The Pennsylvania State University

The Graduate School

Department of Energy and Mineral Engineering

ADSORPTION OF THIOPHENIC COMPOUNDS ON TiO_2-CeO_2 MIXED OXIDES

A Thesis in

Energy and Geo-Environmental Engineering

by

Shingo Watanabe

Submitted in Partial Fulfillment
of the Requirements
for the Degree of

Doctor of Philosophy

December 2007

The thesis of Shingo Watanabe was reviewed and approved* by the following:

Chunshan Song
Professor of Fuel Science
Thesis Advisor
Chair of Committee

Andrè L. Boehman
Professor of Fuel Science and Materials Science and Engineering

Sridhar Komarneni
Distinguished Professor of Clay Mineralogy

Yaw D. Yeboah
Professor of Energy & Mineral Engineering
Head of the Department of Energy & Mineral Engineering

*Signatures are on file in the Graduate School

ABSTRACT

The main theme of this thesis is to understand the adsorption mechanism of thiophenic compounds on $Ti_XCe_{1-X}O_2$ (TiO_2-CeO_2) mixed oxides, particularly $Ti_{0.9}Ce_{0.1}O_2$, in liquid hydrocarbons. The key questions that are addressed in this work are: (1) what is the effect of mixing of TiO_2 and CeO_2 on the structural and surface properties? (2) why does oxidative pretreatment enhance the adsorptive desulfurization capacity? (3) what is the adsorption site of thiophenic compounds over the metal oxide? (4) what is the role of surface components in adsorptive desulfurization and regeneration by oxidation? and (5) what is the possible adsorption mechanism of thiophenic compounds over $Ti_{0.9}Ce_{0.1}O_2$ mixed oxide?

The first part of this thesis focuses on characterization of $Ti_XCe_{1-X}O_2$ mixed oxides, with emphasis on the effect of mixing TiO_2 and CeO_2 on the structural and surface properties of $Ti_XCe_{1-X}O_2$ prepared by urea precipitation using XRD, XPS, TPR and NH_3-TPD techniques. A dominant anatase phase was detected by XRD when X was 0.9 or higher while a cubic fluorite phase was dominant in XRD when X was 0.3 or lower. The $Ti_XCe_{1-X}O_2$ oxides were nano-crystalline, about 4.0 – 8.4 nm in size. Lattice parameters were changed by incorporating Ti into CeO_2 and Ce into TiO_2, respectively. This change reflected distortion of structure, and was attributed to reduction of Ce^{4+} to Ce^{3+} and Ti^{4+} to Ti^{3+}. Due to an effect of mixing TiO_2 and CeO_2, the oxidation state of surface cations decreased, and oxygen deficiency of the surface was significantly enhanced. These structure and surface modifications improved reducibility/oxygen storage capacity of mixed oxides. Weak and strong acidity was enhanced with the

increase of Ti content in NH_3-TPD. Recombinative desorption was observed during NH_3 desorption. This desorption phenomena corresponds to the oxidation property of these TiO_2-CeO_2 mixed oxides. The study in Chapter 2 shows the effect of mixing TiO_2 and CeO_2 on the structural and surface properties of $Ti_XCe_{1-X}O_2$ in multiple ways.

In the following section, the adsorption of thiophene over $Ti_{0.9}Ce_{0.1}O_2$, oxidatively regenerable oxide-based sulfur adsorbent, was studied using probe molecules by XPS, DRIFT and TPD-MS. Special attention was paid to the effect of the oxidative treatment on thiophene adsorption over $Ti_{0.9}Ce_{0.1}O_2$ adsorbent, the adsorption site for thiophenic compound, and the role of surface Ce and Ti cations in the adsorptive desulfurization. The formation of sulfite/sulfate species and enhancement of the sulfite/sulfate formation by oxidative pretreatment was observed in thiophene adsorption. These results suggest that the surface oxygen is the major adsorption site for the thiophenic compounds. The surface Ce and Ti were reduced during the adsorption of thiophenic compounds. This phenomenon is attributed to an electron transfer from adsorbates to the surface Ce and Ti. It appears that the surface Ce and Ti can accept electrons from adsorbate, and also contributes to producing active oxygen to oxidize the sulfur atom in thiophenic compounds. An oxidative treatment, including oxidative regeneration, activates the surface oxygen to forms active oxygen species and also oxidizes the surface Ce and Ti. Based on the results obtained, a possible mechanism was proposed for the adsorption, dissociation and surface reaction of thiophene on $Ti_{0.9}Ce_{0.1}O_2$ mixed metal oxide adsorbent.

Lastly, adsorptive desulfurization of jet fuel (JP-5: 1055 ppmw of sulfur) using high surface area-mesoporous $Ti_{0.9}Ce_{0.1}O_2$ oxide-based adsorbent was studied by N_2,

adsorption-desorption, GC-PFPD, TPD and XPS. The sulfur atom of thiophenic compounds was oxidized by surface oxygen, which could be removed from the organic sulfur molecules, and retained as sulfite/sulfate on the adsorbent surface. Simultaneously the surface cations of adsorbent were reduced during the adsorptive desulfurization. These results concur with the proposed mechanism of thiophene adsorption over the $Ti_{0.9}Ce_{0.1}O_2$ oxide-based adsorbent. The excellent redox property of $Ti_{0.9}Ce_{0.1}O_2$ mixed oxide-based adsorbent allows for the multiple cycles of adsorptive desulfurization by oxidative regeneration using air.

TABLE OF CONTENTS

LIST OF FIGURES viii

LIST OF TABLES xiii

ACKNOWLEDGEMENTS xiv

Chapter 1 Introduction 1

1.1 Background of Research 1
1.2 Thesis Overview 8
1.3 References: 11

Chapter 2 Characterization of Structural and Surface Properties of $Ti_XCe_{1-X}O_2$ Mixed Oxides by XRD, XPS, TPR and TPD 15

2.1 Introduction 17
2.2 Experimental 19
2.2.1 Synthesis of Oxides 19
2.2.2 Characterization of Oxides 19
2.3 Results and Discussion 23
2.3.1 Specific Surface Area 23
2.3.2 XRD 24
2.3.3 XPS 26
2.3.4 H_2-TPR 28
2.3.5 NH_3-TPD 30
2.5 Conclusions 34
References: 55

Chapter 3 Mechanistic Insights into the Adsorption of Thiophene on $Ti_{0.9}Ce_{0.1}O_2$ Mixed Oxide by XPS, in-situ IR and TPD 59

Abstract 59
3.1 Introduction 61
3.2 Experimental 64
3.2.1 Preparation 64
3.2.2 Characterization 65
3.3 Results 68
3.3.1 XPS 68
3.3.2 DRIFT 71
3.3.3 TPD 75
3.4 Discussion 77
3.4.1 Adsorption Mechanism of Thiophenic Compounds over $Ti_{0.9}Ce_{0.1}O_2$ 77

3.4 Conclusions....81
References: 91

Chapter 4 Role of $Ti_{0.9}Ce_{0.1}O_2$ Mixed Oxide as Oxidative Regenerable Adsorbent for the Ultra-Deep Ultra Deep Desulfurization of Jet Fuel 98

Abstract....98
4.1 Introduction....99
4.2 Experimental....101
4.2.1 Preparation....101
4.2.2 Adsorptive Desulfurization of JP-5 101
4.2.3 Characterization....102
4.3 Results and Discussion 105
4.3.1 Nitrogen Adsorption-Desorption Isotherm....105
4.3.2 Adsorptive Desulfurization of JP-5 and Oxidative Regeneration 106
4.3.3 XPS....108
4.3.4 TPD....111
4.4 Conclusions....114
References: 127

Chapter 5 Summary, Conclusions, and Recommended Future Work 130

Recommended future work....133

Appendix A Adsorptive Desulfurization of Liquid Fuels over Metal Oxides: Adsorbent Screening and Study of Thiophene Adsorption by in-situ IR Spectroscopy....135

Abstract....135
A.1 Introduction....136
A.2 Experimental Section....138
A.2.1 Adsorbents....138
A.2.2 Apparatus and Procedure....139
A.3 Results and Discussion 141
A.3.1 Adsorptive Desulfurization over Metal Oxides....141
Sulfur removal of a model fuel 141
Sulfur removal of real fuel (JP-5) 141
A.3.2 In-situ FT-IR....143
IR spectrum of liquid thiophene....144
IR spectra of thiophene adsorption over Cr_2O_3....145
IR spectra of thiophene adsorption over CeO_2....147
IR spectra of thiophene adsorption over NiO....149
IR spectra of thiophene adsorption over ZnO 150
Sulfur removal of liquid fuels and thiophene adsorption over metal oxides 151
A. 4 Conclusions....153

References: 164

Appendix B Preparation Procedure of Oxidatively Regenerable $Ti_{0.9}Ce_{0.1}O_2$ Oxide-based Adsorbent 169

Apparatus 169
Reagent 169
Arrangement 170
Preparation Procedure 170

Appendix C Adsorptive Desulfurization Procedure 175

A fixed-bed Flow System 175
A batch system 177

Appendix D Adsorptive Desulfurization of Liquid Fuels over TiO_2-based Oxide Adsorbents and Investigation of the Effect of Precursor on Desulfurization Performance 178

D-1 Experimental 178
D-1-1 Adsorptive desulfurization 178
D-1-2 Characterization 179
D.2 Results 179
References: 189

Appendix E Adsorptive Desulfurization of Various Fuels over Several Metal Oxides 203

E-1 Experimental 203
E-1-1 Sulfur removal of low sulfur gasoline containing methanol over various metal oxides 204
E-1-2 Sulfur removal of JP-8 over the various metal oxides 205
E-1-3 Sulfur removal of ultra low sulfur diesel over the various metal oxides 206
E-1-4 Sulfur removing performance of $Ti_{0.9}Ce_{0.1}O_2$ for the different fuels 207
E-2 Sulfur Balance in ADS of JP-8 using $Ti_{0.9}Ce_{0.1}O_2$ 208

Appendix F Additional Characterization 209

XPS spectra of two different $Ti_{0.9}Ce_{0.1}O_2$ samples 209

LIST OF FIGURES

Figure **1-1**: Annual Change in SO_2 emission in the US[4] 2

Figure **2-1**: Pore size distributions of TiO_2, $Ti_{0.9}Ce_{0.1}O_2$, $Ti_{0.5}Ce_{0.5}O_2$, $Ti_{0.1}Ce_{0.9}O_2$ and CeO_2 prepared by urea precipitation 37

Figure **2-2**: XRD patterns of commercial TiO_2 and CeO_2, and prepared TiO_2-CeO_2 oxides: (a) TiO_2, (b) $Ti_{0.9}Ce_{0.1}O_2$, (c) $Ti_{0.7}Ce_{0.3}O_2$, (d) $Ti_{0.5}Ce_{0.5}O_2$, (e) $Ti_{0.7}Ce_{0.3}O_2$, (f) $Ti_{0.1}Ce_{0.9}O_2$, and (g) CeO_2. 38

Figure **2-3**: XPS Ce 3d spectra for (a) CeO_2, , (b) $Ti_{0.1}Ce_{0.9}O_2$, (c) $Ti_{0.3}Ce_{0.7}O_2$, (d) $Ti_{0.5}Ce_{0.5}O_2$, (e) $Ti_{0.7}Ce_{0.3}O_2$, (f) $Ti_{0.9}Ce_{0.1}O_2$, after drying at 110 ^oC overnight .. 40

Figure **2-4**: Correlation between the surface Ce^{3+} concentration and the concentration of Ce in TiO_2-CeO_2 oxides. 41

Figure **2-5**: XPS Ti 2p spectra for (a) TiO_2, (b) $Ti_{0.9}Ce_{0.1}O_2$, (c) $Ti_{0.7}Ce_{0.3}O_2$, (d) $Ti_{0.5}Ce_{0.5}O_2$, (e) $Ti_{0.7}Ce_{0.3}O_2$ and (f) $Ti_{0.1}Ce_{0.9}O_2$, and (g) CeO_2, after drying at 110 ^oC overnight. 42

Figure **2-6**: Correlation between binding energy of Ti $2p_{3/2}$ and oxidation state of Ti [57-59] 43

Figure **2-7**: Calculated average oxidation state of Ti in each TiO_2-CeO_2 oxides 44

Figure **2-8**: XPS O 1s spectra for (a) TiO_2, (b) $Ti_{0.9}Ce_{0.1}O_2$, (c) $Ti_{0.7}Ce_{0.3}O_2$, (d) $Ti_{0.5}Ce_{0.5}O_2$, (e) $Ti_{0.7}Ce_{0.3}O_2$ and (f) $Ti_{0.1}Ce_{0.9}O_2$, and (g) CeO_2, after drying at 110 ^oC overnight. 45

Figure **2-9**: The comparison of composition of TiO_2-CeO_2 with stoichiometry of oxides. The measured surface lattice oxygen concentration was obtained based on XPS results, and calculated lattice oxygen concentration was indicated from concentrations of surface Ce^{4+}, Ce^{3+}, T^{i4+} and Ti^{3+}. 46

Figure **2-10**: H_2-TPR profiles of TiO_2-CeO_2 oxides 47

Figure **2-11**: Measured surface oxygen concentration and H_2 consumption in TPR of TiO_2-CeO_2 oxides 48

Figure **2-12**: NH_3-TPD profiles for (a) CeO_2, (b) $Ti_{0.1}Ce_{0.9}O_2$, (c) $Ti_{0.3}Ce_{0.7}O_2$, (d) $Ti_{0.5}Ce_{0.5}O_2$, (e) $Ti_{0.7}Ce_{0.3}O_2$, (f) $Ti_{0.9}Ce_{0.1}O_2$ and (g) TiO_2 49

Figure **2-13**: Correlation between the area of NH_3 desorption peak centered at 270 ^oC and the concentration of Ce in TiO_2-CeO_2 oxides. 50

Figure **2-14**: TPD profiles of NH_3, H_2O, N_2 and O_2 for NH_3 (left) and non-NH_3 (right) adsorbed $Ti_{0.9}Ce_{0.1}O_2$. Sample was treated at 300 ^oC for 1 hr, cooled down to at 110 ^oC, NH3 adsorption was conducted at 110 oC, and desorption was employed under He flow at heating rate 10 oC/min to 700 ^oC. 51

Figure **2-15**: TPD profiles of NH_3, H_2O, N_2 and O_2 for NH_3 (left) and non-NH_3 (right) adsorbed $Ti_{0.5}Ce_{0.5}O_2$. Sample was treated at 300 ^oC for 1 hr, cooled down to at 110 ^oC, NH_3 adsorption was conducted at 110 ^oC, and desorption was employed under He flow at heating rate 10 ^oC/min to 700 ^oC. 52

Figure **2-16**: TPD profiles of NH_3, H_2O, N_2 and O_2 for NH_3 (left) and non-NH_3 (right) adsorbed $Ti_{0.1}Ce_{0.9}O_2$. Sample was treated at 300 ^oC for 1 hr, cooled down to at 110 ^oC, NH_3 adsorption was conducted at 110 ^oC, and desorption was employed under He flow at heating rate 10 ^oC/min to 700 ^oC. 53

Figure **2-17**: Correlation between the difference of H_2O desorption intensities of NH_3 and non-NH_3 adsorbed samples and Ti concentration in TiO_2-CeO_2 oxides 54

Figure **3-1**: S 2p spectra for (a) non-adsorbed $Ti_{0.9}Ce_{0.1}O_2$ surface and (b) THT adsorbed $Ti_{0.9}Ce_{0.1}O_2$ surface. Adsorption of THT was conducted in liquid phase at 25 ^oC for 2 hours. 82

Figure **3-2**: Ce 3d (left) and Ti 2p (right) spectra for (a) non-adsorbed $Ti_{0.9}Ce_{0.1}O_2$ surface and (b) THT adsorbed $Ti_{0.9}Ce_{0.1}O_2$ surface. Adsorption of THT was conducted in liquid phase at 25 ^oC for 2 hours. 83

Figure **3-3**: IR spectra of O_2 adsorbed over $Ti_{0.9}Ce_{0.1}O_2$ at 220 ^oC for 2 hours after vacuum -dried at 200 ^oC for 30 min. 85

Figure **3-4**: IR spectra of thiophene adsorbed on vacuum-dried $Ti_{0.9}Ce_{0.1}O_2$. Thiophene adsorption for (a) 1 min, (b) 5 min, (c) 60 min exposure to thiophene, (d) flowing He for 1 min and (e) flowing He for 60 min, at room temperature. 86

Figure **3-5**: IR spectra of thiophene adsorbed on oxidized $Ti_{0.9}Ce_{0.1}O_2$. (a) exposure to thiophene for 1 min, (b) exposure to thiophene for 60 min, (c) He flow for 1 min, and (d) He flow for 60 min, at room temperature. 87

Figure **3-6**: TPD spectra of m/e=64 for non-adsorbed, vacuum-dried and oxidized $Ti_{0.9}Ce_{0.1}O_2$ oxide adsorbed thiophene in n-C_{10} solution (1000 ppmw-sulfur) at room temperature. 88

Figure **3-7**: TPD spectra of m/e=54, 56, 58 and 84 for (a) vacuum-dried and (b) oxidized $Ti_{0.9}Ce_{0.1}O_2$ oxide adsorbed thiophene in n-C_{10} solution (1000 ppmw-sulfur) at room temperature. 89

Figure **3-8**: Proposed adsorption pathway of thiophene over $Ti_{0.9}Ce_{0.1}O_2$ from this study.....90

Figure **4-1**: Nitrogen adsorption-desorption isotherm of $Ti_{0.9}Ce_{0.1}O_2$. 115

Figure **4-2**: Pore size distribution of $Ti_{0.9}Ce_{0.1}O_2$ before 1st sulfur removal (fresh) and after 3rd oxidative regeneration (spent). 116

Figure **4-3**: Breakthrough curves of JP-5 desulfurization over $Ti_{0.9}Ce_{0.1}O_2$ at room temperature, fuel flow rate, LHSV: 1.2 h^{-1}. 118

Figure **4-4**: Distribution of sulfur compounds in GC-PFPD chromatogram of JP-5. 120

Figure **4-5**: Ce 3d and Ti 2p spectra of $Ti_{0.9}Ce_{0.1}O_2$ (a) dried at 100 ^oC for 2 hours and (b) oxidized at 220 ^oC for 2 hours. 121

Figure **4-6**: Ce 3d spectra of $Ti_{0.9}Ce_{0.1}O_2$ for (a) before and (b) after adsorption of sulfur in JP-5 and (c) after oxidative regeneration. 122

Figure **4-7**: Ti 2p spectra of $Ti_{0.9}Ce_{0.1}O_2$ for (a) before and (b) after adsorption of sulfur in JP-5 and (c) after oxidative regeneration. 123

Figure **4-8**: TPD spectra of m/e=64 for $Ti_{0.9}Ce_{0.1}O_2$ adsorbent before and after adsorption of sulfur in JP-5 at room temperature. 124

Figure **4-9**: TPD spectra of m/e= 48 (SO), 64 (SO_2), 80 (SO_3) and 96 (SO_4) for $Ti_{0.9}Ce_{0.1}O_2$ adsorbent before and after adsorption of sulfur in JP-5 at room temperature. 125

Figure **4-10**: Proposed pathway of adsorptive desulfurization of jet fuel over $Ti_{0.9}Ce_{0.1}O_2$ adsorbent.....126

Figure **A-1**: Sulfur removal capacity of model fuel and JP-5 over metal oxides at room temperature for 2 hrs. Fuel/adsorbent weight ratio= 1:5. 158

Figure **A-2**: Comparison of sulfur removing capacities of model fuel and JP-5 159

Figure **A-3**: FT-IR difference spectra obtained by subtracting the spectrum of vacuumed-dried Cr_2O_3 (200 ^oC for 1 hr) from (a) the spectrum Cr_2O_3 exposed to thiophene/Ar flow for 1 min, (b) the spectrum of Cr_2O_3 exposed to thiophene/Ar flow for 60 min, (c) the spectrum of Cr_2O_3 aged for 60 min after exposed to thiophene/Ar flow for 60 min, (d) the spectrum of Cr_2O_3 under Ar flow for 1 min, (e) the spectrum of Cr_2O_3 under Ar flow for 15 min, at room temperature in the range of 4000 – 2800 cn^{-1} (left) and 1800 - 1000 cm^{-1} (right). 160

Figure **A-4**: FT-IR difference spectra obtained by subtracting the spectrum of vacuumed-dried CeO_2 (200 ^oC for 1 hr) from (a) the spectrum CeO_2 exposed to thiophene/Ar flow for 1 min, (b) the spectrum of CeO_2 exposed to thiophene/Ar flow for 60 min, (c) the spectrum of CeO_2 aged for 60 min after exposed to thiophene/Ar flow, (d) the spectrum of CeO_2 under Ar flow for 5 min, (e) the spectrum of CeO_2 under Ar flow for 60 min, at room temperature in the range of 4000 – 2800 cn^{-1} (left) and 1800 - 1000 cm^{-1} (right). 161

Figure **A-5**: FT-IR difference spectra obtained by subtracting the spectrum of vacuumed-dried NiO (200 ^oC for 1 hr) from (a) the spectrum NiO exposed to thiophene/Ar flow for 1 min, (b) the spectrum of NiO exposed to thiophene/Ar flow for 60 min, (c) the spectrum of NiO aged for 60 min after exposed to thiophene/Ar flow, (d) the spectrum of NiO under Ar flow for 1 min, (e) the spectrum of NiO under Ar flow for 60 min, at room temperature in the range of 4000 – 2800 cn^{-1} (right) and 1800 - 1000 cm^{-1} (left). 162

Figure **A-6**: FT-IR difference spectra obtained by subtracting the spectrum of vacuumed-dried ZnO (200 ^oC for 1 hr) from (a) spectrum ZnO exposed to thiophene/Ar flow for 1 min, (b) the spectrum of ZnO exposed to thiophene/Ar flow for 60 min, (c) the spectrum of ZnO aged for 60 min after exposed to thiophene/Ar flow, (d) the spectrum of ZnO under Ar flow for 1 min, (e) the spectrum of ZnO under Ar flow for 60 min, at room temperature in the range of 4000 – 2800 cn^{-1} (right) and 1800 - 1000 cm^{-1} (left). 163

Figure **B-1**: Changes of pH and temperature in the urea precipitation for $Ti_{0.9}Ce_{0.1}O_2$ preparation (data was provided Mamoru Fujii) 173

Figure **D-1**: Sulfur removal of JP-5 over TiO_2-based adsorbents: JP-5 contained 1055 ppmw-S. Adsorption was conducted in batch system, at room temperature, and adsorbent/fuel weight ratio = 1/10. 182

Figure **D-2**: Benzothiophene removal by adsorption over TiO_2-CeO_2 oxides for 1 h and its products found in washing solvent 183

Figure **D-3**: Sulfur removal of JP-5 over TiO_2-based adsorbents: JP-5 contained 1055 ppmw-S. Adsorption was conducted in batch system, at 100 ^oC, and adsorbent/fuel weight ratio = 1/10. 184

Figure **D-4**: Temperature effect on ADS capacity of JP-5 in the use of batch system at 25 and 100 ^oC. Fuel: Adsorbent=10:1. 185

Figure **D-5**: Effect of sulfur in precursor on the sulfur removal performance over $Ti_{0.9}Ce_{0.1}O_2$: batch testing using JP-5 (1055 ppmw), fuel/adsorbent=10/1 wt. 187

Figure **D-6**: NH_3-TPD profiles of m/e=16 for H_2O for $Ti_{0.9}Ce_{0.1}O_2$ prepared using non- and sulfur containing precursor. 188

Figure **E-1**: Breakthrough curves of ADS of gasoline (26 ppmw-S) containing methanol over various metal oxide adsorbents: LHSV: 1.2 h-1, operation temperature: room temperature. Pretreatment at 300 ^{o}C under air flow.....204

Figure **E-2**: Breakthrough curves of ADS of JP-8 (365 ppmw-S) over various metal oxide adsorbents: operation temperature: LHSV: 1.2 h^{-1}, room temperature. Pretreatment at 300 ^{o}C under air flow. 205

Figure **E-3**: Breakthrough curves of ADS of ultra low diesel (16 ppmw-S) over various metal oxide adsorbents: LHSV: 1.2 h^{-1}, operation temperature: room temperature. Pretreatment at 300 ^{o}C under air flow. 206

Figure **E-4**: Breakthrough curves of ADS for various fuels over $Ti_{0.9}Ce_{0.1}O_2$: operation temperature: room temperature. Pretreatment at 300 ^{o}C under air flow. 207

Figure **F-1**: XPS Ce 3d spectra of two $Ti_{0.9}Ce_{0.1}O_2$ samples prepared different time 209

Figure **F-2**: XPS Ti 2p spectra of two $Ti_{0.9}Ce_{0.1}O_2$ samples prepared different time ..210

Figure **F-3**: XPS O 1s spectra of two $Ti_{0.9}Ce_{0.1}O_2$ samples prepared different time ...211

LIST OF TABLES

Table **1-1**: Breakthrough Capacity, Selectivity and Regenerability of Reported Adsorbents for Adsorptive Desulfurization of Real Fuels. 6

Table **2-1**: Physical Properties of TiO_2-CeO_2 Oxides 36

Table **2-2**: Crystallite Structure, d Value, Lattice Parameter and Mean Crystalline Size in TiO_2-CeO_2 Mixed Oxides 39

Table **3-1**: Concentration of Ce^{3+} and Binding Energy of Ti $2p_{3/2}$ before and after THT Adsorption 84

Table **4-1**: BET Surface Area, Pore Volume and Average Pore Size of Fresh and Regenerated $Ti_{0.9}Ce_{0.1}O_2$ 117

Table **4-2**: Sulfur Removal Capacity for JP-5 at Room Temperature. Initial Sulfur Concentration of JP-5: 1055 ppmw. 119

Table **A-1**: Physical Properties of Metal Oxides 155

Table **A-2**: Sulfur Removal of Model Fuel over Metal Oxides. 156

Table **A-3**: Sulfur Removal of JP-5 Fuel over Metal Oxides 157

Table **D-1**: d- Spacing and Lattice Parameter of Fresh and Spent $Ti_{0.9}Ce_{0.1}O_2$ 186

Table **E-1**: Sulfur Balance in ADS of JP-8 208

ACKNOWLEDGEMENTS

This work was carried out in the Clean Fuels and Catalysis Program at the Energy Institute, the Pennsylvania State University. Funding for research into adsorptive desulfurization provided by the office of Naval Research, U.S. Department of Defense and the Pennsylvania State University is gratefully acknowledged.

I wish to express my sincere gratitude to my advisor, Dr. Chunshan Song for his support, guidance and encouragement. I would also like to thank Dr. André L. Boehman, Dr. Yaw Yeboah and Dr. Sridhar Komarneni for their insightful comments, helpful suggestions and for serving as committee members. I would like to acknowledge the help of members of our research group, particularly Dr. X. Ma for many technical discussions on adsorptive desulfurization and related research Thanks are also extended to Mr. B. Hengstebek, Dr. V. Bojan,, Ms. N. Wonderling, Dr. M. Klimkiewicz and Ms. M. Salama for their help in analysis.

Lastly, my thanks to my parents for their love, encouragement and confidence in me.

Chapter 1

Introduction

1.1 Background of Research

Sulfur was known already in ancient times. It is referred to as brimstone in the earliest literature, such as the Bible.[1] Nowadays, the oxidized compounds SO_X are known as a major pollutant. The anthropogenic SO_X emission is generated mainly from combustion of fossil fuels in the world.[2] About 3/4 of the total SO_X emission originated from the anthropogenic source, which corresponds to 101.8×10^6 ton of sulfur per year in early 1990s.[3] As shown in Figure 1, due to the control of pollutants emissions beginning in the 1970s, the total anthropogenic SO_X emission has started to decline since 1970 in US[4] and since 1980 in Europe.[5] However, the SO_X emission from transportation fuels continued to increase till 1990, and then begun to decrease after 1990 in the US. It is important to note that the onset of reduction in SO_X emission from transportation sector coincided with the sulfur regulations of transportation fuels.[6] In the last two decades, the maximum allowed sulfur concentrations in liquid fuels have been lowered significantly worldwide. Furthermore, the sulfur regulation is expected to be more stringent in future. For example, the sulfur regulations for gasoline and diesel fuels will be set up to lower than 10 ppmw in year 2011 in Europe.[7]

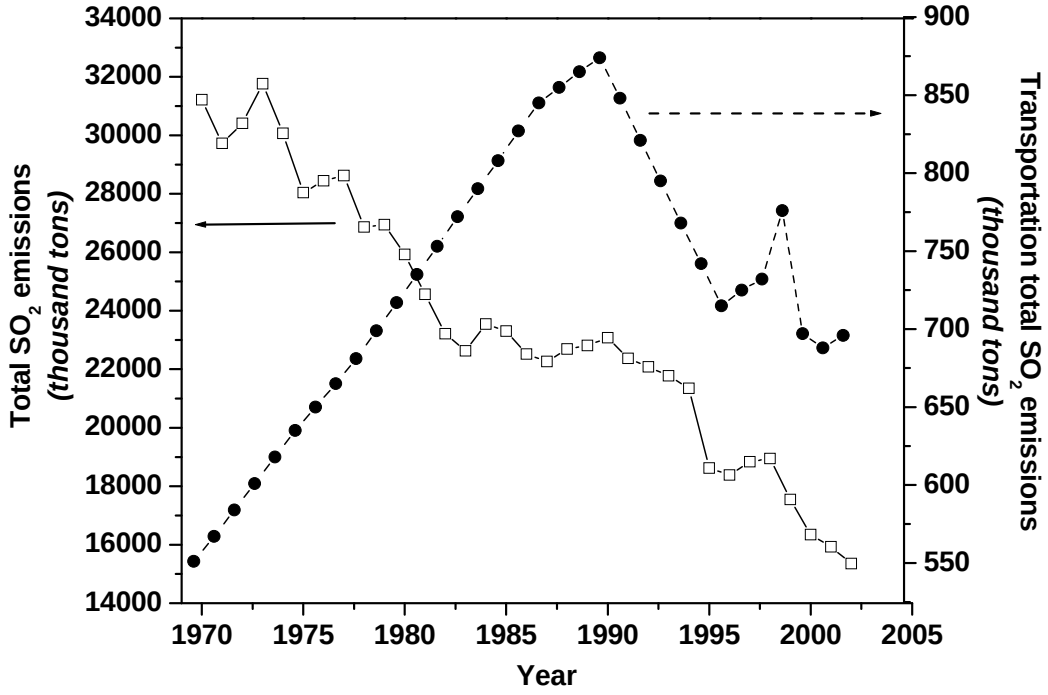

Figure **1-1**: Annual Change in SO_2 emission in the US[4]

Recently, new regulations to reduce the sulfur content in transportation fuels have come into force by the governments in various countries. The U.S. Environmental Protection Agency (EPA) has announced a regulation that mandates refineries to reduce the sulfur content in gasoline and diesel fuels from 300-500 parts per million by weight of sulfur (ppmw) to below the average of 30 and 15 ppmw in 2006, respectively.[6, 8] Although the sulfur contents of transportation fuels are significantly lowered, some organic sulfur compounds still remain in the fuels due to the low reactivity of certain substituted thiophenic compounds. These sulfur compounds are oxidized and converted

to SO_X during combustion of liquid fuels. Combusted gas contains also CO, unburned hydrocarbons (HC) and NO_X along with SO_X, and those compounds need to be further reduced or cleaned up before release to the atmosphere. A catalytic process is employed in automobile exhaust catalytic converter unit by oxidation of CO and unburned hydrocarbons and reduction of NO_X. However, sulfur, which exists in small amount in exhaust gas, causes serious poisoning of the catalyst in the converter, especially the noble metals such as Pt and Rh. Negative influence of sulfur was also found on the reduction of particulate matters which are responsible also for the black smoke out of exhaust gas from diesel trucks.[9]

The ultra-deep desulfurization of liquid fuels is also important for the development of fuel cell applications.[6, 10, 11] The sulfur content in liquid fuels needs to be further reduced to lower than 0.1 ppmw for Proton Exchange Membrane Fuel Cell (PEMFC) and lower than 1 ppmw for Solid Oxide Fuel Cell (SOFC) applications. If an effective desulfurization approach can be developed, utilization of the clean liquid fuels for fuel cell applications is very attractive due to the availability and existing infrastructures.[11] The growth in demand for ultra-low-sulfur transportation fuels, the current and the anticipated future environmental regulations on low-sulfur fuels, and the need for ultra-clean fuels for the promising fuel cell applications all point to the needs for developing more efficient and more effective approaches for removing sulfur from liquid fuels.

Hydrodesulfurization (HDS) is a common industrial process to remove sulfur from petroleum feed stocks, and is widely used to meet the current regulations. However, HDS requires higher temperature, and higher pressure in a pressurized reactor tower and

consumes hydrogen which is expensive. Deep sulfur removal is especially important for diesel fuels where the substituted dibenzothiophenes are more difficult to remove. Therefore, ultra clean diesel fuel (e.g., < 1 ppmw sulfur) production by HDS requires more severer operation conditions such as higher temperature and higher pressure with higher hydrogen consumption, in addition to the larger catalyst bed volume in pressurized reactors.[12] Thus, extensive research has been carried out to explore alternative processes such as adsorption, alkylation, oxidation, and extraction.[6, 13] Among them, the selective adsorption of organic sulfur compounds is attractive because it would require much lower operating costs and greatly reduce the need for high-pressure and high-temperature operations and minimizes consumption of hydrogen. Several materials, such as activated carbon (AC)-based,[14] metal-based,[10, 15] metal oxide-based,[16-18] and zeolite-based [19-22] adsorbents, have been investigated for adsorptive desulfurization (ADS) of liquid fuels (gasoline, jet fuel and diesel fuel). The adsorbents reported for sulfur removal of commercial liquid fuels are summarized in Table 1-1. Activated carbon-based adsorbent was used for sulfur removal of diesel containing 297 ppmw [23] and JP-5 containing 1172 ppmw of sulfur[24] at room temperature. Breakthrough capacities for sulfur removal of diesel and JP-5 jet fuel with the sulfur concentration in the effluent lower than 1 ppmw were obtained as 0.64 and lower than 0.1 milligram of sulfur per gram of adsorbent (mg-S/g-Ads.), respectively. Regeneration for AC-based adsorbent was conducted using a mixture of 30 wt.% of benzene and 70 wt.% of n-octane under ultrasound operation at 50 ^{o}C after sulfur adsorption removal from a model fuel. Approximately 65 % of the sulfur adsorbed over the AC-sorbent desorbed during solvent-regeneration while result of multiple cycles of adsorptive desulfurization was not reported. Sulfur removal from a

gasoline containing 210 ppmw sulfur over Ni-based adsorbent at room temperature was reported.[15] Sulfur removing capacities were about 0.3 mg-S/g-Ads. Breakthrough capacity of sulfur removal from light JP-8 at 220 ^{o}C was 13.5 mg-S/g-Ads.[22] Adsorption of thiophenic compounds over Ni-based adsorbent leads to C-S bond cleavage. Regeneration for this type of adsorbents was not reported. However, H_2 reduction at higher temperature might be needed.

Zeolite-based adsorbents have been examined for adsorptive desulfurization of gasoline,[25, 26] jet fuel[20, 21] and diesel[20, 27]. Among several zeolite based-adsorbents, monovalent Cu ion exchanged-Y zeolite showed the superior desulfurization performance. The sulfur removing capacities for jet and diesel fuels were 12.7 and 8.9 mg-S/g-Ads., respectively.[20] The adsorption mechanism was explained as via π complexation [27]. Sulfur removal by metal cation-exchanged zeolite adsorbents was also suggested to take place via sulfur-metal interaction.[19, 25] Although the zeolite based-adsorbents showed higher sulfur removing capacity, regeneration requires more than one type of treatment steps, which start with oxidation under air flow at 350 ^{o}C for 6 hours, and then reduced under He flow. In addition to the AC-based, metal-based and zeolite-based adsorbents, TiO_2-CeO_2 mixed oxide-based adsorbents have been examined for sulfur removal of gasoline, jet fuel and diesel.[16-18] The previous study showed that the initial sulfur concentration of real fuels can be reduced to lower than 1 ppmw at room temperature. Multiple cycles of adsorptive desulfurization was successfully accomplished by oxidative regeneration using air.[18] Due to a simple regeneration by oxidation, an effective adsorptive system could be developed through the use of metal oxides.

Table **1-1**: Breakthrough Capacity, Selectivity and Regenerability of Reported Adsorbents for Adsorptive Desulfurization of Real Fuels.

Adsorbent	Feed stock (sulfur conc.)	Capacity (mg-S/g-Ads.)	Selectivity	Regenerability
Activated carbon	JP-5 (1172 ppmw)[24] Diesel (297 ppmw)[23]	~ 0.0 0.64	selectivity toward 4,6DMDBT	Washing by polar solvents, and can be aided by ultra sound. dry under N_2 flow
Ni-based	Gasoline (210 ppmw)[15]	0.3	high selectivity towards sulfur. uses ethanol as sacrificing agents for coke formation	H_2 reduction at high temp.
Cu (I)- Y zeolite	Commercial jet fuel (364 ppmw)[20] Diesel (297 ppmw)[20]	8.9 12.7	π complexation. olefins, oxygenates and moisture deactivate.	Oxidation under air flow for 6 hrs and reduction under He flow
$Ti_{0.9}Ce_{0.1}O_2$	JP-5 (1055 ppmw) ** present work	2.4	selectivity toward sulfur	oxidation under air flow for 30 min – 2 hrs

** operation: at room temperature*

A concept is being developed in our laboratory at Penn State University known as "selective adsorption for removal of sulfur (PSU-SARS)" for the selective removal of organic sulfur compounds from gasoline, diesel and jet fuel.[6, 10-12, 15, 16, 19, 21, 22, 28-30] As introduced above, several adsorbents based on zeolites, oxides, supported metal compounds, activated carbons, etc. are being developed and some of them exhibited the excellent desulfurization performance for gasoline, jet fuel and diesel fuel [10, 12, 17-19]. Among the several kinds of materials that have been investigated as adsorbents, the metal oxide-based adsorbents showed promising results in multiple cycles of ADS of liquid hydrocarbon fuels. Due to a simple regeneration by oxidation, an effective adsorptive system could be developed through the use of metal oxides. However, little is known on the mechanism of adsorptive desulfurization of liquid fuels over metal oxide-based adsorbent.

The objective of this research is to gain the insight into the mechanism of adsorptive desulfurization of liquid fuels over TiO_2-CeO_2 ($Ti_xCe_{1-x}O_2$) mixed metal oxide adsorbents, particularly $Ti_{0.9}Ce_{0.1}O_2$. The $Ti_{0.9}Ce_{0.1}O_2$ adsorbents have been found to be one of the most promising adsorbents for ultra deep desulfurization of liquid fuels [17, 18]. The absence of detailed studies, especially those providing a mechanistic understanding of the thiophene adsorption on the metal oxide-based adsorbent, has become the bottleneck in the development of better understanding and improved oxide-based adsorbents. In order to achieve the goal of understanding the mechanism of adsorptive desulfurization, comparative studies had been conducted, which include studies on structural and surface properties of TiO_2-CeO_2 oxides, the effect of oxidative pretreatment on sulfur removal over $Ti_{0.9}Ce_{0.1}O_2$, the adsorption site for thiophenic

compounds, the role of the surface Ce and Ti cations of $Ti_{0.9}Ce_{0.1}O_2$ adsorbent in adsorptive desulfurization. The information obtained from these studies provides the insight into the mechanism of the adsorptive desulfurization of liquid fuels over $Ti_{0.9}Ce_{0.1}O_2$-based adsorbent, and will guide our work in improvement of the adsorbents and development of more effective metal-oxide-based adsorbents.

1.2 Thesis Overview

The following chapters cover several inter-related fundamental and application aspects for the adsorptive desulfurization of liquid fuels over $Ti_{0.9}Ce_{0.1}O_2$ mixed oxide-based adsorbent.

Chapter 2 focuses on the preparation and structural and surface properties of TiO_2-CeO_2 metal oxides. Recent work in our laboratory on the adsorptive desulfurization of liquid fuels indicated that TiO_2-CeO_2 mixed metal oxides adsorbents exhibit excellent sulfur removing performance.[17, 18] Among the different ratios of Ti/Ce in the TiO_2-CeO_2 mixed oxides, $Ti_{0.9}Ce_{0.1}O_2$ showed the various sulfur removing properties from liquid fuels.[17, 18] Published studies, although still very limited, indicate the unique structural or surface properties of TiO_2-CeO_2 mixed oxides.[31-35] On the other hand, there are very few studies on both the structure and the surface properties of TiO_2-CeO_2 mixed oxides. Detailed studies involving both structure and surface chemistry of TiO_2-CeO_2 mixed oxides were not found, especially TiO_2-CeO_2 mixed oxides synthesized by the urea precipitation method. No prior study has been reported on the $Ti_{0.9}Ce_{0.1}O_2$. Thus, the studies in Chapter 2 focused on characterization of TiO_2-CeO_2 ($Ti_XCe_{1-X}O_2$) mixed

oxides, with emphasis on the effect of mixing TiO_2 and CeO_2 on structure and surface properties of TiO_2-CeO_2 mixed oxides. Nitrogen adsorption-desorption and X-ray diffraction (XRD) were conducted to characterize the textural and structural properties of the oxides. The surface properties of TiO_2-CeO_2 oxides were investigated by X-ray photoelectron spectroscopy (XPS), temperature-programmed desorption of ammonia (NH_3-TPD) and temperature-programmed reduction in hydrogen (H_2-TPR). The results show a significant effect of mixing TiO_2 and CeO_2 on changes in structure, crystalline size, and surface properties, including oxygen deficiency, reducibility and acidity, of TiO_2-CeO_2 mixed oxides.

Chapter 3 attempts to provide insights into the adsorption mechanism of thiophene including the effect of the oxidative pretreatment on thiophene adsorption over $Ti_{0.9}Ce_{0.1}O_2$ adsorbent, the adsorption site for thiophenic compound, and the role of surface Ce and Ti cations in the adsorptive desulfurization. Influence of oxidative pretreatment of TiO_2-CeO_2 mixed metal oxides adsorbents was found in the examination using model fuel [18]. Sulfur removing capacity varied with the different pretreatments at 375 ^oC for 2 hours and decreased in the order of air > N_2 > H_2. Mixed oxide adsorbent oxidatively pretreated under air flow showed almost three times higher sulfur removing ability than that with H_2 reduction. Thus, the effect of oxidative treatment on sulfur removal over the $Ti_{0.9}Ce_{0.1}O_2$ adsorbent was investigated here. In addition to the effect of oxidative pretreatment, the adsorption mechanism of thiophene on $Ti_{0.9}Ce_{0.1}O_2$ oxide was studied using probe molecules. Little is known on the mechanism of thiophene adsorption on mixed metal oxides. Therefore, this study led to elucidation of the mechanism of

adsorption of thiophene over $Ti_{0.9}Ce_{0.1}O_2$ including the role of surface Ti and Ce in adsorptive desulfurization by using analytical techniques such as XPS, DRIFT and TPD.

Chapter 4 investigates the role of $Ti_{0.9}Ce_{0.1}O_2$ mixed oxide as oxidatively regenerable adsorbent for the adsorptive desulfurization of a real jet fuel in the multiple cycles including the effect of oxidative treatment, the adsorption selectivity and the role of adsorbent during the sulfur adsorption removal and oxidative regeneration. In contrast to the model study in previous chapter, this chapter discusses the effect of oxidative treatment, the adsorption selectivity and the role of adsorbent in the sulfur removal of a real JP-5 jet fuel and the oxidative regeneration was examined also by XPS and TPD. By comparison of physical property of the fresh and spent adsorbents, the effectiveness of excellent redox property of $Ti_{0.9}Ce_{0.1}O_2$ adsorbent on the adsorptive desulfurization and oxidative regeneration was emphasized.

Chapter 5 summarizes the major observations and new findings with conclusions on the unique feature of $Ti_{0.9}Ce_{0.1}O_2$ adsorbent as a new oxidatively regenerable adsorbent and the insight into the fundamental surface chemical changes during the adsorptive desulfurization over $Ti_{0.9}Ce_{0.1}O_2$ adsorbent and the oxidation regeneration.

1.3 References:

(1) Babor, J. A.; Lehrman, A., In *General College Chemistry*, 3rd ed Crowell: 1953; 'pp 412.

(2) Langner, J.; Rodhe, H.; Crutzen, P. J.; Zimmermann, P., Anthropogenic Influence on the Distribution of Tropospheric Sulfate Aerosol. *Nature* **1992,** 359, (6397), 712.

(3) Graf, H. F.; Feichter, J.; Langmann, B., Volcanic sulfur emissions: Estimates of source strength and its contribution to the global sulfate distribution. *Journal of Geophysical Research-Atmospheres* **1997,** 102, (D9), 10727.

(4) US-EPA National Emissions Inventory (NEI) Air Pollutant Emissions Trends Data. http://www.epa.gov/ttn/chief/trends/ (June 26),

(5) Vestreng, V.; Myhre, G.; Fagerli, H.; Reis, S.; Tarrason, L., Twenty-five years of continuous sulphur dioxide emission reduction in Europe. *Atmospheric Chemistry and Physics* **2007,** 7, (13), 3663.

(6) Song, C. S., An overview of new approaches to deep desulfurization for ultra-clean gasoline, diesel fuel and jet fuel. *Catalysis Today* **2003,** 86, (1-4), 211.

(7) Marcilly, C., Present status and future trends in catalysis for refining and petrochemicals. *Journal of Catalysis* **2003,** 216, (1-2), 47.

(8) Song, C. S., Keynote address. New approaches to deep desulfurization for ultra-clean gasoline and diesel fuels: An overview. *Am. Chem. Soc. Div. Fuel Chem. Prepr.* **2002,** 47, (2), 438.

(9) Inoue, S.; Takatsuka, T., Ultra-deep desulfurization and aromatic saturation of diesel oil. *Sekiyu Gakkaishi-Journal of the Japan Petroleum Institute* **1999,** 42, (6), 365.

(10) Ma, X. L.; Sun, L.; Song, C. S., A new approach to deep desulfurization of gasoline, diesel fuel and jet fuel by selective adsorption for ultra-clean fuels and for fuel cell applications. *Catalysis Today* **2002,** 77, (1-2), 107.

(11) Song, C., Fuel processing for low-temperature and high-temperature fuel cells challenges, and opportunities for sustainable development in the 21st century. *Catalysis Today* **2002,** 77, 17.

(12) Song, C.; Ma, X. L., New design approaches to ultra-clean diesel fuels by deep desulfurization and deep dearomatization. *Applied Catalysis B-Environmental* **2003,** 41, (1-2), 207.

(13) Babich, I. V.; Moulijn, J. A., Science and technology of novel processes for deep desulfurization of oil refinery streams: A review. *Fuel* **2003,** 82, (6), 607.

(14) Zhou, A. N.; Ma, X. L.; Song, C. S., Liquid-phase adsorption of multi-ring thiophenic sulfur compounds on carbon materials with different surface properties. *Journal of Physical Chemistry B* **2006,** 110, (10), 4699.

(15) Ma, X. L.; Sprague, M.; Song, C. S., Deep desulfurization of gasoline by selective adsorption over nickel-based adsorbent for fuel cell applications. *Industrial & Engineering Chemistry Research* **2005,** 44, (15), 5768.

(16) Watanabe, S.; Velu, S.; Ma, X.; Song, C., New ceria-based selective adsorbents for removing sulfur from gasoline for fuel cell application. *Am. Chem. Soc., Div. Fuel Chem. Prepr.* **2003,** 48, (2), 695.

(17) Watanabe, S.; Ma, X.; Song, C. S., Selective sulfur removal from liquid hydrocarbons over regenerable CeO_2-TiO_2 adsorbents for fuel cell applications. *Am. Chem. Soc. Div. Fuel Chem. Prepr.* **2004,** 49, (2), 511.

(18) Watanabe, S. Selective and Regenerable Metal Oxide Adsorbents for the Removal of Sulfur from Liquid Fuels for Fuel Cell Applications. Master of Science, The Pennsylvania State University, University Park, Pennsylvania, 2004.

(19) Velu, S.; Ma, X. L.; Song, C. S., Selective adsorption for removing sulfur from jet fuel over zeolite-based adsorbents. *Industrial & Engineering Chemistry Research* **2003,** 42, (21), 5293.

(20) Hernandez-Maldonado, A. J.; Yang, F. H.; Qi, G.; Yang, R. T., Desulfurization of transportation fuels by pi-complexation sorbents: Cu(I)-, Ni(II)-, and Zn(II)-zeolites. *Applied Catalysis B-Environmental* **2005,** 56, (1-2), 111.

(21) Velu, S.; Song, C. S.; Engelhard, M. H.; Chin, Y. H., Adsorptive removal of organic sulfur compounds from jet fuel over K-exchanged NiY zeolites prepared by impregnation and ion exchange. *Industrial & Engineering Chemistry Research* **2005,** 44, (15), 5740.

(22) Velu, S.; Ma, X. L.; Song, C. S.; Namazian, M.; Sethuraman, S.; Venkataraman, G., Desulfurization of JP-8 jet fuel by selective adsorption over a Ni-based adsorbent for micro solid oxide fuel cells. *Energy & Fuels* **2005,** 19, (3), 1116.

(23) Hernandez-Maldonado, A. J.; Yang, R. T., New sorbents for desulfurization of diesel fuels via pi-complexation. *AIChe Journal* **2004,** 50, (4), 791.

(24) Wang, Y. H.; Yang, R. T., Desulfurization of liquid fuels by adsorption on carbon-based sorbents and ultrasound-assisted sorbent regeneration. *Langmuir* **2007,** 23, (7), 3825.

(25) King, D. L.; Faz, C., Desulfurization of Tier 2 gasoline by divalent copper-exchanged zeolite Y. *Applied Catalysis a-General* **2006,** 311, 58.

(26) Hernandez-Maldonado, A. J.; Yang, R. T., Desulfurization of commercial liquid fuels by selective adsorption via pi-complexation with Cu(I)-Y zeolite. *Industrial & Engineering Chemistry Research* **2003,** 42, (13), 3103.

(27) Hernandez-Maldonado, A. J.; Yang, R. T., Desulfurization of transportation fuels by adsorption. *Catalysis Reviews-Science and Engineering* **2004,** 46, (2), 111.

(28) Ma, X. L.; Sun, L.; Song, C. S., Adsorptive desulfurization of diesel fuel over a metal sulfide-based adsorbent. *Am. Chem. Soc. Div. Fuel Chem. Prepr.* **2003,** 48, (2), 522.

(29) Velu, S.; Watanabe, S.; Ma, X. L.; Song, C. S., Regenerable adsorbents for the adsorptive desulfurization of transportation fuels for fuel cell applications. *Am. Chem. Soc., Div. Fuel Chem. Prepr.* **2003,** 226, U531.

(30) Song, C. S.; Ma, X. L., Ultra-deep desulfurization of liquid hydrocarbon fuels: Chemistry and process. *International Journal of Green Energy* **2004,** 1, (2), 167.

(31) Trovarelli, A.; de Leitenburg, C.; Boaro, M.; Dolcetti, G., The utilization of ceria in industrial catalysis. *Catalysis Today* **1999,** 50, (2), 353.

(32) Trovarelli, A., Catalytic properties of ceria and CeO_2-containing materials. *Catalysis Reviews-Science and Engineering* **1996,** 38, (4), 439.

(33) Diebold, U., The surface science of titanium dioxide. *Surface Science Reports* **2003,** 48, (5-8), 53.

(34) Hadjiivanov, K. I.; Klissurski, D. G., Surface chemistry of titania (anatase) and titania-supported catalysts. *Chemical Society Reviews* **1996,** 25, (1), 61.

(35) Luo, M. F.; Chen, J.; Chen, L. S.; Lu, J. Q.; Feng, Z.; Li, C., Structure and redox properties of $Ce_XTi_{1-X}O_2$ solid solution. *Chemistry of Materials* **2001,** 13, (1), 197.

Chapter 2

Characterization of Structural and Surface Properties of $Ti_XCe_{1-X}O_2$ Mixed Oxides by XRD, XPS, TPR and TPD

Abstract

Previous research in our laboratory showed that TiO_2-CeO_2 ($Ti_XCe_{1-X}O_2$) mixed oxides are good adsorbents for adsorptive desulfurization of liquid fuels. The present work focuses on characterization of $Ti_XCe_{1-X}O_2$ mixed oxides, with emphasis on the effect of mixing TiO_2 and CeO_2 on the structural and surface properties of $Ti_XCe_{1-X}O_2$ prepared by urea precipitation using XRD, XPS, TPR and NH_3-TPD techniques. A dominant anatase phase was detected by XRD when X was 0.9 or higher while a cubic fluorite phase was dominant in XRD when X was 0.3 or lower. The mixed oxides were nano-crystalline, about 4.0 nm in size when X = 0.9 and 4.8 – 5.4 nm when X = 0.1- 0.3, which are significantly smaller than the TiO_2 and CeO_2 single oxides (8.1 to 8.4 nm). Lattice parameters were changed by incorporating Ti into CeO_2 and Ce into and TiO_2, respectively. This change reflected distortion of structure, and was attributed to reduction of Ce^{4+} to Ce^{3+} and Ti^{4+} to Ti^{3+}. Due to an effect of mixing TiO_2 and CeO_2, the oxidation state of surface cations decreased, and oxygen deficiency of the surface was significantly enhanced. These structure and surface modifications improved reducibility/oxygen storage capacity of mixed oxides. Weak and strong acidity was enhanced with the increase of Ti content in NH_3-TPD. Recombinative desorption was observed during NH_3 desorption. This desorption phenomena corresponds to the oxidation property of these

TiO_2-CeO_2 mixed oxides. The current study shows the effect of mixing TiO_2 and CeO_2 on the structural and surface properties of $Ti_XCe_{1-X}O_2$ in multiple ways.

2.1 Introduction

Titania (TiO_2) and ceria (CeO_2) have been extensively studied among metal oxides for their various applications.[31-34] For various technical applications, TiO_2 is known as an excellent material, especially for photocatalysis [36] and environmental catalysis.[34, 37] CeO_2 is known as an excellent support for base metals and noble metals in a variety of catalytic processes due to its high oxygen storage capacity, redox properties and strong metal-support interactions.[38-40] Thus, both TiO_2 and CeO_2 have recently received increasing attention due to their importance for various catalytic applications. In addition to pure TiO_2 and CeO_2, modified TiO_2-based and CeO_2-based mixed oxides have attracted much interest for catalytic applications because of their improved properties. These improvements are attributed to modification of the structure, electronic property, or thermal stability by doping. Several studies of TiO_2-CeO_2 mixed oxides have shown the improvements regarding redox properties,[41, 42] textural and structural properties.[43]

We have found that Ce ion-exchanged Y zeolite shows unique property for adsorption of organic sulfur compounds,[19] and that TiO_2-supported metal catalyst can be more sulfur resistant.[44] There are on-going studies in our laboratory on selective adsorption for removing sulfur from liquid fuels as a new approach to deep desulfurization at ambient temperature under atmospheric pressure without using hydrogen.[6, 10, 12] Further study in our laboratory revealed that CeO_2 mixed with TiO_2 oxide show superior performance than either oxide along for adsorptive desulfurization of liquid fuels such as jet fuels, and TiO_2-CeO_2 mixed oxides synthesized by the urea

precipitation method are potential new adsorbent materials.[16] On the other hand, there are very few studies on either the structure or surface properties of TiO_2-CeO_2 mixed oxides. Detailed studies involving both structure and surface chemistry of TiO_2-CeO_2 mixed oxides were not found, and little has been published on TiO_2-CeO_2 mixed oxides synthesized by the urea precipitation method.

The present work focuses on characterization of TiO_2-CeO_2 ($Ti_XCe_{1-X}O_2$) mixed oxides, with emphasis on the effect of mixing TiO_2 and CeO_2 on structure and surface properties of TiO_2-CeO_2 mixed oxides. Nitrogen adsorption-desorption and X-ray diffraction (XRD) were conducted to characterize the textural and structural properties of the oxides. The surface properties of TiO_2-CeO_2 oxides were investigated by X-ray photoelectron spectroscopy (XPS), temperature-programmed desorption of ammonia (NH_3-TPD) and temperature-programmed reduction in hydrogen (H_2-TPR). The results show a significant effect of mixing TiO_2 and CeO_2 on distortion of structure, crystalline size, and surface properties, including oxygen deficiency, reducibility and acidity, of TiO_2-CeO_2 mixed oxides.

2.2 Experimental

2.2.1 Synthesis of Oxides

Cerium (IV) oxide, titanium (IV) oxide and their mixed oxide were synthesized through a urea precipitation/gelation method from aqueous solutions of inorganic salts.[45] Prior to urea precipitation, aqueous solutions containing metal ions were prepared. The total of cerium ammonium nitrate $(NH_4)_2Ce(NO_3)_6$ (Aldrich, 99.99 %) and titanium oxysulfate $TiOSO_4xH_2SO_4xH_2O$ (Aldrich, Ti: 18.5 wt%) was 0.075 mol. Adequate amounts of cerium ammonium nitrate and titanium oxysulfate were dissolved in 200 mL of distilled water, respectively. Ammonium cerium nitrate aqueous solution was added to the titanium solution. The mixed aqueous solution was then added to 800mL of aqueous solution containing 70 g of urea, $CO(NH_2)_2$, (Aldrich 99+ %), and stirred vigorously by a magnetic stirrer. The solution was maintained 1000 mL at 90 - 95 ^oC for 8 h. The resulting precipitant was filtered and dried overnight in an oven at 110 ^oC. The dried precipitant was crushed into powder. The powder sample was heated at a rate of 1.5 ^oC/min from room temperature to 450 ^oC in static air, subsequently temperature was kept at 450 ^oC for 6 h in a muffle furnace.

2.2.2 Characterization of Oxides

The Brunauer, Emmett, and Teller (BET) surface area and pore size distribution of metal oxides were obtained from 49-point nitrogen adsorption/desorption analysis with

a Quantachrome Autosorb 1. All samples were outgassed at 220 ^{o}C prior to the adsorption-desorption measurements. Micropore surface area and volume was calculated using t-method. The pore size distribution was calculated by applying the Barrett-Joyner-Halenda (BJH) method on the desorption branch of isotherm curve. Analysis parameters were set as follows: five points multiple BET points with relative pressure (P/P_o) from 0.05 to 0.35.

X-ray powder diffraction (XRD) patterns for the samples were collected at scan rate of 1 ^{o}/min in the 2θ range of 20-65 ^{o} using a Scintag-I XRD instrument equipped with Cu Kα radiation. The working voltage of the instrument was 35 kV and the current was 35 mA. Separately, silicon internal standard was analyzed for 2θ corrections. The mean crystallite size of samples was calculated from peak broadening using the Scherrer equation by the function of Jade 6.5, where the Scherrer constant (particle shape factor) was taken as 0.85.

X-ray photoelectron spectroscopy (XPS) spectra were recorded on a Kratos Analytical Axis Ultra spectrometer with monochromatic aluminum (1486.6 eV). The X-ray source operated at 14 kV and 20 mA. The sample powders were pressed into 5 mm x 5 mm 3M double-sided tape using a mortar and pestle and visualized by a stereo microscope to ensure complete coverage and powder uniformity over the tape. Prior to the analysis, adsorbent samples were dried overnight under atmospheric conditions in an oven at 120 ^{o}C. After drying, all samples were immediately stored in a container, and mounted for analysis. Sample height positions were set from O 1s signal at 529 eV following changing of lateral coordinates such that the measured signal from the sample powders were maximized, thus minimizing any possible signal from the 3M double sided

tape. The 3M tape was examined independently and the characteristic shape of the C 1s line was not found when compared to the C 1s line collected from these sample powders. As a reference, we used the C 1s signal of the adventitious carbon (carbon of any surface adsorbed), which we fixed at 285 eV. A survey scan with analyzer pass energy of 80 eV was initially recorded for the sample to identify elements present. The composition and chemical states were determined from the charge corrected high resolution scans with analyzer pass energy of 20 eV. An estimation of the amount of Ce(III) [46, 47] can be obtained from the intensity of the v_0 (u_0) and v' (u') lines, according to the formula:

$$Ce^{III}(\%) = \frac{v_0 + v' + u_0 + u'}{\Sigma(v+u)}$$

Temperature-programmed reduction (TPR) analysis was carried out on a Micrometritics 2910 Autochem (USA) analyzer. In a typical TPR experiment, about 0.2 g of the powder sample was loaded in a U-shaped quartz adsorption cell above a small amount of quartz wool. The TPR profile of sample was recorded by following temperature program between 30 - 750 ^{o}C with heating rate of 10 ^{o}C/min in 4.93 % hydrogen in argon with a flow rate of 50 ml/min. Hydrogen uptake is monitored by TCD detector.

Temperature-programmed desorption (TPD) of ammonia adsorption was conducted to investigate the acidity of the simple and mixed oxides. NH_3-TPD analysis was carried out in a flow apparatus on a Micrometrics 2910 Autochem (USA). In a typical NH_3-TPD experiment, about 0.2 g of the sample was loaded in U-shaped quartz adsorption cell above a small amount of quartz wool. The sample was outgassed under the argon flow at 300 ^{o}C for 60 min. After outgassing, the temperature was cooled down

to 110 ^{o}C. For NH_3 adsorption, outgassed metal oxide samples were saturated with pulse of 1 % NH_3/He mixture 20 times at 110 ^{o}C. The sample was flushed in ultra high purity grade He flow at 110 ^{o}C after pulse NH_3 adsorption for removal of physically adsorbed NH_3 on the oxides. An NH_3-TPD profile of the sample was recorded by increasing the temperature from 110 ^{o}C to 700 ^{o}C with a heating rate of 10 ^{o}C/min under 50 ml/min of UHP He flow. The desorbed ammonia was detected by a mass spectrometer (AMETEK Dycor DM200M). The desorbed ammonia, water, nitrogen and oxygen were identified on the basis of the intensity of the fragment with m/e = 16, 18, 28 and 32, respectively. The peak m/e = 16 was used for ammonia because the parent peak, m/e = 17, was influenced by the desorbed water.

2.3 Results and Discussion

2.3.1 Specific Surface Area

The results of the N_2 adsorption-desorption analysis are summarized in Table **2-1** for surface area and in Figure **2-1** for pore size distribution of TiO_2-CeO_2 mixed oxides along with those of TiO_2 and CeO_2 single oxides. The surface area of CeO_2 and TiO_2 was 101.9 and 223.6 m^2/g, respectively. These oxides exhibit a relatively high surface area. In particular, the surface area of prepared CeO_2 and TiO_2 was significantly high in comparison with that of commercial CeO_2 and TiO_2. The surface area of TiO_2 was twice as high as that of CeO_2. Mixing TiO_2 and CeO_2 in the synthesis stage can lead to a synergetic increase of surface area. In particular, $Ti_{0.7}Ce_{0.3}O_2$ and $Ti_{0.9}Ce_{0.1}O_2$ exhibited the highest surface area in the series of TiO_2-CeO_2 oxides. The enlargement of surface area can be attributed to the effect of mixing TiO_2 and CeO_2 precursors. As reported in the literature, urea co-precipitation method also permits the synthesis of ZrO_2-TiO_2 mixed oxides with high surface area.[48, 49] The resulting high surface area of the mixed oxides was attributed to the inhibition of the individual crystallization during precipitation.[48] Similarly, mixing TiO_2 and CeO_2 precursors in urea co-precipitation process could lead to smaller crystals due to the inhibition of their individual crystallization thus leading to higher surface area. This is confirmed by XRD analysis, as described below. The pore size distribution shows that these samples possess a unimodal mesoporous pore structure with narrow size range. The pore size distribution of TiO_2-CeO_2 mixed oxides intend to

be positioned between those of TiO_2 and CeO_2 single oxides, as can be seen in Figure **2-1**. Mixing TiO_2 and CeO_2 can cause an increment of surface area and change average pore size which may be larger than those of TiO_2 and CeO_2.

2.3.2 XRD

X-ray powder diffraction analysis was conducted to characterize the crystallographic structure and crystallite size of TiO_2-CeO_2 oxide samples. Figure **2-2** shows the XRD spectra of the mixed oxides along with the synthesized TiO_2 and CeO_2 as well as the commercial TiO_2 and CeO_2 samples. Structures of CeO_2 and $Ti_{0.1}Ce_{0.9}O_2$ and $Ti_{0.3}Ce_{0.7}O_2$ oxides were identified as cubic fluorite structure. Anatase structure was shown by the XRD patterns of TiO_2 and $Ti_{0.9}Ce_{0.1}O_2$ (Figure **2-2**). The intensities for these peaks corresponding to fluorite and anatase structure are significantly broader than those of commercial CeO_2 (Aldrich) and TiO_2 (Degussa). The peak intensities of Ti-containing CeO_2 and Ce-containing TiO_2 were lower than those of CeO_2 and TiO_2. In the case of $Ti_{0.5}Ce_{0.5}O_2$ and $Ti_{0.7}Ce_{0.3}O_2$, their XRD patterns exhibited very broad diffraction peaks centered at around $2\theta = 28^o$. The intensity difference and peak broadening were attributed to a reduction of crystalline size.

Table **2-2** shows mean crystalline sizes of CeO_2 and TiO_2 oxides calculated using Scherrer's equation. The mean crystalline sizes of CeO_2 and TiO_2 prepared by urea precipitation were significantly smaller than those of commercial ones. Furthermore, mixed TiO_2-CeO_2 oxides showed smaller mean crystalline sizes than those of laboratory-prepared CeO_2 and TiO_2 single oxides. Inducing a small amount of TiO_2 into CeO_2

significantly decreased the crystalline size from 84 to 48 Å for $Ti_{0.1}Ce_{0.9}O_2$ and to 54 Å for $Ti_{0.3}Ce_{0.7}O_2$. Similarly, introducing CeO_2 to TiO_2 decreased the crystalline size from 81 to 40 Å for $Ti_{0.9}Ce_{0.1}O_2$. When the value of X in the mixed oxides $Ti_XCe_{1-X}O_2$ is in the range of 0.5 to 0.7, the crystalline sizes are so small that they can not be detected clearly by XRD so the calculation of crystalline sizes was difficult. Consequently, it is clear that mixing TiO_2 and CeO_2 oxides in the $Ti_XCe_{1-X}O_2$ synthesis causes a reduction of crystalline sizes.

Changes of lattice parameters in the series of TiO_2-CeO_2 oxides were observed along with the mixing TiO_2 and CeO_2. In the fluorite structure, addition of Ti into CeO_2 increased the lattice parameter of the a-axis from 5.217 to 6.168 Å. The ionic radius of Ti^{4+} is 0.61 Å, which is smaller than that of Ce^{4+} (0.97 Å). Thus, it is clear that this expansion of the lattice parameter did not occur due to a direct substitution of Ce^{4+} by Ti^{4+}. On the other hand, the ionic radius of Ce^{3+} (1.14 Å) is larger than that of Ce^{4+}. Thus, the addition of Ti into CeO_2 contributed to increase in the lattice parameter, which may be cause by reducing of Ce cation from tetravalent to trivalent. The reduction of Ce cation is attributed to decrease in the O 2p-Ce 4f hybridization. This result concurs with the result of a calculation by Skorodumova et al.[50] In contrast to the Ti addition, Zr and Ca addition into CeO_2 resulted in a decrease of the lattice parameter.[51, 52] Thus, the addition of Ti into CeO_2 is comparatively unique.

Anatase structure was identified by XRD for TiO_2 and $Ti_{0.9}Ce_{0.1}O_2$ (Figure **2-2**). Upon Ce addition into TiO_2, an increase of the lattice parameter in the a-axis was observed with a decrease of that in c-axis Table **2-2**). Lattice parameter reduction of the c-axis in anatase structure was arisen from the shortening of metal-oxygen bonding.[53]

This bond shortening resulted from localization that the electron density of Ti cations move to empty lattice sites, which involves formation of oxygen vacancy and reduction of Ti cation.[54] Consequently, the expansion of the lattice parameter in the a-axis was attributed to not only to the substitution of titanium Ti^{4+} (0.61 Å) by Ce^{4+} (0.97 Å)[55] but also the reduction of Ti. In conclusion, the significant effects of mixing TiO_2 and CeO_2 reflected in reduction of crystalline size and the distortion of structure by changing lattice parameter.

2.3.3 XPS

XPS analysis was conducted to understand the surface chemical state of $Ti_XCe_{1-X}O_2$ oxides. Ce 3d spectra of CeO_2 and TiO_2-CeO_2 mixed oxides are shown in Figure **2-3**. The labels of peaks used in Ce 3d identification were established by Burroughs et al.[56] V and U are used for convenience and indicate the spin-orbit coupling $3d_{5/2}$ and $3d_{3/2}$, respectively. The peaks referred to as v, v" and v"' are contributed by CeO_2, and assigned to a mixture of Ce IV ($3d^94f^2$) O ($2p^4$), Ce IV ($3d^94f^1$) O ($2p^5$) and Ce IV ($3d^94f^0$) O ($2p^6$), respectively. The same peak assignment is applied to u structures. The peaks v_o and v' are assigned to a mixture of Ce III ($3d^94f^2$) O ($2p^5$) and Ce III ($3d^94f^1$) O ($2p^6$), respectively. Ce 3d spectrum of CeO_2 (Figure **2-3**-a) shows six peaks at 916.2, 907.2, 900.8, 898.0, 888.9 and 882.1 eV. These peaks represent the presence of Ce^{4+}. The intensity of these six peaks gradually decreased with the increase of Ti concentration. On the contrary, the intensity at 903.9 and 885.4 eV increased with the increase of Ti content. This change in the Ce 3d spectra corresponds to the increase of Ce^{3+}

concentration in TiO_2-CeO_2 oxides with increasing Ti concentration. The curve fitting procedure of Ce 3d spectra indicated that the surface concentration of Ce^{3+} of the TiO_2-CeO_2 oxides varied with the amount of Ti addition from 15.1 % in CeO_2 to 40.7 % in $Ti_{0.9}Ce_{0.1}O_2$. The Ce^{3+} concentration has a linear relationship with the Ti concentration, and is shown in Figure **2-4**. Thus, the introducing TiO_2 into CeO_2 causes the partial reduction of Ce tetravalent cation.

As seen in the change in CeO_2 structure with Ti concentration, the chemical state of Ti changed with Ce concentration. Figure **2-5** shows the Ti $2p_{1/2}$ and Ti $2p_{3/2}$ spectra of TiO_2-CeO_2 mixed oxides. Ti $2p_{3/2}$ peak shifted from 459.4 eV in TiO_2 to 457.9 eV in $Ti_{0.1}Ce_{0.9}O_2$. This shifting represents an intermediate oxidation state of Ti from tetra to trivalent. In Figure **2-6**, the binding energy of Ti $2p^{3/2}$ and the oxidation state of Ti were correlated using literature data,[57-59] and the correlation shows a linear relationship between the binding energy of Ti $2p_{3/2}$ and the oxidation state of Ti. Based on this relationship, oxidation state of Ti in the series of TiO_2-CeO_2 oxides was estimated as lower than 4+, and Ti was found to be significantly reduced with higher Ce content (Figure **2-7**). The reduction of Ti and Ce in the series of TiO_2-CeO_2 oxides was observed by Ce and Ti, respectively. This reduction behavior is similar to what was considered in XRD study. Thus the Ti and Ce metal cations influence each other to change their oxidation states both in surface and bulk.

Figure **2-8** shows O 1s spectra of TiO_2-CeO_2 mixed oxides. Binding energy of O 1s for surface oxygen of these oxides decreased from 530.4 to 529.0 eV with the increasing Ce concentration. The binding energy of the surface oxygen was influenced by the concentration of Ti and Ce in the TiO_2-CeO_2 mixed oxides. Moreover, O 1s peaks

corresponding to TiO_2 and CeO_2 did not individually appear in the spectra of TiO_2-CeO_2 mixed oxides. This observation in O 1s suggests that Ti and Ce are chemically mixed in the TiO_2-CeO_2 mixed oxides.

Figure **2-9** shows a measured and calculated surface oxygen concentration of TiO_2-CeO_2 oxides. The measured surface oxygen concentration was obtained by a curve-fitting of O 1s. The calculated surface oxygen concentration was indicated by the oxidation state of surface Ce and Ti. Both surface oxygen concentrations were described by stoichiometric value. As seen in Figure **2-9**, the measured surface oxygen concentration of TiO_2-CeO_2 oxides is lower than the calculated value. This comparison suggests that mixing TiO_2 and CeO_2 significantly enhanced the formation of oxygen defects on the surface, especially for $Ti_{0.7}Ce_{0.3}O_2$ and $Ti_{0.9}Ce_{0.1}O_2$. These oxides were calcined and thermally treated overnight in an oven before XPS analysis. Thus, their reduced centers are considerably stable. This stability is attributed to the localization of 4f orbital for Ce and 3d orbital for Ti, and those localized orbitals partially increase electron density towards empty oxygen sites.[60-63] Thus, high oxygen deficiency and significant reduction of Ce and Ti were observed by XPS analysis. This high oxygen deficiency arose from the significant effect of mixing CeO_2 and TiO_2.

2.3.4 H_2-TPR

Figure **2-10** shows the H_2-TPR profiles of the series of TiO_2-CeO_2 oxides. A peak appeared at 410 ^oC with shoulder on the higher temperature side in TPR profile of CeO_2. This peak and shoulder correspond to the reduction of surface oxygen and bulk oxygen,

respectively.[64] Increasing the Ti content in TiO_2-CeO_2 oxides revealed the increase of reduction temperature to 580 ^oC for $Ti_{0.1}Ce_{0.9}O_2$, 600 ^oC for $Ti_{0.3}Ce_{0.7}O_2$ and 670 ^oC for $Ti_{0.5}Ce_{0.5}O_2$. The peak intensity of mixed oxides also increased with increase of Ti content. The shoulder on the lower temperature side of the reduction peak was observed for these oxides, and corresponds to reduction of surface oxygen. Thus, this intense peak for $Ti_{0.1}Ce_{0.9}O_2$, $Ti_{0.3}Ce_{0.7}O_2$ and $Ti_{0.5}Ce_{0.5}O_2$ corresponds to the significant reduction of bulk oxygen. Tthe XRD patterns of $Ti_{0.1}Ce_{0.9}O_2$, $Ti_{0.3}Ce_{0.7}O_2$ and $Ti_{0.5}Ce_{0.5}O_2$ showed an increase of lattice parameter with Ti addition in fluorite structure. This increase of lattice parameter contributed to the structure distortion, and as a consequence a larger amount of oxygen was more easily released from bulk.

Reduction of TiO_2 was not observed from 50 to 750 ^oC. However, reduction peak appeared at 545 ^oC for $Ti_{0.9}Ce_{0.1}O_2$. Higher reduction peak with shoulder appeared at 645 ^oC and 513 ^oC by further Ce addition, which was for $Ti_{0.7}Ce_{0.3}O_2$.The distortion of the structure, as revealed by XRD study, could contribute to this change of reduction patterns. Reduction of $Ti_{0.7}Ce_{0.3}O_2$ and $Ti_{0.9}Ce_{0.1}O_2$ was not as significant as that of other mixed oxides. The reason is possibly due to the higher oxygen deficiency as described in the XPS study. Consequently, mixing TiO_2 and CeO_2 modified the reduction property of CeO_2 and TiO_2 significantly.

H_2 consumption during TPR was calculated, and it was plotted in Figure **2-11** with measured surface oxygen concentration of TiO_2-CeO_2 oxides, obtained in the XPS study. H_2 consumption for reduction of $Ti_{0.1}Ce_{0.9}O_2$ was remarkably large. This large H_2 consumption is attributed to large surface oxygen concentration as measured in the XPS study. Although measured surface oxygen concentrations of CeO_2 and TiO_2 were high,

H_2 consumption of those oxides was not comparable. This difference in reduction behavior suggests that mixing CeO_2 and TiO_2 significantly enhances the reduction properties of the oxides. However, although the measured surface oxygen concentration of mixed oxides was moderately low for the TiO_2-CeO_2 mixed oxides, large H_2 consumption indicated the significant reduction of the TiO_2-CeO_2 mixed oxides. This fact suggests that reduction with the bulk oxygen was enhanced by mixing TiO_2 and CeO_2. This property also corresponds to oxygen storage capacity. As discussed in the XRD study, distortion of the structure induced by mixing TiO_2 and CeO_2 promoted the reducibility, including oxygen storage capacity.

2.3.5 NH_3-TPD

Temperature-programmed desorption of adsorbed ammonia has been employed to investigate the acidic and catalytic properties with simultaneous mass spectrometric analysis of desorbed molecules. NH_3-TPD for the series of $Ti_XCe_{1-X}O_2$ oxides was conducted by NH_3 adsorption at 110 ^oC, and desorption from 110 to 700 ^oC at a heating rate of 10 ^oC/min under UHP He flow. The detected response of desorbed NH_3 was normalized by the surface area of the $Ti_XCe_{1-X}O_2$ oxides. The acquired NH_3-TPD profiles of $Ti_XCe_{1-X}O_2$ oxides are shown in Figure **2-12**. NH_3 desorption was observed at 170 – 680 ^oC. The maximum NH_3 desorption temperature for $Ti_XCe_{1-X}O_2$ oxides shifts from 235 ^oC to 260, 260, 260, 265 and 270 ^oC with increasing Ti content, and these peaks correspond to weak acid. This desorption temperature of NH_3 suggests that the surface of

these oxides is dominantly weakly acidic. In addition, some strong acidity was identified for the mixed oxides by deconvolution of the peaks.

Figure **2-13** shows the area obtained by curve fitting in weaker acid region for TiO_2-CeO_2 mixed oxides. The corresponding area was increasing with increase of Ti content. A linear correlation for weak acidity and Ti/Ce ratio was found. NH_3 desorption peaks for the $Ti_XCe_{1-X}O_2$ oxides showed shoulder on the side of higher temperature. The desorption at higher temperature corresponds to stronger acid, and which increased with the increase of Ti concentration. This may be attributed to the NH_3 adsorption on Lewis acid as indicated by Tsyganenko et al.[65] Consequently, acid sites density, especially weak acid, increased with the Ti concentration.

In addition to the NH_3 desorption, products, such as H_2O, N_2 and O_2, were detected during the elevation of temperature. NH_3, H_2O, N_2 and O_2 TPD profiles of NH_3 adsorbed and non-adsorbed on $Ti_{0.9}Ce_{0.1}O_2$, $Ti_{0.5}Ce_{0.5}O_2$ and $Ti_{0.1}Ce_{0.9}O_2$ are plotted and shown in Figure **2-14 -** Figure **2-16**.

Desorption profiles of NH_3, H_2O (m/e=18), N_2 (m/e=28) and O_2 (m/e=32) for NH_3-adsorbed and non-adsorbed $Ti_{0.9}Ce_{0.1}O_2$ are shown in Figure **2-14**. Desorption of H_2O and N_2 appeared at 150 ^oC along with NH_3 for NH_3-adsorbed $Ti_{0.9}Ce_{0.1}O_2$. Although NH_3 desorption did not appear at temperatures higher than 500 ^oC, desorption of H_2O and N_2 continued to 590 and 700 ^oC, respectively. These desorption profiles suggest that strongly adsorbed NH_3 are oxidized effectively at higher than 500 ^oC. In comparison with the desorption profiles of non-NH_3 adsorbed $Ti_{0.9}Ce_{0.1}O_2$, the intensities for desorption of H_2O and N_2 showed higher for NH_3 adsorbed one. This intensity difference suggests clearly that H_2O and N_2 were produced by oxidation of NH_3. When NH_3 desorption

began, O_2 uptake was also observed. Thus, a trace amount of O_2 (< 0.1 %) in He flow was consumed to oxidize NH_3 and produce H_2O and N_2.

Desorption profiles of NH_3, H_2O, N_2 and O_2 for NH_3-adsorbed and non-adsorbed $Ti_{0.5}Ce_{0.5}O_2$ and $Ti_{0.1}Ce_{0.9}O_2$ are shown in Figure **2-15** and Figure **2-16**, respectively. Desorption of H_2O and N_2 appeared at 150 ^oC along with that of NH_3 for NH_3-adsorbed $Ti_{0.5}Ce_{0.5}O_2$ and $Ti_{0.1}Ce_{0.9}O_2$ similar to the desorption profiles for $Ti_{0.9}Ce_{0.1}O_2$ in Figure **2-14**. The maximum temperature of H_2O desorption shifted from 430 to 385 ^oC with decreasing Ti content. H_2O desorption was observed along with N_2 desorption and O_2 uptake. Those desorption in products are attributed to a recombinative desorption of NH_3 with uptake of trace O_2 presented in the He flow.

The H_2O desorption peak was observed in the TPD profiles of both non-NH_3 adsorbed NH_3-adsorbed mixed oxides. The intensity of H_2O desorption for non-NH_3 adsorbed mixed oxides is lower than that of NH_3-adsorbed. Since H_2O desorption was not observed for the non-NH_3 adsorbed sample at lower than 300 ^oC, oxidation of NH_3 is considered to take place along with NH_3 desorption. The difference of intensity for H_2O desorption peaks suggests that oxidation of NH_3 also occurred above 300 ^oC. Interestingly, the significant O_2 uptake was only observed in the TPD profiles of NH_3 adsorbed oxides. Thus, these TiO_2-CeO_2 mixed oxides could function as an oxidation catalyst with utilizing their oxygen storage capacity.

The difference in the intensities of H_2O desorption between NH_3-adsorbed and non-adsorbed were observed for TiO_2-CeO_2 mixed oxides in Figure **2-14** - Figure **2-16**. The difference was plotted in Figure **2-17**. Oxidation of NH_3 over $Ti_{0.9}Ce_{0.1}O_2$ along with

NH_3 desorption was the most significant. Moler ratio Ti/Ce showed influence on the oxidation property.

2.5 Conclusions

The following conclusions may be drawn from the investigation of structural and surface analysis of a series of $Ti_XCe_{1-X}O_2$ oxides synthesized by urea precipitation/gelation:

1. Change in XRD patterns and binding energy in XPS spectra revealed the important structural changes that take place upon mixing TiO_2 and CeO_2.

2. Structural distortion of anatase TiO_2 was caused by introducing CeO_2, and that of fluorite CeO_2, by introducing TiO_2, as reflected by a change of lattice parameters. A dominant anatase phase was detected by XRD when X was 0.9 or higher while a cubic fluorite phase was dominant in XRD when X was 0.3 or lower.

3. Mixing TiO_2 and CeO_2 precursors contributed to decreasing the crystalline size of the $Ti_XCe_{1-X}O_2$ oxides. The mixed oxides were nano-crystalline, about 4.0 nm in size when X = 0.9 and 4.8 – 5.4 nm when X = 0.1 - 0.3, which are significantly smaller than the TiO_2 and CeO_2 single oxides (8.1 to 8.4 nm).

4. Creation of surface oxygen defect sites was enhanced by mixing TiO_2 and CeO_2. Mixing TiO_2 and CeO_2 promoted reducibility and oxygen storage capacity, as revealed by XPS, H_2-TPR and NH_3-TPD.

5. Acid sites were identified for $Ti_XCe_{1-X}O_2$ oxides by NH_3-TPD. Those acid sites increased with increasing concentrations of Ti.

6. Recombinative desorption of NH_3 with H_2O and N_2 was observed in TPD profiles of $Ti_XCe_{1-X)}O$ oxides. This recombinative desorption took place with a trace amount of

oxygen in the carrier gas. Oxidation of ammonia occurred during ammonia desorption over the TiO_2-CeO_2 mixed oxides. TiO_2-CeO_2 mixed oxides showed excellent oxygen storage capacity, and could act as an oxidation catalyst.

Table **2-1**: Physical Properties of TiO_2-CeO_2 Oxides

	Surface area (m^2/g)	Pore Volume (cm^3/g)	Average pore size (Å)
CeO_2	101.9	0.169	56
$Ti_{0.1}Ce_{0.9}O_2$	138.7	0.216	53
$Ti_{0.3}Ce_{0.7}O_2$	119.2	0.365	73
$Ti_{0.5}Ce_{0.5}O_2$	183.4	0.278	46
$Ti_{0.7}Ce_{0.3}O_2$	241.0	0.253	38
$Ti_{0.9}Ce_{0.1}O_2$	249.3	0.460	37
TiO_2	223.6	0.246	37
Commercial oxides			
CeO_2	2.1	0.022	38
TiO_2	12.8	0.132	19

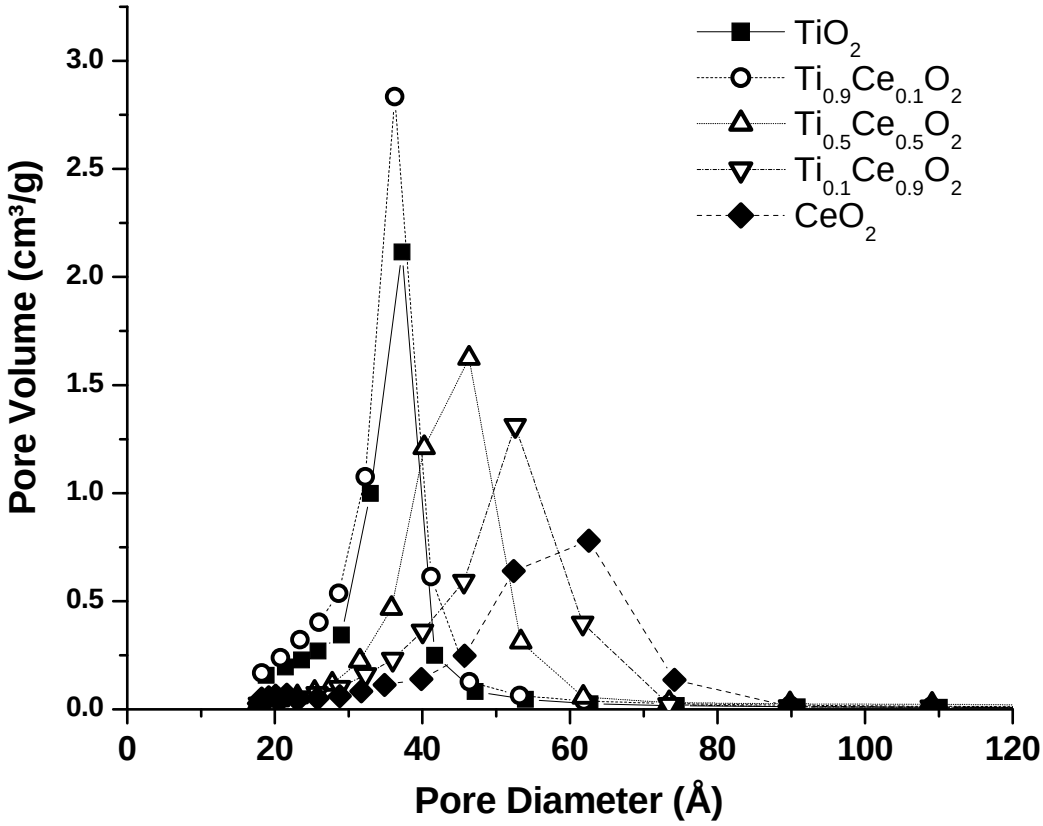

Figure **2-1**: Pore size distributions of TiO_2, $Ti_{0.9}Ce_{0.1}O_2$, $Ti_{0.5}Ce_{0.5}O_2$, $Ti_{0.1}Ce_{0.9}O_2$ and CeO_2 prepared by urea precipitation

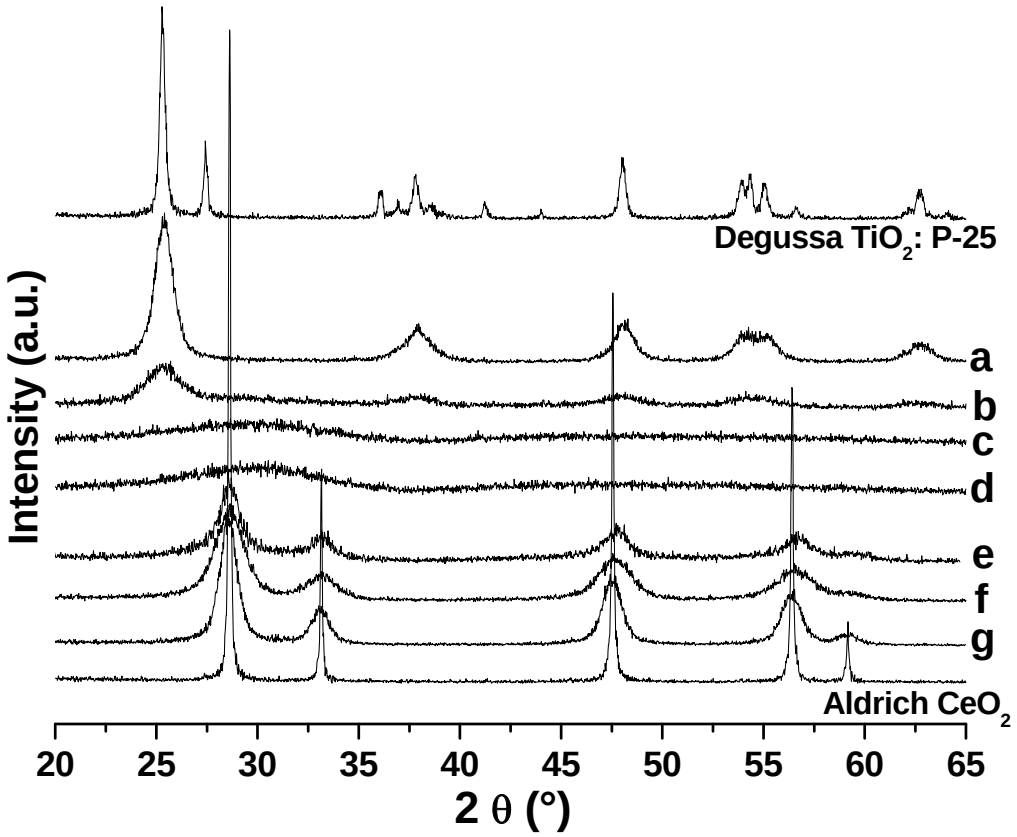

Figure **2-2**: XRD patterns of commercial TiO_2 and CeO_2, and prepared TiO_2-CeO_2 oxides: (a) TiO_2, (b) $Ti_{0.9}Ce_{0.1}O_2$, (c) $Ti_{0.7}Ce_{0.3}O_2$, (d) $Ti_{0.5}Ce_{0.5}O_2$, (e) $Ti_{0.7}Ce_{0.3}O_2$, (f) $Ti_{0.1}Ce_{0.9}O_2$, and (g) CeO_2.

Table **2-2**: Crystallite Structure, d Value, Lattice Parameter and Mean Crystalline Size in TiO_2-CeO_2 Mixed Oxides

	crystallite structure	lattice parameter (Å)		mean crystalline size (Å)
		a	c	
TiO_2	anatase	3.726	10.478	81
$Ti_{0.9}Ce_{0.1}O_2$	anatase	3.808	9.661	40
$Ti_{0.7}Ce_{0.3}O_2$	N/A	–	–	–
$Ti_{0.5}Ce_{0.5}O_2$	N/A	–	–	–
$Ti_{0.3}Ce_{0.7}O_2$	fluorite	6.168	–	54
$Ti_{0.1}Ce_{0.9}O_2$	fluorite	5.477	–	48
CeO_2	fluorite	5.217	–	84
References:				
TiO_2 (P-25): Degussa	anatase + rutile	–	–	311, 519
CeO_2: Aldrich	fluorite	5.402	-	> 1000
TiO_2 [55]	anatase	3.785	9.514	
CeO_2 [55]	fluorite	5.411	–	

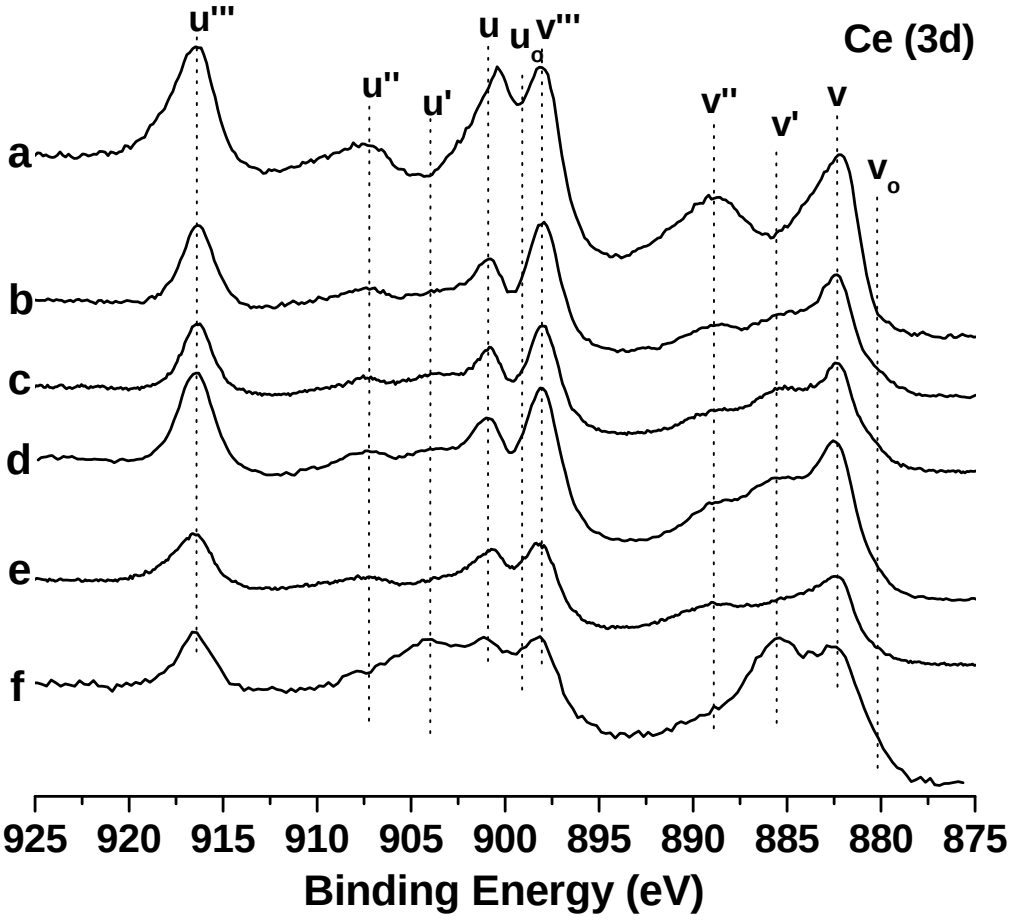

Figure **2-3**: XPS Ce 3d spectra for (a) CeO_2, , (b) $Ti_{0.1}Ce_{0.9}O_2$, (c) $Ti_{0.3}Ce_{0.7}O_2$, (d) $Ti_{0.5}Ce_{0.5}O_2$, (e) $Ti_{0.7}Ce_{0.3}O_2$, (f) $Ti_{0.9}Ce_{0.1}O_2$, after drying at 110 ^oC overnight

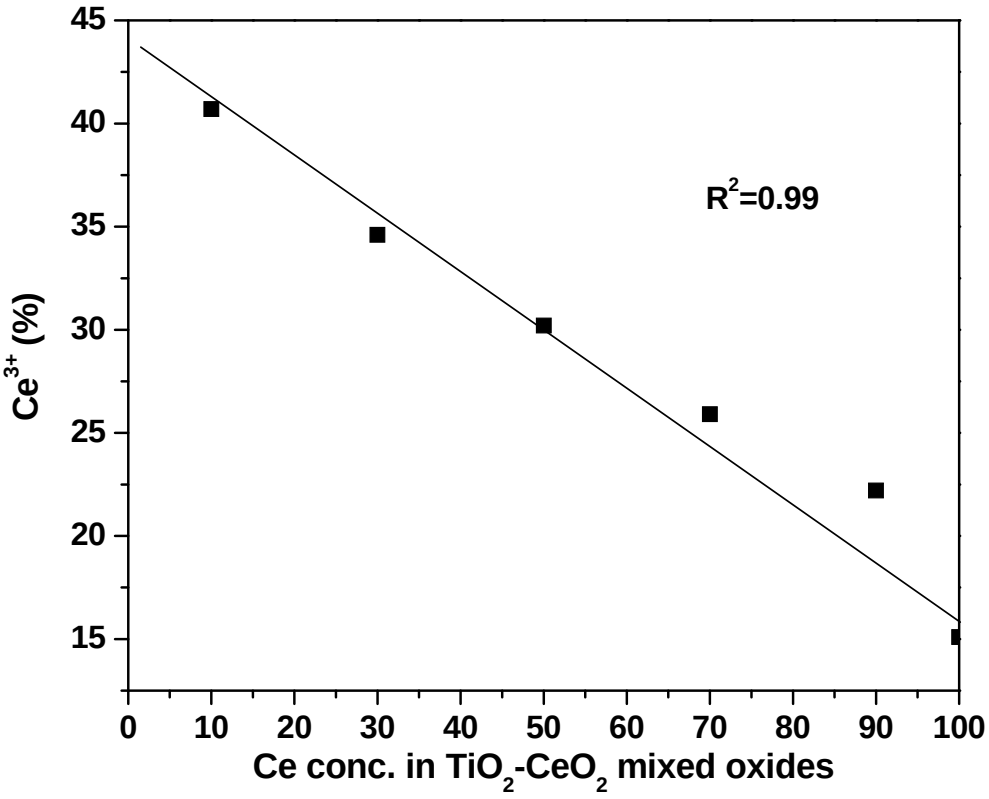

Figure **2-4**: Correlation between the surface Ce^{3+} concentration and the concentration of Ce in TiO_2-CeO_2 oxides.

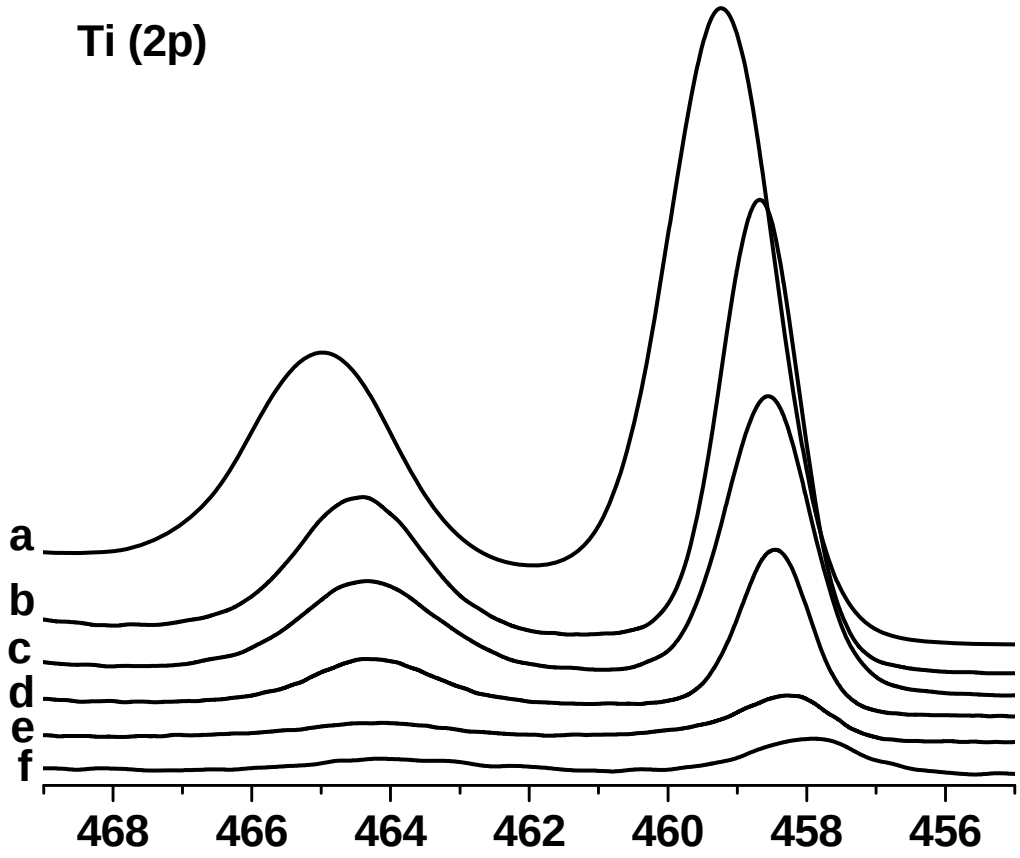

Figure **2-5**: XPS Ti 2p spectra for (a) TiO_2, (b) $Ti_{0.9}Ce_{0.1}O_2$, (c) $Ti_{0.7}Ce_{0.3}O_2$, (d) $Ti_{0.5}Ce_{0.5}O_2$, (e) $Ti_{0.7}Ce_{0.3}O_2$ and (f) $Ti_{0.1}Ce_{0.9}O_2$, and (g) CeO_2, after drying at 110 ^{o}C overnight.

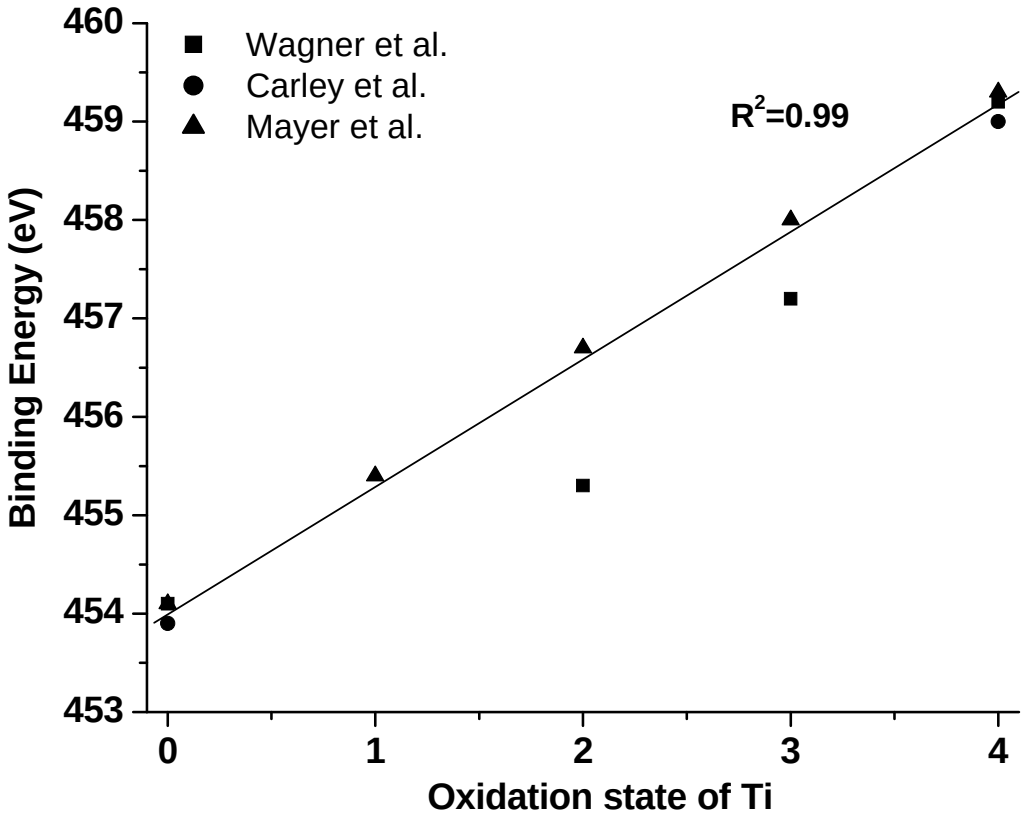

Figure **2-6**: Correlation between binding energy of Ti $2p_{3/2}$ and oxidation state of Ti [57-59]

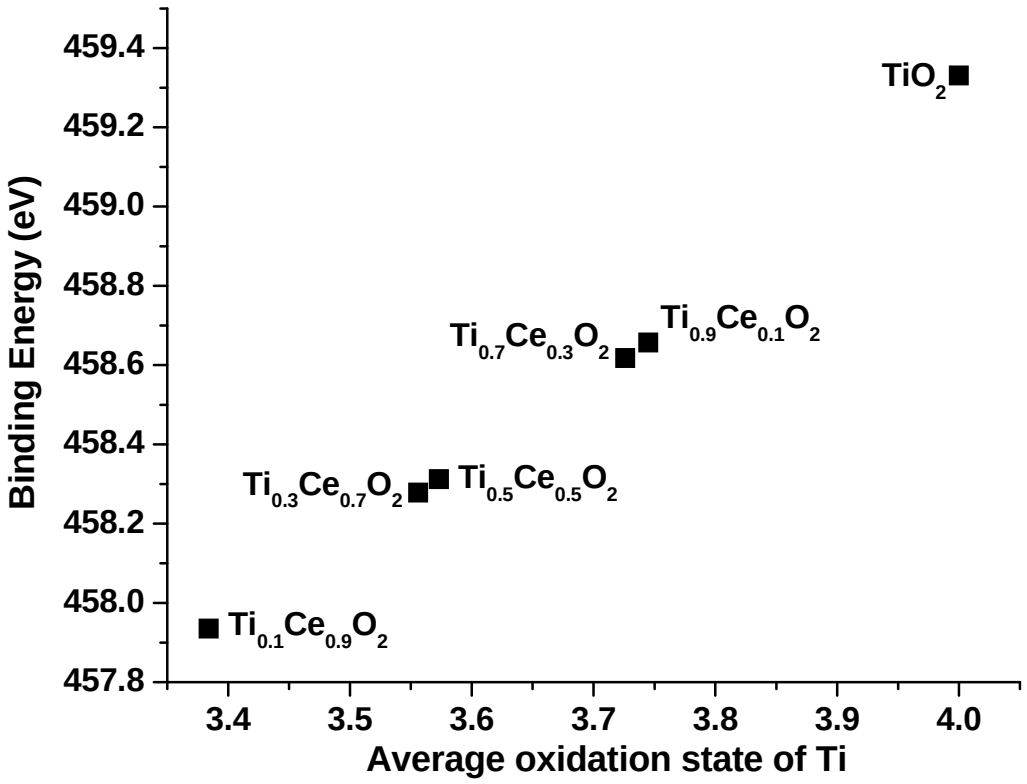

Figure **2-7**: Calculated average oxidation state of Ti in each TiO_2-CeO_2 oxides

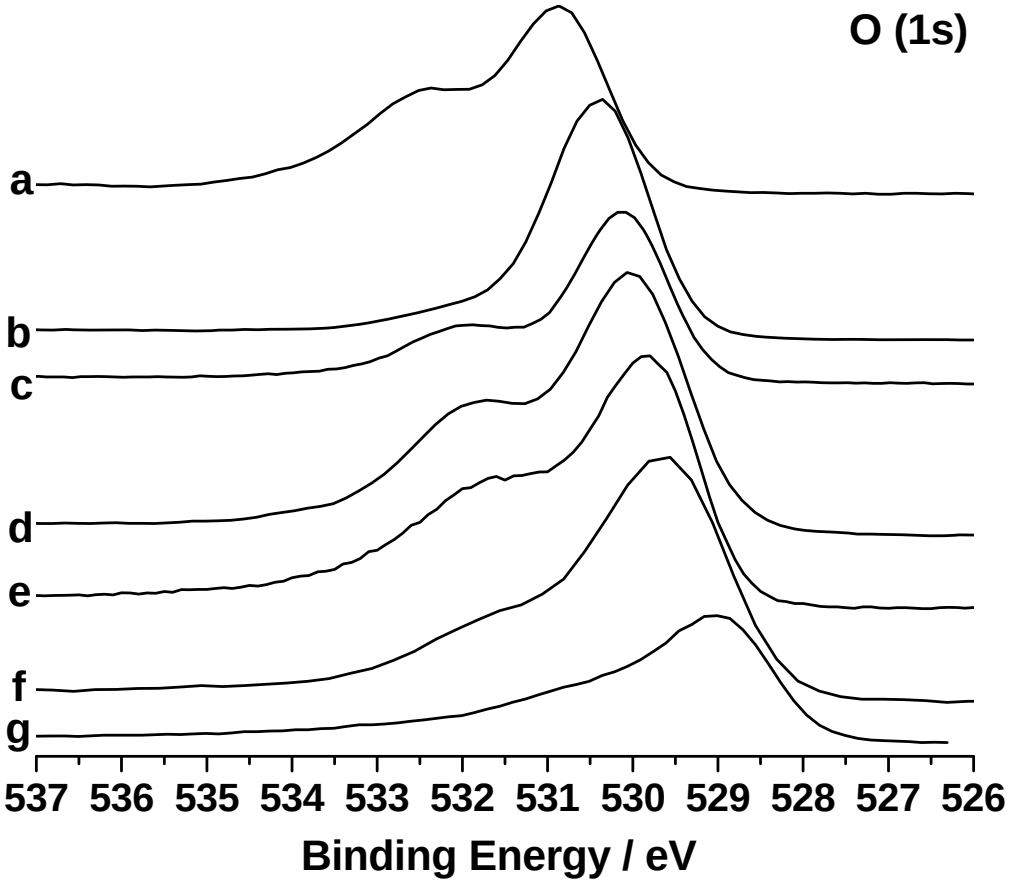

Figure **2-8**: XPS O 1s spectra for (a) TiO_2, (b) $Ti_{0.9}Ce_{0.1}O_2$, (c) $Ti_{0.7}Ce_{0.3}O_2$, (d) $Ti_{0.5}Ce_{0.5}O_2$, (e) $Ti_{0.7}Ce_{0.3}O_2$ and (f) $Ti_{0.1}Ce_{0.9}O_2$, and (g) CeO_2, after drying at 110 ^oC overnight.

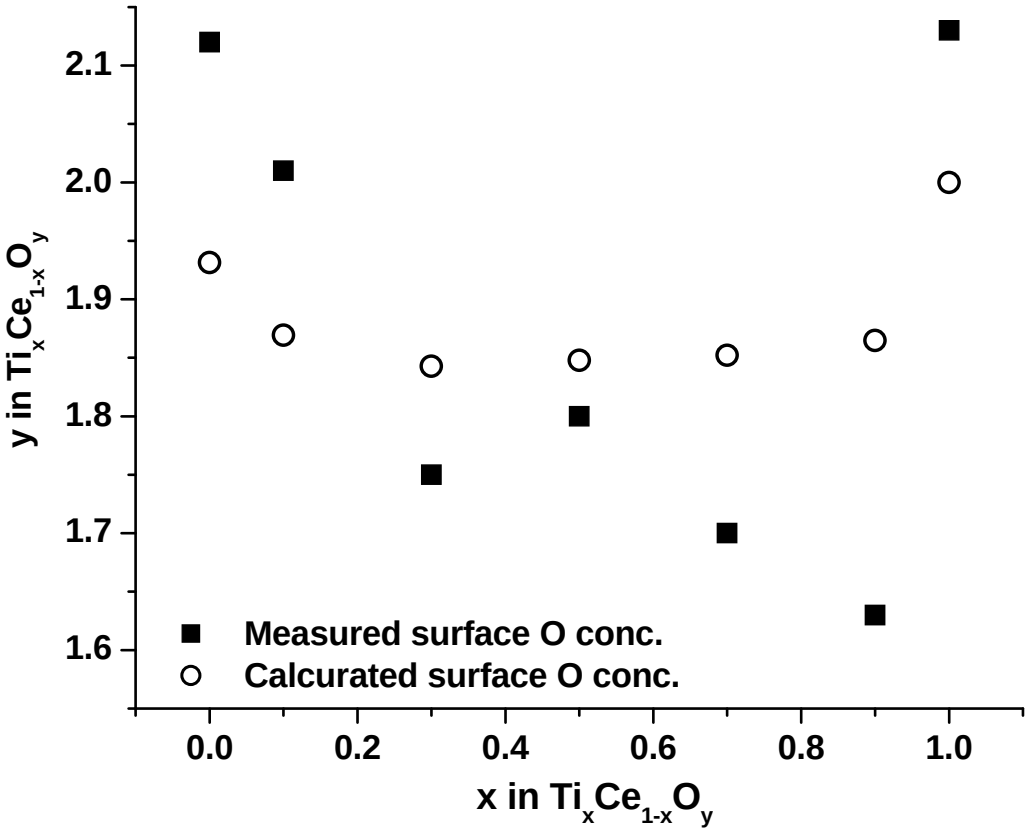

Figure **2-9**: The comparison of composition of TiO_2-CeO_2 with stoichiometry of oxides. The measured surface lattice oxygen concentration was obtained based on XPS results, and calculated lattice oxygen concentration was indicated from concentrations of surface Ce^{4+}, Ce^{3+}, T^{i4+} and Ti^{3+}.

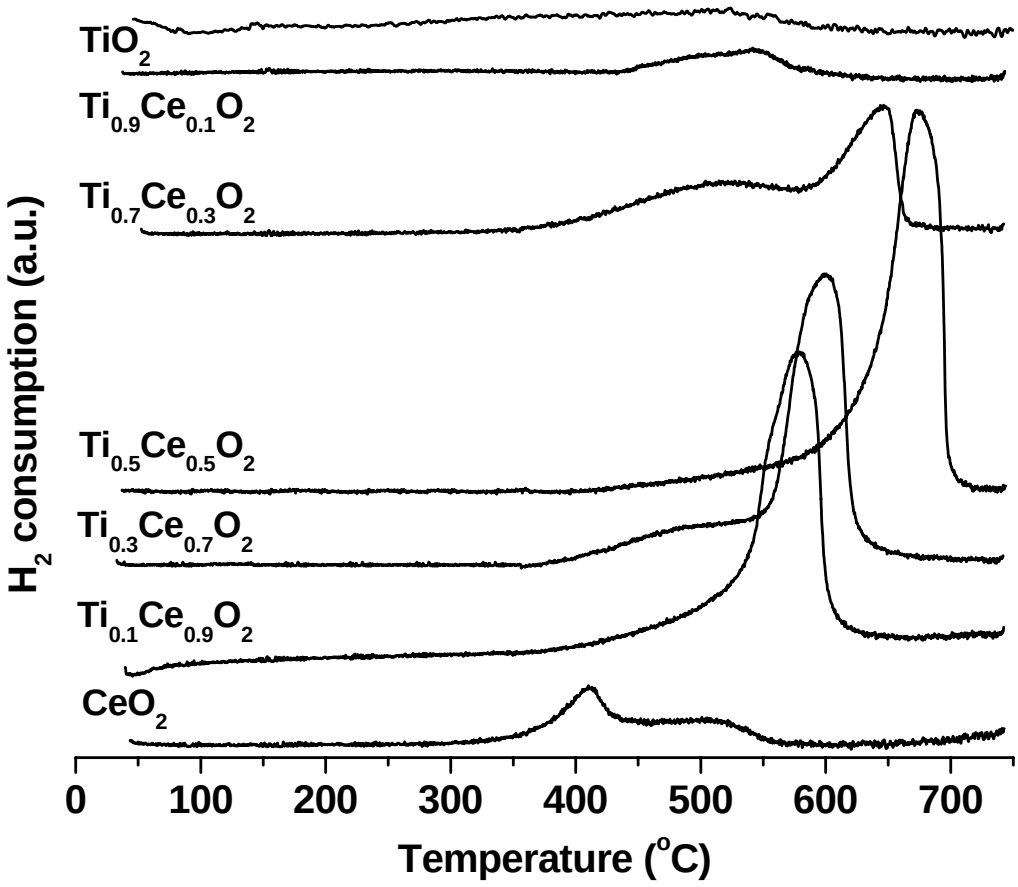

Figure **2-10**: H_2-TPR profiles of TiO_2-CeO_2 oxides

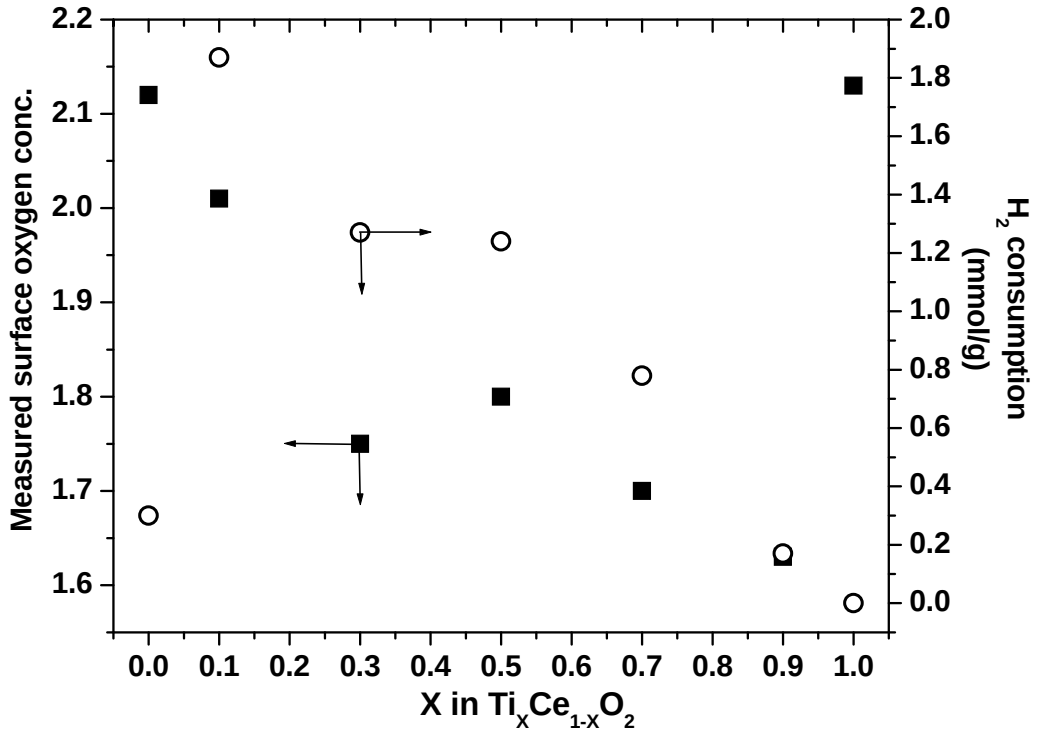

Figure **2-11**: Measured surface oxygen concentration and H_2 consumption in TPR of TiO_2-CeO_2 oxides

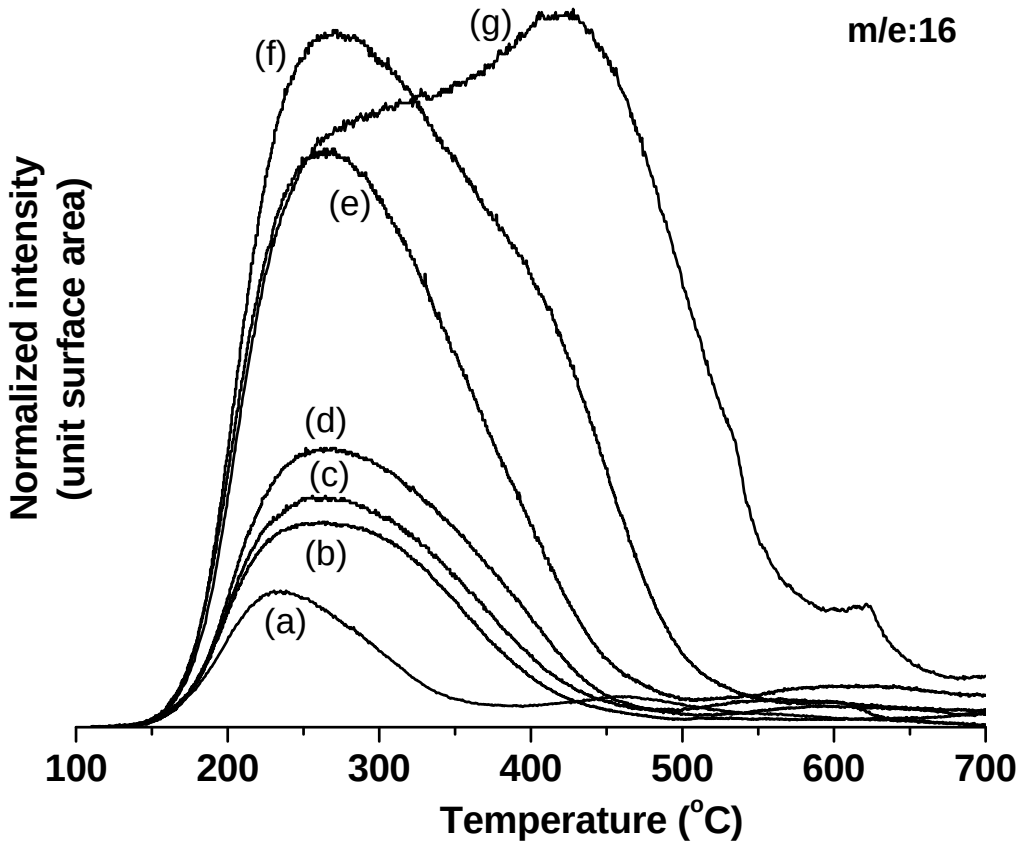

Figure **2-12**: NH_3-TPD profiles for (a) CeO_2, (b) $Ti_{0.1}Ce_{0.9}O_2$, (c) $Ti_{0.3}Ce_{0.7}O_2$, (d) $Ti_{0.5}Ce_{0.5}O_2$, (e) $Ti_{0.7}Ce_{0.3}O_2$, (f) $Ti_{0.9}Ce_{0.1}O_2$ and (g) TiO_2

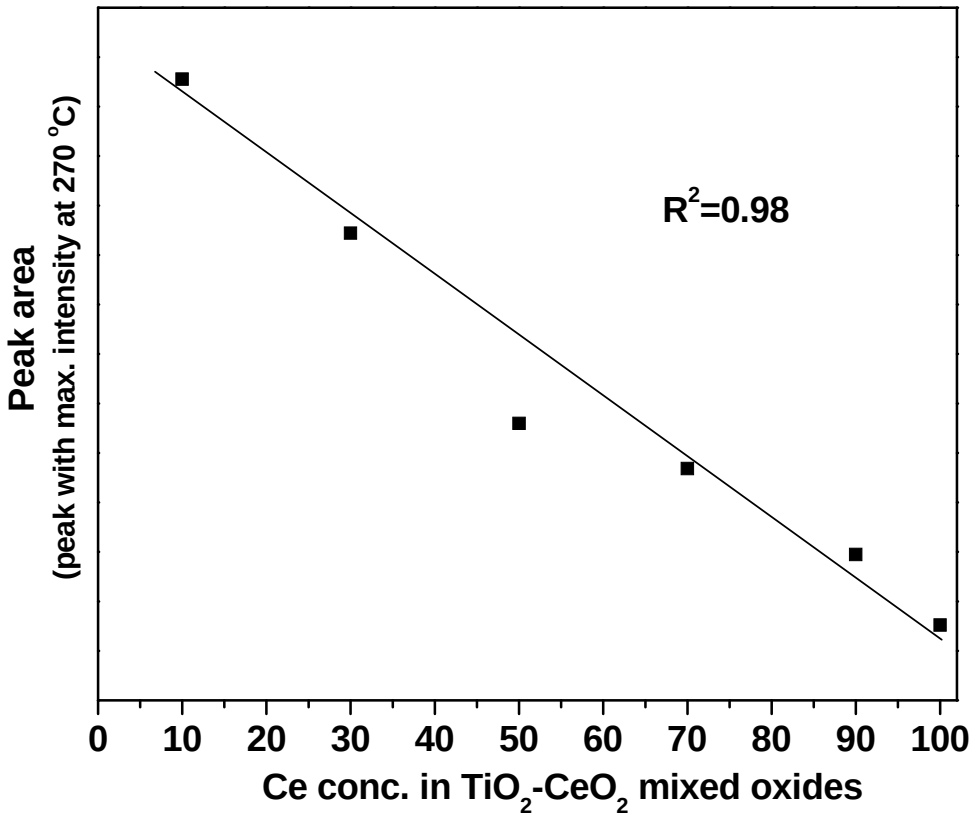

Figure **2-13**: Correlation between the area of NH_3 desorption peak centered at 270 ^oC and the concentration of Ce in TiO_2-CeO_2 oxides.

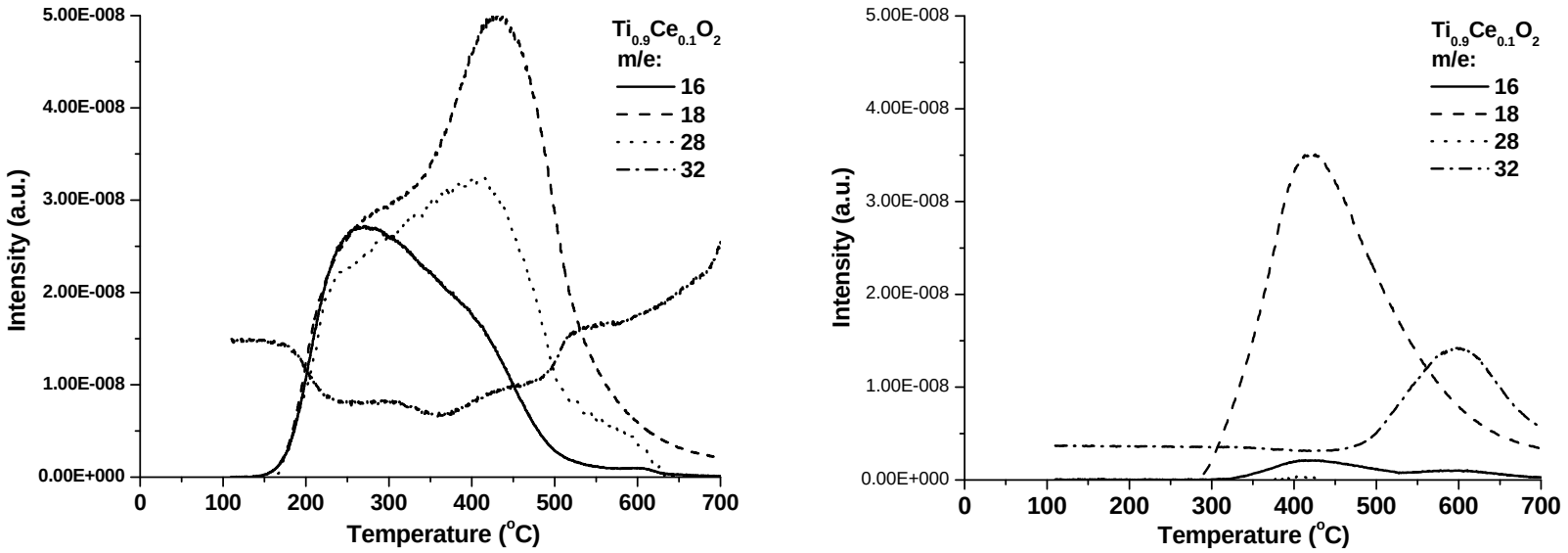

Figure **2-14**: TPD profiles of NH_3, H_2O, N_2 and O_2 for NH_3 (left) and non-NH_3 (right) adsorbed $Ti_{0.9}Ce_{0.1}O_2$. Sample was treated at 300 ^oC for 1 hr, cooled down to at 110 ^oC, NH3 adsorption was conducted at 110 oC, and desorption was employed under He flow at heating rate 10 oC/min to 700 ^oC.

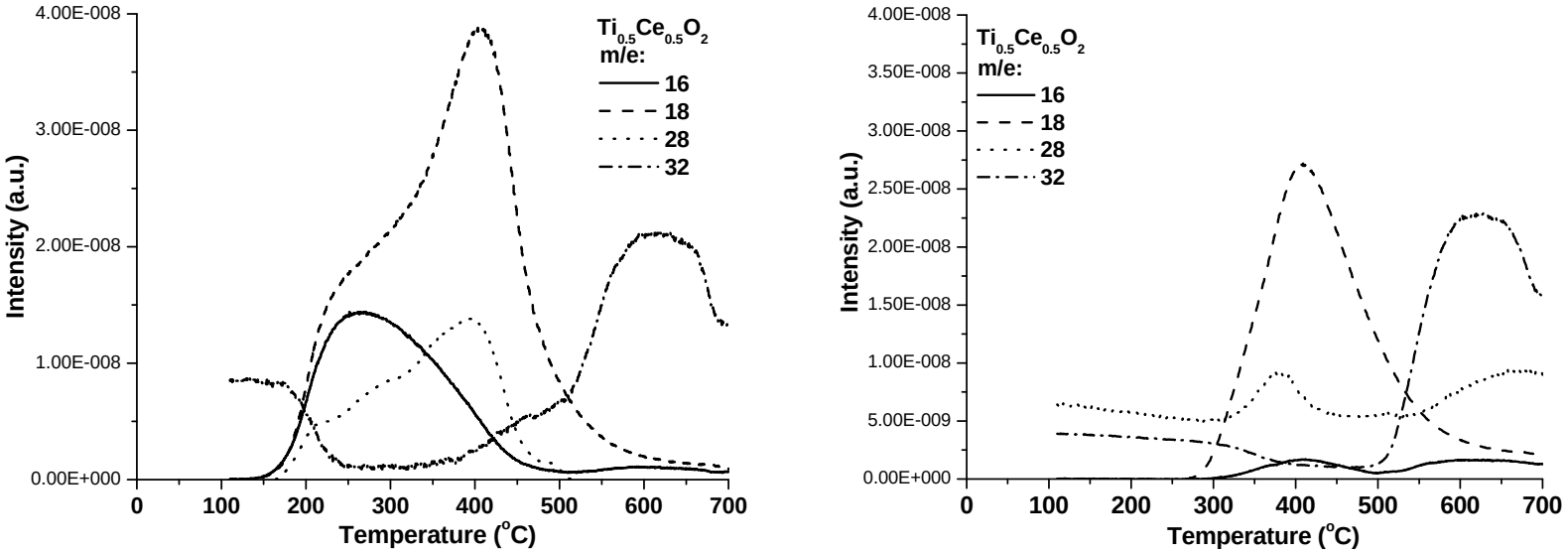

Figure **2-15**: TPD profiles of NH_3, H_2O, N_2 and O_2 for NH_3 (left) and non-NH_3 (right) adsorbed $Ti_{0.5}Ce_{0.5}O_2$. Sample was treated at 300 ^oC for 1 hr, cooled down to at 110 ^oC, NH_3 adsorption was conducted at 110 ^oC, and desorption was employed under He flow at heating rate 10 ^oC/min to 700 ^oC.

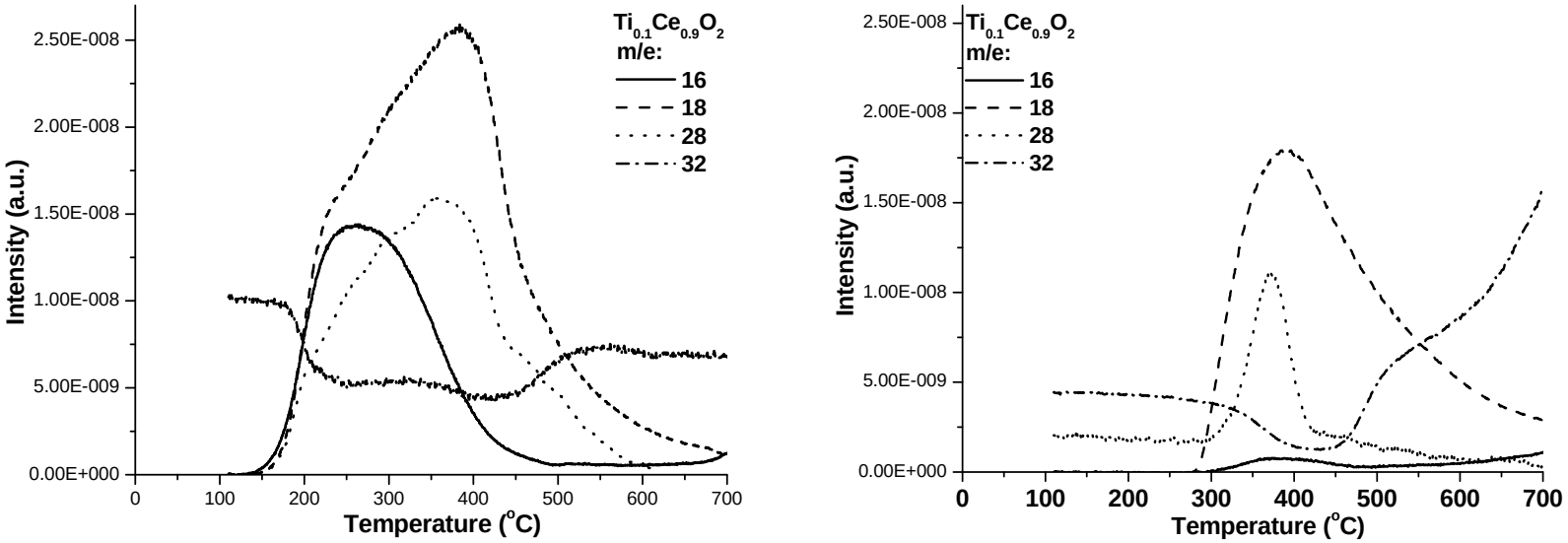

Figure **2-16**: TPD profiles of NH_3, H_2O, N_2 and O_2 for NH_3 (left) and non-NH_3 (right) adsorbed $Ti_{0.1}Ce_{0.9}O_2$. Sample was treated at 300 ^oC for 1 hr, cooled down to at 110 ^oC, NH_3 adsorption was conducted at 110 ^oC, and desorption was employed under He flow at heating rate 10 ^oC/min to 700 ^oC.

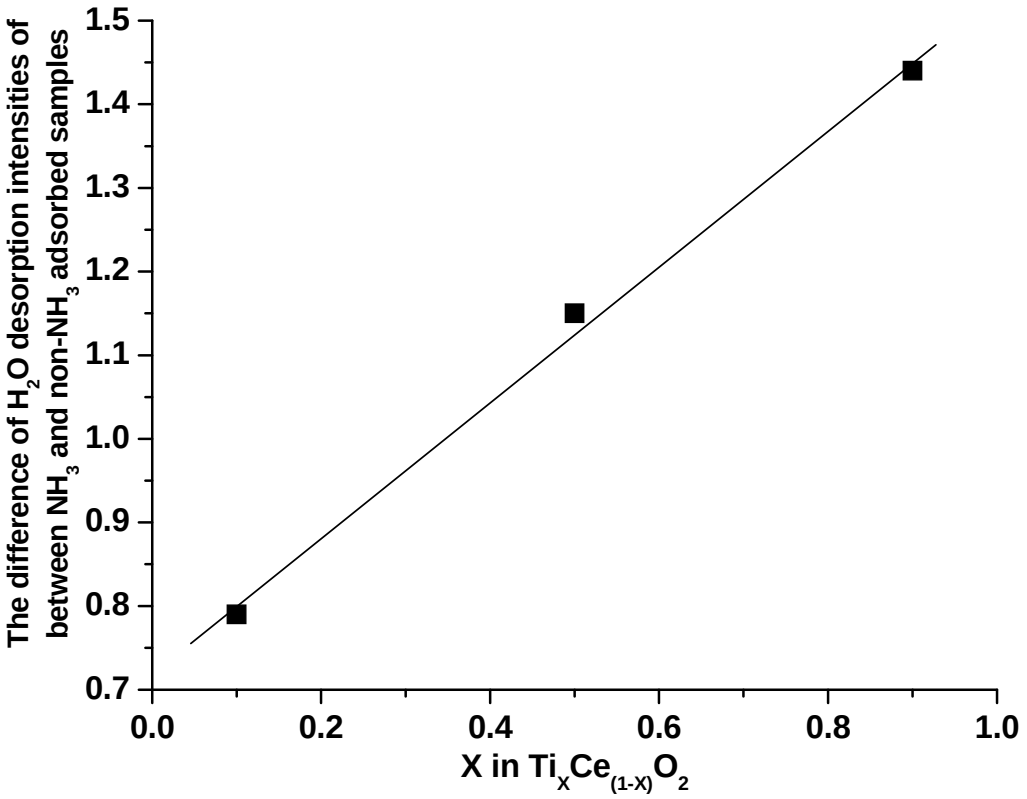

Figure **2-17**: Correlation between the difference of H_2O desorption intensities of NH_3 and non-NH_3 adsorbed samples and Ti concentration in TiO_2-CeO_2 oxides

References:

(1) Trovarelli, A.; de Leitenburg, C.; Boaro, M.; Dolcetti, G., The utilization of ceria in industrial catalysis. *Catalysis Today* **1999,** 50, (2), 353.

(2) Trovarelli, A., Catalytic properties of ceria and CeO_2-containing materials. *Catalysis Reviews-Science and Engineering* **1996,** 38, (4), 439.

(3) Diebold, U., The surface science of titanium dioxide. *Surface Science Reports* **2003,** 48, (5-8), 53.

(4) Hadjiivanov, K. I.; Klissurski, D. G., Surface chemistry of titania (anatase) and titania-supported catalysts. *Chemical Society Reviews* **1996,** 25, (1), 61.

(5) Hoffmann, M. R.; Martin, S. T.; Choi, W. Y.; Bahnemann, D. W., Environmental Applications of Semiconductor Photocatalysis. *Chemical Reviews* **1995,** 95, (1), 69.

(6) Pieplu, A.; Saur, O.; Lavalley, J. C.; Legendre, O.; Nedez, C., Claus catalysis and H_2S selective oxidation. *Catalysis Reviews-Science and Engineering* **1998,** 40, (4), 409.

(7) Flytzani-Stephanopoulos, M.; Zhu, T. L.; Li, Y., Ceria-based catalysts for the recovery of elemental sulfur from SO_2-laden gas streams. *Catalysis Today* **2000,** 62, (2-3), 145.

(8) Liu, W.; Wadia, C.; Flytzani-Stephanopoulos, M., Transition metal/fluorite-type oxides as active catalysts for reduction of sulfur dioxide to elemental sulfur by carbon monoxide. *Catalysis Today* **1996,** 28, (4), 391.

(9) Zeng, Y.; Zhang, S.; Groves, F. R.; Harrison, D. P., High temperature gas desulfurization with elemental sulfur production. *Chemical Engineering Science* **1999,** 54, (15-16), 3007.

(10) Koebrugge, G. W.; Winnubst, L.; Burggraaf, A. J., Thermal-Stability of Nanostructured Titania and Titania Ceria Ceramic Powders Prepared by the Sol-Gel Process. *Journal of Materials Chemistry* **1993,** 3, (11), 1095.

(11) Shi, Z. M.; Yu, W. G.; Bayar, X., Study of crystallization behavior of Ce^{4+}-modified titania gels. *Scripta Materialia* **2004,** 50, (6), 885.

(12) Lopez, T.; Rojas, F.; Alexander-Katz, R.; Galindo, F.; Balankin, A.; Buljan, A., Porosity, structural and fractal study of sol-gel TiO_2-CeO_2 mixed oxides. *Journal of Solid State Chemistry* **2004,** 177, (6), 1873.

(13) Velu, S.; Ma, X. L.; Song, C. S., Selective adsorption for removing sulfur from jet fuel over zeolite-based adsorbents. *Industrial & Engineering Chemistry Research* **2003,** 42, (21), 5293.

(14) Lin, S. D.; Song, C. S., Noble metal catalysts for low-temperature naphthalene hydrogenation in the presence of benzothiophene. *Catalysis Today* **1996,** 31, (1-2), 93.

(15) Ma, X. L.; Sun, L.; Song, C. S., A new approach to deep desulfurization of gasoline, diesel fuel and jet fuel by selective adsorption for ultra-clean fuels and for fuel cell applications. *Catalysis Today* **2002,** 77, (1-2), 107.

(16) Song, C.; Ma, X. L., New design approaches to ultra-clean diesel fuels by deep desulfurization and deep dearomatization. *Applied Catalysis B-Environmental* **2003,** 41, (1-2), 207.

(17) Song, C. S., An overview of new approaches to deep desulfurization for ultra-clean gasoline, diesel fuel and jet fuel. *Catalysis Today* **2003,** 86, (1-4), 211.

(18) Watanabe, S.; Velu, S.; Ma, X.; Song, C., New ceria-based selective adsorbents for removing sulfur from gasoline for fuel cell application. *Am. Chem. Soc. Div. Fuel Chem. Prepr.* **2003,** 48, (2), 695.

(19) Wang, Z.; Flytzani-Stephanopoulos, M., Cerium oxide-based sorbents for regenerative hot reformate gas desulfurization. *Energy & Fuels* **2005,** 19, (5), 2089.

(20) Karvinen, S., The effects of trace elements on the crystal properties of TiO_2. *Solid State Sciences* **2003,** 5, (5), 811.

(21) Subrt, J.; Stengl, V.; Bakardjieva, S.; Szatmary, L., Synthesis of spherical metal oxide particles using homogeneous precipitation of aqueous solutions of metal sulfates with urea. *Powder Technology* **2006,** 169, (1), 33.

(22) Reddy, B. M.; Khan, A., Recent advances on TiO_2-ZrO_2 mixed oxides as catalysts and catalyst supports. *Catalysis Reviews-Science and Engineering* **2005,** 47, (2), 257.

(23) Lukac, J.; Klementova, M.; Bezdicka, P.; Bakardjieva, S.; Subrt, J.; Szatmary, L.; Gruskova, A., Characterization of Zr-doped TiO_2 prepared by homogenous co-

precipitation without high-temperature treatment. *Journal of Materials Science* **2007,** 42, (22), 9421.

(24) Skorodumova, N. V.; Simak, S. I.; Lundqvist, B. I.; Abrikosov, I. A.; Johansson, B., Quantum origin of the oxygen storage capability of ceria. *Physical Review Letters* **2002,** 89, (16), 166601.

(25) Rodriguez, J. A.; Hanson, J. C.; Kim, J. Y.; Liu, G.; Iglesias-Juez, A.; Fernandez-Garcia, M., Properties of CeO_2 and $Ce_{1-X}Zr_XO_2$ nanoparticles: X-ray absorption near-edge spectroscopy, density functional, and time-resolved x-ray diffraction studies. *Journal of Physical Chemistry B* **2003,** 107, (15), 3535.

(26) Rodriguez, J. A.; Wang, X. Q.; Hanson, J. C.; Liu, G.; Iglesias-Juez, A.; Fernandez-Garcia, M., The behavior of mixed-metal oxides: Structural and electronic properties of $Ce_{1-X}Ca_XO_2$ and $Ce_{1-x}Ca_xO_{2-x}$. *Journal of Chemical Physics* **2003,** 119, (11), 5659.

(27) Dutta, G.; Waghmare, U. V.; Baidya, T.; Hegde, M. S.; Priolkar, K. R.; Sarode, P. R., Origin of enhanced reducibility/oxygen storage capacity of $Ce_{1-X}Ti_XO_2$ compared to CeO_2 or TiO_2. *Chemistry of Materials* **2006,** 18, (14), 3249.

(28) Henrich, V. E.; Dresselhaus, G.; Zeiger, H. J., Observation of Two-Dimensional Phases Associated with Defect States on Surface of TiO_2. *Physical Review Letters* **1976,** 36, (22), 1335.

(29) CRC-Handbook, Handbook of chemistry and physics. In 77th ed.; Lide, D. R., 'Ed.'^'Eds.' CRC Press: Boca Raton, Florida, 1996-1997; 'Vol.' p^pp **12**.

(30) Burroughs, P.; Hamnett, A.; Orchard, A. F.; Thornton, G., Satellite Structure in the X-Ray Photoelectron Spectra of some Binary and Mixide Oxides of Lanthanum and Cerium. *Journal of the Chemical Society-Dalton Transactions* **1976,** 17, 1686.

(31) Wagner, C. D.; Riggs, W. M.; Davis, L. E.; Moulder, J. F.; Muilenbedrg, G. E., *Handbook of X-Ray Photoelectron Spectroscopy*. ed.; Perkin-Elmer Corporation: Minnesota, 1978.

(32) Carley, A. F.; Chalker, P. R.; Riviere, J. C.; Roberts, M. W., The Identification and Characterization of Mixed Oxidation-States at Oxidized Titanium Surfaces by Analysis of X-Ray Photoelectron-Spectra. *Journal of the Chemical Society-Faraday Transactions I* **1987,** 83, 351.

(33) Mayer, J. T.; Diebold, U.; Madey, T. E.; Garfunkel, E., Titanium and Reduced Titania Overlayers on Titanium Dioxide(110). *Journal of Electron Spectroscopy and Related Phenomena* **1995,** 73, (1), 1.

(34) Leung, C. M.; Weinert, M.; Allen, P. B.; Wentzcovitch, R. M., First-principles study of titanium oxides. *Physical Review B* **1996,** 54, (11), 7857.

(35) Mullins, D. R.; Overbury, S. H.; Huntley, D. R., Electron spectroscopy of single crystal and polycrystalline cerium oxide surfaces. *Surface Science* **1998,** 409, (2), 307.

(36) Mullins, D. R.; Radulovic, P. V.; Overbury, S. H., Ordered cerium oxide thin films grown on Ru(0001) and Ni(111). *Surface Science* **1999,** 429, (1-3), 186.

(37) Henderson, M. A.; Perkins, C. L.; Engelhard, M. H.; Thevuthasan, S.; Peden, C. H. F., Redox properties of water on the oxidized and reduced surfaces of CeO_2 (111). *Surface Science* **2003,** 526, (1-2), 1.

(38) Yao, H. C.; Yao, Y. F. Y., Ceria in automotive exhaust catalysts I.Oxygen storage. *Journal of Catalysis* **1984,** 86, 254.

(39) Tsyganenko, A. A.; Pozdnyakov, D. V.; Filimonov, V. N., Infrared Study of Surface Species Arising from Ammonia Adsorption on Oxide Surfaces. *Journal of Molecular Structure* **1975,** 29, (2), 299.

Chapter 3

Mechanistic Insights into the Adsorption of Thiophene on $Ti_{0.9}Ce_{0.1}O_2$ Mixed Oxide by XPS, in-situ IR and TPD

Abstract

The adsorption of thiophenic compounds over $Ti_{0.9}Ce_{0.1}O_2$, oxidatively regenerable oxide-based sulfur adsorbent, was studied by XPS, DRIFT and TPD-MS. Previous research in our laboratory showed that $Ti_{0.9}Ce_{0.1}O_2$ mixed oxide adsorbent is promising for adsorptive desulfurization of liquid fuels and suitable for oxidative regeneration using air. In the present work, special attention was paid to the effect of the oxidative treatment on thiophene adsorption over $Ti_{0.9}Ce_{0.1}O_2$ adsorbent, the adsorption site for thiophenic compound, and the role of surface Ce and Ti cations in the adsorptive desulfurization. The formation of sulfite/sulfate species and enhancement of the sulfite/sulfate formation by oxidative pretreatment was observed in thiophene adsorption. These results suggest that the surface oxygen is the major adsorption site for the thiophenic compounds. The surface Ce and Ti were reduced during the adsorption of thiophenic compounds. This phenomenon is attributed to an electron transfer from adsorbates to the surface Ce and Ti. It appears that the role of the surface Ce and Ti can accept electrons from adsorbate, and also contributes to producing active oxygen to oxidize the sulfur atom in thiophenic compounds. An oxidative treatment, including oxidative regeneration, activates the surface oxygen to forms active oxygen species and oxidizes the surface Ce and Ti. Based on the results obtained, a possible mechanism was

proposed for the adsorption, dissociation and surface reaction of thiophene on $Ti_{0.9}Ce_{0.1}O_2$ mixed metal oxide adsorbent.

3.1 Introduction

Most efficient production of ultra clean fuel, particularly ultra low sulfur fuel, has become an important research subject worldwide.[1-3] The sulfur compounds remaining in liquid transportation fuels are much less reactive compared to many of the sulfur compounds in the crude oils.[1] The oxidized sulfur compounds SO_X are major pollutants. The combustion of fossil fuels is major source of anthropogenic SO_X emission on a global basis.[4] In order to improve the air quality, the new regulations on much lower sulfur concentration in transportation fuels announced by U.S. Environmental Protection Agency were implemented recently in year 2006.[1] The new sulfur levels allowed in transportation fuels were lowered from 300-500 parts per million by weight of sulfur (ppmw) to less than 30 ppmw for gasoline and 15 ppmw for diesel fuel in the US.[1] Further regulations for even lower sulfur contents and also for lower-sulfur off-load fuels are expected in the future. In Europe, the sulfur regulations for gasoline and diesel fuels will be set up to lower than 10 ppmw in year 2011.[5] In the last two decades, the maximum allowed sulfur concentrations in liquid fuels have been lowered significantly worldwide.

Hydrodesulfurization (HDS), a common process to remove sulfur from petroleum feed stocks, is widely used to meet the current regulations. However, in addition to the larger catalyst bed volume in pressurized reactors, HDS for a deeper sulfur removal requires higher temperature, higher pressure and larger hydrogen consumption due to the low reactivity of substituted thiophenic compounds.[1, 6-8] Due to the increasingly lower

quality of crude oils and progressively more and more severe requirements of low-sulfur fuels, the development of more efficient and effective approaches and new methods for removing sulfur from the petroleum feed stocks has become the focus of many recent studies world wide.[1, 3] Among these processes, adsorptive desulfurization (ADS) of liquid hydrocarbon fuels has recently received much attention as a potential new approach to produce ultra clean fuel.[1-3, 9] The major advantages of ADS are, (1) the refractory sulfur compounds (thiophenic and alkylated thiophenic compounds) can be removed under mild condition (at lower temperature and under lower pressure) without hydrogen consumption, and (2) it is a very simple process,[1, 10, 11] Among the several kinds of materials that have been investigated as adsorbents, the metal oxide-based adsorbents showed promising results in multiple cycles of ADS of liquid hydrocarbon fuels.[12, 13] Due to a simple regeneration by oxidation, an effective adsorptive system could be developed through the use of metal oxides.[11-13]

Understanding of ADS mechanism is crucial to develop and improve regenerable adsorbents. Some of the fundamental studies on ADS by metal oxides were found in literature.[14-18] These studies have used thiophene as a model organic sulfur compound because it is representative of the sulfur compounds in petroleum feed stock and its structure and chemistry are well-known.[17-20] As a part of mechanistic study of the HDS, the adsorption of thiophene on HDS catalysts has been studied by several analytical techniques, such as vibrational spectroscopy,[19-25] X-ray photoelectron spectroscopy[26-29] and thermal desorption mass spectroscopy.[30] These analytical techniques are useful to study the interaction of adsorbates and adsorbents. However, little is known on the mechanism of thiophene adsorption on mixed metal oxides.

The objective of this research is to understand the adsorption mechanism of thiophenic compounds on $Ti_{0.9}Ce_{0.1}O_2$ oxide which previously was shown to have an excellent performance for sulfur removal from real fuels.[11, 13] The absence of detailed studies, especially those providing a mechanistic understanding of the thiophene adsorption on the metal oxide-based adsorbent, has become the bottleneck in the further development and improvement of the oxide-based adsorbents. Thus, the investigation on adsorption of thiophene on the metal oxide was conducted by means of XPS, DRIFT and TPD. Special attention was also paid to the effect of the oxidative pretreatment on thiophene adsorption over $Ti_{0.9}Ce_{0.1}O_2$ adsorbent, the adsorption site for thiophenic compound, and the role of surface Ce and Ti cations in the adsorptive desulfurization. The information obtained from the present work provided new insight into the adsorption mechanism of thiophene on $Ti_{0.9}Ce_{0.1}O_2$-based adsorbents for sulfur removal from the liquid hydrocarbon fuels.

3.2 Experimental

3.2.1 Preparation

The metal oxide adsorbent ($Ti_{0.9}Ce_{0.1}O_2$) was synthesized through a urea precipitation/gelation method from aqueous solutions of inorganic salts [31, 32]. Prior to urea precipitation/gelation, aqueous solutions containing metal ion were prepared. 8.2 g of cerium ammonium nitrate $(NH_4)_2Ce(NO_3)_6$ (Aldrich, 99.99 %) was dissolved in deionized water to make 100 mL of solution. A 100 mL of aqueous solution dissolving 32.68 g of $TiOSO_4xH_2SO_4xH_2O$ (Aldrich, Ti: 18.5 wt%) was prepared as well. Ammonium cerium nitrate aqueous solution was added to the titanium oxysulfate solution. The mixed aqueous solutions was added to 800 mL of aqueous solution containing 70 g of urea, $CO(NH_2)_2$, (Aldrich 99+ %), and vigorously stirred by a magnetic stirrer. The solution volume was kept at 1000 mL during the entire precipitation process. The temperature of the solution was kept at 90 - 95 ^oC for 8 hours. The resulting precipitate was filtered and washed with 1000 mL of distilled water. The precipitate was dried overnight in an oven at 110 ^oC and then calcined in a muffle furnace in static air for 6 hours at 450 ^oC. The temperature was reached at a heating rate of 1.5^oC/min from room temperature.

3.2.2 Characterization

X-ray photoelectron spectroscopy (XPS) spectra were recorded on a Kratos Analytical Axis Ultra spectrometer with monochromatic aluminum (1486.6 eV). The X-ray source operated at 14 kV and 20 mA. As a sample preparation for XPS analysis, sulfur loaded and unloaded samples were prepared for XPS analysis. Sulfur was loaded on $Ti_{0.9}Ce_{0.1}O_2$ oxide sample by using a model fuel in a batch system. The model fuel consisted of tetrahydrothiophene (THT) dissolved in n-decane (n-C_{10}), and the sulfur concentration was 1000 ppmw. The powder adsorbent was placed in a glass tube with an internal diameter of 22 mm and a length of 150 mm. Pretreatment was conducted in the glass tube at 350 ^{o}C for 1 hour in atmospheric condition without any gas flow before adsorption. 5.0 g of a model fuel and 0.5 g of metal oxide (fuel/ adsorbent ratio= 10) were stirred at 25 ^{o}C for 1 hour with a magnetic stirrer. The adsorbent was filtered and dried under vacuum at room temperature overnight. After drying, all samples were immediately stored in a container, and mounted for analysis. The dried sample powders were pressed into 5 mm x 5 mm 3M double-sided tape using a mortar and pestle. The mounted sample was visualized by a stereo microscope to ensure complete coverage and powder uniformity over the tape. Sample height positions were set from O 1s signal at 529 eV following changing of lateral coordinates such that the measured signal from the sample powders were maximized, thus minimizing any possible signal from the 3M double sided tape. The 3M tape was examined independently and the characteristic shape of the C 1s line was not found when compared to the C 1s line collected from these sample powders. As a reference, we used the C 1s signal of the adventitious carbon

(carbon of any surface adsorbed), which we fixed at 285 eV. A survey scan with analyzer pass energy of 80 eV was initially recorded for the sample to identify elements present. The composition and chemical states were determined from the charge corrected high resolution scans with analyzer pass energy of 20 eV. An estimation of the amount of Ce(III) [33, 34] can be obtained from the intensity of the v_0 (u_0) and v' (u') lines, according to the formula:

$$Ce^{III}(\%) = \frac{v_0 + v' + u_0 + u'}{\Sigma(v+u)}$$

Diffuse reflectance infrared Fourier transform (DRIFT) spectra were obtained on a NICOLET NEXUS 470 FT-IR spectrometer recorded with a resolution of 4 cm^{-1} and 126 scans. DRIFT cell equipped with a ZnSe window was attached to a line that allows performing in situ treatment of the samples in either a gas flow or in a vacuum at different temperatures. A sample of metal oxide powders was treated at 200 ^oC for 1 hour under vacuum or oxygen flow. Subsequently thiophene (T) was introduced into the IR cell with 30 cm^3/min of Ar flow (1 % thiophene vapor in Ar) for 60 min. At last, 30 cm^3/min of Ar or O_2 flow was introduced to remove adsorbate from the oxide surface. All spectra were acquired at room temperature. As a reference, IR spectrum of liquid thiophene was obtained by using KBr pellets.

Temperature-programmed desorption measurements (TPD) were conducted using TGA 2050 (TA Instrument) in UHV system (2.3×10^{-6} mbar) outfitted with ThermoStar G301 (Pfeiffer) quadrupole mass spectrometer capable of monitoring 64 masses simultaneously. Sulfur loaded and unloaded samples were prepared for TPD experiments. Sulfur was loaded on $Ti_{0.9}Ce_{0.1}O_2$ oxide sample by using a model fuel in a batch system.

The model fuel consisted of thiophene in n-decane (n-C_{10}). The sulfur concentration was 1000 ppmw. The powder adsorbent was placed in a glass tube with an internal diameter of 22 mm and length of 150 mm. Pretreatment was conducted in the glass tube at 220 ^{o}C for 1 hour in atmosphere or 30 cc/min of O_2 flow before adsorption of thiophene. 5.0 g of the model fuel and 0.5 g of the metal oxide (fuel/ adsorbent ratio= 10) were stirred at 25 ^{o}C for 1 hours with a magnetic stirrer. The adsorbent was filtered with the aid of an aspirator and kept at room temperature for 30 min. The thiophene adsorbed sample was placed in an alumina holder, and TPD experiments were carried out at a heating rate of 10 ^{o}C/min under 130 cc/min argon gas flowing while acquiring data at a sampling frequency of 4 points/^{o}C.

3.3 Results

3.3.1 XPS

XPS analysis was conducted to gain insight into the adsorption site of the thiophenic compound and the role of $Ti_{0.9}Ce_{0.1}O_2$ surface for the interaction with the thiophenic compound. Tetrahydrothiophene (THT) was used as a probe molecule because it is known to be one of the most strongly-adsorbing organic sulfur compounds in ADS.[35] Fig. **3-1** shows the XPS S 2p spectra of $Ti_{0.9}Ce_{0.1}O_2$ adsorbents with and without THT adsorbate. The photoemission S 2p core-level spectra of THT adsorbed and non-adsorbed $Ti_{0.9}Ce_{0.1}O_2$ showed a peak centered at binding energy of 168.3 eV, which was assigned to sulfate species, SO_4^{2-}.[36-38] Sulfate species in the sample without THT adsorbate was originated from the Ti precursor salt. The S 2p spectra of THT adsorbed $Ti_{0.9}Ce_{0.1}O_2$ clearly showed the additional peaks at 166.3 and 163.3 eV, in addition to the sulfate peak. Comparison with published data allows unambiguous assignment of these S 2p features to sulfite-like (SO_3^{2-}) species (~166.3 eV) and tetrahydrothiophene (~162.8 eV).[39] The sulfite species arose as a result of the adsorption of THT on $Ti_{0.9}Ce_{0.1}O_2$. This result suggests that sulfur atom of THT interacted with surface oxygen. The formation of sulfite implies that the interaction of THT over the $Ti_{0.9}Ce_{0.1}O_2$ involves oxidation of sulfur atom by surface oxygen. Thus, sulfur atom of adsorbed tetrahydrothiophene was oxidized moderately, and shifted to the higher binding energy. The binding energy of the peak at 163.3 eV is higher than that of THT. It should be attributed to chemisorption of THT over

the surface. In the S 2p spectra, any peaks corresponding sulfide species were not identified.

This observation suggests that there was no strong direct bond-forming interaction between sulfur atom of THT and surface metal cation, which would involve electron transfer from sulfur to metal cations. Therefore, the formation of sulfate and sulfite species on the surface of $Ti_{0.9}Ce_{0.1}O_2$ upon adsorption of THT suggests that a major interaction between sulfur in thiophenic compound and $Ti_{0.9}Ce_{0.1}O_2$ surface could take place through oxygen on the surface of the adsorbent.

Fig. **3-2** presents the Ce 3d spectra of $Ti_{0.9}Ce_{0.1}O_2$ before and after THT loading. The labels of peaks used in Ce 3d identification were established by Burroughs et al.[40] The V and U indicate the spin-orbit coupling $3d_{5/2}$ and $3d_{3/2}$, respectively. The peaks marked as v, v" and v"' are attributed to CeO_2, and assigned to a mixture of Ce IV ($3d^9 4f^2$) O ($2p^4$), Ce IV ($3d^9 4f^1$) O ($2p^5$) and Ce IV ($3d^9 4f^0$) O ($2p^6$), respectively. The same assignment is applied to U structures. The peaks, v_o and v', are assigned to a mixture of Ce III ($3d^9 4f^2$) O ($2p^5$) and Ce III ($3d^9 4f^1$) O ($2p^6$), respectively. Intense peaks appeared at 882.7, 898.4, 901.1 and 916.8 eV in the Ce 3d spectra. These peaks correspond to tetravalent Ce. Thus, the predominant oxidation state of surface Ce of $Ti_{0.9}Ce_{0.1}O_2$ is 4+ both in the absence and presence of THT adsorbed. However, the intensity at 885.2 and 903.6 eV slightly increased after THT adsorption over $Ti_{0.9}Ce_{0.1}O_2$. This change implies that the concentration of trivalent Ce increased after THT adsorption. The concentration of trivalent Ce in the total surface Ce was clarified by quantitative XPS analysis via curve fitting procedure and the data are shown in Table **3-1**. After THT adsorption, the concentration of Ce^{3+} increased from 21.9 to 25.1 %. The

reduction of adsorbent was similarly seen in the adsorption of SO_2 over CeO_2.[36-38] Thus, the reducibility of the adsorbent may play an important role in sulfur adsorption.

Fig. **3-2** shows the Ti 2p spectra before and after THT adsorption. Before THT adsorption, Ti $2p_{3/2}$ peal is located at 458.7 eV. After THT adsorption, the peak of Ti $2p_{3/2}$ shifted to 458.4 eV. This binding energy is lower by 0.3 eV than Ti $2p_{3/2}$ before adsorption. Since XPS analysis confirmed the absence of any sulfide formation, this peak shift could not be attributed to S-Ti interaction. Such a shift corresponds to reduction of Ti cation that occurred after THT adsorption. Therefore, the role of both surface Ce and Ti could be to accept electrons during the ADS.

Although there are few reported adsorption studies of thiophenic compounds over metal oxides, adsorption of inorganic sulfur compounds, such as SO_2 and H_2S over metal oxides has been extensively studied. XPS and NEXAFS, for example, were used to elucidate the chemistry of SO_2 adsorption.[41-44] The formation of sulfite and sulfate was observed in the SO_2 adsorption over TiO_2. These SO_X-like species were found to involve the bridging oxygen of TiO_2 surface. In fact, the bridging oxygen of stoichiometric TiO_2 surface is the adsorption site for SO_2. In the SO_2 adsorption over TiO_2, the peak shift of Ti $2p_{3/2}$ by 0.3 eV was observed,[41] and a very similar shift in binding energy was also observed in our thiophene adsorption study. This result suggests that electron transfer took place in the SO_2 adsorption. In contrast to SO_2 adsorption, methanethiol and thiophene adsorption over TiO_2 showed the SO_X formation in S 2p spectra of XPS analysis.[17, 45] Therefore, a bridging oxygen over metal oxides is a possible adsorption site for sulfur compounds, such as thiophenic compounds, and electron transfer could occur to metal cations through the surface oxygen.

3.3.2 DRIFT

Oxidative treatment on $Ti_{0.9}Ce_{O.1}O_2$

We undertook the investigation of the influence of oxidative treatment on $Ti_{0.9}Ce_{O.1}O_2$ using in-situ infrared spectroscopy, because the improvement of sulfur removing ability from liquid hydrocarbon fuels was reported.[46] The FT-IR difference spectra were obtained by subtracting the spectrum of vacuum-dried $Ti_{0.9}Ce_{O.1}O_2$ (200 ^oC for 1 hr) from the spectrum $Ti_{0.9}Ce_{O.1}O_2$ exposed to O_2 flow at 200 ^oC for 1 hour after degassing under the vacuum at 200 ^oC for 30 min. The resulting IR spectrum is shown in Figure **3-3**. Two prominent bands appeared after the treatment under O_2 flow at 200 ^oC at around 1558 cm^{-1} and 1363 – 1281 cm^{-1} and two moderate bands at 1090 and 1022 cm^{-1} with a shoulder at 1146 cm^{-1}. The bands that appeared at around 1363 – 1281 cm^{-1} upon oxidative treatment may be ascribed to carboxylate species formed by reaction of oxygen with carbonaceous species. These bands were similarly observed in the IR spectra of oxygen adsorption over CeO_2.[47-50] The carbonaceous entities might be derived from the residue of precipitating agent (urea). Bands appearing at 1558, 1146, 1090 and 1022 cm^{-1} are assigned to adsorbed oxygen species.[48, 49, 51] The sharp intense band at 1558 cm^{-1} was assigned to adsorbed neutral O_2, which is assumed to be bonding through the anti π orbital without acquiring negative charge.[52] The two moderate bands appearing at 1090 and 1022 cm^{-1} with a shoulder at 1146 cm^{-1} were assigned to superoxide species, O_2^-. Superoxide species formed by the interaction of molecular oxygen and neighboring reduced centers, such as Ce^{3+} or Ti^{3+}. Our previous study showed that the significant oxygen deficiency accompanied with reduced centers presented over $Ti_{0.9}Ce_{O.1}O_2$ oxide

surface.[46] The interaction of molecular oxygen and $Ti_{0.9}Ce_{O.1}O_2$ resulted in the reoxidation of the surface reduced centers and the subsequent formation of superoxide species.

IR spectrum of liquid thiophene

The IR spectrum of the liquid thiophene was obtained as a reference. Liquid thiophene was placed between two KBr pellets to minimize evaporation of thiophene for the IR measurement. The bands of liquid thiophene were assigned based on previous publications.[20, 25, 53, 54] IR bands for liquid thiophene appeared at 3110, 3075, 1588, 1409, 1252, 1082, and 1034 cm^{-1} corresponding to the C-H stretching vibration (ν(C-H) α-position), the C-H stretching vibration (ν(C-H) β-position), the asymmetric C=C stretching ($\nu(C=C)_{asym}$), the symmetric C=C stretching ($\nu(C=C)_{sym}$) and the in-plane C-H bending vibration (δ(C-H)) for the last three bands, respectively. In comparison with these bands of liquid thiophene, adsorption behavior of thiophene over $Ti_{0.9}Ce_{O.1}O_2$ oxide was examined.

IR spectrum of thiophene adsorbed on dried $Ti_{0.9}Ce_{O.1}O_2$

Figure **3-4** shows the FT-IR difference spectra obtained by subtracting the spectrum of vacuum-dried $Ti_{0.9}Ce_{O.1}O_2$ (200 ^oC for 1 hr) from (a) the spectrum of $Ti_{0.9}Ce_{O.1}O_2$ exposed to thiophene/Ar flow for 1 min, (b) the spectrum of $Ti_{0.9}Ce_{O.1}O_2$ exposed to thiophene/Ar flow for 5 min, (c) the spectrum of $Ti_{0.9}Ce_{O.1}O_2$ exposed to thiophene/Ar flow for 60 min, (d) the spectrum of $Ti_{0.9}Ce_{O.1}O_2$ under He flow for 1 min after adsorption, and (e) the spectrum of $Ti_{0.9}Ce_{O.1}O_2$ under He flow for 60 min after adsorption.

The absorbance features at 1653, 1408, 1253 and 1193 cm^{-1} were observed in Figure **3-4**-a. Bands at 1408 and 1253 cm^{-1} are assigned to thiophene, and those at 1653 and 1193 cm^{-1} are assigned to C=C and S-O stretching vibration, respectively. The C=C stretching vibration corresponds to a double bond with the higher bond order, which was assigned to olefin. The spectrum b in Figure **3-4** showed bands at 1653, 1593, 1408, 1360, 1254, 1193, 1082 and 849 cm^{-1}. Bands at 1593, 1408, 1254, 1082 and 849 cm^{-1} are assigned to thiophene. New bands appeared at 1360 and 1193 cm^{-1}, which are assigned to S-O stretching vibration. These frequencies correspond to SO_2 complex-like species.[55] For more significant quantities of thiophene introduced into the DRIFT cell, the bands due to thiophene increased in intensity, and appeared at 1408, 1253 and 1082 cm^{-1} with shoulder at 1419 cm^{-1} (Figure **3-4**-c). The larger quantity of thiophene exposure to $Ti_{0.9}Ce_{O.1}O_2$ dominantly increased the intensity of physically adsorbed thiophene. The shoulder of the band at 1408 cm^{-1} is assigned to the η^1-(S)-coordination of thiophene.[20, 25] This adsorption mode is attributed to thiophene adsorption via sulfur atom with increased electron density within the C=C−C=C fragment and decreased its aromaticity.

After introducing He flow into the DRIFT cell, the intensity of bands corresponding to thiophene dramatically decreased (Figure **3-4**-d and 4-e). The bands corresponding to thiophene at 1408, 1253 and 1082 cm^{-1} disappeared after introducing He flow for 60 min (Figure **3-4**-e). This result implies that physically adsorbed thiophene desorbs easily. On the other hand, broad bands appeared at 1192 and 926 cm^{-1} after introducing He flow for 60 min. They are assigned to sulfite species that remained on the surface as products.

As seen in Figure **3-4**-a, S-O stretching frequencies were found at the beginning of thiophene exposure. Thus, these S-O bondings were formed at the beginning of thiophene adsorption over $Ti_{0.9}Ce_{O.1}O_2$. The formation of sulfite species due to a thiophene adsorption concurs with the result of the XPS study. Consequently, surface oxygen is possibly an adsorption site of thiophene.

IR spectrum of thiophene adsorbed on oxidized $Ti_{0.9}Ce_{O.1}O_2$

Analysis of thiophene adsorption over oxidized $Ti_{0.9}Ce_{O.1}O_2$ by in-situ FT-IR was conducted to elucidate the influence of oxidative pretreatment on thiophene adsorption. Figure **3-5** presents the FT-IR difference spectra obtained by subtracting the spectrum of oxidatively pretreated $Ti_{0.9}Ce_{O.1}O_2$ (200 ^oC for 1 hr under oxygen flow) from (a) the spectrum $Ti_{0.9}Ce_{O.1}O_2$ exposed to thiophene/Ar flow for 1 min, (b) the spectrum of $Ti_{0.9}Ce_{O.1}O_2$ exposed to thiophene/Ar flow for 60 min, and (c) the spectrum of $Ti_{0.9}Ce_{O.1}O_2$ under He flow for 1 min after thiophene adsorption, (d) the spectrum of $Ti_{0.9}Ce_{O.1}O_2$ under He flow for 60 min after thiophene adsorption.

IR spectrum of thiophene adsorbed on oxidized $Ti_{0.9}Ce_{O.1}O_2$ by exposure to thiophene for 1 min is shown in Figure **3-5**-a. While broad bands appeared at 1570 and 1373 cm^{-1}, the infrared absorbance bands corresponding to thiophene were not observed. Absorbance at 1570 cm^{-1} is assigned to C=C stretching vibration. Due to the absence of bands corresponding to thiophene, the C=C bond is not assigned to thiophene. The band at 1373 cm^{-1} is assigned to S-O stretching vibration of sulfate.[56-58] After further exposure to thiophene, significant bands corresponding to thiophene appeared at 1408 and 1082 cm^{-1} (Figure **3-5**-b).

Figure **3-5**-c and 5-d show the difference spectra after introducing He flow into the IR cell. The intensity of peaks at 1408, 1254 and 1082 cm^{-1} corresponding to thiophene decreased significantly. The bands assigned to thiophene disappeared after introduction of He flow. Along with disappearance of thiophene bands, a large broad band appeared at 925 cm^{-1}. This broad band is assigned to S-O stretching vibration of SO_3^{2-} species.[55] This result suggests that oxidative treatment prior to thiophene adsorption contributes to the sulfite formation during thiophene adsorption. The formation of superoxide species was observed in the different IR spectrum of oxidative treatment of $Ti_{0.9}Ce_{O.1}O_2$. Thus, this reactive oxygen species plays an important role in adsorption of thiophene over metal oxides.

3.3.3 TPD

Identification of adsorbates was conducted by temperature-programmed desorption accompanying mass spectrometry. Figure **3-6** shows the TPD spectra species with m/e = 64 corresponding to mass-to-charge ratio of SO_2. Intense peaks appeared with the maximum desorption rate at 785 ^oC for non-thiophene adsorbed $Ti_{0.9}Ce_{0.1}O_2$. This desorption peak corresponds to sulfate species.[59] This result is in good agreement with the XPS study. This sulfate species originates from the residue of Ti precursor salt that remains after calcination in air.

In addition, the desorption profiles of thiophene adsorbed on vacuum-dried and oxidized $Ti_{0.9}Ce_{0.1}O_2$ oxide shows the sulfate species-corresponding desorption peak. While the desorption profiles of non-thiophene adsorbed and thiophene-adsorbed dried

$Ti_{0.9}Ce_{0.1}O_2$ resemble each other, TPD of oxidized $Ti_{0.9}Ce_{0.1}O_2$ with thiophene adsorbed revealed the maximum SO_2 desorption at 765 ^oC with a shoulder extending to 1000 ^oC. This enlarged SO_2 desorption profile implies that significant sulfate formation occurred upon thiophene adsorption over oxidized $Ti_{0.9}Ce_{0.1}O_2$. Besides sulfate corresponding desorption peak, a low-temperature desorption peak of SO_2 appeared at around 480 ^oC for thiophene adsorbed on dried and oxidized $Ti_{0.9}Ce_{0.1}O_2$. These peaks were attributed to decomposition of sulfite species. Formation of sulfite species in adsorption of thiophene over the oxidized $Ti_{0.9}Ce_{0.1}O_2$ was prominent in sharp contrast to that of dried $Ti_{0.9}Ce_{0.1}O_2$. It could be due to the oxidation of sulfur atom of thiophene by the superoxide formed during oxidative pretreatment.

Figure **3-7** shows the desorption profiles of species with m/e = 54, 56, 58 and 84. The mass-to-charge ratios 56, 58 and 84 correspond to butene, butane and thiophene, respectively. Although m/e = 54 could result from ionization and decomposition of butene and butane, the mass-to-charge ratio 54 could be assigned to butadiene. Desorption profile of butene exhibited the significant maximum rate of desorption at 150 ^oC. In addition to butene desorption, the moderate intensities of butane and thiophene desorption also appeared with at 100 - 150 ^oC. The butene desorption in TPD profiles of thiophene adsorbed on dried and oxidized $Ti_{0.9}Ce_{0.1}O_2$ mixed oxide indicate that thiophene mostly adsorbs dissociatively. The product containing C=C found in DRIFT study can be assigned to butene. The results obtained from TPD study concurs with the results of XPS and DRIFT study.

3.4 Discussion

3.4.1 Adsorption Mechanism of Thiophenic Compounds over $Ti_{0.9}Ce_{0.1}O_2$

The results of our study on thiophene adsorption over $Ti_{0.9}Ce_{0.1}O_2$ mixed oxide indicate the influence of oxidative treatment on ADS, the possible thiophene adsorption site and the role of surface Ce and Ti in ADS. The experimental results and findings are elaborated by the following discussion.

Surface oxygen was identified as an adsorption site for thiophene. In this in-situ IR study, the formation of S-O and C=C bonding corresponding to SO_2-complex species and butene, respectively, occurs at the beginning of thiophene adsorption. This formation of SO_X species is the possible evidences that sulfur interact with surface oxygen. After the significant exposure to the thiophene and removal of adsorbates by He flow, sulfite/sulfate species appeared in the IR spectra. A peak corresponding to sulfite species newly appeared in the XPS S 2p spectrum of sulfur adsorbed $Ti_{0.9}Ce_{0.1}O_2$. This sulfite peak was attributed to thiophene adsorption over $Ti_{0.9}Ce_{0.1}O_2$. Furthermore, the formation of SO_X species was shown in TPD results. TPD of SO_2 appeared at 480 ^oC on the thiophene adsorbed $Ti_{0.9}Ce_{0.1}O_2$. This desorption peak was assigned to sulfite species.

The presence of sulfite and sulfate species on the surface, and the formation of SO_X species due to the thiophene adsorption were confirmed by XPS, IR and TPD. These results are indicative of a sequential adsorption and reaction pathway beginning with the interaction of sulfur atom of thiophene with surface oxygen. While this sulfur-oxygen bonding leads to SO_2-complex like species at the beginning, this SO_2-complex like species could transform to sulfite/sulfate. This trend was observed in SO_2 adsorption on

oxides.[44] In the present study, formation of superoxide species was revealed as a result of oxidative treatment. The superoxide formed by the interaction of molecular oxygen with reduced surface centers and as a result of surface oxygen exchanging by molecular oxygen.[60] Similarly, the superoxide formation due to thermal treatment was observed for TiO_2[60-62] and CeO_2.[63] As an activation of surface oxygen, the influence of oxidative thermal treatment has been reported by Yu et al. [62] and Sato et al.[61] Thus, the above discussion suggests that activated surface oxygen and superoxide species are the adsorption sites and they can oxidize the sulfur atom.

In terms of the effect of oxidative thermal treatment, change in the band structure of anatase was observed.[64] After oxidative treatment, valence band of anatase was extended toward higher binding energy. It implies that the contribution of O 2p in the valence band increases by oxidative thermal treatment. On the other hand, reduction of TiO_2 under 5 % H_2 flow at 650 ^oC for 3 hours did not improve catalytic activity because valence band of anatase was not altered by the reduction.[64] In addition to the investigation of pure oxides, enhancement of oxygen exchange property was observed for Pr and Zr doped CeO_2.[63] As shown for the formation of superoxide species in the case of oxidative thermal treatment on Zr-doped CeO_2,[65] these active oxygen species could be effectively formed over $Ti_{0.9}Ce_{0.1}O_2$.

As for the role of surface Ce and Ti, they could contribute to not only producing superoxide species but also interacting with molecules by accepting electrons. Adsorption accompanying with receiving electrons may similarly be seen in benzene adsorption.[66] The oxidative pretreatment of $Ti_{0.9}Ce_{0.1}O_2$ increases the valence state from 3 to 4 for both Ti and Ce. The Ti^{4+} and Ce^{4+} with d^0 and f^0 electron configuration could play a role as

electron acceptor, and contribute to a weak interaction with π bonding. Thus, the role of oxidative thermal treatment to $Ti_{0.9}Ce_{0.1}O_2$ oxide is to activate surface oxygen and oxidize the surface cations.

Based on the above discussion, we could propose a possible adsorption mechanism of thiophenic compounds over $Ti_{0.9}Ce_{0.1}O_2$. The proposed adsorption pathway is shown in **Figure 3-8**. The results obtained in current study provide a basis for understanding the adsorption mechanism of thiophene over $Ti_{0.9}Ce_{0.1}O_2$ as discussed further below.

The first step of adsorptive desulfurization over $Ti_{0.9}Ce_{0.1}O_2$ oxide starts with oxidative treatment. It involves mainly the adsorption of gaseous O_2 on reduced center (1). In the O_2 adsorption, an electron is transferred from reduced center to oxygen to form O_2^- (2). This superoxide species is known to be strongly electrophilic.[51, 52] Reactive oxygen species, such as superoxide and also the bridging oxygen species oxidize sulfur atom, and form sulfinyl. Subsequently the neighboring active oxygen species further oxidize the sulfur atom to form sulfonyl (3). It resembles the step of oxidative desulfurization.[67, 68] The oxidation of sulfur atom contributes to the reduction of bond energy between the carbon and the sulfur.[69] In other words, the oxidation of sulfur caused the localization of the thiophene ring due to charge transfer to oxygen, and the aromaticity was decreased. As a result, the sulfur atom positions at out of the plane in the thiophene ring (3).[70] Due to the strong electrophilic nature of superoxide, sulfur of sulfonyl group interacts with another active oxygen species,[71, 72] and the localization of the ring becomes further significant (4). In the localized ring, high π electron density of C=C bonds could easily transfer electron to interact with surface cations, Ti^{4+} and Ce^{4+}

(5). Interaction of cations with π electron of C=C bond possibly decreases the valence state of cations. As a result, adsorbed thiophene forms sulfite and η^4 complex over the surface (5). The resulting oxygen addition to form sulfite and η^4 complex significantly weakens C-S bond (6). C-S bond cleavage of thiophene takes place and sulfur atom remains as sulfite/sulfate over the surface (7). Subsequently, hydrogen, which may be subtracted by the metal cations from co-existing hydrocarbons, reacted to leave a double bond at the end of the hydrocarbon chain. Some of the double bonds may be further hydrogenated. At last, both butene and butane can be found as decomposed hydrocarbons from thiophene (8). In current study, removal of sulfur atom from the molecules occurred along with the formation of sulfite species during the adsorption of thiophene over $Ti_{0.9}Ce_{0.1}O_2$. It is similar to what was reported in alkali-coexisting oxidation of dihydrothiophene[73-76] and photo-oxidative desulfurization.[77, 78] For example, oxidation of dibenzothiophene (DBT) using NaOH was conducted as the mixture of 16.6 mmol of DBT-sulfone with 83 mmol or NaOH stirred under N_2 for 5 h at 300 ^oC primarily produced 2-phenylphenol and SO_3^{2-}.[76] Jenks et al. employed the photo-oxidation for biphenyl production from DBT by ultra violet ($\lambda > 300$ nm) irradiation, and induced the decomposition of DBT sulfone in the presence of hydrogen donor, such as 2-isoproponol.[78] In contrast to these studies, $Ti_{0.9}Ce_{0.1}O_2$ adsorbent can remove sulfur atom from thiophenic compounds, and this occurs at room temperature with activation by using air. Thus, this process is very promising due to the high efficiency and simplicity of sulfur removing procedure.

3.4 Conclusions

On the basis of the above results and discussion, the following conclusions can be drawn regarding the study of adsorption mechanism of thiophenic compounds over $Ti_{0.9}Ce_{0.1}O_2$ metal oxide.

1. Oxidative thermal treatment produces superoxide species over $Ti_{0.9}Ce_{0.1}O_2$. Presumably molecular oxygen is involved in the interaction with surface reduced centers. The roles of oxidative pretreatment are formation of active oxygen species over the surface and increasing valence state of surface cations.
2. The surface oxygen species were identified as adsorption sites for thiophene over $Ti_{0.9}Ce_{0.1}O_2$. Dominantly thiophene adsorption forms sulfite/sulfate species by sulfur-oxygen interaction. The oxidation of sulfur atom is involved in the adsorption of thiophenic compounds over $Ti_{0.9}Ce_{0.1}O_2$ adsorbent.
3. Thiophene adsorption on $Ti_{0.9}Ce_{0.1}O_2$ was mainly dissociative adsorption, and produced C_4 hydrocarbons, such as butene and butane.
4. The role of surface Ce and Ti is to form superoxide species and possibly to accept electrons in interaction with π electron of localized thiophene ring. The possible η^1(S)-coordination and η^4 adsorption mode enhances the localization of the ring, and as a result, would cause dissociation of thiophene by C-S bond cleavage.

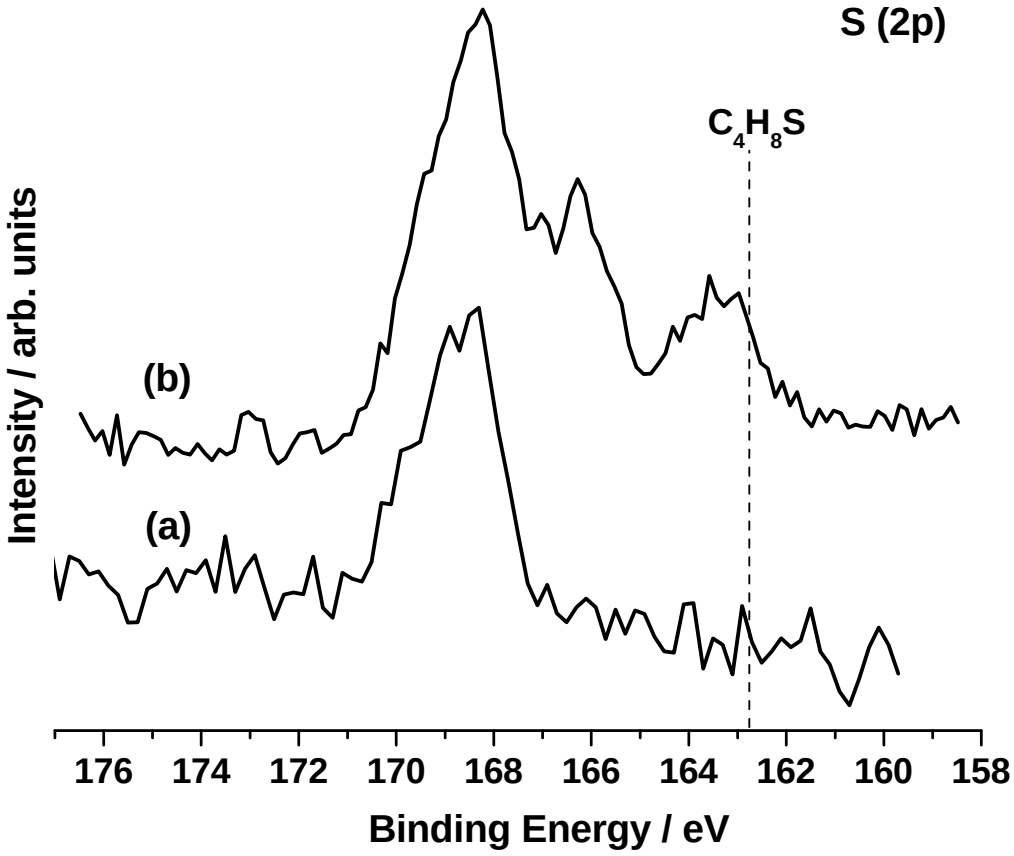

Figure **3-1**: S 2p spectra for (a) non-adsorbed $Ti_{0.9}Ce_{0.1}O_2$ surface and (b) THT adsorbed $Ti_{0.9}Ce_{0.1}O_2$ surface. Adsorption of THT was conducted in liquid phase at 25 ^{o}C for 2 hours.

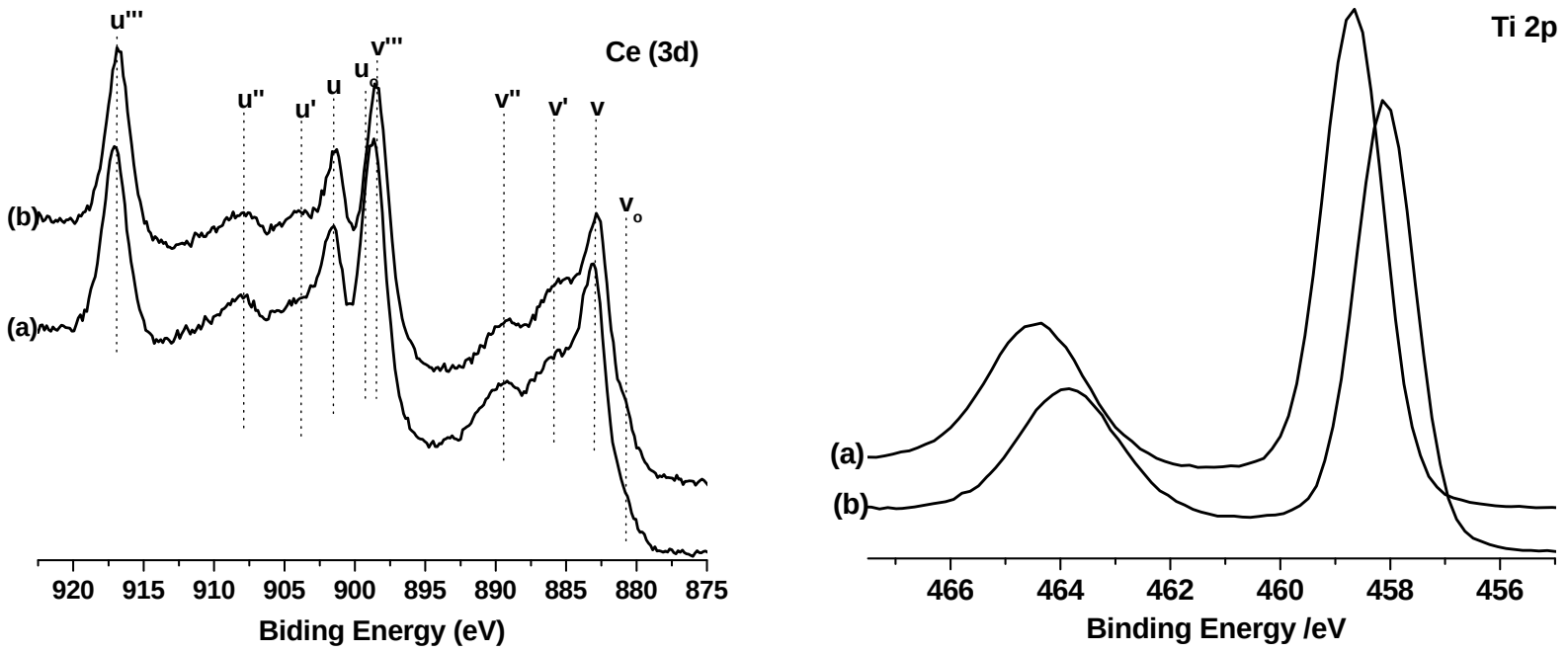

Figure **3-2**: Ce 3d (left) and Ti 2p (right) spectra for (a) non-adsorbed $Ti_{0.9}Ce_{0.1}O_2$ surface and (b) THT adsorbed $Ti_{0.9}Ce_{0.1}O_2$ surface. Adsorption of THT was conducted in liquid phase at 25 ^{o}C for 2 hours.

Table **3-1**: Concentration of Ce^{3+} and Binding Energy of Ti $2p_{3/2}$ before and after THT Adsorption

	THT adsorption	
	before	after
	Ce^{3+} concentration (%)	
Ce	21.9	25.1
	Binding Energy (eV)	
Ti	458.7	458.4

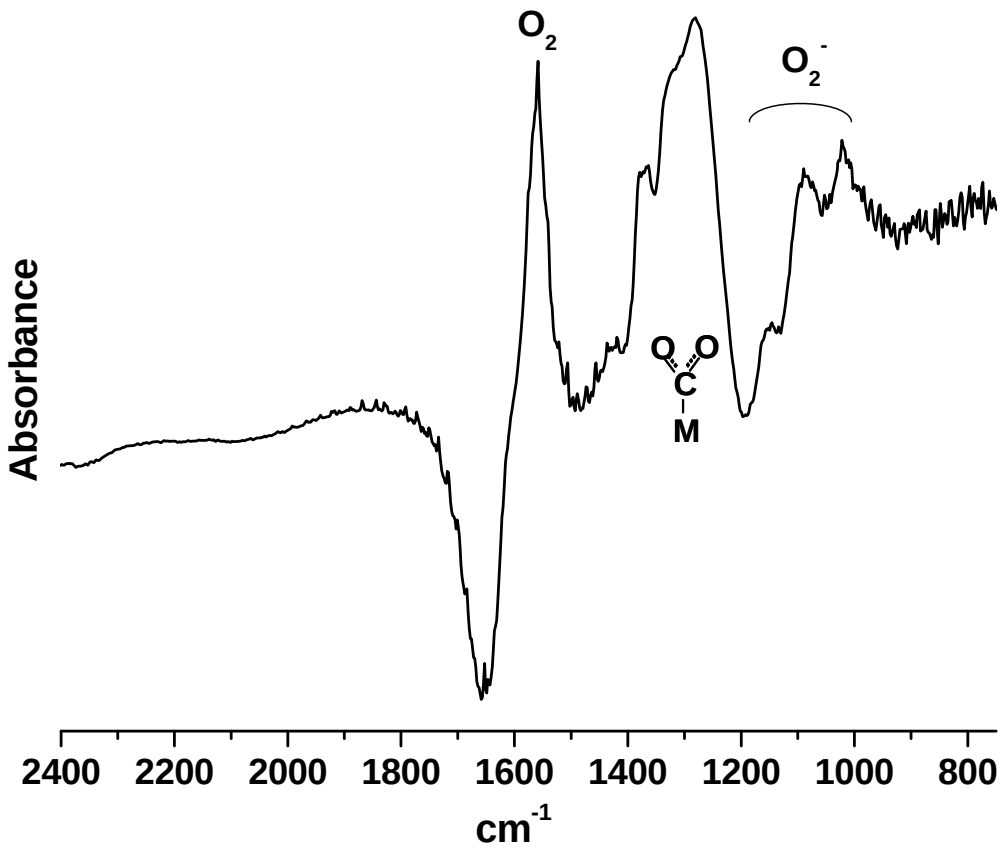

Figure **3-3**: IR spectra of O_2 adsorbed over $Ti_{0.9}Ce_{0.1}O_2$ at 220 ^oC for 2 hours after vacuum -dried at 200 ^oC for 30 min.

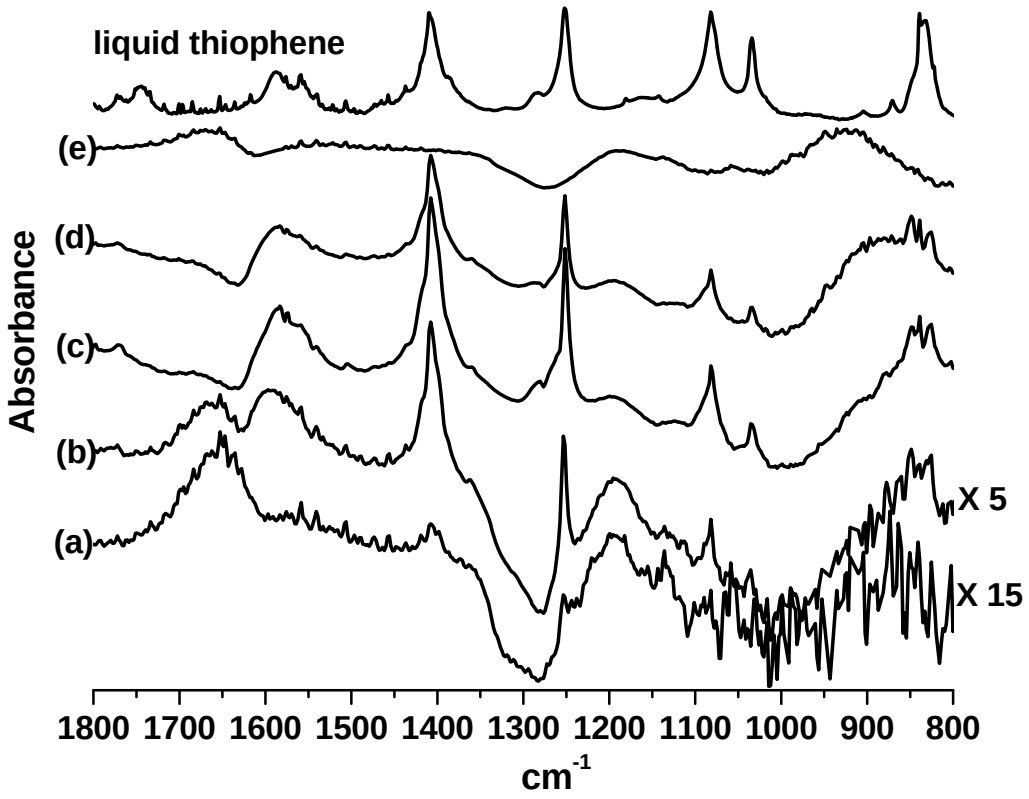

Figure **3-4**: IR spectra of thiophene adsorbed on vacuum-dried $Ti_{0.9}Ce_{0.1}O_2$. Thiophene adsorption for (a) 1 min, (b) 5 min, (c) 60 min exposure to thiophene, (d) flowing He for 1 min and (e) flowing He for 60 min, at room temperature.

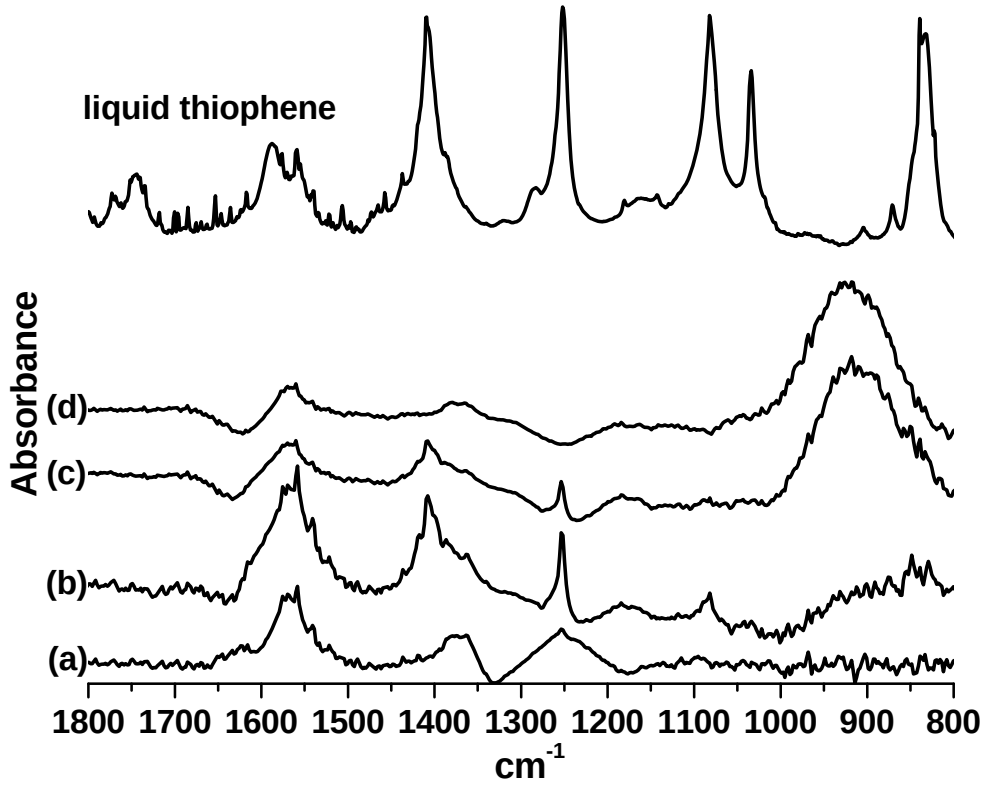

Figure **3-5**: IR spectra of thiophene adsorbed on oxidized $Ti_{0.9}Ce_{0.1}O_2$. (a) exposure to thiophene for 1 min, (b) exposure to thiophene for 60 min, (c) He flow for 1 min, and (d) He flow for 60 min, at room temperature.

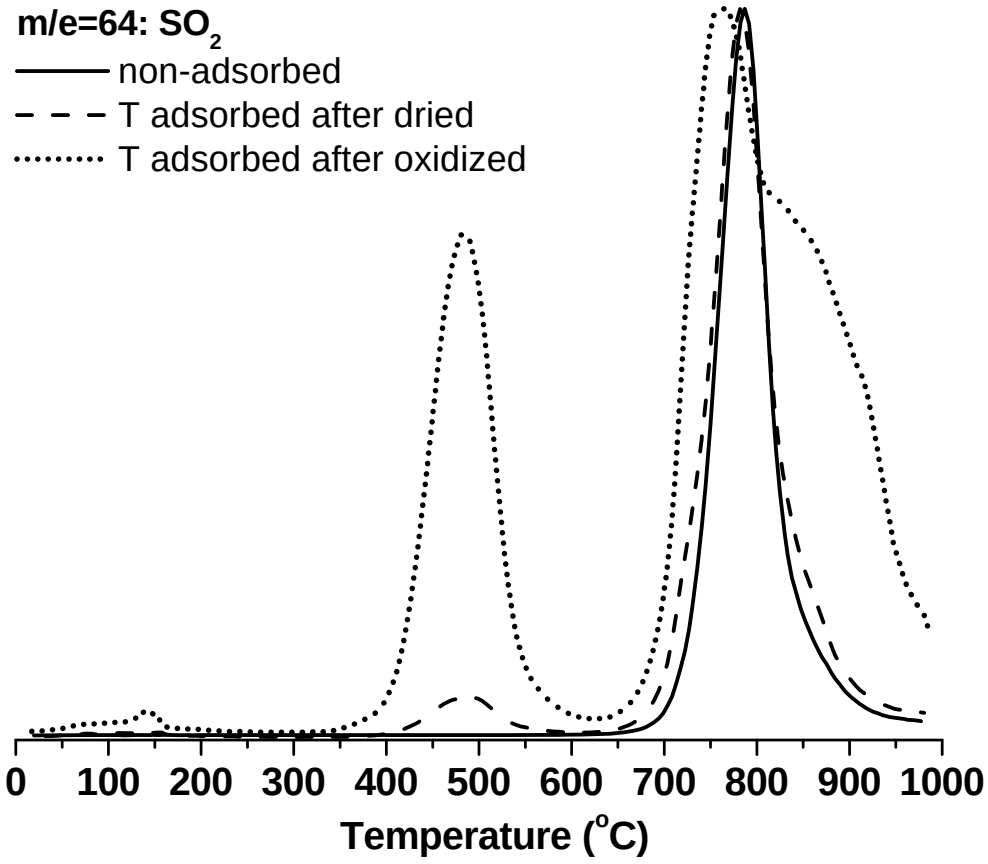

Figure **3-6**: TPD spectra of m/e=64 for non-adsorbed, vacuum-dried and oxidized $Ti_{0.9}Ce_{0.1}O_2$ oxide adsorbed thiophene in n-C_{10} solution (1000 ppmw-sulfur) at room temperature.

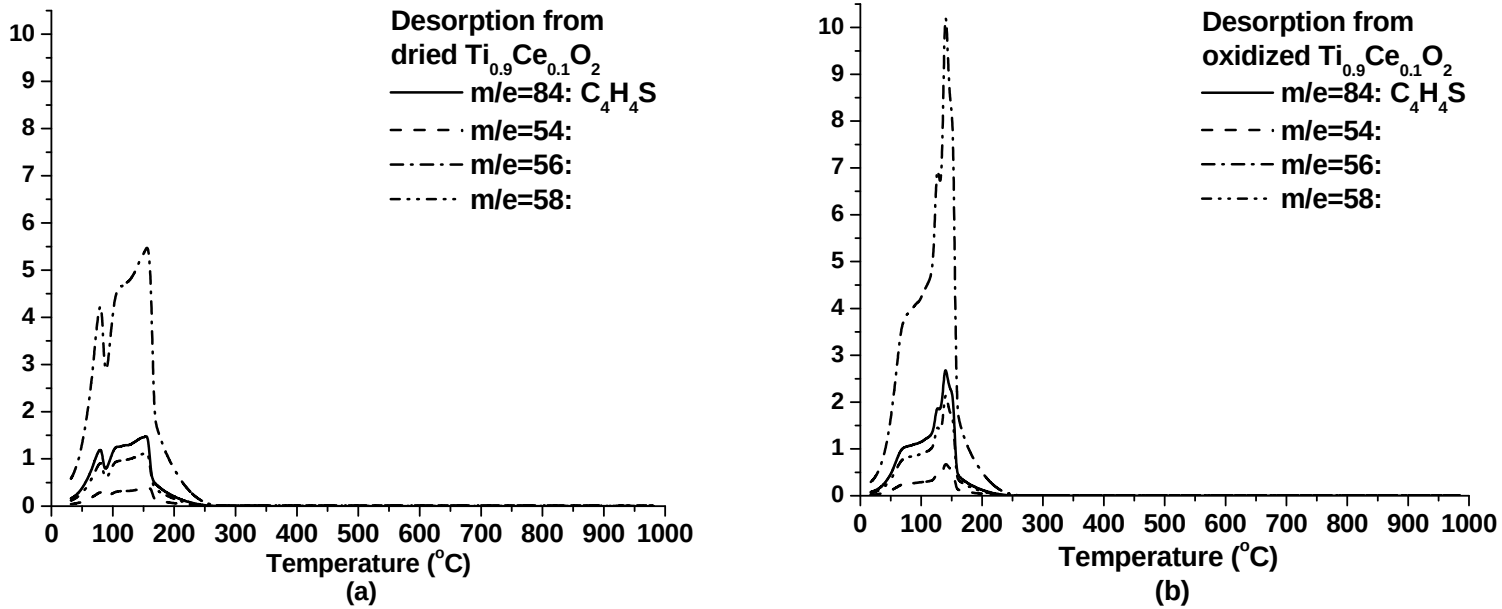

Figure **3-7**: TPD spectra of m/e=54, 56, 58 and 84 for (a) vacuum-dried and (b) oxidized $Ti_{0.9}Ce_{0.1}O_2$ oxide adsorbed thiophene in n-C_{10} solution (1000 ppmw-sulfur) at room temperature.

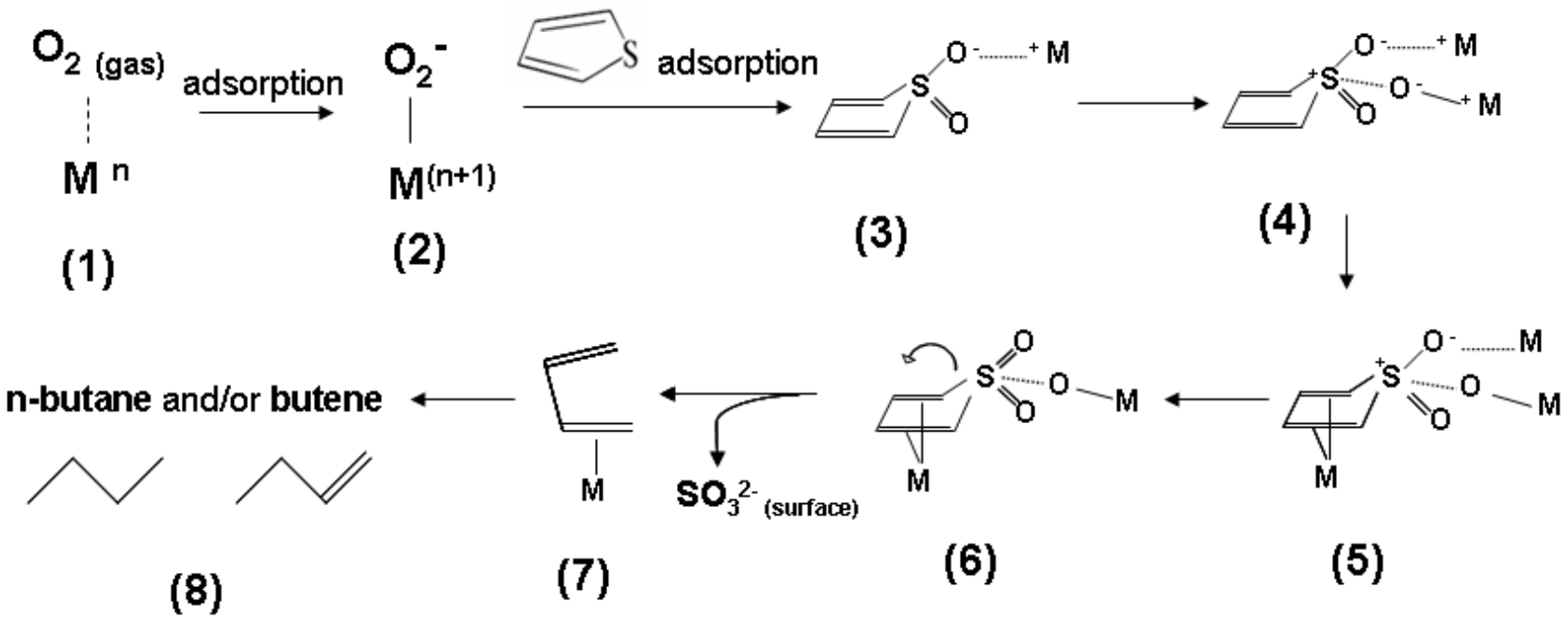

Figure **3-8**: Proposed adsorption pathway of thiophene over $Ti_{0.9}Ce_{0.1}O_2$ from this study

References:

(1) Song, C. S., An overview of new approaches to deep desulfurization for ultra-clean gasoline, diesel fuel and jet fuel. *Catalysis Today* **2003,** 86, (1-4), 211.

(2) Song, C.; Ma, X. L., New design approaches to ultra-clean diesel fuels by deep desulfurization and deep dearomatization. *Applied Catalysis B-Environmental* **2003,** 41, (1-2), 207.

(3) Babich, I. V.; Moulijn, J. A., Science and technology of novel processes for deep desulfurization of oil refinery streams: A review. *Fuel* **2003,** 82, (6), 607.

(4) Langner, J.; Rodhe, H.; Crutzen, P. J.; Zimmermann, P., Anthropogenic Influence on the Distribution of Tropospheric Sulfate Aerosol. *Nature* **1992,** 359, (6397), 712.

(5) Marcilly, C., Present status and future trends in catalysis for refining and petrochemicals. *Journal of Catalysis* **2003,** 216, (1-2), 47.

(6) Gates, B. C.; Topsoe, H., Reactivities in deep catalytic hydrodesulfurization: Challenges, opportunities, and the importance of 4-methyldibenzothiophene and 4,6-dimethyldibenzothiophene. *Polyhedron* **1997,** 16, (18), 3213.

(7) Topsoe, H.; Clausen, B. S.; Massoth, F. E., *Hydrotreating Catalysis*. ed.; Springer-Verlag: Berlin, 1996.

(8) Song, C. S.; Ma, X. L., Ultra-deep desulfurization of liquid hydrocarbon fuels: Chemistry and process. *International Journal of Green Energy* **2004,** 1, (2), 167.

(9) Hernandez-Maldonado, A. J.; Yang, R. T., Desulfurization of transportation fuels by adsorption. *Catalysis Reviews-Science and Engineering* **2004,** 46, (2), 111.

(10) Ma, X. L.; Sun, L.; Song, C. S., A new approach to deep desulfurization of gasoline, diesel fuel and jet fuel by selective adsorption for ultra-clean fuels and for fuel cell applications. *Catalysis Today* **2002,** 77, (1-2), 107.

(11) Watanabe, S. Selective and Regenerable Metal Oxide Adsorbents for the Removal of Sulfur from Liquid Fuels for Fuel Cell Applications. Master of Science, The Pennsylvania State University, University Park, Pennsylvania, 2004.

(12) Watanabe, S.; Velu, S.; Ma, X.; Song, C., New ceria-based selective adsorbents for removing sulfur from gasoline for fuel cell application. *Am. Chem. Soc., Div. Fuel Chem. Prepr.* **2003,** 48, (2), 695.

(13) Watanabe, S.; Ma, X.; Song, C. S., Selective sulfur removal from liquid hydrocarbons over regenerable CeO_2-TiO_2 adsorbents for fuel cell applications. *Am. Chem. Soc. Div. Fuel Chem. Prepr.* **2004,** 49, (2), 511.

(14) Tsyganenko, A. A.; Can, F.; Mauge, F., IR study of the adsorption and isotopic scrambling of thiophene on CaO. *Journal of physical Chemistry B* **2003,** 107, 8578.

(15) Quigley, W. W. C.; Yamamoto, H. D.; Aegerter, P. A.; Simpson, G. J.; Bussell, M. E., Infrared spectroscopy and temperature-programmed desorption study of adsorbed thiophene on gamma-Al_2O_3. *Langmuir* **1996,** 12, (6), 1500.

(16) Jirsak, T.; Dvorak, J.; Rodriguez, J. A., Chemistry of thiophene on ZnO, S/ZnO, and Cs/ZnO surfaces: Effects of cesium on desulfurization processes. *Journal of Physical Chemistry B* **1999,** 103, (26), 5550.

(17) Liu, G.; Rodriguez, J. A.; Hrbek, J.; Long, B. T.; Chen, D. A., Interaction of thiophene with stoichiometric and reduced rutile TiO_2(110) surfaces: role of Ti^{3+} sites in desulfurization activity. *Journal of Molecular Catalysis a-Chemical* **2003,** 202, (1-2), 215.

(18) Hedhili, M. N.; Yakshinskiy, B. V.; Schlereth, T. W.; Gouder, T.; Madey, T. E., The interactions of thiophene with polycrystalline UO_2. *Surface Science* **2005,** 574, (1), 17.

(19) Tarbuck, T. L.; McCrea, K. R.; Logan, J. W.; Heiser, J. L.; Bussell, M. E., Identification of the adsorption mode of thiophene on sulfided Mo catalysts. *Journal of Physical Chemistry B* **1998,** 102, (40), 7845.

(20) Mills, P.; Phillips, D. C.; Woodruff, B. P.; Main, R.; Bussell, M. E., Investigation of the adsorption and reactions of thiophene on sulfided Cu, Mo, and Rh catalysts. *Journal of Physical Chemistry B* **2000,** 104, (14), 3237.

(21) Wu, W. C.; Wu, Z. L.; Feng, Z. C.; Ying, P. L.; Li, C., Adsorption and reaction of thiophene and H_2S on Mo_2C/Al_2O_3 catalyst studied by in situ FT-IR spectroscopy. *Physical Chemistry Chemical Physics* **2004,** 6, (24), 5596.

(22) Wu, Z. L.; Li, C.; Wei, Z. B.; Ying, P. L.; Xin, Q., FT-IR spectroscopic studies of thiophene adsorption and reactions on Mo_2N/gamma-Al_2O_3 catalysts. *Journal of Physical Chemistry B* **2002,** 106, (5), 979.

(23) Nicholson, D. E., Identification of Adsorbed Species by Intrared Spectrometry. *Analytical Chemistry* **1962,** 34, (3), 370.

(24) Ratnasam.P; Fripiat, J. J., Surface Chemistry of Sulphides .1. Infra-red Study of Molybdenum and Germanium Sulphides and of Their Reaction with H_2, H_2O, Thiophene and Ethanethiol. *Transactions of the Faraday Society* **1970,** 66, (575), 2897.

(25) Mills, P.; Korlann, S.; Bussell, M. E.; Reynolds, M. A.; Ovchinnikov, M. V.; Angelici, R. J.; Stinner, C.; Weber, T.; Prins, R., Vibrational study of organometallic complexes with thiophene ligands: Models for adsorbed thiophene on hydrodesulfurization catalysts. *Journal of Physical Chemistry A* **2001,** 105, (18), 4418.

(26) Sengupta, S. K.; Ahn, H.; Whitten, J. E., Adsorption of thiophene on Al(111) and deposition of aluminum on condensed thiophene. *Surface Science* **2002,** 520, (3), 207.

(27) Whitten, J. E., Adsorption of thiophene and pyridine on W(110). *Surface Science* **2003,** 546, (2-3), 107.

(28) St Clair, T. P.; Oyama, S. T.; Cox, D. F., Adsorption and reaction of thiophene on alpha-Mo_2C(0001). *Surface Science* **2002,** 511, (1-3), 294.

(29) Huntley, D. R.; Mullins, D. R.; Wingeier, M. P., Desulfurization of thiophenic compounds by Ni(111): Adsorption and reactions of thiophene, 3-methylthiophene, and 2,5-dimethylthiophene. *Journal of Physical Chemistry* **1996,** 100, (50), 19620.

(30) Schoofs, G. R.; Preston, R. E.; Benziger, J. B., Adsorption and Desulfurization of Thiophene on Nickel(111). *Langmuir* **1985,** 1, (3), 313.

(31) Kobayashi, M.; Flytzani-Stephanopoulos, M., Reduction and sulfidation kinetics of cerium oxide and Cu-modified cerium oxide. *Industrial & Engineering Chemistry Research* **2002,** 41, (13), 3115.

(32) Watanabe, S.; Ma, X.; Song, C., Characterization of Structural and Surface Properties of $Ti_XCe_{1-X}O_2$ Mixed Oxides by XRD, XPS, TPR and TPD. **in submission**.

(33) Karvinen, S., The effects of trace elements on the crystal properties of TiO_2. *Solid State Sciences* **2003,** 5, (5), 811.

(34) Subrt, J.; Stengl, V.; Bakardjieva, S.; Szatmary, L., Synthesis of spherical metal oxide particles using homogeneous precipitation of aqueous solutions of metal sulfates with urea. *Powder Technology* **2006,** 169, (1), 33.

(35) Velu, S.; Ma, X. L.; Song, C. S., Selective adsorption for removing sulfur from jet fuel over zeolite-based adsorbents. *Industrial & Engineering Chemistry Research* **2003,** 42, (21), 5293.

(36) Smirnov, M. Y.; Kalinkin, A. V.; Pashis, A. V.; Sorokin, A. M.; Noskov, A. S.; Bukhtiyarov, V. I.; Kharas, K. C.; Rodkin, M. A., Comparative XPS study of Al_2O_3 and CeO_2 sulfation in reactions with SO_2, SO_2+O_2, SO_2+H_2O, and SO_2+O_2+H_2O. *Kinetics and Catalysis* **2003,** 44, (4), 575.

(37) Smirnov, M. Y.; Kalinkin, A. V.; Pashis, A. V.; Sorokin, A. M.; Noskov, A. S.; Kharas, K. C.; Bukhtiyarov, V. I., Interaction of Al_2O_3 and CeO_2 surfaces with SO_2 and SO_2+O_2 studied by X-ray photoelectron spectroscopy. *Journal of Physical Chemistry B* **2005,** 109, (23), 11712.

(38) Ferrizz, R. M.; Gorte, R. J.; Vohs, J. M., TPD and XPS investigation of the interaction of SO_2 with model ceria catalysts. *Catalysis Letters* **2002,** 82, (1-2), 123.

(39) Wagner, C. D.; Riggs, W. M.; Davis, L. E.; Moulder, J. F.; Muilenbedrg, G. E., *Handbook of X-Ray Photoelectron Spectroscopy*. ed.; Perkin-Elmer Corporation: Minnesota, 1978.

(40) Burroughs, P.; Hamnett, A.; Orchard, A. F.; Thornton, G., Satellite Structure in the X-Ray Photoelectron Spectra of some Binary and Mixide Oxides of Lanthanum and Cerium. *Journal of the Chemical Society-Dalton Transactions* **1976,** 17, 1686.

(41) Smith, K. E.; Mackay, J. L.; Henrich, V. E., Interaction of SO_2 with Nearly Perfect and Defect TiO_2(110) Surfaces. *Physical Review B* **1987,** 35, (11), 5822.

(42) Sayago, D. I.; Serrano, P.; Bohme, O.; Goldoni, A.; Paolucci, G.; Roman, E.; Martin-Gago, J. A., Adsorption and desorption of SO_2 on the TiO_2(110)-(1X1) surface: A photoemission study. *Physical Review B* **2001,** 6420, (20).

(43) Sayago, D. I.; Serrano, P.; Bohme, O.; Goldoni, A.; Paolucci, G.; Roman, E.; Martin-Gago, J. A., A photoemission study of the SO_2 adsorption on TiO_2 (110) surfaces. *Surface Science* **2001,** 482, 9.

(44) Raza, H.; Harte, S. P.; Muryn, C. A.; Wincott, P. L.; Thornton, G.; Casanova, R.; Rodriguez, A., NEXAFS studies of the reaction of SO_2 with TiO_2(100)-(1x1) and -(1x3). *Surface Science* **1996,** 366, (3), 519.

(45) Liu, G.; Rodriguez, J. A.; Chang, Z.; Hrbek, J.; Gonzalez, L., Adsorption of methanethiol on stoichiometric and defective TiO_2(110) surfaces: A combined experimental and theoretical study. *Journal of Physical Chemistry B* **2002,** 106, (38), 9883.

(46) Watanabe, S.; Ma, X.; Song, C., **in submission**.

(47) Bozon-Verduraz, F.; Bensalem, A., IR Studies of Cerium Dioxide : Influence of Impurities and Defects. *Journal of the Chemical Society-Faraday Transactions* **1994,** 90, (4), 653.

(48) Li, C.; Domen, K.; Maruya, K.; Onishi, T., Dioxygen Adsorption on Well-Outgassed and Partially Reduced Cerium Oxide Studied by FT-IR. *Journal of the American Chemical Society* **1989,** 111, (20), 7683.

(49) Li, C.; Domen, K.; Maruya, K.; Onishi, T., IR Spectra of Dioxygen Species Formed on CeO_2 at Room-Temperature. *Journal of the Chemical Society-Chemical Communications* **1988**, (23), 1541.

(50) Li, C.; Domen, K.; Maruya, K.; Onishi, T., Oxygen-Exchange Reactions over Cerium Oxide - an FT-IR Study. *Journal of Catalysis* **1990,** 123, (2), 436.

(51) Che, M.; Tench, A. J., Characterization and Reactivity of Molecular Oxygen Species on Oxide Surfaces. *Advances in Catalysis* **1983,** 32, 1.

(52) Bielanski, A.; Haber, J., *Oxygen in Catalysis*. ed.; Marcel Dekker, Inc.: New York, 1991.

(53) Rico, M.; Orza, J. M.; Morcillo, J., Fundamental vibrations of thiophene and its deuterated derivatives. *Spectrochimica Acta* **1965,** 21, 689.

(54) El-Azhary, A. A.; Hilal, R. H., Vibrational analysis of the spectra of furan and thiophene. *Spectrochimica Acta Part a-Molecular and Biomolecular Spectroscopy* **1997,** 53, (9), 1365.

(55) Nakamoto, K., *Infrared and Raman Spectra of Inorganic and Coordination Compounds Part B: Applications in Coordination, Organometallic, and Bioinorganic Chemistry*. Fifth ed.; John Wiley & Sons, Inc.: New York, 1997.

(56) Saur, O.; Bensitel, M.; Saad, A. B. M.; Lavalley, J. C.; Tripp, C. P.; Morrow, B. A., The Structure and Stability of Sulfated Alumina and Titania. *Journal of Catalysis* **1986,** 99, (1), 104.

(57) Waqif, M.; Saur, O.; Lavalley, J. C.; Perathoner, S.; Centi, G., Nature and Mechanism of Formation of Sulfate Species on Copper Alumina Sorbent Catalysts for SO_2 Removal. *Journal of Physical Chemistry* **1991,** 95, (10), 4051.

(58) Bensitel, M.; Saur, O.; Lavalley, J. C.; Morrow, B. A., An Infrared Study of Sulfated Zirconia. *Materials Chemistry and Physics* **1988,** 19, (1-2), 147.

(59) Luo, T.; Vohs, J. M.; Gorte, R. J., An examination of sulfur poisoning on Pd/ceria catalysts. *Journal of Catalysis* **2002,** 210, (2), 397.

(60) Tanaka, K. I., Intermediate of Oxygen-Exchange Reaction over Illuminated Titanium-Dioxide. *Journal of Physical Chemistry* **1974,** 78, (5), 555.

(61) Sato, S.; Kadowaki, T.; Yamaguti, K., Photocatalytic Oxygen Isotopic Exchange between Oxygen Molecule and the Lattice Oxygen of TiO_2 Prepared from Titanium Hydroxide. *Journal of Physical Chemistry* **1984,** 88, (14), 2930.

(62) Yu, J. C.; Lin, J.; Lo, D.; Lam, S. K., Influence of thermal treatment on the adsorption of oxygen and photocatalytic activity of TiO_2. *Langmuir* **2000,** 16, (18), 7304.

(63) Takami, A.; Harada, K.; Tsushio, Y., Behavior of oxygen of cerium composite oxides on catalytic combustion of carbon particulate. *Journal of the Japan Petroleum Institute* **2007,** 50, (2), 102.

(64) Sanjines, R.; Tang, H.; Berger, H.; Gozzo, F.; Margaritondo, G.; Levy, F., Electronic-Structure of Anatase TiO_2 Oxide. *Journal of Applied Physics* **1994,** 75, (6), 2945.

(65) Descorme, C.; Madier, Y.; Duprez, D., Infrared study of oxygen adsorption and activation on cerium-zirconium mixed oxides. *Journal of Catalysis* **2000,** 196, (1), 167.

(66) Suda, Y., Interaction of Benzene, Cyclohexene, and Cyclohexane with the Surface of Titanium-Dioxide (Rutile). *Langmuir* **1988,** 4, (1), 147.

(67) Corma, A.; Garcia, H., Lewis Acids as Catalysts in Oxidation Reactions: Form Homogeneous to Heterogeneous Systems. *Chemical Reviews* **2002,** 102, 3837.

(68) Brown, K. N.; Espenson, J. H., Stepwise oxidation of thiophene and its derivatives by hydrogen peroxide catalyzed by methyltrioxorhenium(VII). *Inorganic Chemistry* **1996,** 35, (25), 7211.

(69) Attar, A.; Corcoran, W. H., Desulfurization of Organic Sulfur-Compounds by Selective Oxidation .1. Regenerable and Nonregenerable Oxygen Carriers. *Industrial & Engineering Chemistry Product Research and Development* **1978,** 17, (2), 102.

(70) Pouzet, P.; Erdelmeier, I.; Ginderow, D.; Mornon, J. P.; Dansette, P.; Mansuy, D., Thiophene S-Oxides - Convenient Preparation, First Complete Structural Characterization and Unexpected Dimerization of One of Them, 2,5-Diphenylthiophene-1-Oxide. *Journal of the Chemical Society-Chemical Communications* **1995**, (4), 473.

(71) Heldt, W. Z., Coupling of Aromatic Rings .I. Pyrolysis of Aryl Sulfides and Aryl Sulfones to Substituted Biphenyls. *Journal of Organic Chemistry* **1965,** 30, (11), 3897.

(72) Pitchen, P.; Dunach, E.; Deshmukh, M. N.; Kagan, H. B., An Efficient Asymmetric Oxidation of Sulfides to Sulfoxides. *Journal of the American Chemical Society* **1984,** 106, (26), 8188.

(73) McGregor, S. D.; Lemal, D. M., Fragmentations . Thermal 5 to 4+1 Reaction. *Journal of the American Chemical Society* **1966,** 88, (12), 2858.

(74) Chou, T. S.; Chang, S. Y., A Convenient Method for the Extrusion of Sulfur-Dioxide from 2,2,5,5-Tetrasubstituted 3-Sulfolenes. *Journal of the Chemical Society-Perkin Transactions 1* **1992**, (12), 1459.

(75) Mock, W. L., Stereochemical Consequences of Orbital Symmetry Control in Reversible Combining of Sulfur-Dioxide with Conjugated Systems (Sulfolene Reactions). *Journal of the American Chemical Society* **1975,** 97, (13), 3666.

(76) LaCount, R. B.; Friedman, S., Oxidation of Dibenzothiophene and Reaction of Dibenzothiophene 5,5-Dioxide with Aqueous Alkali. *Journal of Organic Chemistry* **1977,** 42, (16), 2751.

(77) Shiraishi, Y.; Tachibana, K.; Hirai, T.; Komasawa, I., Photochemical production of biphenyls from oxidized sulfur compounds obtained by oxidative desulfurization of light oils. *Energy & Fuels* **2003,** 17, (1), 95.

(78) Jenks, W. S.; Taylor, L. M.; Guo, Y. S.; Wan, Z. H., Photochemistry of Dibenzothiophene-S,S-Dioxide - Reactions of a Highly Constrained Biradical. *Tetrahedron Letters* **1994,** 35, (39), 7155.

Chapter 4

Role of $Ti_{0.9}Ce_{0.1}O_2$ Mixed Oxide as Oxidative Regenerable Adsorbent for the Ultra-Deep Ultra Deep Desulfurization of Jet Fuel

Abstract

High surface area-mesoporous $Ti_{0.9}Ce_{0.1}O_2$ oxide-based adsorbent was studied for adsorptive desulfurization of a jet fuel (JP-5: 1055 ppmw of sulfur) using several techniques including GC-PFPD, TPD and XPS. $Ti_{0.9}Ce_{0.1}O_2$ oxide-based adsorbent selectively adsorbes sulfur and achieved the sulfur reduction of the jet fuel from 1055 ppmw to lower than 1 ppmw in multiple cycles of adsorption in fixed-bed flow system and regeneration in-situ by oxidative teeatment using air. This ultra deep desulfurization was attributed to the selective sulfur removal by the adsorbent. The analysis of treated fuels indicated that $Ti_{0.9}Ce_{0.1}O_2$ oxide-based adsorbent is selective towards sulfur atom. The sulfur atom in the organic sulfur compounds was oxidized, while the surface (Ti^{4+}, Ce^{4+}) cations of adsorbent were reduced simultaneously upon the adsorption of sulfur compounds. The sulfur atom oxidized by surface oxygen may be removed from the organic sulfur molecules, and remained as sulfite and sulfate species the adsorbent surface. These results are consistent with the previously proposed mechanism of adsorptive desulfurization over the $Ti_{0.9}Ce_{0.1}O_2$ oxide-based adsorbent. The $Ti_{0.9}Ce_{0.1}O_2$ mixed oxide-based adsorbent shows excellent redox property, which makes it possible to carry out the multiple cycles of adsorptive desulfurization in flow system and oxidative regeneration using air.

4.1 Introduction

Deep desulfurization of liquid fuels has received much attention due to the stringent environmental regulations on sulfur concentrations in transportation fuels. In year 2006, new regulations on sulfur concentrations in transportation fuels previously announced by the U.S. Environmental Protection Agency were implemented in order to improve the quality of the air.[6] The maximum allowed sulfur levels of transportation fuels were decreased from about 350 ppmw to less than 30 ppmw for gasoline, and from 500 to 15 ppmw for diesel fuel.[6] Further lower sulfur contents may be regulated for transportation fuels and new regulations are also exptected for off-road fuels that usually have higher sulfur contents such as those for construction vehicles. Therefore, its is highly desirable to develop more effective and efficient technologies for removing sulfur from the petroleum feed stocks that are becoming heavier and higher in sulfur contents.

As a common industrial process, hydrodesulfurization (HDS) has been utilized to remove sulfur from petroleum feed stocks. This process can be used to meet the current regulations. However, HDS for a deeper desulfurization requires higher temperature, higher pressure and higher hydrogen consumption in addition to the larger catalyst bed volume due to the lower reactivity of alkylated benzothiophene- and dibenzothiophene-type compounds.[6, 30, 66, 67] Thus, extensive research has been carried out on the improvement of HDS and the exploration of alternative processes for the production of ultra clean fuels.[6, 13] Among these processes, adsorptive desulfurization (ADS) of liquid hydrocarbon fuels has recently received much attention for being able to produce ultra clean fuel without using hydrogen.[6, 12, 13, 27] The major advantages of ADS are: (1) the

refractory sulfur compounds (thiophenic and alkylated thiophenic compounds) can be removed under mild condition (at lower temperature and under lower pressure) without using hydrogen gas, (2) there is no need for pressurized vessel and no need for high-temperature and high-pressure operations, and (3) it is a very simple process,[6, 10, 18] Several types of materials have been investigated for their use as adsorbents. The metal oxide-based adsorbents, particularly TiO_2-CeO_2 mixed oxides, has shown promising results in multiple cycles ADS of liquid hydrocarbon fuels.[16, 17] Due to the simplicity of regeneration by oxidation, we have explored the use of metal oxides for developing an effective adsorptive system.[16-18]

In a prior work, a detailed study on adsorption mechanism of thiophenic compounds over $Ti_{0.9}Ce_{0.1}O_2$ oxide was conducted using x-ray photoelectron spectroscopy (XPS), diffuse reflectance infrared fourier transform (DRIFT) spectroscopy and temperature-programmed desorption (TPD).[95] These results suggested that adsorption of thiophene occurs through its sulfur atom with the interaction of surface oxygen to form SO_X species over the oxide surface. Thiophene dissociatively adsorbed over $Ti_{0.9}Ce_{0.1}O_2$, and sulfur atom was removed from thiophene molecule.[128] This mechanistic study suggested that this process using $Ti_{0.9}Ce_{0.1}O_2$ adsorbent is promising due to the high efficiency and simplicity for sulfur removal.

The aim of the present work is to understand the role of $Ti_{0.9}Ce_{0.1}O_2$ mixed oxide as an oxidatively regenerrable adsorbent for adsorptive desulfurization of a real jet fuel by examining the effect of oxidative treatment, the adsorption selectivity and the changes of the Ti and Ce species in the adsorbent during the sulfur adsorption removal and oxidative regeneration. The adsorption selectivity was estimated by analyzing the sulfur

compounds in the desulfurized fuels by GC-PFPD. The role of $Ti_{0.9}Ce_{0.1}O_2$ adsorbent in adsorptive desulfurization was investigated by examining the surface properties of the fresh activated, spent and regenerated adsorbents using XPS and TPD.

4.2 Experimental

4.2.1 Preparation

Preparation of metal oxide adsorbent, $Ti_{0.9}Ce_{0.1}O_2$, was described in section 3.2.1 of Chapter 3.

4.2.2 Adsorptive Desulfurization of JP-5

Adsorptive desulfurization was conducted using a jet fuel (JP-5) containing 1055 ppmw in a fixed-bed flow system. The powder adsorbents were packed in a stainless steel column with an internal diameter of a 4.6 mm and length of 150 mm. The adsorbent bed volume was 2.49 cc. The pretreatment includes activation of adsorbent under the dry air flow at 375 ^{o}C for 2 hours prior to fuel flow for sulfur removal. The JP-5 fuel was fed into the column using an HPLC pump. The feed flow rate was 0.05 cc/min with LHSV: of 1.2 h^{-1}. The adsorption was conducted at room temperature under atmospheric pressure. After adsorption, 100 cc/min of air was flown into the column for 5 min to remove the liquid fuel from the adsorbent bed. Subsequently, the temperature of the adsorbent bed was increased up to 400 ^{o}C within 10 min, and the temperature was kept constant for 30 min. Air flow was continued until the bed was cooled down to room

temperature. Then the subsequent cycle of adsorptive desulfurization test was conducted. Antek 9000 Series Sulfur Analyzer (detection limit 0.5 ppmw) was used to determine the total sulfur concentration of the treated JP-5.

4.2.3 Characterization

Gas chromatograph with pulsed flame photometric detector (GC-PFPD, O.I. Analytical 5380) was used for identification of the sulfur compounds in the JP-5 fuel. A Hewlett 5890 Packard series II gas chromatograph with a capillary column, XTI-5 (Restek, bonded 5 %, 30 m x 0.25 mm ID x 0.25 μm film thickness) and a split mode injector (ratio: 100:1) was used with ultra-high purity helium as a carrier gas. The injector temperature was kept at 290 ˚C. The column temperature was set at 50 ˚C for 4 min, 6 ˚C/min from 50 ˚C to 290 ˚C for GC-PFPD analysis.

The Brunauer, Emmett, and Teller (BET) surface area and pore size distribution of metal oxides were obtained from 49-point nitrogen adsorption/desorption analysis with a Micrometrics ASAP 2020. All samples were outgassed at 220 ^{o}C prior to the adsorption-desorption measurements. The pore size distribution was calculated by applying the Barrett-Joyner-Halenda (BJH) method on the desorption branch of isotherm curve. Analysis parameters were set as follows: five points multiple BET points with relative pressure (P/P_o) from 0.05 to 0.35.

X-ray photoelectron spectroscopic (XPS) analysis was conducted on a Kratos Analytical Axis Ultra spectrometer with monochromatic aluminum (1486.6 eV) X-ray source operated at 14 kV and 20 mA. The first analysis was conducted to investigate the

effect of pretreatment on chemical state of the adsorbent surface. A set of samples was prepared by treating adsorbent at 100 ^{o}C in an oven for 2 hours and oxidized at 220 ^{o}C under oxygen flow for 2 hours. The second set of analysis was conducted to clarify the chemical state of adsorbent surface before and after sulfur removal of JP-5, and after oxidative regeneration. Three samples were prepared for this analysis. The first sample was oxidatively pretreated $Ti_{0.9}Ce_{0.1}O_2$ oxide. The second sample was dried at 80 ^{o}C after conducting first cycle of adsorptive desulfurization of JP-5. The third sample was oxidatively regenerated $Ti_{0.9}Ce_{0.1}O_2$ oxide after third cycle of adsorptive desulfurization. The sample powders were pressed into 5mm x 5mm 3M double-sided tape, and visualized by a stereo microscope to ensure complete coverage and powder uniformity over the tape. Sample height positions were set from O 1s signal at 529 eV followed by changing of lateral coordinates such that the measured signal from the sample powders were maximized. Thus, any possible signal from the 3M double sided tape was minimized. The 3M tape was examined independently and the characteristic shape of the C 1s line was not found when compared to the C 1s line collected from these sample powders. As a reference, we used the C 1s signal of the adventitious carbon (carbon of any surface adsorbed), which was fixed at 285 eV. A survey scan was initially recorded for the sample to identify elements present with analyzer pass energy of 80 eV. Composition and chemical states were determined from the charge corrected high resolution scans with analyzer pass energy of 20 eV. The amount of Ce(III) was estimated from the intensity of the v_0 (u_0) and v' (u') lines,[61, 129] according to the following equation:

$$Ce^{III}(\%) = \frac{v_0 + v' + u_0 + u'}{\Sigma(v+u)}$$

Temperature-programmed desorption (TPD) measurements were conducted using TGA 2050 (TA Instrument) in UHV system (2.3×10^{-6} mbar) outfitted with ThermoStar G301 (Pfeiffer) quadrupole mass spectrometer capable of monitoring 64 masses simultaneously. Fresh and spent $Ti_{0.9}Ce_{0.1}O_2$ adsorbents for desulfurization of JP-5 fuel were prepared for TPD experiments. The fresh and spent adsorbent samples were placed in an alumina holder, and TPD experiments were carried out at a heating rate of 10 ^{o}C/min under 130 cc/min argon gas flowing while acquiring data at a sampling frequency of 4 points/^{o}C.

4.3 Results and Discussion

4.3.1 Nitrogen Adsorption-Desorption Isotherm

Figure **4-1** shows shows the nitrogen adsorption-desorption isotherm of the fresh $Ti_{0.9}Ce_{0.1}O_2$ mixed oxide adsorbent. The isotherm of $Ti_{0.9}Ce_{0.1}O_2$ exhibits the Type IV adsorption-desorption isotherm according to IUPAC classification.[130] The hysteresis loop observed in this isotherm can be attributed to capillary condensation in the mesopore. Figure **4-2** shows that the average pore size of $Ti_{0.9}Ce_{0.1}O_2$ before 1st cycle of ADS and after regeneration of 3rd cycle. As N_2 adsorption-desorption isotherm indicated, average pore size of the fresh $Ti_{0.9}Ce_{0.1}O_2$ was 36 Å. This mixed oxide adsorbent is classified as a mesoporous material. The average pore size of the spent adsorbent was 48 Å. The pore size of the adsorbent was increased after three cycles of adsorptive desulfurization and regeneration.

Table **4-1** shows the specific surface area, pore volume and average pore size of the fresh and regenerated $Ti_{0.9}Ce_{0.1}O_2$. The surface area of the fresh $Ti_{0.9}Ce_{0.1}O_2$ adsorbent was 321.0 m^2/g. The surface area of the spent adsorbent was 171.9 m^2/g. Therefore, it is clear that the surface area of the adsorbent decreased was significantly after three ADS cycles. This increase of the pore size and decrease of surface area of adsorbent was associated with oxidative regeneration. Although the regeneration temperature was lower than calcination temperature, the decrease of surface area was

attributed to the sintering caused by higher rise of temperature due to the oxidative regeneration.

4.3.2 Adsorptive Desulfurization of JP-5 and Oxidative Regeneration

The breakthrough curves of sulfur adsorption removal from the JP-5 using the $Ti_{0.9}Ce_{0.1}O_2$ mixed oxide are shown in Figure **4-3**. Although JP-5 contains various kinds of organic sulfur compounds, as shown in Figure **4-4** adsorptive desulfurization using the $Ti_{0.9}Ce_{0.1}O_2$ mixed oxide adsorbent accomplished the major reduction of sulfur from 1055 ppmw to lower than 1 ppmw at room temperature without using any hydrogen gas. This ultra deep desulfurization was attributed to the selectivity of $Ti_{0.9}Ce_{0.1}O_2$ mixed oxide adsorbent towards the sulfur compounds.

Several researchers showed that thiophenic compounds and co-existing aromatics compete for the surface sites on the adsorbents.[10, 15, 19, 131] The JP-5 fuel used for this study contains about 0.1 wt% of sulfur, and aromatic content of JP-5 jet fuels could be up to 25 % which is the maximum allowed aromatics content.[132] Thus, the selectivity of the $Ti_{0.9}Ce_{0.1}O_2$ adsorbent developed in our laboratory towards sulfur compounds in the real jet fuel is significantly high. The sulfur concentration in the effluent gradually increased up to 100 ppmw. After 6 gram of treated fuel per gram of adsorbent, the sulfur concentration in the effluent significantly increased.

For the first cycle of sulfur removal, the breakthrough adsorption capacity of the $Ti_{0.9}Ce_{0.1}O_2$ mixed oxide adsorbent at the sulfur level of 30 ppmw in the effluent was 3.9 mg-S/g-Ads (milligram of sulfur per gram of the adsorbent). This value corresponds to

5.2 mL-fuel/g-Ads (milliliter of fuel per gram of the adsorbent) for the breakthrough volume. Subsequently, the oxidative regeneration was conducted, and second and third cycle sulfur removal was employed. The sulfur level was significantly reduced from 1055 ppmw in second and third cycle of ADS as well. The corresponding breakthrough capacities were 3.5 and 3.0 mg-S/g-Ads., respectively (Figure **4-3**). In contrast to the sulfur removing capacity in first cycle, the loss of the capacity in second cycle was 10 % and 21 % in the third cycle. This reduction of sulfur removing capacity resulted from the reduction of surface area (Table **4-1**). However, oxidative regeneration of $Ti_{0.9}Ce_{0.1}O_2$ mixed oxide adsorbent effectively recovered the sulfur removal capacity at 400 ^{o}C under air flow.

The sulfur compounds in JP-5 were identified by a GC-PFPD. The resulting chromatograms are shown in Figure **4-4**. Alkylated benzothiophenes and some alkylated thiophenes were observed as the main sulfur compounds in the GC-PFPD chromatogram of JP-5. Among the alkylated benzothiophenes, 2,3-dimethyl-benzothiophene (2,3-DMBT) and 2,3,7-thrimethyl-benzothiophene are the major constituents of organic sulfur compounds in JP-5 jet fuel.

The distribution of sulfur compounds in the treated JP-5 is shown in Figure **4-4**. Alkylated benzothiophenes were presented in the treated fuel fraction containing 7 ppmw of sulfur, The intense peak corresponding to 2,3,7-TMBT appeared in the effluent containing 58 ppmw of sulfur. This result suggest that 2,3,7-TMBT was not selectively removed. Our previous study indicated that thiophenic compounds mainly adsorb through their sulfur atom over the oxide-based adsorbent. Thus, the presence of 2,3,7-TMBT in the effluent was attributed to the steric hindrance by the 2 and 7 positions of alkyl group.

This result concurs that selective sulfur removal of thiophenic compounds over $Ti_{0.9}Ce_{0.1}O_2$ adsorbent takes place through their sulfur atom. The high peak intensity of 2,3,7-TMBT was observed in the effluent containing 84 and 101 ppmw of sulfur along with that of 2,3-DMBT. This result indicates that the 2 and 7 positions of alkyl groups affects the adsorption due to the steric hindrance because the selective adsorption of organic sulfur compounds takes place through the interaction of sulfur atom of the thiophenic compounds with the surface sites on $Ti_{0.9}Ce_{0.1}O_2$ adsorbent.

In the GC-PFPD chromatogram of treated JP-5, a new peak appeared at the retention time 34.2 min in addition to the 2,3-DMBT and 2,3,7-TMBT. This peak could be assigned to oxidized sulfur compounds, such as sulfoxide or sulfone via the comparison with the literature data.[133] The formation of oxidized sulfur compounds is in good agreement with a previously proposed adsorption mechanism of thiophene over the $Ti_{0.9}Ce_{0.1}O_2$ adsorbent.[95] The analysis of treated JP-5 indicates that the adsorption of sulfur compounds occur through the sulfur atom with surface oxygen to form sulfoxide/sulfone species.

4.3.3 XPS

XPS spectra of $Ti_{0.9}Ce_{0.1}O_2$ before and after oxidative treatment are shown in Figure **4-5**. The labels of peaks used in Ce 3d identification were established by Burroughs et al.[56] V and U are used for convenience indicating the spin-orbit coupling $3d_{5/2}$ and $3d_{3/2}$, respectively. The peaks referred to as v, v" and v"' are contributed by Ce^{4+} (CeO_2), and assigned to a mixture of Ce IV ($3d^9 4f^2$) O ($2p^4$), Ce IV ($3d^9 4f^1$) O ($2p^5$)

and Ce IV ($3d^9 4f^0$) O ($2p^6$), respectively. The same peak assignment is applied to u structures. The peaks, v_o and v', are assigned to a mixture of Ce III ($3d^9 4f^2$) O ($2p^5$) and Ce III ($3d^9 4f^1$) O ($2p^6$), respectively.

The influence of the oxidative treatment on Ce in $Ti_{0.9}Ce_{0.1}O_2$ is shown in Figure **4-5**. Intense peaks were found at 882.9, 889.2, 898.6 901.6, and 917.0 eV in the Ce 3d spectra of Figure **4-5**-(a) and **4-5**-(b). These peaks indicate that the dominant oxidation state of the surface Ce is tetravalent. In comparison to the spectrum of the dried adsorbent, the intensities for v' and u' decreased after oxidation. This decrease was attributed to oxidation of surface Ce. The peak deconvolution by curve fitting procedure indicated the concentration of Ce^{3+} decreased from 23.0 to 35.9 %. This result suggests that oxidative treatment oxidized Ce^{3+} in the sample to Ce^{4+} in the treatment process.

The binding energy of Ti $2p_{3/2}$ of dried $Ti_{0.9}Ce_{0.1}O_2$ is 458.4 eV. This corresponds to the average valence state of surface Ti at about 3.6 based on the peak position of Ti $2p_{3/2}$ of TiO_2.[57-59] After the oxidative treatment, the binding energy of Ti $2p_{3/2}$ of the adsorbent shifted to 458.7 eV. This peak shift corresponds to the oxidation of surface Ti cation to tetravalent. The oxidation of Ce and Ti were attributed to the interaction of molecular oxygen with the surface reduced center by transfer of electrons. This result is in good agreement with our previous study using in-situ IR spectroscopy.[18] Thus, oxidation of the Ce and Ti cations and formation of active oxygen species (O_2^-) take place in the oxidative pretreatment.

Figure **4-6** shows the results of XPS analysis in Ce 3d spectra of $Ti_{0.9}Ce_{0.1}O_2$ before and after the first adsorptive desulfurization of JP-5 and after the third oxidative regeneration. The intensities in Ce 3d XPS peaks changed at 882.9, 886.0, 898.6, 901.5,

904.4 and 916.9 eV. These changes reflect the changes of Ce^{3+} and Ce^{4+} concentrations. By peak deconvolution via the curve-fitting procedure, we found that the concentration of Ce^{3+} increased from 23.0 to 50.5 % after sulfur adsorption. This trend reveals the surface reduction of Ce^{4+} species following the adsorption of organic sulfur compounds. On the other hand, the surface Ce^{3+} decreased from about 50% to 24 % after oxidative regeneration in air. Thus the oxidation involves regeneration of Ce^{4+} species while the sulfur adsorption leads to more Ce^{3+} species on the surface.

The above XPS results reveal that reduction-oxidation cycle of surface Ce is involved in the adsorptive desulfurization-regeneration cycle. Our previous study showed that thiophenic compounds adsorb through their sulfur atom with the surface oxygen of the adsorbent.[95] The formation of sulfite/sulfate was observed in the adsorption of thiophenic compounds. Therefore, the surface Ce serves as indirect oxidizing agent by receiving electrons through the oxygen. The accepted electron may be taken by the oxygen in oxidative regeneration. Thus the redox property of Ce should be a significant factor and may be important in multiple cycles of adsorptive sulfur removal from JP-5 jet fuel.

Figure **4-7** shows the Ti $2p_{3/2}$ XP spectra before and after sulfur adsorption from JP-5 and after oxidative regeneration of the adsorbent. The Ti $2p_{3/2}$ peak shifted from 458.7 to 458.4 eV after the sulfur adsorption. This shift is characteristic of reduction of Ti species on the surface of $Ti_{0.9}Ce_{0.1}O_2$ adsorbent. After the oxidative regeneration, the Ti $2p_{3/2}$ peak shifted back from 458.4 to 458.7 eV. This shift corresponds to oxidation of Ti species on the surface of $Ti_{0.9}Ce_{0.1}O_2$ adsorbent. Surface Ti showed an excellent redox property, in a way similar to the trends observed for the surface Ce species in Figure 6. It

is clear that the oxidation-reduction cycle of Ti species plays an important role in the process of adsorptive desulfurization with regeneration.

The oxidation or reduction of Ce and Ti species is involved in all the major steps including pretreatment, adsorption of sulfur compounds and regeneration of the used adsorbent in air. The redox property of the adsorbent was found to be an important property for multiple cycles of adsorptive desulfurization. This redox property contributes to form the active surface oxygen species and to oxidize the sulfur atom of thiophenic compounds. Due to the excellent redox property of $Ti_{0.9}Ce_{0.1}O_2$ adsorbent, multiple cycles of adsorptive desulfurization of liquid hydrocarbons can proceed at room temperature, ambient pressure and no hydrogen consumption with oxidative regeneration.

4.3.4 TPD

Identification of adsorbates was conducted by temperature-programmed desorption accompanying mass spectrometry. Figure **4-8** shows the TPD profiles of species with m/e = 64 corresponding to mass-to-charge ratio of SO_2 for $Ti_{0.9}Ce_{0.1}O_2$ before and after adsorption of sulfur compounds from JP-5 jet fuel. Intense peaks appeared with the maximum desorption rate at 795 ^oC for the fresh $Ti_{0.9}Ce_{0.1}O_2$ adsorbent. This desorption peak corresponds to sulfate species.[108] Since this adsorbent sample was not exposed to fuel prior to the TPD, these peaks can be attributed to residue of sulfate species in Ti precursor.

In addition, the desorption profiles of $Ti_{0.9}Ce_{0.1}O_2$ adsorbent used for adsorption desulfurization of JP-5 shows the desorption peak at 745 and 860 ^oC corresponding to

sulfate species. The TPD profiles with the maximum desorption rate at 860 ^{o}C for spent adsorbent could correspond to that appeared at 795 ^{o}C for fresh adsorbent based on the similar desorption patterns. In our previous study, the desorption profiles of thiophene adsorbed oxidized $Ti_{0.9}Ce_{0.1}O_2$ showed the maximum SO_2 desorption peak at 765 ^{o}C with TPD peak shoulder extending to 1000 ^{o}C.[95] These results suggest that sulfate formation occurred in adsorptive desulfurization over oxidized $Ti_{0.9}Ce_{0.1}O_2$. Furthermore, desorption peak of SO_2 was observed at 465 ^{o}C for the spent $Ti_{0.9}Ce_{0.1}O_2$ adsorbent. This peak was attributed to decomposition of sulfite species. Similar TPD profile pattern was observed in the TPD of thiophene adsorption on the $Ti_{0.9}Ce_{0.1}O_2$.[95] Thus, formation of sulfite and sulfate species takes place in adsorptive desulfurization of liquid fuels.

Figure **4-9** shows that the TPD spectra of species with m/e = 48, 64, 80 and 96 corresponding to mass-to-charge ratio of SO, SO_2, SO_3 and SO_4 for the $Ti_{0.9}Ce_{0.1}O_2$ after adsorption desulfurization of JP-5. The desorption profiles of SO_4 and SO_3 appeared with the maximum desorption rate at 145 ^{o}C. These desorption profiles appeared with the shoulder of the desorption profiles of SO_2 and SO. This SO_4 species weakly adsorb over the adsorbent surface. The formation of SO_4 species could be attributed to the superoxide formed during oxidative pretreatment.

The ADS of JP-5 by using $Ti_{0.9}Ce_{0.1}O_2$ adsorbent is summarized and the adsorption pathway is depicted with benzothiophene as a representative sulfur compound in Figure **4-10**. Adsorptive desulfurization process begins with oxidative pretreatment. The oxidative pretreatment produces superoxide species over the $Ti_{0.9}Ce_{0.1}O_2$ adsorbent.[95] The formation of superoxide is attributed to electron transfer from cations of the adsorbent to molecular oxygen adsorbed on surface. The sulfur atom of organic sulfur compounds in

JP-5 adsorbed over the adsorbent surface via interaction with surface oxygen, such as superoxides. The superoxides are electrophilic species. Therefore, electron was accepted from sulfur atom, and was transferred to surface cations. This was observed as reduction (Ti^{4+}, Ce^{4+}) and oxidation of (Ti^{3+}, Ce^{3+}) cations in XPS. Consequently, the sulfur atom remains as sulfite/sulfate over the adsorbent surface. Subsequent oxidative regeneration contributed to removing adsorbed sulfur, replenishment of active oxygen species and oxidation of surface cations for next sulfur adsorption-removal cycle. Accordingly, the excellent redox property of $Ti_{0.9}Ce_{0.1}O_2$ oxide-based adsorbent plays an important role in the multi-cycle adsorptive desulfurization including activation, sulfur adsorption-removal and regeneration of the adsorbent in the production of ultra clean fuels.

4.4 Conclusions

Based on the results presented herein, we have elucidated the roles of $Ti_{0.9}Ce_{0.1}O_2$ adsorbent in the adsorptive desulfurization of a jet fuel. The conclusions can be drawn as follows:

1. Mesoporous metal oxide-based $Ti_{0.9}Ce_{0.1}O_2$ adsorbent selectively adsorbs organic sulfur compounds in the JP-5 jet fuel and thus effectively reduces sulfur level from 1055 to lower than 1 ppmw at room temperature under ambient pressure without using any hydrogen. The ADS using $Ti_{0.9}Ce_{0.1}O_2$ adsorbent can be carried out in multiple cycles of adsorption and oxidative regeneration.
2. The sulfur atom of organic sulfur compounds interact with surface oxygen on the $Ti_{0.9}Ce_{0.1}O_2$ adsorbent in adsorptive desulfurization. This consideration is further supported by the observation of steric hindrance on sulfur adsorption by the alkyl groups in the analysis of treated JP-5 and the formation of sulfite/sulfate in adsorptive desulfurization of JP-5.
3. The redox property of $Ti_{0.9}Ce_{0.1}O_2$ adsorbent is one of the most important features observed for oxidatively regenerable adsorbent. The excellent redox property of the adsorbent plays an important role in the adsorptive desulfurization including oxidative regeneration.

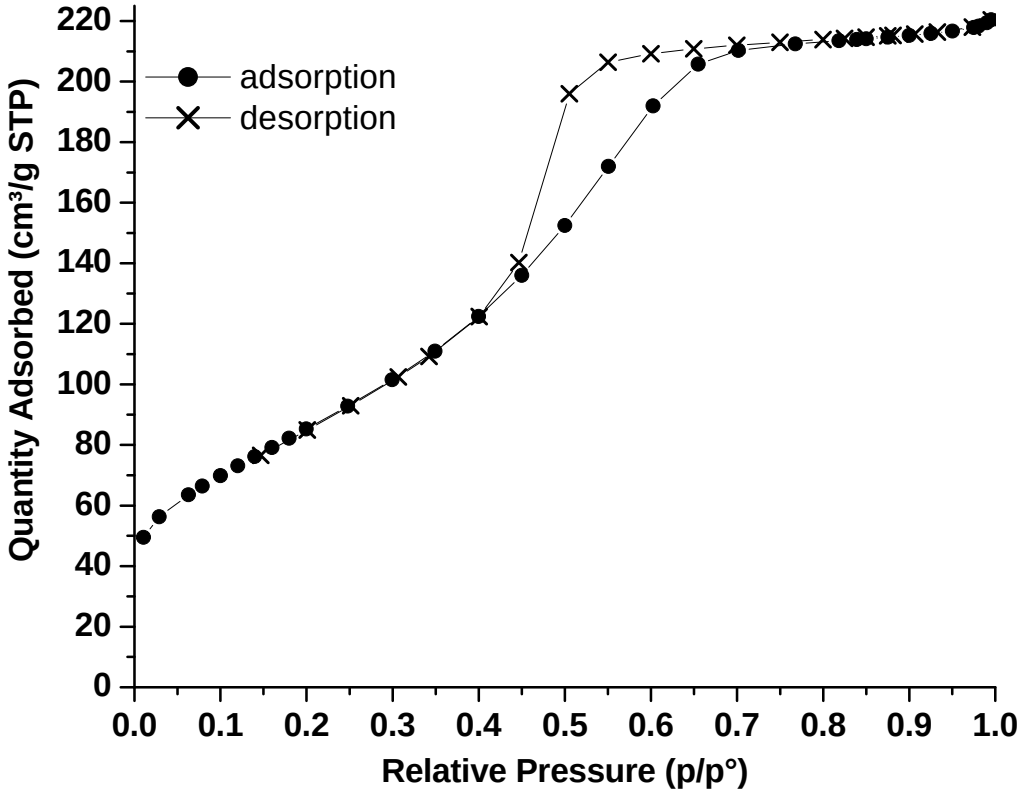

Figure **4-1**: Nitrogen adsorption-desorption isotherm of $Ti_{0.9}Ce_{0.1}O_2$.

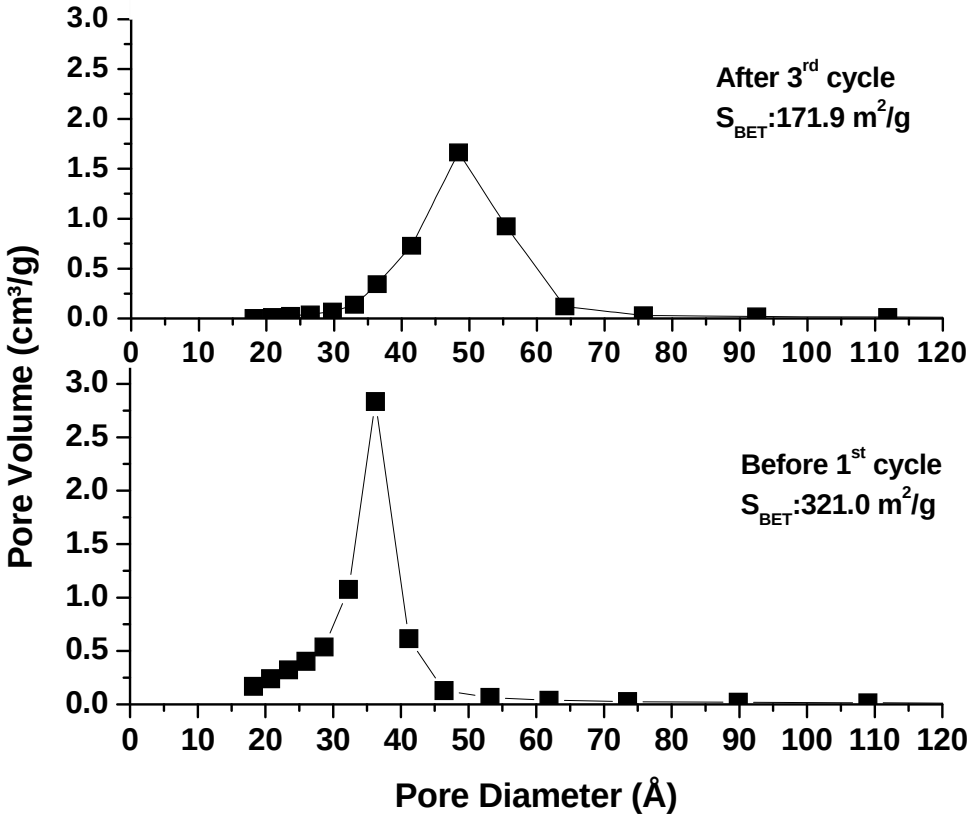

Figure **4-2**: Pore size distribution of $Ti_{0.9}Ce_{0.1}O_2$ before 1st sulfur removal (fresh) and after 3rd oxidative regeneration (spent).

Table **4-1**: BET Surface Area, Pore Volume and Average Pore Size of Fresh and Regenerated $Ti_{0.9}Ce_{0.1}O_2$

	BET surface area (m^2/g)	pore volume (cm^3/g)	ave. pore size (Å)
Before 1st cycle	321.0	0.359	36
After 3rd cycle	171.9	0.217	48

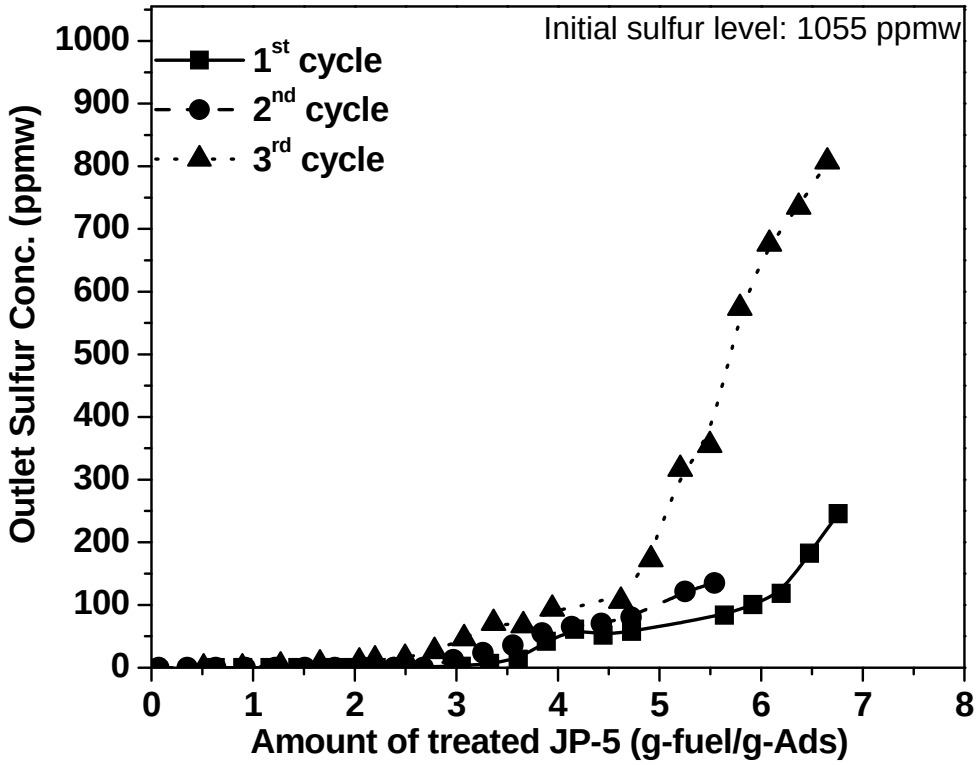

Figure **4-3**: Breakthrough curves of JP-5 desulfurization over $Ti_{0.9}Ce_{0.1}O_2$ at room temperature, fuel flow rate, LHSV: 1.2 h^{-1}.

Table **4-2**: Sulfur Removal Capacity for JP-5 at Room Temperature. Initial Sulfur Concentration of JP-5: 1055 ppmw.

ADS Cycle	1st	2nd	3rd
Capacity* (mg-S/g-Ads.)	3.9	3.5	3.0

* Sulfur removing capacity was calculated based on breakthrough capacity < 30 ppm-S in effluent.

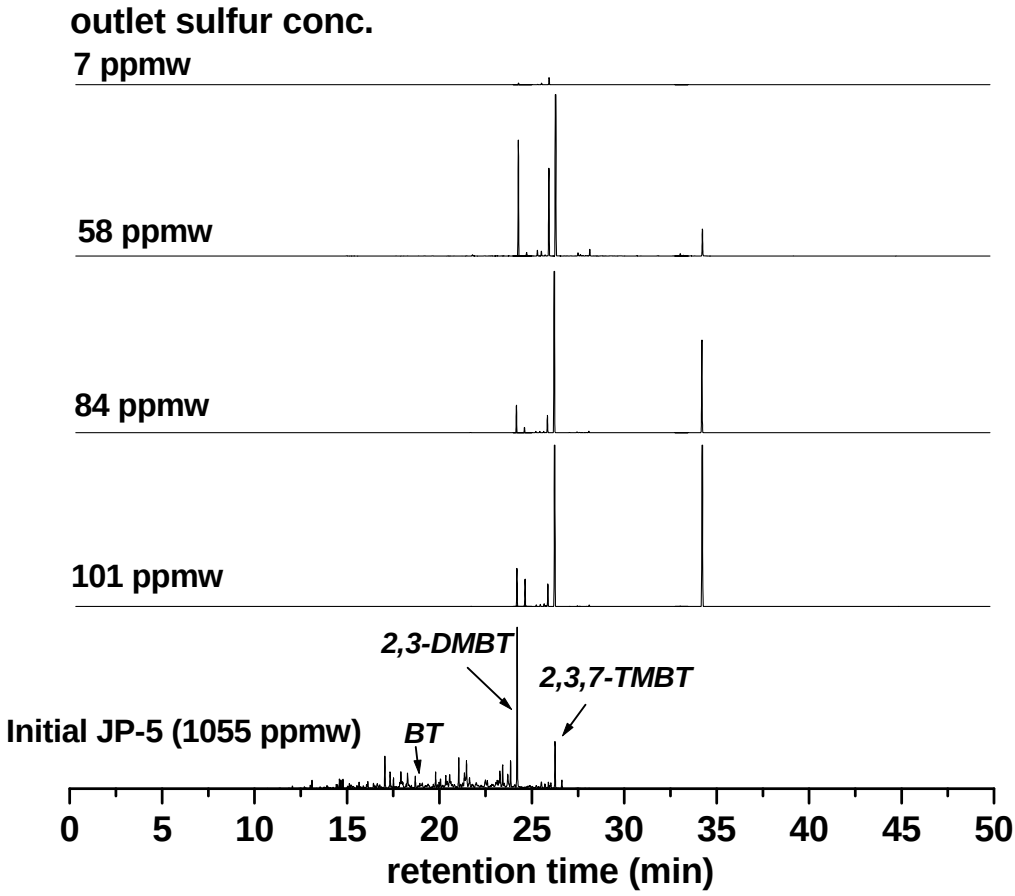

Figure **4-4**: Distribution of sulfur compounds in GC-PFPD chromatogram of JP-5.

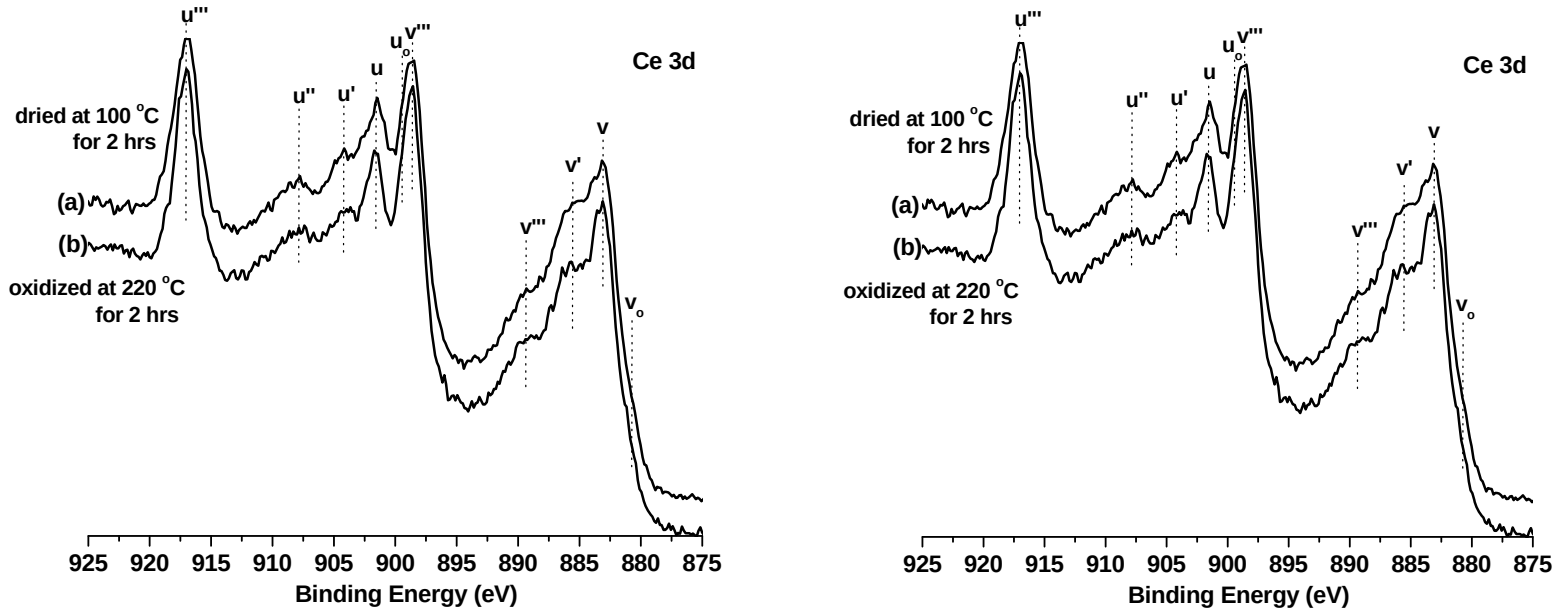

Figure **4-5**: Ce 3d and Ti 2p spectra of $Ti_{0.9}Ce_{0.1}O_2$ (a) dried at 100 °C for 2 hours and (b) oxidized at 220 °C for 2 hours.

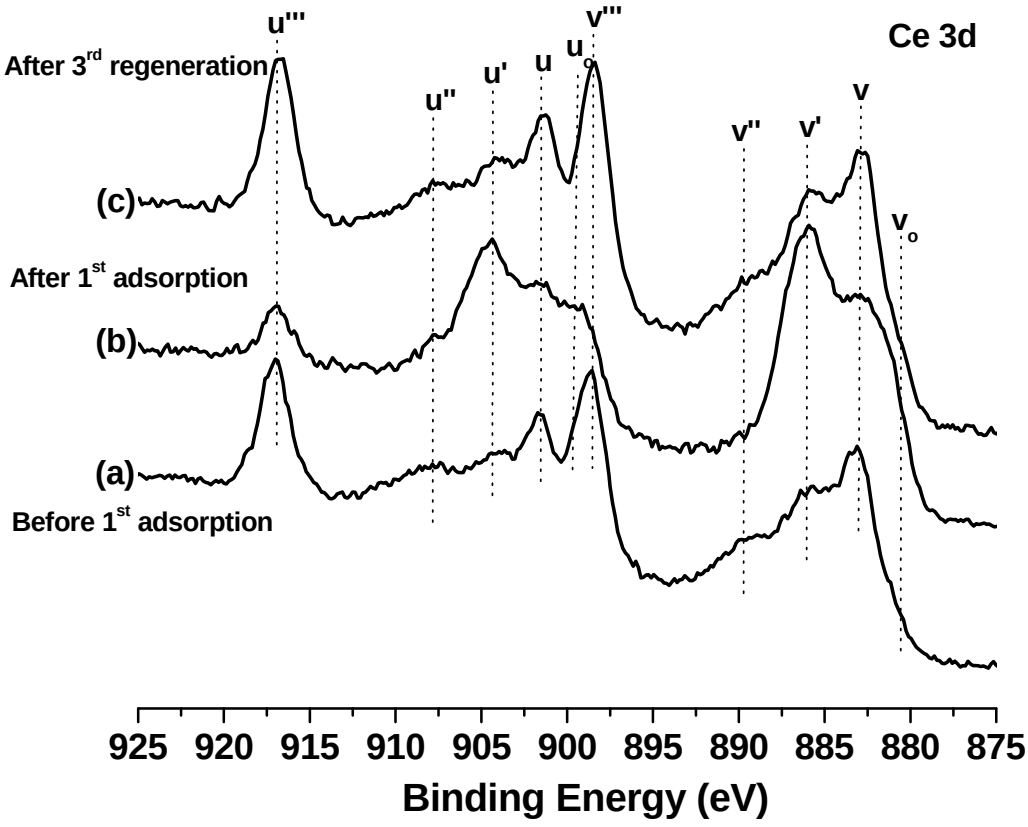

Figure **4-6**: Ce 3d spectra of $Ti_{0.9}Ce_{0.1}O_2$ for (a) before and (b) after adsorption of sulfur in JP-5 and (c) after oxidative regeneration.

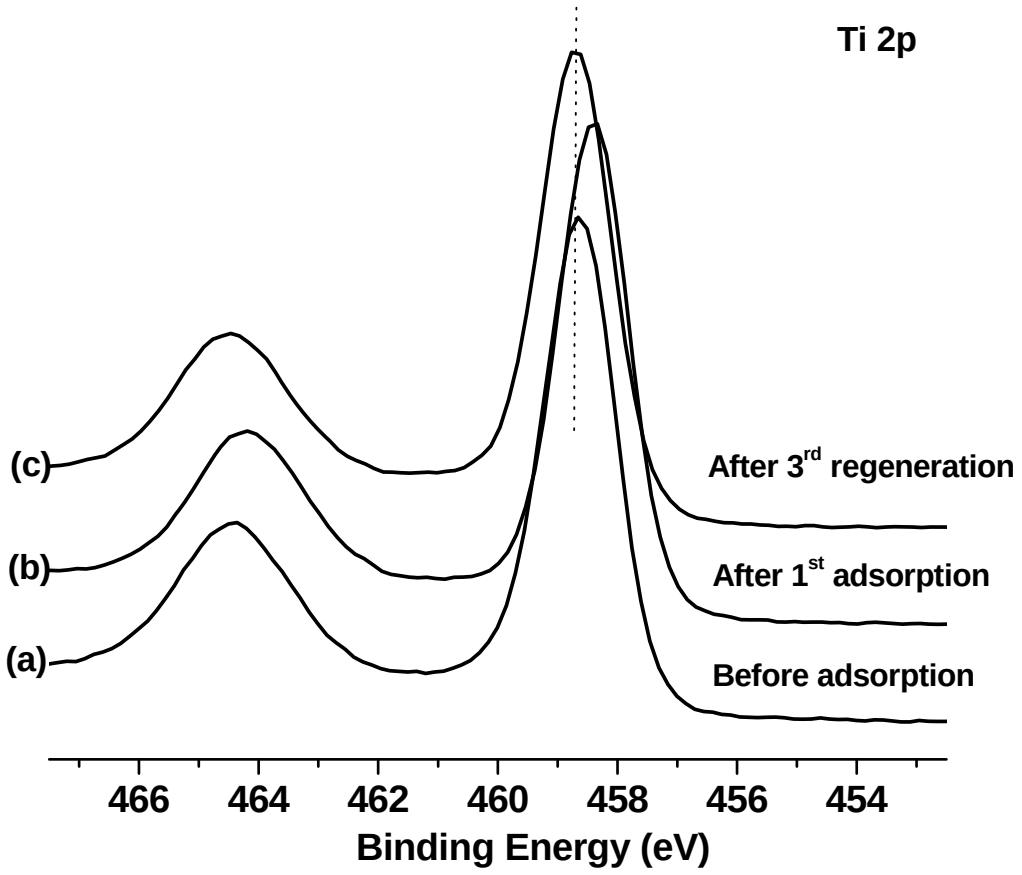

Figure **4-7**: Ti 2p spectra of $Ti_{0.9}Ce_{0.1}O_2$ for (a) before and (b) after adsorption of sulfur in JP-5 and (c) after oxidative regeneration.

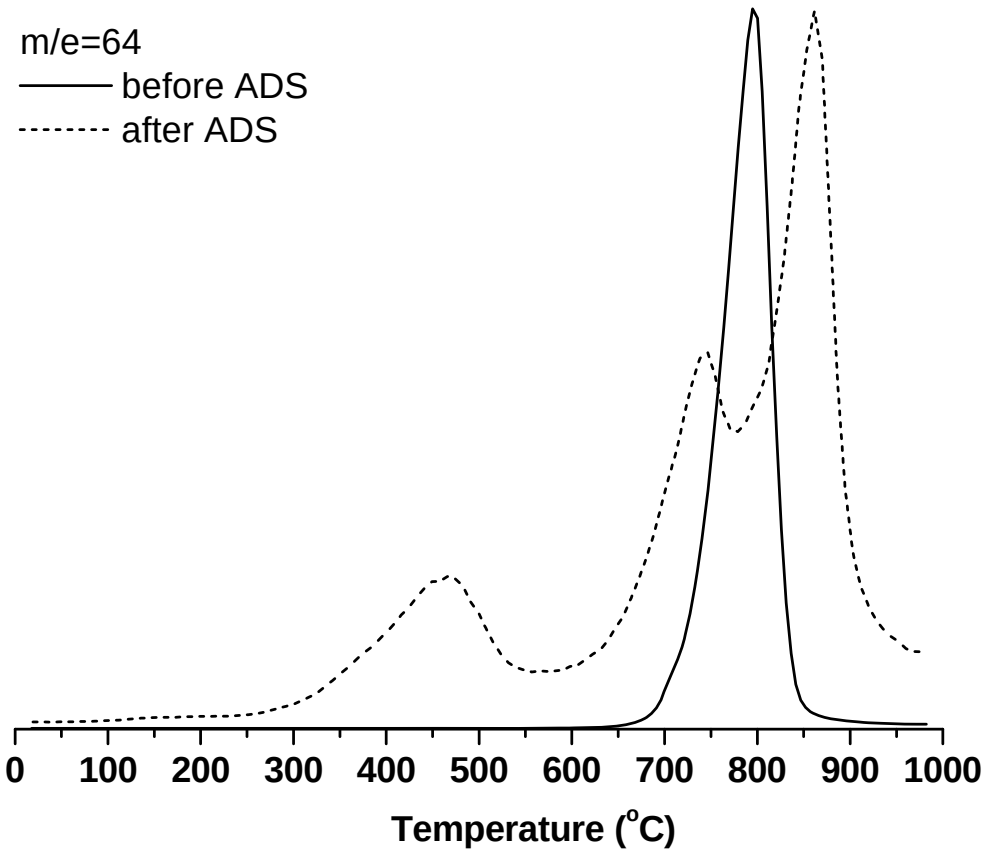

Figure **4-8**: TPD spectra of m/e=64 for $Ti_{0.9}Ce_{0.1}O_2$ adsorbent before and after adsorption of sulfur in JP-5 at room temperature.

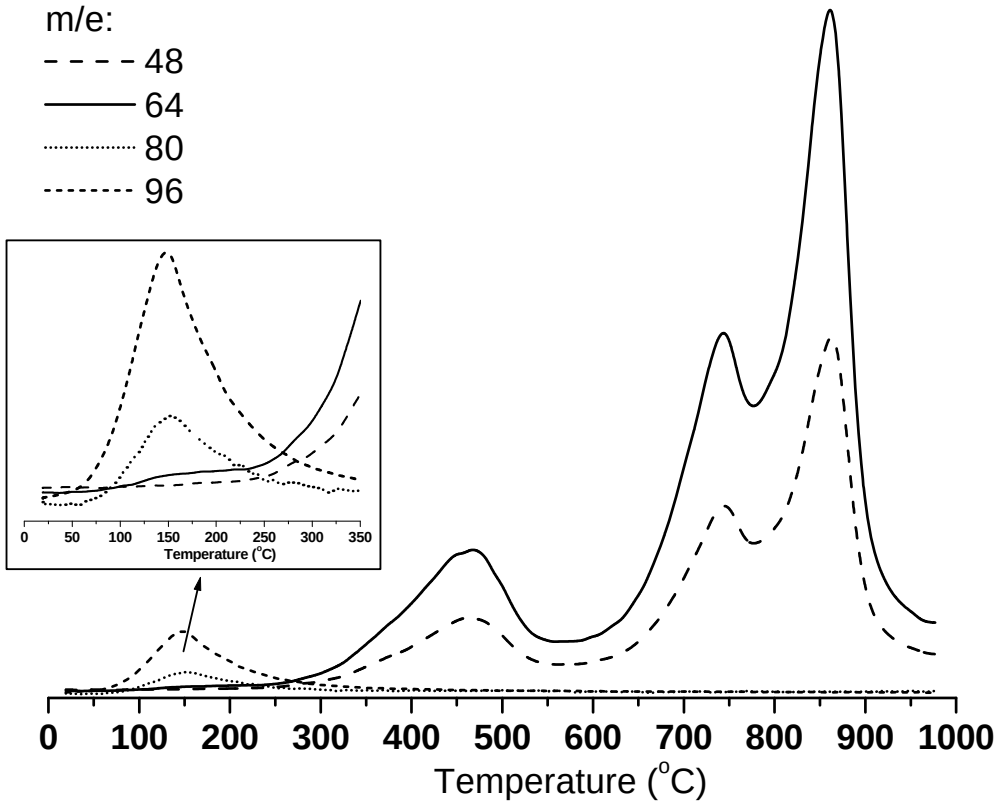

Figure **4-9**: TPD spectra of m/e= 48 (SO), 64 (SO_2), 80 (SO_3) and 96 (SO_4) for $Ti_{0.9}Ce_{0.1}O_2$ adsorbent before and after adsorption of sulfur in JP-5 at room temperature.

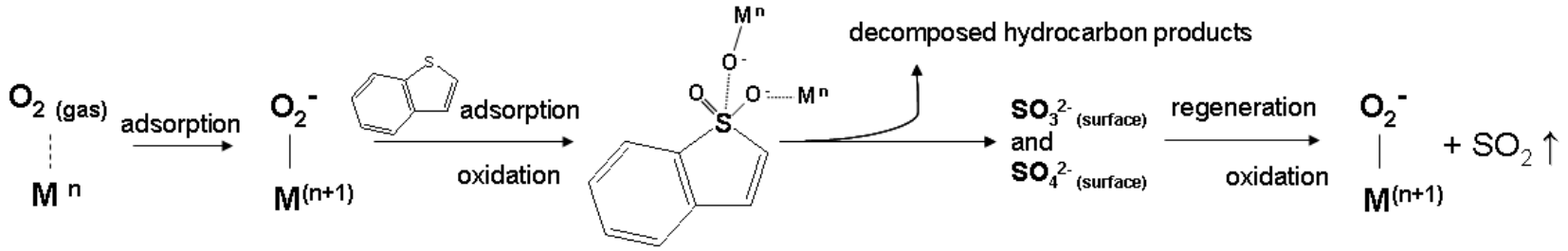

Figure **4-10**: Proposed pathway of adsorptive desulfurization of jet fuel over $Ti_{0.9}Ce_{0.1}O_2$ adsorbent

References:

(1) Song, C. S., An overview of new approaches to deep desulfurization for ultra-clean gasoline, diesel fuel and jet fuel. *Catalysis Today* **2003,** 86, (1-4), 211.

(2) Gates, B. C.; Topsoe, H., Reactivities in deep catalytic hydrodesulfurization: Challenges, opportunities, and the importance of 4-methyldibenzothiophene and 4,6-dimethyldibenzothiophene. *Polyhedron* **1997,** 16, (18), 3213.

(3) Topsoe, H.; Clausen, B. S.; Massoth, F. E., *Hydrotreating Catalysis*. Springer-Verlag: Berlin, 1996.

(4) Song, C. S.; Ma, X. L., Ultra-deep desulfurization of liquid hydrocarbon fuels: Chemistry and process. *International Journal of Green Energy* **2004,** 1, (2), 167.

(5) Babich, I. V.; Moulijn, J. A., Science and technology of novel processes for deep desulfurization of oil refinery streams: A review. *Fuel* **2003,** 82, (6), 607.

(6) Song, C.; Ma, X. L., New design approaches to ultra-clean diesel fuels by deep desulfurization and deep dearomatization. *Applied Catalysis B-Environmental* **2003,** 41, (1-2), 207.

(7) Hernandez-Maldonado, A. J.; Yang, R. T., Desulfurization of transportation fuels by adsorption. *Catalysis Reviews-Science and Engineering* **2004,** 46, (2), 111.

(8) Ma, X. L.; Sun, L.; Song, C. S., A new approach to deep desulfurization of gasoline, diesel fuel and jet fuel by selective adsorption for ultra-clean fuels and for fuel cell applications. *Catalysis Today* **2002,** 77, (1-2), 107.

(9) Watanabe, S. Selective and Regenerable Metal Oxide Adsorbents for the Removal of Sulfur from Liquid Fuels for Fuel Cell Applications. Master of Science, The Pennsylvania State University, University Park, Pennsylvania, 2004.

(10) Watanabe, S.; Velu, S.; Ma, X.; Song, C., New ceria-based selective adsorbents for removing sulfur from gasoline for fuel cell application. *Prepr. Pap. - Am. Chem. Soc., Div. Fuel Chem.* **2003,** 48, (2), 695.

(11) Watanabe, S.; Ma, X.; Song, C. S., Selective sulfur removal from liquid hydrocarbons over regenerable CeO_2-TiO_2 adsorbents for fuel cell applications. *Am. Chem. Soc. Div. Fuel Chem. Prepr.* **2004,** 49, (2), 511.

(12) Watanabe, S.; Ma, X.; Song, C., **in submission**.

(13) Watanabe, S.; Sun, F.; Ma, X.; Song, C., Mechanistic Insights into the Adsorption of Thiophene on $Ti_{0.9}Ce_{0.1}O_2$ Mixed Oxide by XPS, in-situ IR and TPD. **in submission**.

(14) Laachir, A.; Perrichon, V.; Badri, A.; Lamotte, J.; Catherine, E.; Lavalley, J. C.; Elfallah, J.; Hilaire, L.; Lenormand, F.; Quemere, E.; Sauvion, G. N.; Touret, O., Reduction of CeO_2 by Hydrogen - Magnetic-Susceptibility and Fourier-Transform Infrared, Ultraviolet and X-Ray Photoelectron-Spectroscopy Measurements. *Journal of the Chemical Society-Faraday Transactions* **1991,** 87, (10), 1601.

(15) Mullins, D. R.; Overbury, S. H.; Huntley, D. R., Electron spectroscopy of single crystal and polycrystalline cerium oxide surfaces. *Surface Science* **1998,** 409, (2), 307.

(16) Sing, K. S. W.; Everett, D. H.; Haul, R. A. W.; Moscou, L.; Pierotti, R. A.; Rouquerol, J.; Siemieniewska, T., Reporting Physisorption Data for Gas Solid Systems with Special Reference to the Determination of Surface-Area and Porosity (Recommendations 1984). *Pure and Applied Chemistry* **1985,** 57, (4), 603.

(17) Velu, S.; Ma, X. L.; Song, C. S., Selective adsorption for removing sulfur from jet fuel over zeolite-based adsorbents. *Industrial & Engineering Chemistry Research* **2003,** 42, (21), 5293.

(18) Ma, X. L.; Sprague, M.; Song, C. S., Deep desulfurization of gasoline by selective adsorption over nickel-based adsorbent for fuel cell applications. *Industrial & Engineering Chemistry Research* **2005,** 44, (15), 5768.

(19) Kim, J. H.; Ma, X. L.; Zhou, A. N.; Song, C. S., Ultra-deep desulfurization and denitrogenation of diesel fuel by selective adsorption over three different adsorbents: A study on adsorptive selectivity and mechanism. *Catalysis Today* **2006,** 111, (1-2), 74.

(20) Gray, J. H.; Handwerk, G. E., Petroleum Refining. 4thed. Marcel Dekker: 2001 pp 16.

(21) Ma, X. L.; Zhou, A. N.; Song, C. S., A novel method for oxidative desulfurization of liquid hydrocarbon fuels based on catalytic oxidation using molecular oxygen coupled with selective adsorption. *Catalysis Today* **2007,** 123, (1-4), 276.

(22) Burroughs, P.; Hamnett, A.; Orchard, A. F.; Thornton, G., Satellite Structure in the X-Ray Photoelectron Spectra of some Binary and Mixide Oxides of Lanthanum and Cerium. *Journal of the Chemical Society-Dalton Transactions* **1976,** 17, 1686.

(23) Wagner, C. D.; Riggs, W. M.; Davis, L. E.; Moulder, J. F.; Muilenbedrg, G. E., *Handbook of X-Ray Photoelectron Spectroscopy*. Perkin-Elmer Corporation: Minnesota, 1978.

(24) Carley, A. F.; Chalker, P. R.; Riviere, J. C.; Roberts, M. W., The Identification and Characterization of Mixed Oxidation-States at Oxidized Titanium Surfaces by Analysis of X-Ray Photoelectron-Spectra. *Journal of the Chemical Society-Faraday Transactions I* **1987,** 83, 351.

(25) Mayer, J. T.; Diebold, U.; Madey, T. E.; Garfunkel, E., Titanium and Reduced Titania Overlayers on Titanium Dioxide (110). *Journal of Electron Spectroscopy and Related Phenomena* **1995,** 73, (1), 1.

(26) Luo, T.; Vohs, J. M.; Gorte, R. J., An examination of sulfur poisoning on Pd/ceria catalysts. *Journal of Catalysis* **2002,** 210, (2), 397.

Chapter 5

Summary, Conclusions, and Recommended Future Work

This thesis focused on investigating the adsorptive desulfurization of liquid fuels over TiO_2-CeO_2 ($Ti_xCe_{1-x}O_2$) mixed metal oxide adsorbents, particularly $Ti_{0.9}Ce_{0.1}O_2$. The emphasis was placed on the mechanistic aspects including the characterization of structural and surface properties of TiO_2-CeO_2 mixed oxides prepared by urea precipitation, the mechanistic study of thiophene adsorption over $Ti_{0.9}Ce_{0.1}O_2$, and the investigation of the role of $Ti_{0.9}Ce_{0.1}O_2$ adsorbent in adsorptive desulfurization of JP-5 jet fuel in the multiple cycles using several analytical techniques.

Chapter 2 showed that the important structural changes took place upon mixing TiO_2 and CeO_2. Structural distortion of anatase TiO_2 was caused by introducing CeO_2, and that of fluorite CeO_2, by introducing TiO_2, as reflected by a change of lattice parameters. A dominant anatase phase was observed when X was 0.9 or higher in $Ti_xCe_{1-x}O_2$ while a cubic fluorite phase was dominant when X was 0.3 or lower. Mixing TiO_2 and CeO_2 precursors contributed to decreasing the crystalline size of the $Ti_XCe_{1-X}O_2$ oxides. The mixed oxides were nano-crystalline, about 4.0 nm in size when X = 0.9 and 4.8 – 5.4 nm when X = 0.1 - 0.3, which are significantly smaller than the TiO_2 and CeO_2 single oxides (8.1 to 8.4 nm). Mixing TiO_2 and CeO_2 enhanced the creation of surface oxygen defect sites, promotion of reducibility and oxygen storage capacity. Acid sites were identified for $Ti_XCe_{1-X}O_2$ oxides by NH_3-TPD, and those acid sites increased with increasing concentrations of Ti. In addition, the recombinative desorption of NH_3 with

H_2O and N_2 was observed in TPD profiles of $Ti_XCe_{1-X}O_2$ oxides. This recombinative desorption took place with a trace amount of oxygen in the carrier gas. Oxidation of ammonia occurred during ammonia desorption over the TiO_2-CeO_2 mixed oxides. TiO_2-CeO_2 mixed oxides showed excellent oxygen storage capacity, and could act as an oxidation catalyst.

In Chapter 3, the adsorption mechanism of thiophene over $Ti_{0.9}Ce_{0.1}O_2$ was proposed based on insights into the adsorption study of thiophene including the effect of the oxidative pretreatment on thiophene adsorption over $Ti_{0.9}Ce_{0.1}O_2$ adsorbent, the adsorption site for thiophenic compound, and the role of surface Ce and Ti cations in the adsorptive desulfurization. Oxidative thermal treatment produces superoxide species over $Ti_{0.9}Ce_{0.1}O_2$. Presumably molecular oxygen is involved in the interaction with surface reduced centers. The roles of oxidative pretreatment are formation of active oxygen species over the surface and increasing valence state of surface cations. These surface oxygen species were identified as adsorption sites for thiophene over $Ti_{0.9}Ce_{0.1}O_2$. The oxidation of sulfur atom is involved in the adsorption of thiophenic compounds over $Ti_{0.9}Ce_{0.1}O_2$ adsorbent, and dominantly forms sulfite and sulfate species. The role of surface Ce and Ti is to form superoxide species and possibly to accept electrons in interaction with π electron of localized thiophene ring. The possible η^1(S)-coordination and η^4 adsorption mode enhances the localization of the ring, and as a result, would cause dissociation of thiophene by C-S bond cleavage. Thiophene adsorption on $Ti_{0.9}Ce_{0.1}O_2$ mainly involved dissociation, and produced C_4 hydrocarbons, such as butene and butane.

In Chapter 4, the role of $Ti_{0.9}Ce_{0.1}O_2$ mixed oxide in the adsorptive desulfurization of a real jet fuel in the multiple cycles was investigated in fixed-bed flow system with in-

situ oxidative regeneration using air. Mesoporous metal oxide-based $Ti_{0.9}Ce_{0.1}O_2$ adsorbent selectively adsorbs organic sulfur compounds in the JP-5 jet fuel and thus effectively reduces sulfur level from 1055 to lower than 1 ppmw at room temperature under ambient pressure without using any hydrogen. The ADS using $Ti_{0.9}Ce_{0.1}O_2$ adsorbent can be carried out in multiple cycles of adsorption and oxidative regeneration. The sulfur atom of organic sulfur compounds interact with surface oxygen on the $Ti_{0.9}Ce_{0.1}O_2$ adsorbent in adsorptive desulfurization. This consideration is further supported by the observation of steric hindrance on sulfur adsorption by the alkyl groups in the analysis of treated JP-5 and the formation of sulfite and sulfate species in adsorptive desulfurization of JP-5. The redox property of $Ti_{0.9}Ce_{0.1}O_2$ adsorbent is one of the most important features observed for oxidatively regenerable adsorbent. The excellent redox property of the adsorbent plays an important role in the adsorptive desulfurization including oxidative regeneration.

The major observations and new findings clearly established the unique features of TiO2-CeO2 mixed oxides, particularly $Ti_{0.9}Ce_{0.1}O_2$, as new oxidatively regenerable adsorbents, and provided new insight into the fundamental surface chemical changes during the adsorptive desulfurization over $Ti_{0.9}Ce_{0.1}O_2$ adsorbent and the oxidation regeneration. $Ti_{0.9}Ce_{0.1}O_2$ can selectively adsorb sulfur compounds in the presence of aromatics, and can remove sulfur atom from thiophenic compounds. This occurs at room temperature with $Ti_{0.9}Ce_{0.1}O_2$ adsorbent activated by using air. The excellent redox property of $Ti_{0.9}Ce_{0.1}O_2$ oxide-based adsorbent plays an important role in the multiple-cycle adsorptive desulfurization including activation, sulfur adsorption-removal and regeneration of the adsorbent in the production of ultra clean fuels. Thus, this process is

very promising due to the high efficiency and simplicity of the selective adsorption for sulfur removal at room temperature.

Recommended future work

1. Low temperature DRIFT study using thiophene and thiophene-olefin-aromatic mixture is recommended for the future work. The details of dissociative adsorption of thiophene over the oxide could be obtained. Related analytical characterization using XPS and TPD before and after the adsorption and after the regeneration is also recommended.

2. It would be important to examine how the temperature of adsorptive desulfurization may affect the sulfur removal performance. Sulfur removal of JP-5 at 100 ^{o}C was less efficient at 30 min. However, the sulfur removal capacity was twice larger than that done at room temperature. This suggests that adsorption phenomena of thiophenic compounds should differ at the different temperatures. In addition, XRD analysis of the spent adsorbent showed the lattice parameter expansion in c-axis and reduction in a-axis. It suggests that ADS at high temperature may involve solid state reaction, or in other words anion exchange. It is worth to investigate the effect of temperature on sulfur removal performance along with the influence on the structure.

3. Adsorptive desulfurization takes place with dissociation of thiophenic compounds over the $Ti_{0.9}Ce_{0.1}O_2$ adsorbent. Model study using dibenzothiophene (DBT) is recommended for further investigation of adsorption mechanism. DBT is an ideal model compound to confirm the dissociative adsorption pathway because the clear comparison

can be conducted with several studies, such as photo-oxidative desulfurization, chemical and catalytic oxidative desulfurization and biodesulfurization.

4. It would be interesting to investigate the effect of hydrogen donor on sulfur removing performance including dissociation. During dissociative adsorption, decomposed hydrocarbons were expected to be hydrogenated. Thus, ADS of DBT with or without hydrogen donor, such as tetralin and/or decalin under the various conditions is recommended for the future work.

Appendix A

Adsorptive Desulfurization of Liquid Fuels over Metal Oxides: Adsorbent Screening and Study of Thiophene Adsorption by in-situ IR Spectroscopy

Abstract

Adsorptive desulfurization of a model fuel and JP-5 jet fuel was conducted using metal oxides (Y_2O_3, La_2O_3, CeO_2, TiO_2, ZrO_2, V_2O_5, Nb_2O_5, Cr_2O_3, MoO_2, WO_2, MnO, Fe_2O_3, RuO_2, CoO, CuO, and Ag_2O) at room temperature, under atmospheric pressure and without hydrogen usage. In particular, Cr_2O_3, V_2O_5, MoO_2, Fe_2O_3, RuO_2 and Ag_2O significantly reduced the sulfur concentration of the model fuel. However, Cr_2O_3 was the only oxide which significantly removed sulfur from the jet fuel among the 18 metal oxides. The selectivity could contribute to the deeper sulfur removal from a real fuel, such as jet fuel. CuO, Cr_2O_3, CeO_2, NiO and ZnO were chosen for selective oxides for sulfur removal of the liquid fuels based on the comparison of sulfur removing capacities of model fuel and jet fuel. Those oxides were further investigated their adsorption configurations using thiophene as a probe molecule by means of in-situ IR spectroscopy. The adsorption geometry of thiophene was observed as both through η^1(S)-coordination and π electrons on Cr_2O_3, CeO_2, NiO and ZnO. However, η^1(S)-coordination found to be a key for the selective adsorption. The surface oxygen was identified as a possible adsorption site by absorbance of S-O stretching vibration. As a result, η^1(S)-coordinated thiophene decomposed and sulfur atom remains as sulfite particularly over Cr_2O_3 and

CeO_2. Consequently, η^1-(S)-coordination of thiophene to surface oxygen could be relevant to the selective adsorption for removing sulfur from the liquid fuels.

A.1 Introduction

In various countries, the sulfur content in transportation fuels has been restricted significantly in order to achieve a better air quality. Starting from the year 2006, the US Environmental Protection Agency stated that the regulations for the sulfur concentration of diesel fuel has to be lower than 15 parts per million by weight (ppmw) and 30 ppmw for gasoline from 500 and 300 ppmw, respectively.[6] Such strict environmental regulations emphasize the importance of developing more efficient and effective process to remove sulfur from the liquid fuels.

Hydrodesulfurization (HDS) has been a widely used and common process to remove sulfur from petroleum feed stocks. HDS can achieve the current regulations. However, due to the lower reactivity of alkylated benzothiophenes and dibenzothiophenes, this process requires severer operation condition, such as the higher temperature, higher pressure and larger hydrogen consumption, to reduce the sulfur concentration significantly.[6, 66, 67] Furthermore, a larger volume of catalyst bed is also required besides these severer operation conditions.[30] Thus, extensive research has been carried out to improve the HDS and to explore alternative processes, such as the adsorptive desulfurization.[6, 13]

Adsorptive desulfurization (ADS) has recently received much attention due to an ultra clean fuel production.[6, 12, 13, 27] Major advantages of the ADS are: (1) the refractory

sulfur compounds (thiophenic and alkylated thiophenic compounds) can be removed under mild condition (at lower temperature and under lower pressure) without using hydrogen gas, (2) there is no need for pressurized vessel and no need for high-temperature and high-pressure operations, and (3) it is a very simple process,[6, 10, 18] Many materials, such as metal-based,[10, 15] zeolite-based,[19-22] and activated carbon-based[14] adsorbents, have been investigated for their utilization as adsorbents in ADS of commercial fuels (gasoline, jet fuel and diesel fuel). However, the challenge settles on findings a regenerable adsorbent that selectively adsorbs the sulfur compounds but dose not adsorb aromatic and olefinic compounds co-existing in the fuels.[6]

A few of utilization of metal oxides for ADS were reported.[134, 135] In addition, only several studies are found regarding the thiophene adsorption on metal oxides such as CaO,[68] Al_2O_3,[69] TiO_2[71] and UO_2.[72] Thiophene is typically used as a model organic sulfur compound because it is representative of the aromatic sulfur compounds and the structure and chemistry are well-known.[79, 102, 136-138] Adsorption of thiophene on solid surfaces has been studied by using infrared (IR) spectroscopy since it is particularly informative on the bonding mode of adsorbed thiophene. The main adsorption geometry of thiophene studied by IR spectroscopy was reported to be as η^1(S)-bonded on sulfide Mo catalysts,[73, 74] on Mo_2C/Al_2O_3,[75] and Mo_2N/γ-Al_2O_3.[76] Other possible bonding configurations, such as the η^2-bonded,[77, 78] η^4-bonded,[77, 78] and η^5-bonded,[79] were also observed.

The aims of this work were to investigate the sulfur removing ability of the metal oxides from liquid fuels and to obtain the insight into the adsorption of thiophene over the metal oxides. The comparison of sulfur removing capacities between the model fuel and the commercial fuel allowed us to select a suitable metal oxide for ADS application

because sulfur compounds are adsorbed competitively with co-existing olefins and aromatics in the real fuels.[131] Metal oxides, which selectively adsorb sulfur compounds, were chosen and further studied the adsorption chemistry of thiophene by in-situ infrared spectroscopy.

A.2 Experimental Section

A.2.1 Adsorbents

Yttrium oxide (Y_2O_3), lanthanum oxide (La_2O_3), cerium oxide (CeO_2), titanium oxide (TiO_2), zirconium oxide (ZrO_2), vanadium oxide (V_2O_5), niobium oxide (Nb_2O_5), chromium oxide (Cr_2O_3), molybdenum oxide (MoO_2), tungsten oxide (WO_2), manganese oxide (MnO), iron oxide (Fe_2O_3), ruthenium oxide (RuO_2), cobalt oxide (CoO), copper oxide (CuO), and silver oxide (Ag_2O) were obtained from Aldrich Chemical Co. Nickel oxide (NiO) and zinc oxide (ZnO) were prepared by urea precipitation method using nickel nitrate and zinc nitrate (Aldrich Chemical Co.).[139] During precipitation, the temperature was kept at 90 - 95 ^oC for 8 hours, and the amount of the aqueous solution was maintained at 1000 mL. Resulting precipitates were dried overnight in an oven at 110 ^oC. The dried precipitants were calcined in a muffle furnace at 450 ^oC in static air for 6 hours. The calcination temperature was reached by employing a temperature ramp of 2 ^oC/min. Surface area, pore size and pore volume of metal oxides were calculated by the BET equation and BJH method resulting from nitrogen adsorption-desorption using

Autosorb-1. The metal oxide samples were outgassed at 220 ^{o}C prior to measuring the surface area.

A.2.2 Apparatus and Procedure

A model fuel consisted of thiophene dissolved in n-decane, and the sulfur concentration was 968 parts per million by weight of sulfur (ppmw). JP-5 jet fuel was provided by the US Navy Office of Naval Research. This JP-5 fuel contained 1055 ppmw of sulfur. The adsorptive desulfurization test was conducted in a batch system, and repeated three times. 0.2 g of the powder metal oxide was placed in a glass tube (22 mm of internal diameter and 150 mm in length). The metal oxide sample was dried in an uncovered glass tube at 220 ^{o}C for 2 hours under atmospheric pressure before adsorption. When the temperature of glass tube reaches at room temperature, 1 g of liquid fuel was added and stirred by a magnetic stirrer at 25 ^{o}C for 2 hours.

The total sulfur concentration of the treated model fuel and JP-5 was analyzed by using an ANTEK 9000 Series total sulfur analyzer. A detailed analysis of the method has been reported previously.[140]

Diffuse reflectance infrared Fourier transform (DRIFT) spectra were obtained on a NICOLET NEXUS 470 FT-IR spectrometer and recorded with a resolution of 4 cm^{-1} and 126 scans. DRIFT cell equipped with a ZnSe window was attached to a line that allows performing in situ treatment of the samples in either a gas flow or in a vacuum at different temperatures. A powder metal oxide sample was treated at 200 ^{o}C for 1 hour under vacuum. Subsequently a powder sample was exposed to thiophene for 60 min.

Thiophene was introduced into the DRIFT cell with the aid of Ar flow at 100 cm^3/min (1 % thiophene vapor in Ar). After the thiophene exposure, 30 cm^3/min of Ar flow was introduced into the IR cell to remove weakly adsorbed adsorbate from the oxide surface at room temperature. All spectra were acquired by in-situ spectroscopy at room temperature. As a reference, IR spectrum of liquid thiophene was obtained by using KBr pellets.

A.3 Results and Discussion

A.3.1 Adsorptive Desulfurization over Metal Oxides

Sulfur removal of a model fuel

Sulfur removing capacities of various metal oxides were determined using a model fuel at room temperature. The sulfur removal of the model fuel was performed to establish the static equilibrium capacities of the metal oxides for one specific sulfur compound, such as thiophene. The sulfur concentration after thiophene adsorption and the sulfur removing capacities is shown in Table **A-2**. Among the 18 metal oxides evaluated, Cr_2O_3, V_2O_5, MoO_2, Fe_2O_3, RuO_2 and Ag_2O effectively reduced sulfur concentration from 968 ppmw to 588, 662, 667, 672, 678, and 690 ppmw, respectively. Those metal oxides are acidic oxides.[141] Therefore, the acidic nature of the metal oxide may contribute to the thiophene removal. In contrast, the higher sulfur removing capacity on the base of the surface area revealed for WO_2, MnO, Ag_2O, and CuO. This result suggests that WO_2, MnO, Ag_2O, and CuO have the higher density of adsorption site for thiophene.

Sulfur removal of real fuel (JP-5)

The equilibrium adsorption capacities for sulfur removal of JP-5 fuel using 18 metal oxides is summarized in Table **A-3**. The most significant sulfur reduction, 1055 to

806 ppmw, was observed in adsorptive desulfurization of JP-5 by Cr_2O_3. Although, sulfur reduction of treated fuel was not significant, sulfur removing capacities on the base of surface area for WO_2, MnO, Ag_2O, and CuO were higher than in other oxides as seen in Figure **A-1**. Figure **A-2** shows a linear correlation between the sulfur removing capacity of the model fuel and the JP-5 jet fuel. If this correlation is extrapolated, it may be possible to expect that sulfur reduction of a real fuel could be significant by the adsorbent removing a large amount of sulfur from a simple model fuel.

The relative sulfur removing capacities between sulfur removal of the model fuel and that of the jet fuel, which corresponding to selectivity of metal oxides, is shown in Table **A-3**. The JP-5 fuel used for this study contains about 0.1 wt% of sulfur. These sulfur compounds are presumably various types of alkylated benzothiophenes.[19] Kim et al. showed that the electron density on the sulfur atom seems to influence on the adsorption selectivity more than the π electron density in the sulfur adsorption over oxide-based adsorbents.[131] Therefore, the alkyl groups neighboring sulfur atom could cause the steric hindrance effect. Aromatic content of JP-5 in jet fuels could be up to 25 % which is the maximum allowed aromatics content.[132] The sulfur removal of JP-5 fuel was less effective due to the competitive adsorption of thiophenic compounds and co-existing aromatics for the surface sites on the adsorbents.[10, 15, 19, 131] Competitive adsorption of sulfur compounds was observed over the other solid surfaces in the presence of aromatics.[131, 142, 143] Therefore, the selective adsorption for removing sulfur could take place via sulfur atom of thiophenic compounds over the metal oxides.

The relative sulfur removing capacities of CuO, Cr_2O_3, NiO, ZnO and CeO_2, were higher than those of others. This result suggests that CuO, Cr_2O_3, NiO, ZnO and CeO_2,

are capable to selectively remove sulfur from liquid fuels. The metal oxides, CuO, Cr_2O_3 and NiO, particularly showed the highest relative sulfur removing capacities. As commonly known, these metal oxides, CuO, Cr_2O_3 and NiO, are oxidative catalysts.[144] Thus, oxidation characteristics may play an important role on the selective adsorptive desulfurization of liquid hydrocarbon fuels by using metal oxides. Another commonality of these oxides is the electron configuration of metal ion, which is between d^1-d^9. These electron configurations suggest that the metal ions may act as an electron acceptor to fill in the d orbital during adsorption of organic sulfur compounds since the d^5 and d^{10} configurations are stable (known in Aufbau principle). Hence, the oxidation nature of metal oxides and electron configuration of metal ions may contribute to the selective adsorptive desulfurization.

A.3.2 In-situ FT-IR

In-situ FT-IR studies were conducted to obtain a better understanding of thiophene adsorption over the metal oxides. Metal oxides, CuO, Cr_2O_3, NiO, ZnO and CeO_2, were selected due to the superior selectivity in the sulfur removal of the model and JP-5 jet fuel. The adsorption properties of thiophene over the metal oxides were studied using in-situ FT-IR. The metal oxides were exposed to thiophene, and thiophene adsorbed metal oxide was aged after exposure to thiophene. At last, the argon was flown into the DRIFT cell to remove weakly adsorbed adsorbates.

IR spectrum of liquid thiophene

The IR spectrum of liquid thiophene was obtained as a reference. The band patterns of the liquid thiophene were assigned based on the literature.[74, 79, 102, 103] IR bands for liquid thiophene appeared at 3110, 3075, 1588, 1409, 1252, 1082, and 1034 cm^{-1} corresponding to the C-H stretching vibration (ν(C-H) α-position), the C-H stretching vibration (ν(C-H) β-position), the asymmetric C=C stretching ($\nu(C=C)_{asym}$), the symmetric C=C stretching ($\nu(C=C)_{sym}$) and the in-plane C-H bending vibration (δ(C-H)) for the last three bands, respectively. Assignment of the bonding geometry of adsorbed thiophene is indicated by the observation of the $\nu(C=C)_{sym}$ mode of the thiophene because $\nu(C=C)_{sym}$ band is the most sensitive to the adsorption mode.[79] IR spectra of the thiophene adsorbed on metal oxides, Cr_2O_3, CeO_2, ZnO, and NiO, followed by adsorbate removal by Ar flow at room temperature are shown in Figure **A-3**, Figure **A-4**, Figure **A-5** and Figure **A-6**. Each figure shows the difference IR spectra obtained by subtracting the spectrum of dried metal oxide (200 ^{o}C for 1 hr) from (a) the spectrum of metal oxide exposed to thiophene in Ar flow for 1 min, (b) the spectrum of spectrum of metal oxide exposed to thiophene in Ar flow for 60 min, (c) the spectrum of metal oxide aged for 60 min after stopped exposure to thiophene, (d) the spectrum of metal oxide under Ar flow for 1 min, and (e) the spectrum of metal oxide under Ar flow for 60 min. Although relative sulfur removing capacity of CuO was one of the highest (Table **A-3**), the clear spectra of thiophene adsorbed on CuO were not available due to the strong absorbance by CuO, and the spectra are not shown in here.

IR spectra of thiophene adsorption over Cr_2O_3

Figure **A-3** shows that the difference spectra indicating changes in adsorption mode of thiophene over Cr_2O_3. The IR bands appeared at 3574, 3410, 3113, 3102, 3085, 1415, 1252, 1082 and 1032 cm^{-1} (Figure **A-3**-a). The absorbance observed at 3113, 3102, 3085, 1415, 1252, 1082 and 1032 cm^{-1} is assigned to the bands of the thiophene. When compared to the bands of liquid thiophene, the $\nu(C=C)_{sym}$ band shifted by +6 cm^{-1}. The band shifts are attributed to thiophene adsorption via sulfur atom with decreasing electron density within the C=C−C=C fragment.[79] This shift indicates that the initial thiophene adsorption mode is η^1-(S)-coordination. A broad band at around 3574 cm^{-1} is attributed to an OH group. This O–H stretching vibration is assigned to hydrogen bonding between hydrogen of the thiophene and the surface oxygen.[68, 145] After more significant quantities of thiophene introduced into the DRIFT cell, the intensity of the bands increased at 3574, 3410, 3113, 3102, 3085, 1589, 1539, 1415, 1252, 1082 and 1032 cm^{-1} (Figure **A-3**-b). These bands previously assigned to thiophene significantly increased their intensities. The $\nu(C=C)_{sym}$ band at 1415 cm^{-1} increased the intensity with the shoulder at 1423 and 1404 cm^{-1}. This increase at 1423 and 1404 cm^{-1} is attributed to the increase of the amount of thiophene adsorbed by η^1-(S)-coordination and adsorption via π electrons.[79]

The difference spectrum shown in Figure **A-3**-c illustrates the absorbance features of thiophene adsorbed over Cr_2O_3 kept for 60 min after stopped thiophene flow into the DRIFT cell. The intensity of the bands corresponding to the thiophene appeared at 3113, 3085, 1589, 1415, 1252 and 1032 cm^{-1} was significantly decreased. On the other hand, the new bands appeared at 1705, 1571, 1315, 1205 and 1139 cm^{-1}. The decrease of

intensity suggests that the number of adsorbed thiophene via η^1-(S)-coordination decreased and might be decomposed over the oxide surface. This decomposition of thiophene resulted in decrease of bands corresponding to thiophene and the appearance of the new bands at 1315, 1205 and 1138 cm^{-1} corresponding to S-O stretching frequencies of sulfite and/or sulfate.[104, 146-148] Thus, η^1-(S)-coordinated thiophene possibly decomposed and formed sulfite and sulfate species.

After aging, Ar flow was introduced into the DRIFT cell to remove physically adsorbed adsorbates. The difference spectra showed the further decrease of the intensity corresponding to thiophene including ν(C-H) in between 3120 – 2850 cm^{-1} along with the further increase of the intensity at 1315, 1205 and 1138 cm^{-1} (Figure **A-3**-d and **A-3**-e). After the further Ar flow into the DRIFT cell, absorbance feature at 1401 cm^{-1} remained. This band is assigned to sulfate due to the disappearance of bands corresponding to thiophene. The initially observed intensity at 1404 cm^{-1} after exposure to thiophene may not only be attributed to the ν(C=C) of thiophene adsorption via π electrons but also S-O stretching vibration of sulfate species.

The difference spectra of thiophene adsorption over Cr_2O_3 indicates that the major bonding geometry of thiophene is η^1-(S)-coordination along with hydrogen bonding. Along with the disappearance of the molecularly adsorbed thiophene, new bands corresponding to S-O binding appeared. This result suggests that η^1-(S)-coordinated thiophene started to decomposed as similarly seen in thiophene adsorption on catalysts[73, 74] and form sulfite or sulfate-like species. The formation of SO_X species is similar to what was observed in SO_2 adsorption on Cr_2O_3.[149] Surface oxygen is the possible adsorption site to interact with sulfur compounds. Consequently, thiophene adsorption over Cr_2O_3

mainly undergoes through the sulfur atom with surface oxygen of Cr_2O_3, and as a result, the adsorbed thiophene is decomposed with formation of SO_X species.

IR spectra of thiophene adsorption over CeO_2

The difference spectra in Figure **A-4** show the sequence of adsorption and desorption of thiophene over the CeO_2. Broad peaks appeared at 3420, 1673, 1538, 1311 and 1068 cm^{-1} after thiophene exposure for 1 min (Figure **A-4**-a). These broad bands did not correspond to thiophene. Therefore, thiophene did not physically adsorb at the beginning of thiophene exposure over CeO_2. After further thiophene exposure, the significant difference was observed as the increase of intensity at 3593, 3109, 3097, 3091, 3082, 1539, 1443, 1419, 1409, 1400, 1381, 1342, 1252 and 1082 cm^{-1} in the difference spectrum (Figure **A-4**-b). The bands at 3109, 3082, 1419, 1409, 1400, 1252 and 1082 cm^{-1} are assigned to thiophene. Bands at 1419 and 1400 cm^{-1} are assigned to the $\nu(C=C)_{sym}$ band of thiophene by shifted by +10 and -9 cm^{-1}, respectively. These bands are attributed to thiophene adsorption through η^1-(S)-coordination and π electrons, respectively.[74, 79] The IR band at 3593 cm^{-1} is attributed to hydrogen bonding. This O-H band infers that hydrogen of thiophene forms hydrogen bonding with surface oxygen. The broad band at around 1539 cm^{-1} is assigned to C=C stretching, and does not correspond to the band of thiophene. The bands at 1383 and 1342 cm^{-1} are assigned to S-O stretching frequency, and correspond to ν(S-O) of sulfate and sulfite complexes, respectively.[104, 150] The absorbance of S-O bonding implies that thiophene adsorption over CeO_2 occurs through

the interaction between sulfur and surface oxygen. Because of the observation of S-O bonding, adsorption site of η^1-(S)-coordination of thiophene could be surface oxygen.

The difference spectrum Figure **A-4**-c shows that the bands corresponding to thiophene significantly lowered the intensities, while the intensities at 1697, 1587, 1532, 1441, 1383 and 1342 cm^{-1} increased after stopped exposure to thiophene. The intensity corresponding to thiophene adsorbing via hydrogen bonding and π electron significantly decreased. Intensity of the bands corresponding to thiophene significantly declined along with the increase of the bands at 1383 and 1342 cm^{-1} corresponding to S-O stretching vibration. As a consequence the decomposition of thiophene adsorption via π electron may change the adsorption mode and result in the appearance of S-O bonding and the decreasing of the band intensities of thiophene.

After introducing Ar flow into the DRIFT cell, the intensity of IR bands corresponding to the S-O, especially at 1342 and 1126 cm^{-1} increased more (Figure **A-4**-d and -e). All bands assigning to thiophene disappeared after Ar flow introduction. This change regarding bands of thiophene suggests that thiophene easily desorbs molecularly from the surface of CeO_2 and the S-O bonding is strong enough to remain over the CeO_2 surface as sulfite and sulfate species.

Thiophene adsorbs through η^1-(S)-coordination with surface oxygen over CeO_2. Thiophene adsorption via π electron may be changed to η^1-(S)-coordination with time. Subsequently, η^1-(S)-coordinated thiophene decomposed with formation of SO_X species. Formation of SO_X species was reported for SO_2 adsorption over CeO_2.[88, 89, 151] Thus, surface oxygen of CeO_2 is an adsorption site for sulfur compounds and attributed to oxidation of sulfur atom.

IR spectra of thiophene adsorption over NiO

Figure **A-5**-a did not show any distinguishable bands after thiophene exposure for 1 min. After significant thiophene exposure, the bands corresponding to thiophene appeared at 3670 3656, 3097, 3082, 1562, 1419, 1409, 1400, 1348, 1252 and 1082 cm^{-1} in the difference spectrum (Figure **A-5**-b). The bands assigning to thiophene showed peak shift 1409 to 1419 and 1400 cm^{-1}. Peak shifts from 1409 to 1419 and 1400 cm^{-1} are attributed to η^1-(S)-coordination and adsorption through π electrons in thiophene adsorption.[74, 79] The bands that appeared at 3670 and 3656 cm^{-1} correspond to hydrogen bonding, and the one at 1348 cm^{-1} corresponds to ν(S-O). The difference spectrum Figure **A-5**-b suggests that the adsorption of thiophene occurs through π electrons, η^1-(S)-coordination and hydrogen bonding. Since η^1-(S)-coordination appeared along with S-O band, η^1-(S)-coordinated thiophene adsorbs at surface oxygen.

Figure **A-5**-c shows the difference spectrum after stopped thiophene/Ar flow into the cell. This spectrum did not show any significant difference. This observation suggests that adsorbed thiophene molecule does not change the adsorption mode with time over NiO. The difference spectra Figure **A-5**-d to **A-5**-e shows the significant decrease of bands corresponding to thiophene due to the Ar flow introduction. This result suggests that molecular thiophene easily desorbed from the NiO surface by Ar flow and the formation of S-O bonding is not strong. Thus, thiophene associatively and weakly adsorbs over NiO.

IR spectra of thiophene adsorption over ZnO

Figure **A-6**-a showed no distinguishable bands in the IR difference spectrum. For more quantities of thiophene introduced, bands appeared at 3624, 3107, 3097, 3081, 1583, 1417, 1410, 1400, 1389, 1354, 1282, 161, 1252, 1090, 1082 and 1036 cm^{-1} in Figure **A-6**-b. The bands previously assigned to thiophene appeared along with new bands, such as bands at 1389, 1354, and 1282 cm^{-1}. The bands assigned to thiophene appeared with peak shifts from 1588 to 1583 cm^{-1}, 1409 to 1419 and 1400 cm^{-1}, 1252 to 1254 cm^{-1}. This peak shift from 1409 to 1417 and 1400 cm^{-1} represents the attribution of η^1-(S)-coordination of thiophene and adsorption of thiophene through π electrons.[74, 79] Intensity of the band at 1400 cm^{-1} is stronger than the intensity at 1417 cm^{-1}. This demonstrates that thiophene adsorbs on ZnO dominantly through π electrons. The new bands that appeared at 1389, 1354, and 1282 cm^{-1}, along with thiophene adsorption, are possibly assigned to S-O stretching vibration of sulfite. This result is in good agreement with the XPS result by Jirsak et al.[70] They showed the S 2p XPS spectra of thiophene adsorbed on ZnO studied by XPS. The binding energy of adsorbed thiophene on ZnO at room temperature corresponds to sulfite. However, molecular thiophene adsorbs over ZnO by the more than one type of bonding configurations as seen in the difference IR spectrum.

After the incoming Ar flow with thiophene into the DRIFT cell was stopped and kept it for 60 min, the bands did not show the significant difference in the difference spectrum (Figure **A-6**-c). This observation indicates that most of the adsorbed thiophene does not change the adsorption mode over ZnO. After introduction of Ar flow into the DRIFT cell, the bands corresponding to thiophene decreased the intensity (Figure **A-6**-d),

and further significant Ar flow into the DRIFT cell did not show any distinguishable bands in the difference spectrum (Figure **A-6**-e). This results suggests that thiophene adsorbs weakly over ZnO

Sulfur removal of liquid fuels and thiophene adsorption over metal oxides

Adsorption of thiophene over the selected metal oxides was studied by using in-situ FT-IR. The IR spectral measurements of adsorbed thiophene over Cr_2O_3, CeO_2, NiO and ZnO showed that thiophene adsorption occurs through both η^1-(S)-coordination, π electrons and hydrogen bonding. Molecular thiophene adsorption through hydrogen bonding over Cr_2O_3, CeO_2, NiO and ZnO was observed as reported previously.[68] Thiophene adsorption through η^1-(S)-coordination was observed with absorbance feature assigned to S-O bonding over Cr_2O_3, CeO_2, NiO and ZnO. This result indicates that surface oxygen is the major adsorption site for η^1-(S)-coordination. Therefore, the selective sulfur removal from the liquid hydrocarbons was achieved by the oxides used as oxidative catalyst. The associative adsorption of thiophene was observed for Cr_2O_3, CeO_2, NiO and ZnO. Dissociative adsorption of thiophene occurred only over Cr_2O_3 and CeO_2. The surface oxygen of Cr_2O_3 and CeO_2 oxidize the sulfur atom of thiophene, and this nature could play an important role on the selective sulfur removal from liquid hydrocarbons. As seen in this study, if the surface oxygen is the major active sites for adsorption of thiophene, metal oxides, such as Cr_2O_3 and CeO_2, are very beneficial to use in practical applications because the hydrogen usage may not be required to activate the

oxides. These results suggest that Cr_2O_3 and CeO_2 are particularly promising adsorbents for adsorptive desulfurization of liquid hydrocarbon fuels.

A. 4 Conclusions

On the basis of the above discussion, the following conclusions can be drawn regarding the adsorptive desulfurization of liquid fuels over metal oxides and in-situ IR studies of thiophene adsorption.

(1) Eighteen metal oxides (Y_2O_3, La_2O_3, CeO_2, TiO_2, ZrO_2, V_2O_5, Nb_2O_5, Cr_2O_3, MoO_2, WO_2, MnO, Fe_2O_3, RuO_2, CoO, CuO, Ag_2O, NiO, and ZnO) used as adsorbents were tested for their ability to remove sulfur compounds from a model fuel and a jet fuel at room temperature, under ambient pressure and without H_2 usage. The results of this study showed that MnO, Ag_2O, and WO_2 had the highest sulfur removal performance according to their adsorption capacity on the base of the surface area.

(2) V_2O_5, MoO_2, RuO_2 and Ag_2O effectively removed sulfur compounds from the simple model fuel more effectively than from JP-5 jet fuel. This difference was due to a competitive adsorption with co-existing aromatic compounds and variety of alkylated benzothiophenes present in the jet fuel. On the other hand, the adsorption selectivity toward sulfur compounds over CuO, Cr_2O_3, NiO, ZnO and CeO_2 was higher based on the relative sulfur removing capacities. The electron configuration of metal cation d^1-d^9 of the metal oxides in the oxidative properties may play an important role on the selective sulfur removal of the liquid fuels.

(3) Thiophene molecularly adsorbs through η^1-(S)-coordination, π electron and hydrogen bonding over Cr_2O_3, CeO_2, NiO and ZnO. Adsorption of thiophene in η^1-(S)-coordination occurs with surface oxygen.

(4) Thiophene associatively and dissociatively adsorb on Cr_2O_3 and CeO_2. Surface oxygen plays an important role on the dissociative adsorption through η^1-(S)-coordination over Cr_2O_3 and CeO_2. Due to the sulfur selectivity and strong adsorption through η^1-(S)-coordination with surface oxygen, Cr_2O_3 and CeO_2 can be the promising oxidatively regenerable metal oxide-based adsorbents to be utilized for adsorptive desulfurization of liquid fuels.

Table **A-1**: Physical Properties of Metal Oxides

Metal Oxides	S_{BET} (m^2/g)	Pore Volume (cm^3/g)	Pore Diameter (nm)
Y_2O_3	7.6	0.04	21.1
La_2O_3	4.4	0.02	17.7
CeO_2	6.1	0.02	14.3
TiO_2	7.0	0.04	20.0
ZrO_2	6.7	0.03	19.7
V_2O_5	4.7	0.02	14.2
Nb_2O_5	6.3	0.03	19.8
Cr_2O_3	42.5	0.16	15.4
MoO_2	4.6	0.00	15.5
WO_2	0.6	0.00	21.5
MnO	0.3	0.00	12.3
Fe_2O_3	8.9	0.11	47.3
RuO_2	9.1	0.05	21.1
CoO	10.0	0.03	11.2
NiO	30.7	0.15	19.7
CuO	1.6	0.02	38.7
Ag_2O	0.8	0.00	23.7
ZnO	6.8	0.09	52.7

Table **A-2**: Sulfur Removal of Model Fuel over Metal Oxides.

Metal oxides	S conc. after treatment (ppmw)	Capacity (mg-S/g-Ads.)	Capacity (mg-S/m^2-Ads.)
Initial	968	-	-
Y_2O_3	712	1.28	0.168
La_2O_3	714	1.27	0.28
CeO_2	754	1.07	0.18
TiO_2	734	1.17	0.17
ZrO_2	750	1.09	0.16
V_2O_5	662	1.54	0.33
Nb_2O_5	714	1.22	0.19
Cr_2O_3	588	1.90	0.045
MoO_2	667	1.49	0.33
WO_2	726	1.23	2.05
MnO	715	1.25	4.03
Fe_2O_3	672	1.50	0.17
RuO_2	675	1.48	0.16
CoO	718	1.25	0.13
NiO	768	1.01	0.03
CuO	757	1.06	0.67
Ag_2O	690	1.42	1.89
ZnO	780	0.96	0.14

* Initial sulfur conc. of model fuel: 968 ppmw. Metal oxide: fuel ratio= 1:5 wt. Contact time: 2 hrs.

Table **A-3**: Sulfur Removal of JP-5 Fuel over Metal Oxides

Metal oxides	S conc. after treatment	Capacity		Relative Capacity
	(ppmw)	(mg-S/g-Ads.)	(mg-S/m^2-Ads.)	$Capa._{JP5}/Capa._{ModelFuel}$
initial	1055	-	-	-
Y_2O_3	951	0.51	0.07	0.39
La_2O_3	938	0.52	0.12	0.42
CeO_2	953	0.51	0.08	0.48
TiO_2	992	0.35	0.05	0.30
ZrO_2	975	0.37	0.06	0.34
V_2O_5	954	0.51	0.11	0.33
Nb_2O_5	982	0.36	0.06	0.30
Cr_2O_3	806	1.25	0.03	0.61
MoO_2	976	0.39	0.09	0.26
WO_2	956	0.49	0.82	0.40
MnO	969	0.42	1.35	0.34
Fe_2O_3	961	0.47	0.05	0.31
RuO_2	944	0.56	0.06	0.38
CoO	966	0.44	0.04	0.35
NiO	948	0.54	0.02	0.53
CuO	921	0.67	0.42	0.63
Ag_2O	962	0.46	0.61	0.32
ZnO	948	0.49	0.07	0.51

* Initial sulfur conc. of JP-5: 1055 ppmw. Metal oxide: fuel ration=1:5 wt. Contact time: 2 hrs.

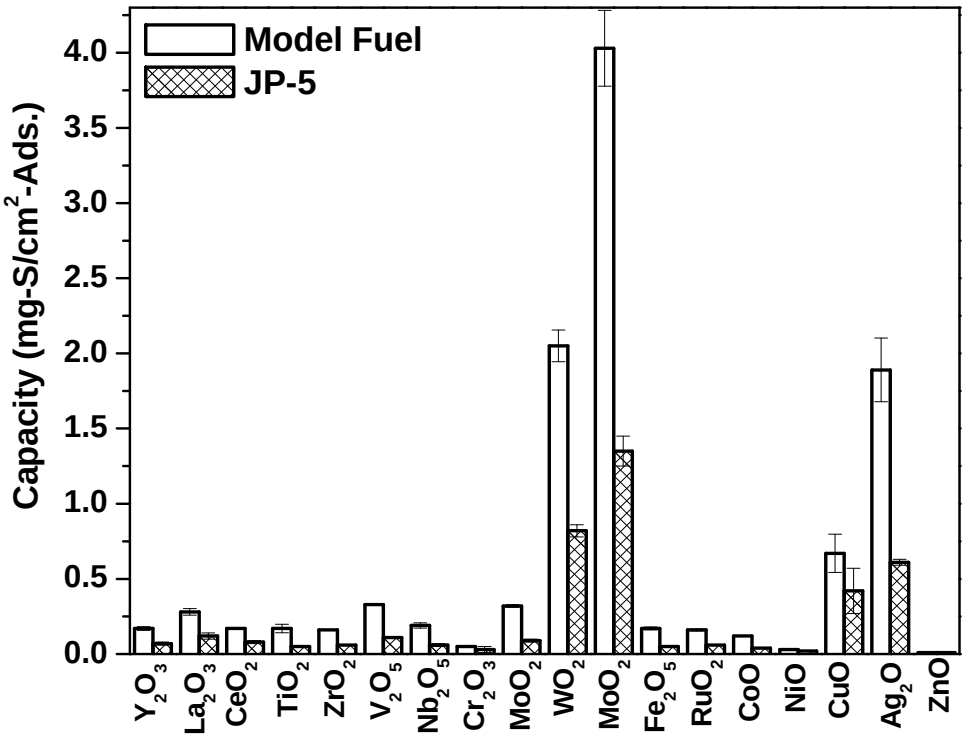

Figure **A-1**: Sulfur removal capacity of model fuel and JP-5 over metal oxides at room temperature for 2 hrs. Fuel/adsorbent weight ratio= 1:5.

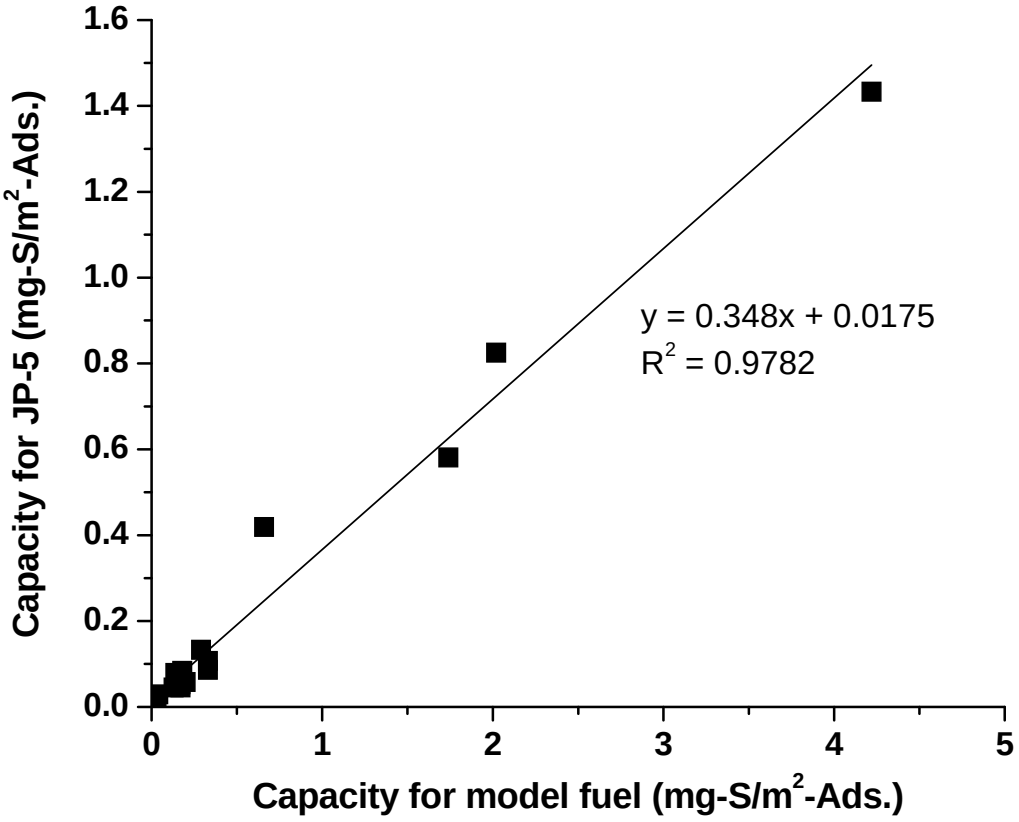

Figure **A-2**: Comparison of sulfur removing capacities of model fuel and JP-5

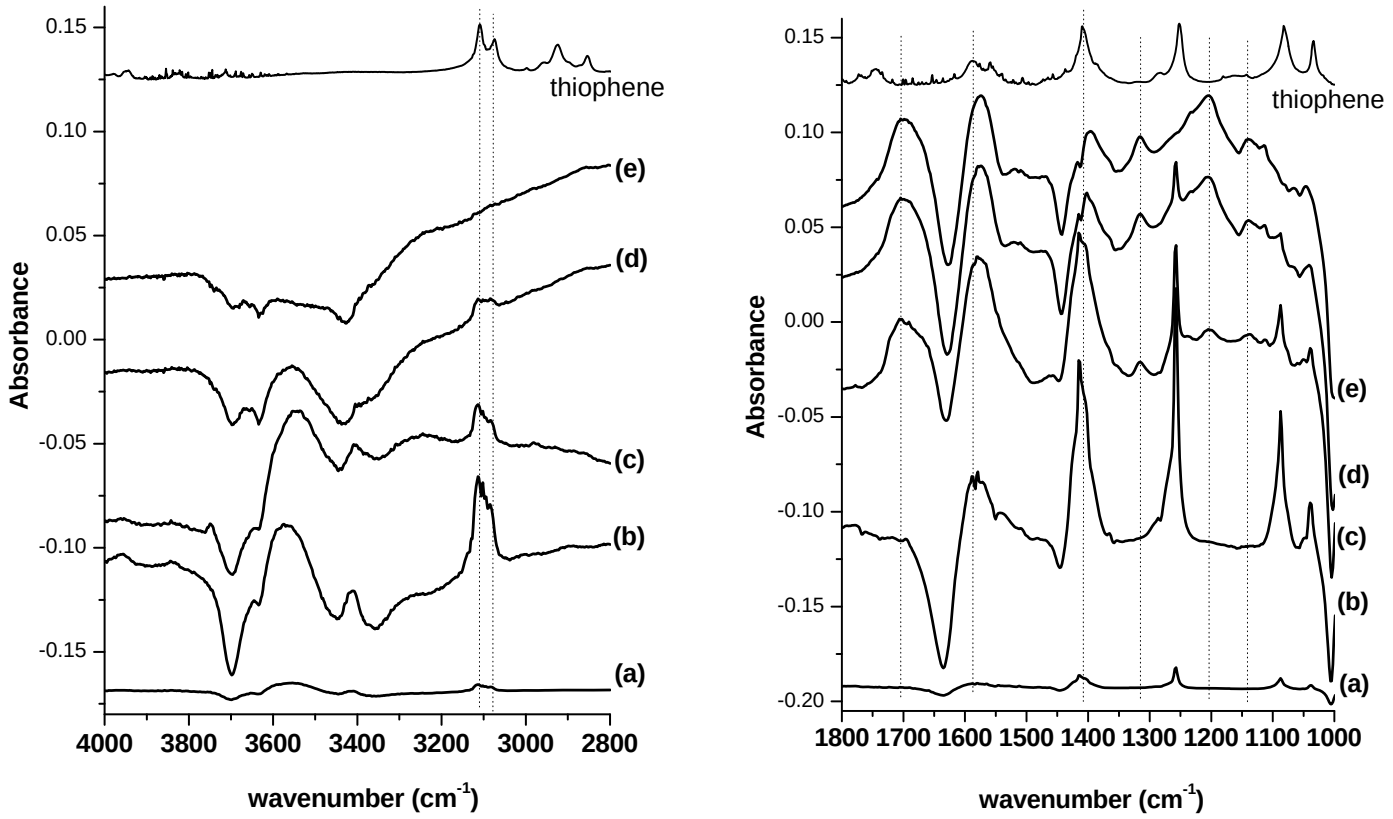

Figure **A-3**: FT-IR difference spectra obtained by subtracting the spectrum of vacuumed-dried Cr_2O_3 (200 ^oC for 1 hr) from (a) the spectrum Cr_2O_3 exposed to thiophene/Ar flow for 1 min, (b) the spectrum of Cr_2O_3 exposed to thiophene/Ar flow for 60 min, (c) the spectrum of Cr_2O_3 aged for 60 min after exposed to thiophene/Ar flow for 60 min, (d) the spectrum of Cr_2O_3 under Ar flow for 1 min, (e) the spectrum of Cr_2O_3 under Ar flow for 15 min, at room temperature in the range of 4000 – 2800 cn^{-1} (left) and 1800 - 1000 cm^{-1} (right).

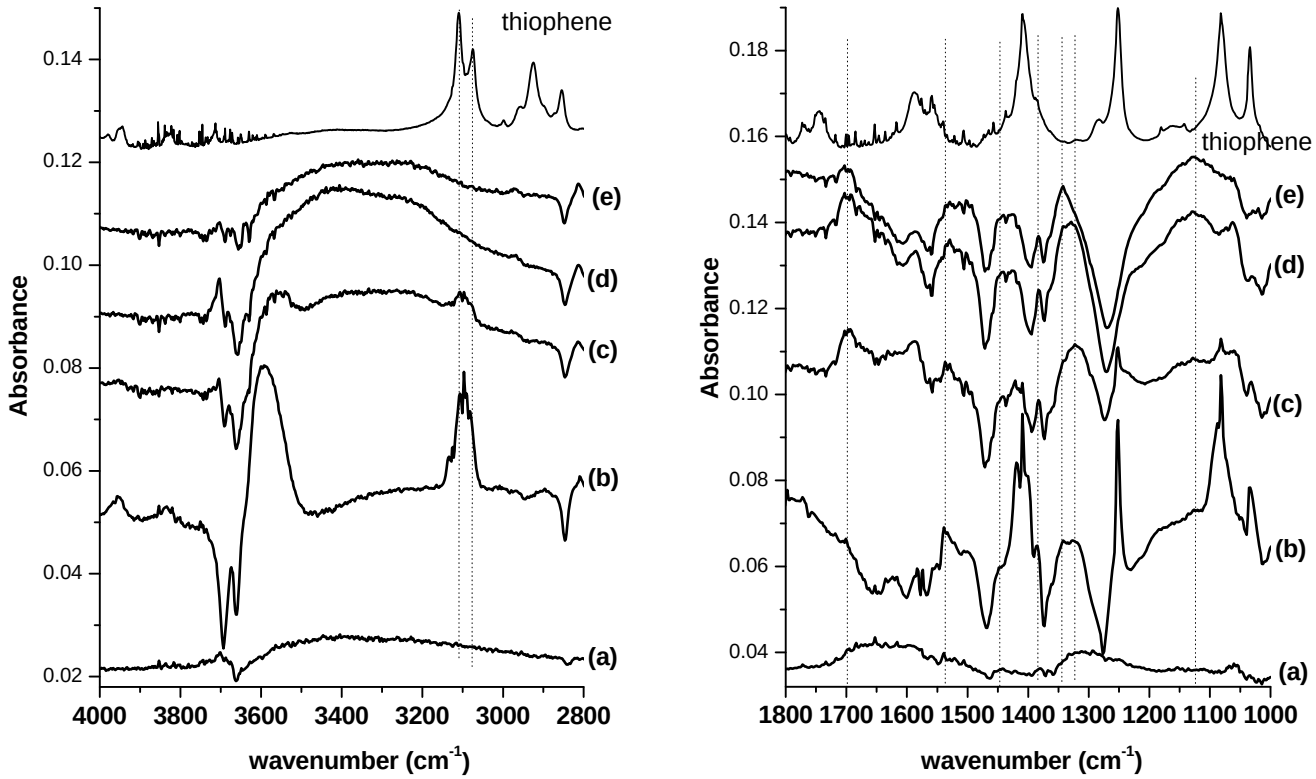

Figure **A-4**: FT-IR difference spectra obtained by subtracting the spectrum of vacuumed-dried CeO_2 (200 ^oC for 1 hr) from (a) the spectrum CeO_2 exposed to thiophene/Ar flow for 1 min, (b) the spectrum of CeO_2 exposed to thiophene/Ar flow for 60 min, (c) the spectrum of CeO_2 aged for 60 min after exposed to thiophene/Ar flow, (d) the spectrum of CeO_2 under Ar flow for 5 min, (e) the spectrum of CeO_2 under Ar flow for 60 min, at room temperature in the range of 4000 – 2800 cn^{-1} (left) and 1800 - 1000 cm^{-1} (right).

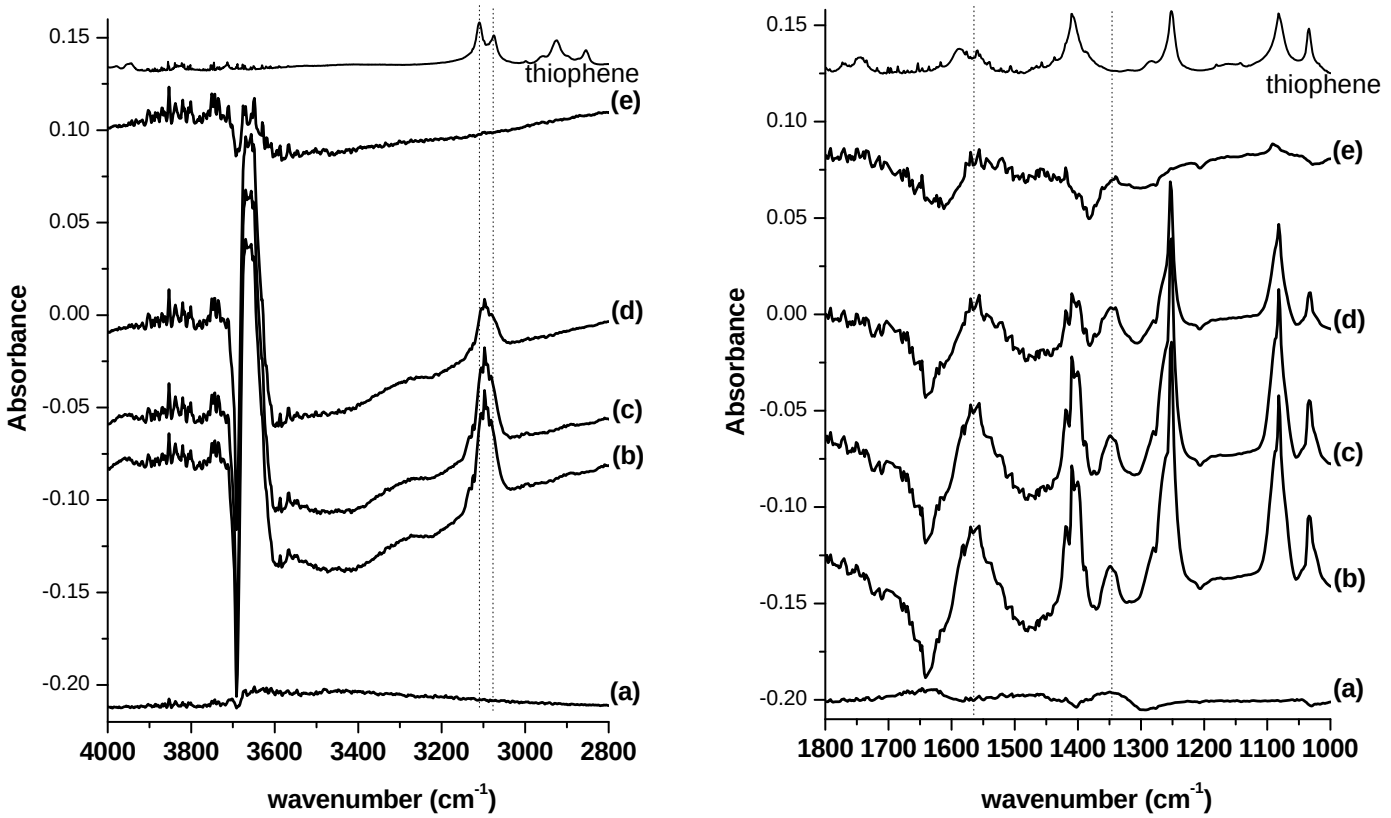

Figure **A-5**: FT-IR difference spectra obtained by subtracting the spectrum of vacuumed-dried NiO (200 ^{o}C for 1 hr) from (a) the spectrum NiO exposed to thiophene/Ar flow for 1 min, (b) the spectrum of NiO exposed to thiophene/Ar flow for 60 min, (c) the spectrum of NiO aged for 60 min after exposed to thiophene/Ar flow, (d) the spectrum of NiO under Ar flow for 1 min, (e) the spectrum of NiO under Ar flow for 60 min, at room temperature in the range of 4000 – 2800 cn^{-1} (right) and 1800 - 1000 cm^{-1} (left).

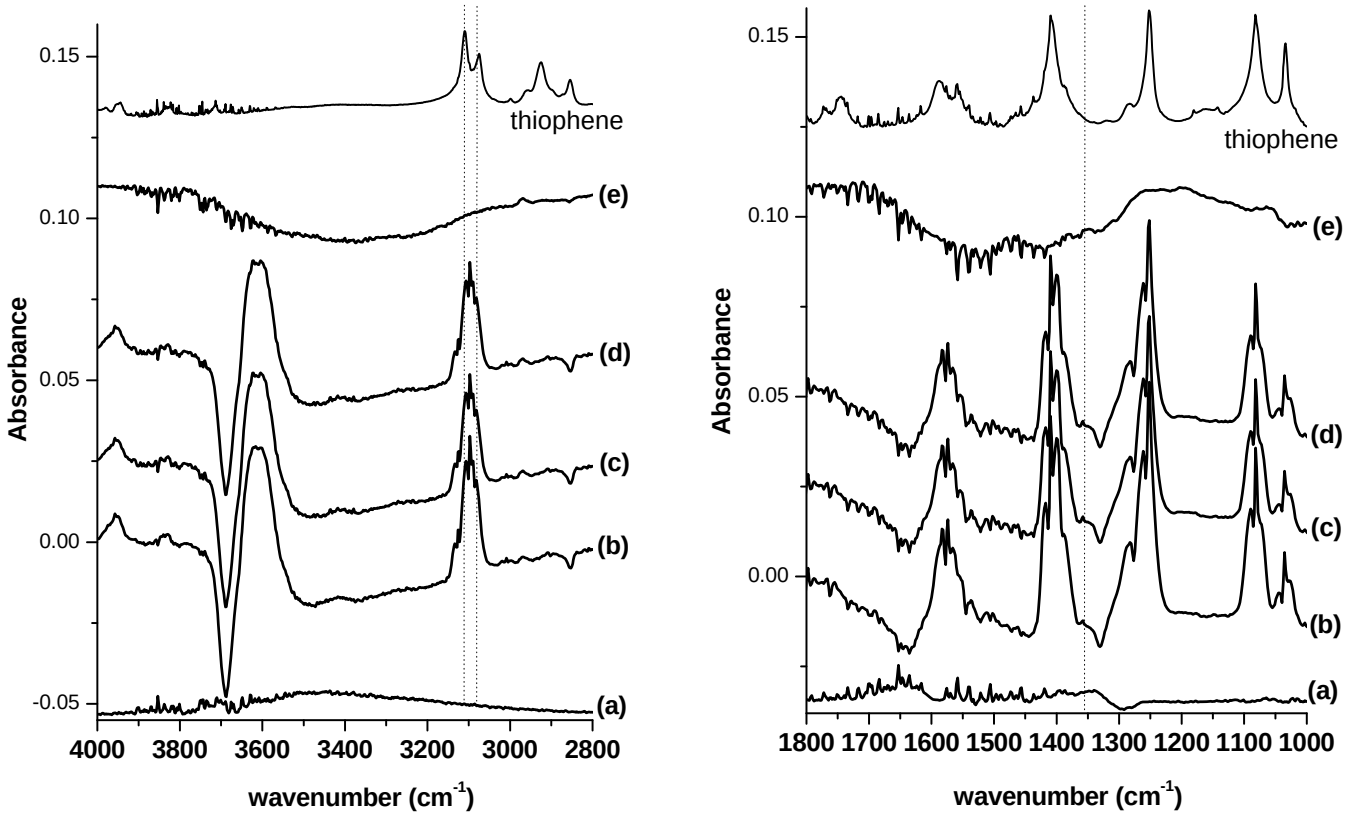

Figure **A-6**: FT-IR difference spectra obtained by subtracting the spectrum of vacuumed-dried ZnO (200 ^{o}C for 1 hr) from (a) spectrum ZnO exposed to thiophene/Ar flow for 1 min, (b) the spectrum of ZnO exposed to thiophene/Ar flow for 60 min, (c) the spectrum of ZnO aged for 60 min after exposed to thiophene/Ar flow, (d) the spectrum of ZnO under Ar flow for 1 min, (e) the spectrum of ZnO under Ar flow for 60 min, at room temperature in the range of 4000 – 2800 cn^{-1} (right) and 1800 - 1000 cm^{-1} (left).

References:

(1) Song, C. S., An overview of new approaches to deep desulfurization for ultra-clean gasoline, diesel fuel and jet fuel. *Catalysis Today* **2003,** 86, (1-4), 211.

(2) Gates, B. C.; Topsoe, H., Reactivities in deep catalytic hydrodesulfurization: Challenges, opportunities, and the importance of 4-methyldibenzothiophene and 4,6-dimethyldibenzothiophene. *Polyhedron* **1997,** 16, (18), 3213.

(3) Topsoe, H.; Clausen, B. S.; Massoth, F. E., *Hydrotreating Catalysis*. ed.; Springer-Verlag: Berlin, 1996.

(4) Song, C. S.; Ma, X. L., Ultra-deep desulfurization of liquid hydrocarbon fuels: Chemistry and process. *International Journal of Green Energy* **2004,** 1, (2), 167.

(5) Babich, I. V.; Moulijn, J. A., Science and technology of novel processes for deep desulfurization of oil refinery streams: A review. *Fuel* **2003,** 82, (6), 607.

(6) Song, C.; Ma, X. L., New design approaches to ultra-clean diesel fuels by deep desulfurization and deep dearomatization. *Applied Catalysis B-Environmental* **2003,** 41, (1-2), 207.

(7) Hernandez-Maldonado, A. J.; Yang, R. T., Desulfurization of transportation fuels by adsorption. *Catalysis Reviews-Science and Engineering* **2004,** 46, (2), 111.

(8) Ma, X. L.; Sun, L.; Song, C. S., A new approach to deep desulfurization of gasoline, diesel fuel and jet fuel by selective adsorption for ultra-clean fuels and for fuel cell applications. *Catalysis Today* **2002,** 77, (1-2), 107.

(9) Watanabe, S. Selective and Regenerable Metal Oxide Adsorbents for the Removal of Sulfur from Liquid Fuels for Fuel Cell Applications. Master of Science, The Pennsylvania State University, University Park, Pennsylvania, 2004.

(10) Ma, X. L.; Sprague, M.; Song, C. S., Deep desulfurization of gasoline by selective adsorption over nickel-based adsorbent for fuel cell applications. *Industrial & Engineering Chemistry Research* **2005,** 44, (15), 5768.

(11) Velu, S.; Ma, X. L.; Song, C. S., Selective adsorption for removing sulfur from jet fuel over zeolite-based adsorbents. *Industrial & Engineering Chemistry Research* **2003,** 42, (21), 5293.

(12) Hernandez-Maldonado, A. J.; Yang, F. H.; Qi, G.; Yang, R. T., Desulfurization of transportation fuels by pi-complexation sorbents: Cu(I)-, Ni(II)-, and Zn(II)-zeolites. *Applied Catalysis B-Environmental* **2005,** 56, (1-2), 111.

(13) Velu, S.; Song, C. S.; Engelhard, M. H.; Chin, Y. H., Adsorptive removal of organic sulfur compounds from jet fuel over K-exchanged NiY zeolites prepared by impregnation and ion exchange. *Industrial & Engineering Chemistry Research* **2005,** 44, (15), 5740.

(14) Velu, S.; Ma, X. L.; Song, C. S.; Namazian, M.; Sethuraman, S.; Venkataraman, G., Desulfurization of JP-8 jet fuel by selective adsorption over a Ni-based adsorbent for micro solid oxide fuel cells. *Energy & Fuels* **2005,** 19, (3), 1116.

(15) Zhou, A. N.; Ma, X. L.; Song, C. S., Liquid-phase adsorption of multi-ring thiophenic sulfur compounds on carbon materials with different surface properties. *Journal of Physical Chemistry B* **2006,** 110, (10), 4699.

(16) Turk, B. S.; Gupta, R. P., RTI's trend process for deepdesulfurization of naphtha. *Prepr. Pap. - Am. Chem. Soc., Div. Fuel Chem.* **2001,** 46, 392.

(17) Rehms, D. L., Laboratory evaluation of promoted alumina adsorbent for fuel desulfurization. *Prepr. Pap. - Am. Chem. Soc., Div. Fuel Chem.* **2002,** 47, (2), 454

(18) Tsyganenko, A. A.; Can, F.; Mauge, F., IR study of the adsorption and isotopic scrambling of thiophene on CaO. *Journal of physical Chemistry B* **2003,** 107, 8578.

(19) Quigley, W. W. C.; Yamamoto, H. D.; Aegerter, P. A.; Simpson, G. J.; Bussell, M. E., Infrared spectroscopy and temperature-programmed desorption study of adsorbed thiophene on gamma-Al_2O_3. *Langmuir* **1996,** 12, (6), 1500.

(20) Liu, G.; Rodriguez, J. A.; Hrbek, J.; Long, B. T.; Chen, D. A., Interaction of thiophene with stoichiometric and reduced rutile TiO_2(110) surfaces: role of Ti^{3+} sites in desulfurization activity. *Journal of Molecular Catalysis a-Chemical* **2003,** 202, (1-2), 215.

(21) Hedhili, M. N.; Yakshinskiy, B. V.; Schlereth, T. W.; Gouder, T.; Madey, T. E., The interactions of thiophene with polycrystalline UO_2. *Surface Science* **2005,** 574, (1), 17.

(22) Rico, M.; Orza, J. M.; Morcillo, J., Fundamental vibrations of thiophene and its deuterated derivatives. *Spectrochimica Acta* **1965,** 21, 689.

(23) Mills, P.; Korlann, S.; Bussell, M. E.; Reynolds, M. A.; Ovchinnikov, M. V.; Angelici, R. J.; Stinner, C.; Weber, T.; Prins, R., Vibrational study of organometallic complexes with thiophene ligands: Models for adsorbed thiophene on hydrodesulfurization catalysts. *Journal of Physical Chemistry A* **2001,** 105, (18), 4418.

(24) Angelici, R. J., Structural Aspects of Thiophene Coordination in Transition-Metal Complexes. *Coordination Chemistry Reviews* **1990,** 105, 61.

(25) Angelici, R. J., Thiophenes in organotransition metal chemistry: Patterns of reactivity. *Organometallics* **2001,** 20, (7), 1259.

(26) Harris, S., Bonding and Reactivity in Transition-Metal Complexes Containing Thiophenic Ligands. *Organometallics* **1994,** 13, (7), 2628.

(27) Tarbuck, T. L.; McCrea, K. R.; Logan, J. W.; Heiser, J. L.; Bussell, M. E., Identification of the adsorption mode of thiophene on sulfided Mo catalysts. *Journal of Physical Chemistry B* **1998,** 102, (40), 7845.

(28) Mills, P.; Phillips, D. C.; Woodruff, B. P.; Main, R.; Bussell, M. E., Investigation of the adsorption and reactions of thiophene on sulfided Cu, Mo, and Rh catalysts. *Journal of Physical Chemistry B* **2000,** 104, (14), 3237.

(29) Wu, W. C.; Wu, Z. L.; Feng, Z. C.; Ying, P. L.; Li, C., Adsorption and reaction of thiophene and H_2S on Mo_2C/Al_2O_3 catalyst studied by in situ FT-IR spectroscopy. *Physical Chemistry Chemical Physics* **2004,** 6, (24), 5596.

(30) Wu, Z. L.; Li, C.; Wei, Z. B.; Ying, P. L.; Xin, Q., FT-IR spectroscopic studies of thiophene adsorption and reactions on Mo_2N/gamma-Al_2O_3 catalysts. *Journal of Physical Chemistry B* **2002,** 106, (5), 979.

(31) Nicholson, D. E., Identification of Adsorbed Species by Intrared Spectrometry. *Analytical Chemistry* **1962,** 34, (3), 370.

(32) Ratnasam.P; Fripiat, J. J., Surface Chemistry of Sulphides .1. Infra-red Study of Molybdenum and Germanium Sulphides and of Their Reaction with H_2, H_2O, Thiophene and Ethanethiol. *Transactions of the Faraday Society* **1970,** 66, (575), 2897.

(33) Kim, J. H.; Ma, X. L.; Zhou, A. N.; Song, C. S., Ultra-deep desulfurization and denitrogenation of diesel fuel by selective adsorption over three different adsorbents: A study on adsorptive selectivity and mechanism. *Catalysis Today* **2006,** 111, (1-2), 74.

(34) Kundakovic, L.; Flytzani-Stephanopoulos, M., Reduction characteristics of copper oxide in cerium and zirconium oxide systems. *Applied Catalysis a-General* **1998,** 171, (1), 13.

(35) Ma, X. L.; Velu, S.; Kim, J. H.; Song, C. S., Deep desulfurization of gasoline by selective adsorption over solid adsorbents and impact of analytical methods on ppm-level sulfur quantification for fuel cell applications. *Applied Catalysis B-Environmental* **2005,** 56, (1-2), 137.

(36) Kung, H. H., Desirable Catalyst Properties in Selective Oxidation Reactions. *Industrial & Engineering Chemistry Product Research and Development* **1986,** 25, (2), 171.

(37) Gray, J. H.; Handwerk, G. E., Petroleum Refining. In 4 ed.; 'Ed.'^'Eds.' Marcel Dekker: 2001; 'Vol.' p^pp 16.

(38) King, D. L.; Faz, C.; Flynn, T., Desulfurization of gasoline feedstocks for application in fuel reforming. *Society of automotive engineers papaer 2000-01-0002* **2000**, 1.

(39) Weitkamp, J.; Schwark, M.; Ernst, S., Removal of Thiophene Impurities from Benzene by Selective Adsorption in Zeolite Zsm-5. *Journal of the Chemical Society-Chemical Communications* **1991**, (16), 1133.

(40) Iwamoto, M.; Yoda, Y.; Yamazoe, N.; Seiyama, T., Study of Metal-Oxide Catalysts by Temperature Programmed Desorption .4. Oxygen-Adsorption on Various Metal-Oxides. *Journal of Physical Chemistry* **1978,** 82, (24), 2564.

(41) El-Azhary, A. A.; Hilal, R. H., Vibrational analysis of the spectra of furan and thiophene. *Spectrochimica Acta Part a-Molecular and Biomolecular Spectroscopy* **1997,** 53, (9), 1365.

(42) Garcia, C. L.; Lercher, J. A., Adsorption and Surface-Reactions of Thiophene on ZSM-5 Zeolites. *Journal of Physical Chemistry* **1992,** 96, (6), 2669.

(43) Smith, A. L., *Applied Infrared Spectroscopy*. ed.; John Wiley & Sons: 1979.

(44) Nakamoto, K., *Infrared and Raman Spectra of Inorganic and Coordination Compounds Part B: Applications in Coordination, Organometallic, and Bioinorganic Chemistry*. Fifth ed.; John Wiley & Sons, Inc.: New York, 1997.

(45) Kataoka, S.; Lee, E.; Tejedor-Tejedor, M. I.; Anderson, M. A., Photocatalytic degradation of hydrogen sulfide and in situ FT-IR analysis of reaction products on surface of TiO2. *Applied Catalysis B-Environmental* **2005,** 61, (1-2), 159.

(46) Waqif, M.; Pieplu, A.; Saur, O.; Lavalley, J. C.; Blanchard, G., Use of CeO_2-Al_2O_3 as a SO_2 sorbent. *Solid State Ionics* **1997,** 95, (1-2), 163.

(47) Rodriguez, J. A.; Jirsak, T.; Perez, M.; Chaturvedi, S.; Kuhn, M.; Gonzalez, L.; Maiti, A., Studies on the behavior of mixed-metal oxides and desulfurization: Reaction of H_2S and SO_2 with Cr_2O_3(0001), MgO(100), and $Cr_XMg_{1-X}O$(100). *Journal of the American Chemical Society* **2000,** 122, (49), 12362.

(48) Davydov, A. A., *Molecular spectroscopy of oxide catalyst surfaces*. ed.; Jon Wiley & Sons Inc.: 2003.

(49) Smirnov, M. Y.; Kalinkin, A. V.; Pashis, A. V.; Sorokin, A. M.; Noskov, A. S.; Kharas, K. C.; Bukhtiyarov, V. I., Interaction of Al_2O_3 and CeO_2 surfaces with SO_2 and SO_2+O_2 studied by X-ray photoelectron spectroscopy. *Journal of Physical Chemistry B* **2005,** 109, (23), 11712.

(50) Ferrizz, R. M.; Gorte, R. J.; Vohs, J. M., TPD and XPS investigation of the interaction of SO_2 with model ceria catalysts. *Catalysis Letters* **2002,** 82, (1-2), 123.

(51) Rodriguez, J. A.; Jirsak, T.; Freitag, A.; Hanson, J. C.; Larese, J. Z.; Chaturvedi, S., Interaction of SO2 with CeO2 and Cu/CeO2 catalysts: photoemission, XANES and TPD studies. *Catalysis Letters* **1999,** 62, (2-4), 113.

(52) Jirsak, T.; Dvorak, J.; Rodriguez, J. A., Chemistry of thiophene on ZnO, S/ZnO, and Cs/ZnO surfaces: Effects of cesium on desulfurization processes. *Journal of Physical Chemistry B* **1999,** 103, (26), 5550.

Appendix B

Preparation Procedure of Oxidatively Regenerable $Ti_{0.9}Ce_{0.1}O_2$ Oxide-based Adsorbent

Apparatus

1. Hot Plate/Stirrer
2. Digital pH meter equipped with thermometer (Corning Ph meter 340)

   Probe: Mettler Toledo InLab® Power Pro pH
3. Griffin beaker: 1000 mL × 1, 200 mL × 2
4. Magnetic stir Bar: 3" (leng.) × ½" (dia.), 1½" (leng.) × ⅜" (dia.)
5. Vacuum pump
6. Büchner funnel
7. Filter paper and filtering flask (1000 mL)
8. HPLC column (½" OD x 10 mm ID x 25 cm)

Reagent

1. Titanium (IV) oxysulfate - sulfuric acid complex hydrate (synthesis grade)
2. Ammonium cerium (IV) nitrate (99.99 %)
3. Urea (reagent grade, 98 %)
4. Deionized water

Arrangement

1. pH meter calibration
    a. Calibrate pH meter using three pH standard solutions with pH = 4, 7 and 10. Check the discrepancies in the measurements, record pH values at all the points before adjustment. The calibration has to be carried out before the experiment periodically.

Preparation Procedure

1. Ti aqueous solution
    a. Weigh Ti oxysulfate-sulfuric acid complex hydrate (32.68 g)
    b. Record supplier, type and lot number of the raw materials. Weigh as dry base.
    c. Place weighed Ti salt in 250 mL beaker. Add deionized water into the same beaker to prepare 100 mL of aqueous solution.
    d. Mix the solution by using a small magnetic stir bar. It takes 1 ~ 2 hrs to completely dissolve. Mix by a small stir bar until pH stabilizes.
    e. Measure the pH of the solution (I). The pH of the solution could be < 1.
2. Ce aqueous solution
    a. Weigh Ammonium cerium nitrate (8.2 g)

b. Record supplier, type and lot number of the raw materials. Weigh as dry base.

c. Place weighed Ce salt in 250 mL beaker. Add deionized water into the same beaker to prepare 100 mL of aqueous solution.

d. Mix the solution by using a small magnetic stir bar. It takes 1 ~ 2 min to completely dissolve. Mix by a small stir bar until pH stabilizes.

e. Measure the pH of the solution (II). The pH of the solution could be ~ 1.

3. Urea aqueous solution

a. Weigh urea (70 g)

b. Record supplier, type and lot number of the raw materials. Weigh as dry base.

c. Place weighed urea in 1000 mL beaker. Add deionized water into the same beaker to prepare 800 mL of aqueous solution.

d. Mix the solution by using a large magnetic stir bar. It takes 1 ~ 2 min to completely dissolve. Mix by a large stir bar until pH stabilizes. T

e. Measure the pH of the solution (III). he pH of the solution could be ~ 8.

4. Mixing of the aqueous solutions

a. Add solution (II) into (I): solution (IV). Mix by a small stir bar until pH stabilizes. The pH of the solution could be ~ 1.

b. Add solution (IV) into (III): solution (V). Mix by a large stir bar until pH stabilizes. The pH of the solution could be ~ 1.5.

5. Heating the mixed aqueous solution (V)

   a. Apply the heating (set at 300 ^{o}C, if possible).

   b. Record the pH and temperature of the solution with time. The pH and temperature change as a function of time as seen in Figure **B-1**.

   c. Stop heating 2 hrs after the pH reaches above 6 with continuous stirring.

   d. Stop stirring when the solution temperature reaches below 30 ^{o}C.

   e. Wait all the precipitate sit bottom of the beaker. The precipitate is yellow.

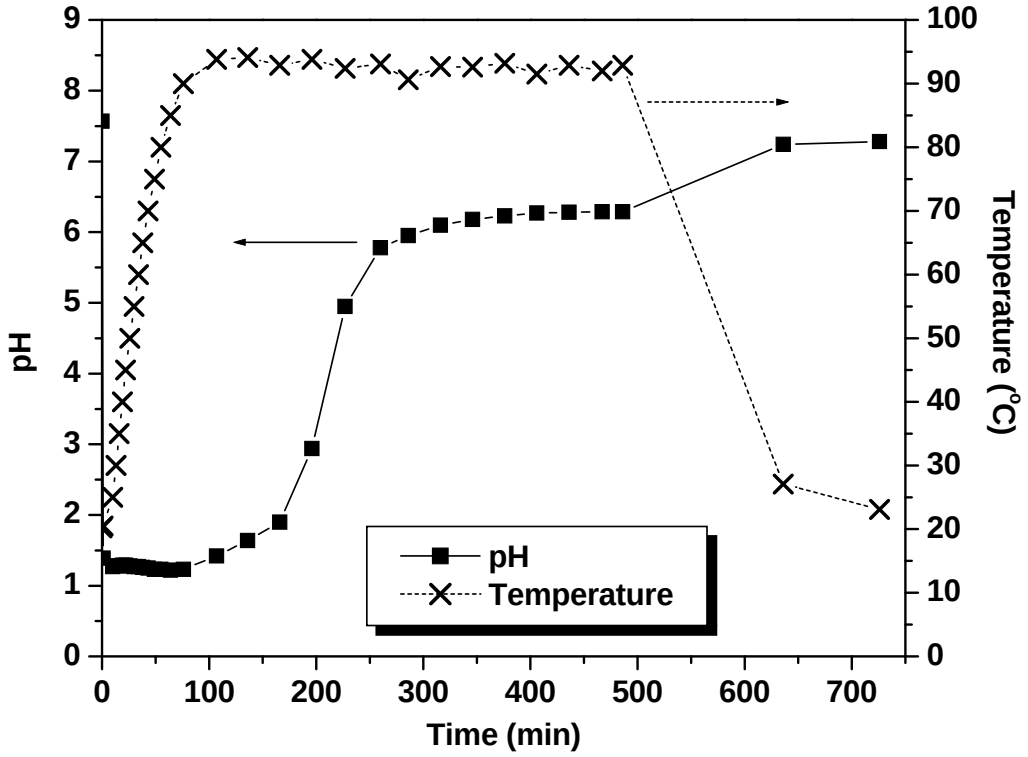

Figure **B-1**: Changes of pH and temperature in the urea precipitation for $Ti_{0.9}Ce_{0.1}O_2$ preparation (data was provided Mamoru Fujii)

6. Filtration
    a. Arrange the filtration system with vacuum pump. Record the funnel diameter and the type of filter paper.
    b. Filter the precipitate. Keep filtration with vacuum for 3 hrs after the most of liquid removed from the precipitate.
    c. Record the starting and final time of filtration.
    d. Measure and record the pH of filtered solution.
7. Drying and Calcination

a. Place the filtered precipitate into the HPLC column.

b. Weigh the amount of precipitant in the column.

c. Connect air flow line to the packed column, and place the packed column in the furnace.

d. Use zero air. Set the inlet air flow rate, 50 mL/min.

e. Set the temperature program of drying and calcination:

   25 ^{o}C → temperature ramp 10 ^{o}C/min → 100 ^{o}C

   100 ^{o}C hold for 3 hrs

   100 ^{o}C → temperature ramp 1.5 ^{o}C/min → 400 ^{o}C

   400 ^{o}C hold for 6 hrs

   400 ^{o}C → 25 ^{o}C with constant air flow

f. Weigh the packed column, and record the weight. Yellow powder should be obtained.

8. Preservation

   a. Label and describe the lot number, precipitation date and your name.

   b. Store the sample in desiccator with drying agent.

Appendix C

Adsorptive Desulfurization Procedure

A fixed-bed Flow System

1. Confirm that the stainless steel column have been cleaned up.
2. Weigh the empty column with two end plugs and two frits.
3. Pack the column with the powder adsorbent.
4. Seal the columns, weigh the packed column with two end plugs, and calculate the weight of the adsorbent, and check whether the weight is reasonable. If not, the column should be repacked again.
5. Confirm whether the pumps, inlet and outlet lines of the device have been cleaned up. If not, clean up them by sulfur-free hexane (Please not use polar solvents for cleaning).
6. Turn on air flow to remove the hexane in the inlet lines before connecting the columns to the system.
7. Connect the columns to the system, and then, turn on air/O_2 flow, and check whether there is a leak. If leak, reconnect the columns again until there is not any leak.
8. Set an inlet air/O_2 flow rate of 50 ml/min for each column.
9. Increase the oven temperature up to 400 ˚C within 30 min under the constant air/O_2 flow and keep at 400 ˚C for 2 hour.

10. Decrease the oven temperature to room temperature under air/O_2 flow by turning off heating and opening oven door. Stop flowing gas at this time when the temperature reaches at 25 ^{o}C.
11. Disconnect the columns, seal two sides of the columns with end plugs soon, weigh the columns with two end plugs, and calculate the net weight of the adsorbent.
12. Clean the pumps and inlet lines by using the testing fuel, and allow about 5 ml of the fuel to pass through each inlet line before connecting the columns to the system.
13. Connect the columns to the system.
14. Increase the oven temperature to the desired temperature, and keep the oven at the desired temperature, and then, turn on the pumps to send the fuel into the columns. Check whether there is a leak.
15. Record the time when the first drop gets out.
16. Collect the samples from the outlet periodically until the sulfur concentration in the effluent reaches at the initial concentration.
17. Weigh the collected samples to calculate the treated fuel.
18. After finish the experiment, decrease the temperature by turning off heating and opening the oven door and flush the remaining fuel out of the column by flowing N_2/air.
19. Disconnect the columns, and weigh the dried spent columns again.
20. Clean the pumps and lines by using sulfur-free hexane.

Regeneration Procedure:

1. After adsorption, flow 50 ml/min of air/O_2 into adsorbent bed.
2. Keep flowing gas for 5 min to remove remaining fuel in adsorbent bed.
3. After any liquid coming out from adsorbent bed, elevate the oven/furnace temperature up to desired temperature (400~550 ^oC) with heating rate 10 ^oC/min.
4. Hold for 1 ~ 2 hrs at the desired temperature.
5. Cool adsorbent bed down to room temperature under the constant flow of air/O_2.
6. Disconnect adsorbent bed from line when the oven/furnace temperature reaches at room temperature. Weigh the adsorbent bed.

A batch system

1. Add 1 g of metal oxides into the clean tube.
2. Place the tube (1) in a batch system and heated up under with or without 30 mL of air flow at 220 ^oC for 1 hour.
3. Seal the tube when it is still hot. Wait the tube temperature reach at room temperature.
4. Add 5 g of fuel and a magnetic stir bar into the tube (3).
5. Turn on heat to set desired temperature, start stirring at 200 rpm, and turn on water circulation to prevent gas evaporation.
6. After the sufficient adsorbent-fuel contact time, separate fuel and metal oxide by filtration or centrifuge.

Appendix D

Adsorptive Desulfurization of Liquid Fuels over TiO_2-based Oxide Adsorbents and Investigation of the Effect of Precursor on Desulfurization Performance

D-1 Experimental

D-1-1 Adsorptive desulfurization

Adsorptive desulfurization of model fuel and real fuel (JP-5) over various TiO_2-based oxide sorbents was conducted. The model fuel consisted of benzothiophene (BT) dissolved in n-decane (n-C_{10}), and the sulfur concentration was 300 ppmw. Jet fuel, JP-5, contained 1055 ppmw of sulfur. The powder adsorbent was placed in a glass tube with an internal diameter of 22 mm and length 150 mm. Adsorbent was pretreated in the glass tube at 350 ^{o}C for 1 hour in atmospheric condition without any gas flow before adsorption. About 5.0 g of a fuel and 0.5 g of metal oxide (fuel/ adsorbent ratio= 10) were stirred by a magnetic stirrer in the test using model fuel for 1 hour and for sulfur removal of JP-5 for up to 18 hours. The adsorbent was separated by filtration after the sulfur removal. Filtered adsorbent used for model fuel testing was placed in the same glass tube, and added 20 g of washing solvent, which consist of 50 vol. % of methanol and 50 wt. % of toluene. Ultrasound was applied for washing for 30 min. The adsorbent was separated by filtration.

D-1-2 Characterization

Antek 9000 Series Sulfur Analyzer (detection limit 0.5 ppmw) was used to determine the total sulfur concentration of the treated JP-5. The used washing solvent was analyzed by GC-FID, O.I. Analytical 5380. A Hewlett 5890 Packard series II gas chromatograph with a capillary column, XTI-5 (Restek, bonded 5 %, 30 m x 0.25 mm ID x 0.25 μm film thickness) and a split mode injector (ratio: 100:1) was used with ultra-high purity helium as a carrier gas. The injector temperature was kept at 290 ˚C.

X-ray powder diffraction (XRD) patterns for the fresh and spent $Ti_{0.9}Ce_{0.1}O_2$were collected at scan rate of 1 ^{o}/min in the 2θ range of 20-65 ^{o} using a Scintag-I XRD instrument equipped with Cu Kα radiation. The working voltage of the instrument was 35 kV and the current was 35 mA. The mean crystallite size of samples was calculated from peak broadening using the Scherrer equation by the function of Jade 6.5, where the Scherrer constant (particle shape factor) was taken as 0.85.

NH_3-TPD was carried out to investigate the acidity of the sorbent. The detailed procedure is described in Chapter 2.

D.2 Results

Figure **D-1** shows the sulfur removal of JP-5 over various TiO_2-based sorbent at room temperature. Ce doped TiO_2 sorbent most efficiently removed sulfur from JP-5 at room temperature. In the previous study, adsorption of thiophene over $Ti_{0.9}Ce_{0.1}O_2$ showed the dissociative adsorption, and as a result decomposed products, such as butene and butane, were observed. Thus, model adsorption study for TiO_2 and $Ti_{0.9}Ce_{0.1}O_2$ was

conducted using benzothiophene as a probe molecule. The results are shown in Figure **D-2**.

Figure **D-2** shows the sulfur removal capacity and product found in the washing solvent. $Ti_{0.9}Ce_{0.1}O_2$ removed more benzothiophene from the model fuel than TiO_2. Spent adsorbents were washed by solvent to identify adsorbates. As a result, ethylbenzene and m- or p-xylene were identified as products of benzothiophene adsorption. Ethylbenzene possibly formed during adsorption or washing using ultrasound. Yield of ethylbenzene resemble the results of previous study. However, production of xylene was unpredictable. It might be attributed to isomerization along with sulfur atom removal of benzothiophene over the adsorbents because these materials showed certain acidity on the surface [152].

Figure **D-3** shows the sulfur removal performance of various TiO_2-based sorbents at 100 oC. Interestingly, sulfur removing capacity of sorbents containing Ce gradually increased up to 8 hours. It may be attributed to desorption of decomposed products from the surface. Among various doped-TiO_2 sorbents, the Ce doped TiO_2 is the most effective for removing sulfur from JP-5 at both room temperature and 100 ^oC. Figure **D-4** shows the adsorption capacity of the TiO_2 and $Ti_{0.9}Ce_{0.1}O_2$ sorbents as a function of adsorption time. The adsorption equilibrium for TiO_2 and $Ti_{0.9}Ce_{0.1}O_2$ was reached within the first 30 min at room temperature. However, it takes about 8 hours to reach maximum of sulfur removal at 100 ^oC for $Ti_{0.9}Ce_{0.1}O_2$. Consequently, Ce dopants may contribute to not only surface modification but also maybe structural modification as mentioned in previous study. Table **D-1** shows the results of XRD analysis of fresh and spent sorbent. The results of the structure analysis by XDR for $Ti_{0.9}Ce_{0.1}O_2$ sorbent prepared using Ti oxy-sulfate before and

after desulfurization of JP-5 at 100 ^{o}C are listed in Table 1. It clearly showed a significant expansion of lattice in anatase structure of $Ti_{0.9}Ce_{0.1}O_2$. It implies that some of oxygen anion in the structure was substituted by sulfur anion because sulfur anion is larger than oxygen anion (S^{2-} is 1.84, O^{2-} is 1.40 Å).

In order to investigate the influence of sulfur in the precursor on sulfur removing performance, the desulfurization performance of $Ti_{0.9}Ce_{0.1}O_2$-based sorbents prepared using two different starting materials was conducted using JP-5 in a batch system at 100 ºC. The influence by presence of sulfur on sulfur removing at 100 ºC is shown in Figure **D-5**. The sulfur removal of JP-5 over both $Ti_{0.9}Ce_{0.1}O_2$ sorbents at 100 ^{o}C increased with increasing contact time. Both sorbents achieved maximum sulfur removing capacity at around 8 hours. Sorbent prepared using Ti oxy-sulfate showed a capacity of 9.1 mg-S/g-Ads, while sorbent prepared using non-sulfur containing precursor gave a capacity of 5.1 mg-S/g-ads. Presence of sulfur in the precursor may contribute to improvement of sulfur removal performance. As seen in Figure **D-6**, the presence of sulfur in the precursor contributed to acidity of sorbent. Thus, the number of acid sites was increased due to the presence of sulfur, and the acidity may play an important role on ADS.

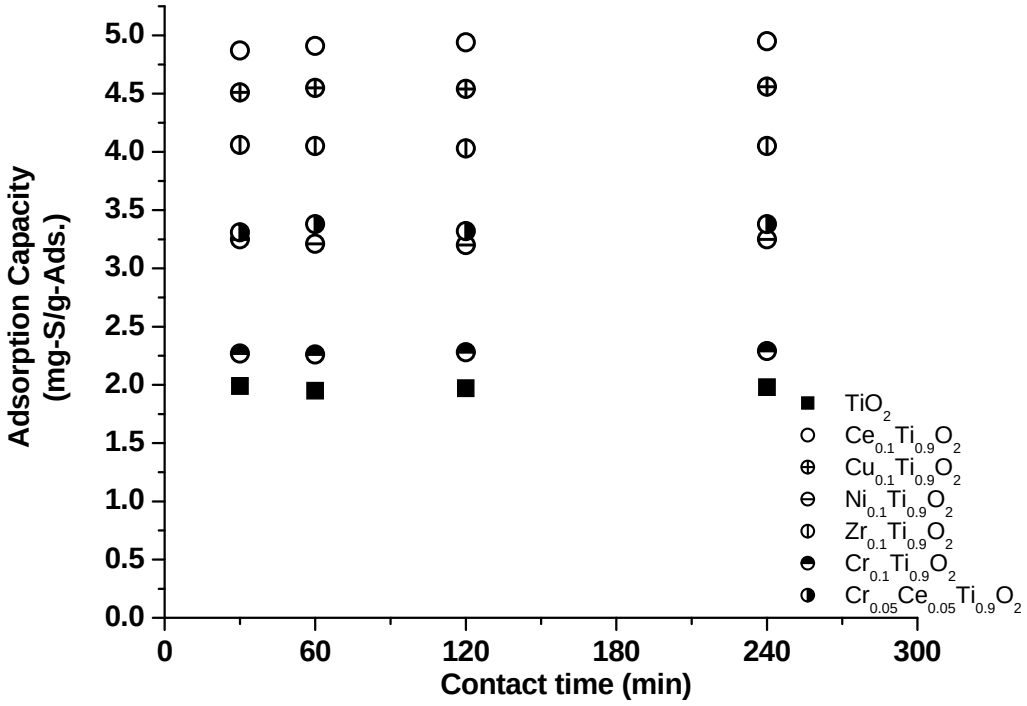

Figure **D-1**: Sulfur removal of JP-5 over TiO_2-based adsorbents: JP-5 contained 1055 ppmw-S. Adsorption was conducted in batch system, at room temperature, and adsorbent/fuel weight ratio = 1/10.

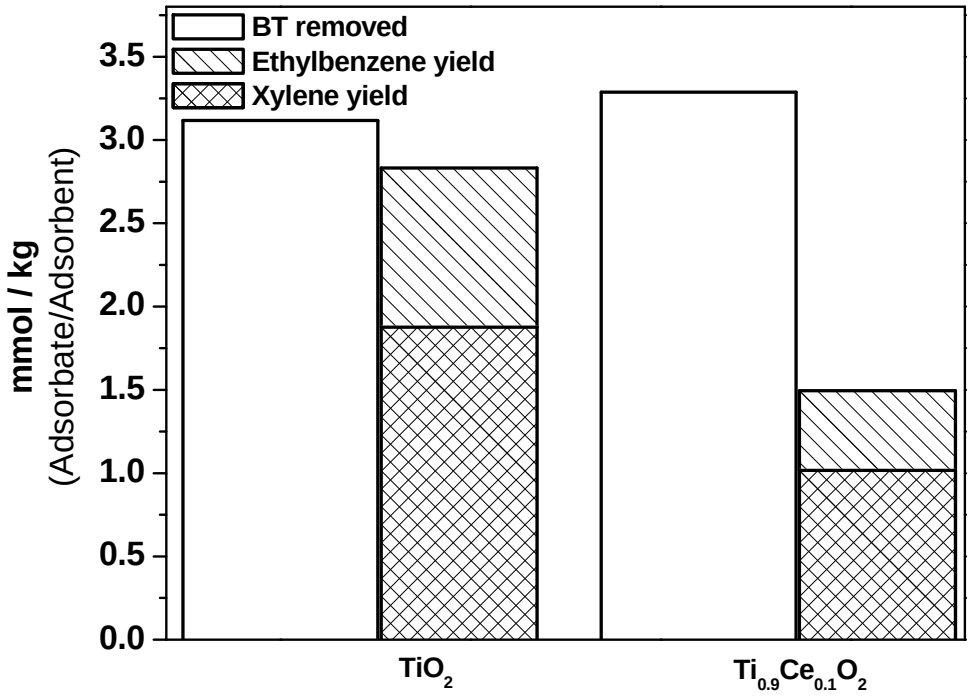

Figure **D-2**: Benzothiophene removal by adsorption over TiO_2-CeO_2 oxides for 1 h and its products found in washing solvent

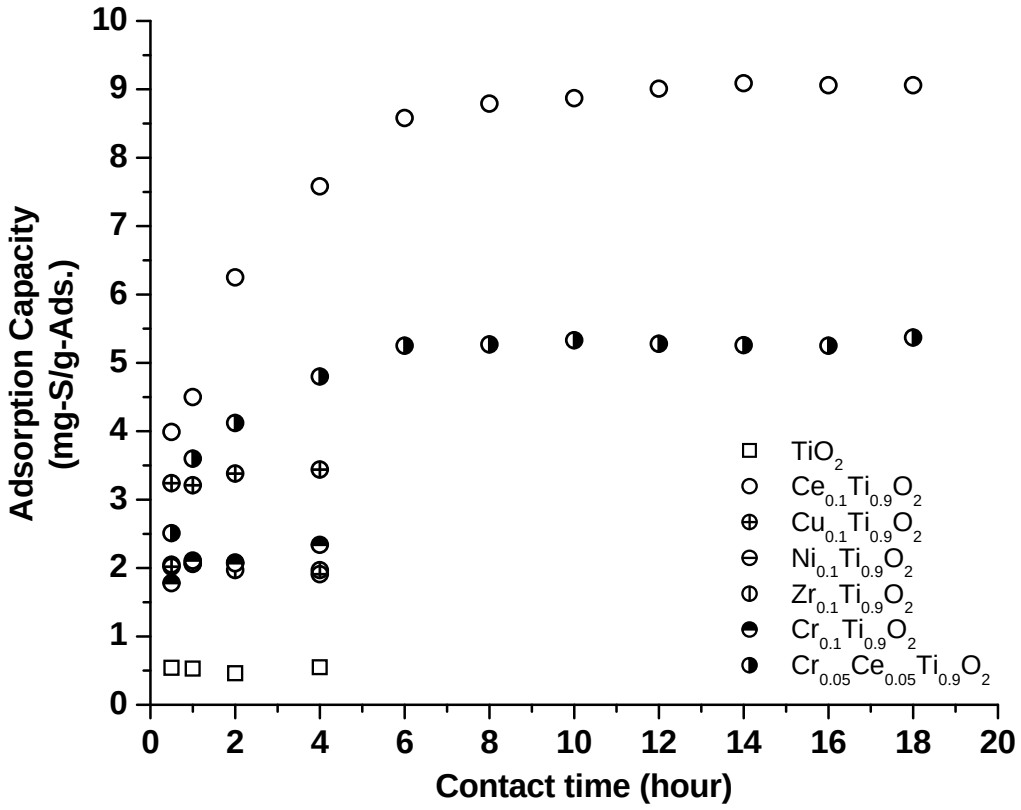

Figure **D-3**: Sulfur removal of JP-5 over TiO_2-based adsorbents: JP-5 contained 1055 ppmw-S. Adsorption was conducted in batch system, at 100 ^oC, and adsorbent/fuel weight ratio = 1/10.

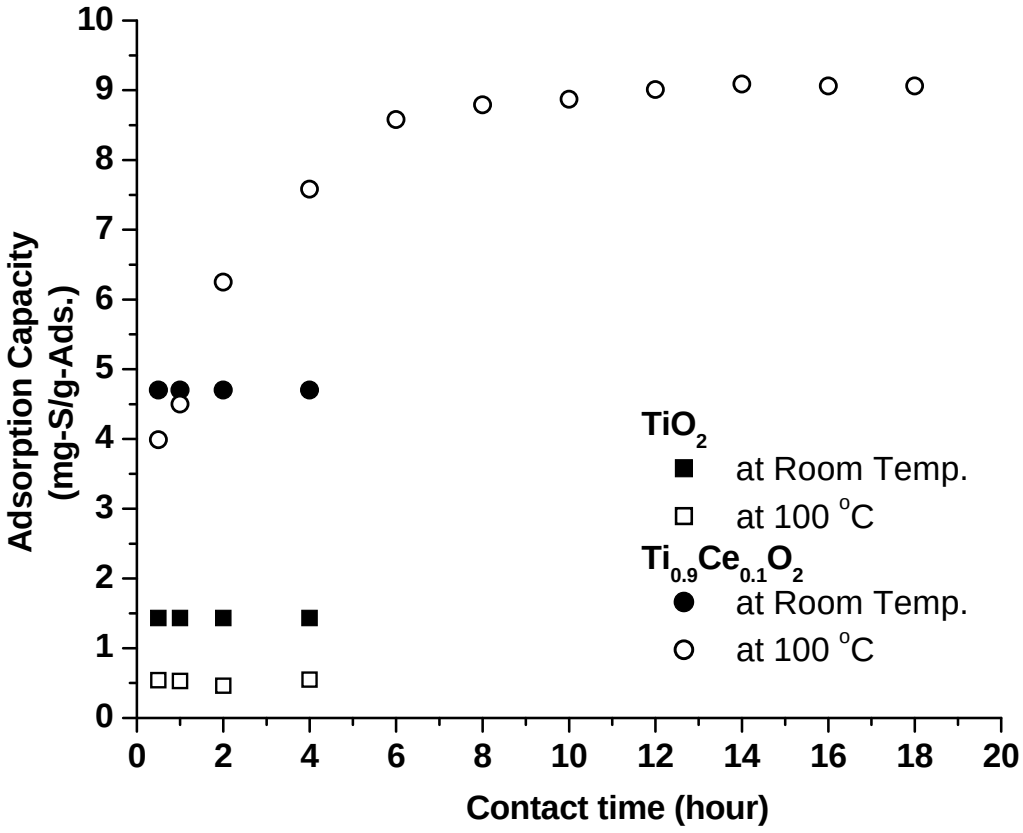

Figure **D-4**: Temperature effect on ADS capacity of JP-5 in the use of batch system at 25 and 100 °C. Fuel: Adsorbent=10:1.

Table **D-1**: d- Spacing and Lattice Parameter of Fresh and Spent $Ti_{0.9}Ce_{0.1}O_2$

		Lattice parameter (Å)	
	d-spacing	a-axis	c-axis
Before use	3.526	3.791	9.593
After use	3.522	3.700	11.473

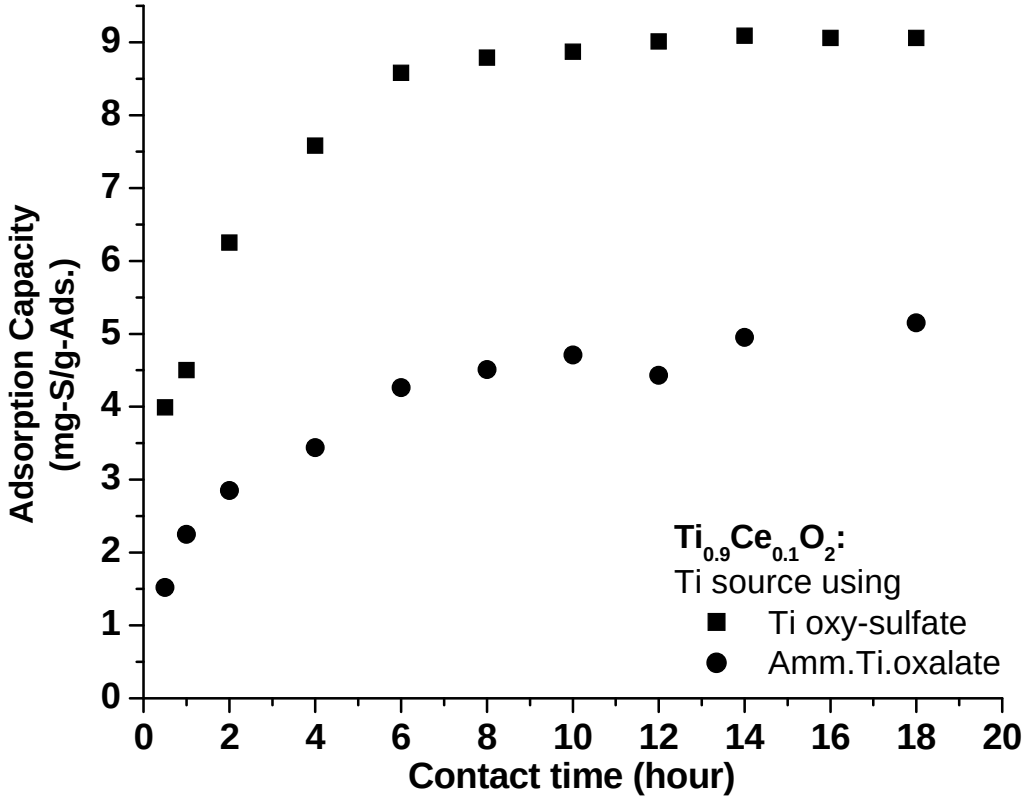

Figure **D-5**: Effect of sulfur in precursor on the sulfur removal performance over $Ti_{0.9}Ce_{0.1}O_2$: batch testing using JP-5 (1055 ppmw), fuel/adsorbent=10/1 wt.

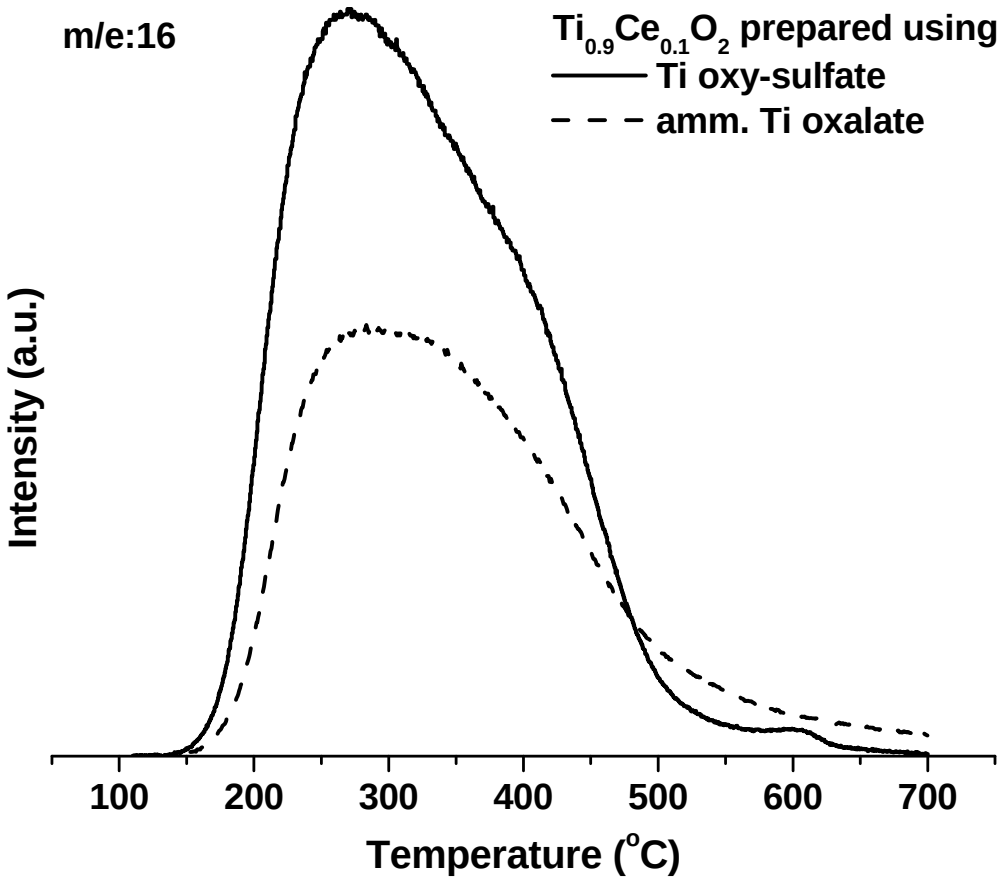

Figure **D-6**: NH_3-TPD profiles of m/e=16 for H_2O for $Ti_{0.9}Ce_{0.1}O_2$ prepared using non- and sulfur containing precursor.

References:

(1) Babor, J. A.; Lehrman, A., In *General College Chemistry*, 3rd ed.; 'Ed.'^'Eds.' Crowell: 1953; 'Vol.' p^pp 412.

(2) Langner, J.; Rodhe, H.; Crutzen, P. J.; Zimmermann, P., Anthropogenic Influence on the Distribution of Tropospheric Sulfate Aerosol. *Nature* **1992,** 359, (6397), 712.

(3) Graf, H. F.; Feichter, J.; Langmann, B., Volcanic sulfur emissions: Estimates of source strength and its contribution to the global sulfate distribution. *Journal of Geophysical Research-Atmospheres* **1997,** 102, (D9), 10727.

(4) US-EPA National Emissions Inventory (NEI) Air Pollutant Emissions Trends Data. http://www.epa.gov/ttn/chief/trends/ (June 26),

(5) Vestreng, V.; Myhre, G.; Fagerli, H.; Reis, S.; Tarrason, L., Twenty-five years of continuous sulphur dioxide emission reduction in Europe. *Atmospheric Chemistry and Physics* **2007,** 7, (13), 3663.

(6) Song, C. S., An overview of new approaches to deep desulfurization for ultra-clean gasoline, diesel fuel and jet fuel. *Catalysis Today* **2003,** 86, (1-4), 211.

(7) Marcilly, C., Present status and future trends in catalysis for refining and petrochemicals. *Journal of Catalysis* **2003,** 216, (1-2), 47.

(8) Song, C. S., Keynote address. New approaches to deep desulfurization for ultra-clean gasoline and diesel fuels: An overview. *Am. Chem. Soc. Div. Fuel Chem. Prepr.* **2002,** 47, (2), 438.

(9) Inoue, S.; Takatsuka, T., Ultra-deep desulfurization and aromatic saturation of diesel oil. *Sekiyu Gakkaishi-Journal of the Japan Petroleum Institute* **1999,** 42, (6), 365.

(10) Ma, X. L.; Sun, L.; Song, C. S., A new approach to deep desulfurization of gasoline, diesel fuel and jet fuel by selective adsorption for ultra-clean fuels and for fuel cell applications. *Catalysis Today* **2002,** 77, (1-2), 107.

(11) Song, C., Fuel processing for low-temperature and high-temperature fuel cells challenges, and opportunities for sustainable development in the 21st century. *Catalysis Today* **2002,** 77, 17.

(12) Song, C.; Ma, X. L., New design approaches to ultra-clean diesel fuels by deep desulfurization and deep dearomatization. *Applied Catalysis B-Environmental* **2003,** 41, (1-2), 207.

(13) Babich, I. V.; Moulijn, J. A., Science and technology of novel processes for deep desulfurization of oil refinery streams: A review. *Fuel* **2003,** 82, (6), 607.

(14) Zhou, A. N.; Ma, X. L.; Song, C. S., Liquid-phase adsorption of multi-ring thiophenic sulfur compounds on carbon materials with different surface properties. *Journal of Physical Chemistry B* **2006,** 110, (10), 4699.

(15) Ma, X. L.; Sprague, M.; Song, C. S., Deep desulfurization of gasoline by selective adsorption over nickel-based adsorbent for fuel cell applications. *Industrial & Engineering Chemistry Research* **2005,** 44, (15), 5768.

(16) Watanabe, S.; Velu, S.; Ma, X.; Song, C., New ceria-based selective adsorbents for removing sulfur from gasoline for fuel cell application. *Am. Chem. Soc., Div. Fuel Chem. Prepr.* **2003,** 48, (2), 695.

(17) Watanabe, S.; Ma, X.; Song, C. S., Selective sulfur removal from liquid hydrocarbons over regenerable CeO_2-TiO_2 adsorbents for fuel cell applications. *Am. Chem. Soc. Div. Fuel Chem. Prepr.* **2004,** 49, (2), 511.

(18) Watanabe, S. Selective and Regenerable Metal Oxide Adsorbents for the Removal of Sulfur from Liquid Fuels for Fuel Cell Applications. Master of Science, The Pennsylvania State University, University Park, Pennsylvania, 2004.

(19) Velu, S.; Ma, X. L.; Song, C. S., Selective adsorption for removing sulfur from jet fuel over zeolite-based adsorbents. *Industrial & Engineering Chemistry Research* **2003,** 42, (21), 5293.

(20) Hernandez-Maldonado, A. J.; Yang, F. H.; Qi, G.; Yang, R. T., Desulfurization of transportation fuels by pi-complexation sorbents: Cu(I)-, Ni(II)-, and Zn(II)-zeolites. *Applied Catalysis B-Environmental* **2005,** 56, (1-2), 111.

(21) Velu, S.; Song, C. S.; Engelhard, M. H.; Chin, Y. H., Adsorptive removal of organic sulfur compounds from jet fuel over K-exchanged NiY zeolites prepared by impregnation and ion exchange. *Industrial & Engineering Chemistry Research* **2005,** 44, (15), 5740.

(22) Velu, S.; Ma, X. L.; Song, C. S.; Namazian, M.; Sethuraman, S.; Venkataraman, G., Desulfurization of JP-8 jet fuel by selective adsorption over a Ni-based adsorbent for micro solid oxide fuel cells. *Energy & Fuels* **2005,** 19, (3), 1116.

(23) Hernandez-Maldonado, A. J.; Yang, R. T., New sorbents for desulfurization of diesel fuels via pi-complexation. *AIChe Journal* **2004,** 50, (4), 791.

(24) Wang, Y. H.; Yang, R. T., Desulfurization of liquid fuels by adsorption on carbon-based sorbents and ultrasound-assisted sorbent regeneration. *Langmuir* **2007,** 23, (7), 3825.

(25) King, D. L.; Faz, C., Desulfurization of Tier 2 gasoline by divalent copper-exchanged zeolite Y. *Applied Catalysis a-General* **2006,** 311, 58.

(26) Hernandez-Maldonado, A. J.; Yang, R. T., Desulfurization of commercial liquid fuels by selective adsorption via pi-complexation with Cu(I)-Y zeolite. *Industrial & Engineering Chemistry Research* **2003,** 42, (13), 3103.

(27) Hernandez-Maldonado, A. J.; Yang, R. T., Desulfurization of transportation fuels by adsorption. *Catalysis Reviews-Science and Engineering* **2004,** 46, (2), 111.

(28) Ma, X. L.; Sun, L.; Song, C. S., Adsorptive desulfurization of diesel fuel over a metal sulfide-based adsorbent. *Am. Chem. Soc. Div. Fuel Chem. Prepr.* **2003,** 48, (2), 522.

(29) Velu, S.; Watanabe, S.; Ma, X. L.; Song, C. S., Regenerable adsorbents for the adsorptive desulfurization of transportation fuels for fuel cell applications. *Am. Chem. Soc., Div. Fuel Chem. Prepr.* **2003,** 226, U531.

(30) Song, C. S.; Ma, X. L., Ultra-deep desulfurization of liquid hydrocarbon fuels: Chemistry and process. *International Journal of Green Energy* **2004,** 1, (2), 167.

(31) Trovarelli, A.; de Leitenburg, C.; Boaro, M.; Dolcetti, G., The utilization of ceria in industrial catalysis. *Catalysis Today* **1999,** 50, (2), 353.

(32) Trovarelli, A., Catalytic properties of ceria and CeO_2-containing materials. *Catalysis Reviews-Science and Engineering* **1996,** 38, (4), 439.

(33) Diebold, U., The surface science of titanium dioxide. *Surface Science Reports* **2003,** 48, (5-8), 53.

(34) Hadjiivanov, K. I.; Klissurski, D. G., Surface chemistry of titania (anatase) and titania-supported catalysts. *Chemical Society Reviews* **1996,** 25, (1), 61.

(35) Luo, M. F.; Chen, J.; Chen, L. S.; Lu, J. Q.; Feng, Z.; Li, C., Structure and redox properties of $Ce_XTi_{1-X}O_2$ solid solution. *Chemistry of Materials* **2001,** 13, (1), 197.

(36) Hoffmann, M. R.; Martin, S. T.; Choi, W. Y.; Bahnemann, D. W., Environmental Applications of Semiconductor Photocatalysis. *Chemical Reviews* **1995,** 95, (1), 69.

(37) Pieplu, A.; Saur, O.; Lavalley, J. C.; Legendre, O.; Nedez, C., Claus catalysis and H_2S selective oxidation. *Catalysis Reviews-Science and Engineering* **1998,** 40, (4), 409.

(38) Flytzani-Stephanopoulos, M.; Zhu, T. L.; Li, Y., Ceria-based catalysts for the recovery of elemental sulfur from SO_2-laden gas streams. *Catalysis Today* **2000,** 62, (2-3), 145.

(39) Liu, W.; Wadia, C.; Flytzani-Stephanopoulos, M., Transition metal/fluorite-type oxides as active catalysts for reduction of sulfur dioxide to elemental sulfur by carbon monoxide. *Catalysis Today* **1996,** 28, (4), 391.

(40) Zeng, Y.; Zhang, S.; Groves, F. R.; Harrison, D. P., High temperature gas desulfurization with elemental sulfur production. *Chemical Engineering Science* **1999,** 54, (15-16), 3007.

(41) Koebrugge, G. W.; Winnubst, L.; Burggraaf, A. J., Thermal-Stability of Nanostructured Titania and Titania Ceria Ceramic Powders Prepared by the Sol-Gel Process. *Journal of Materials Chemistry* **1993,** 3, (11), 1095.

(42) Shi, Z. M.; Yu, W. G.; Bayar, X., Study of crystallization behavior of Ce^{4+}-modified titania gels. *Scripta Materialia* **2004,** 50, (6), 885.

(43) Lopez, T.; Rojas, F.; Alexander-Katz, R.; Galindo, F.; Balankin, A.; Buljan, A., Porosity, structural and fractal study of sol-gel TiO_2-CeO_2 mixed oxides. *Journal of Solid State Chemistry* **2004,** 177, (6), 1873.

(44) Lin, S. D.; Song, C. S., Noble metal catalysts for low-temperature naphthalene hydrogenation in the presence of benzothiophene. *Catalysis Today* **1996,** 31, (1-2), 93.

(45) Wang, Z.; Flytzani-Stephanopoulos, M., Cerium oxide-based sorbents for regenerative hot reformate gas desulfurization. *Energy & Fuels* **2005,** 19, (5), 2089.

(46) Karvinen, S., The effects of trace elements on the crystal properties of TiO_2. *Solid State Sciences* **2003,** 5, (5), 811.

(47) Subrt, J.; Stengl, V.; Bakardjieva, S.; Szatmary, L., Synthesis of spherical metal oxide particles using homogeneous precipitation of aqueous solutions of metal sulfates with urea. *Powder Technology* **2006,** 169, (1), 33.

(48) Reddy, B. M.; Khan, A., Recent advances on TiO_2-ZrO_2 mixed oxides as catalysts and catalyst supports. *Catalysis Reviews-Science and Engineering* **2005,** 47, (2), 257.

(49) Lukac, J.; Klementova, M.; Bezdicka, P.; Bakardjieva, S.; Subrt, J.; Szatmary, L.; Gruskova, A., Characterization of Zr-doped TiO_2 prepared by homogenous co-precipitation without high-temperature treatment. *Journal of Materials Science* **2007,** 42, (22), 9421.

(50) Skorodumova, N. V.; Simak, S. I.; Lundqvist, B. I.; Abrikosov, I. A.; Johansson, B., Quantum origin of the oxygen storage capability of ceria. *Physical Review Letters* **2002,** 89, (16), 166601.

(51) Rodriguez, J. A.; Hanson, J. C.; Kim, J. Y.; Liu, G.; Iglesias-Juez, A.; Fernandez-Garcia, M., Properties of CeO_2 and $Ce_{1-X}Zr_XO_2$ nanoparticles: X-ray absorption near-edge spectroscopy, density functional, and time-resolved x-ray diffraction studies. *Journal of Physical Chemistry B* **2003,** 107, (15), 3535.

(52) Rodriguez, J. A.; Wang, X. Q.; Hanson, J. C.; Liu, G.; Iglesias-Juez, A.; Fernandez-Garcia, M., The behavior of mixed-metal oxides: Structural and electronic properties of $Ce_{1-X}Ca_XO_2$ and $Ce_{1-x}Ca_xO_{2-x}$. *Journal of Chemical Physics* **2003,** 119, (11), 5659.

(53) Dutta, G.; Waghmare, U. V.; Baidya, T.; Hegde, M. S.; Priolkar, K. R.; Sarode, P. R., Origin of enhanced reducibility/oxygen storage capacity of $Ce_{1-X}Ti_XO_2$ compared to CeO_2 or TiO_2. *Chemistry of Materials* **2006,** 18, (14), 3249.

(54) Henrich, V. E.; Dresselhaus, G.; Zeiger, H. J., Observation of Two-Dimensional Phases Associated with Defect States on Surface of TiO_2. *Physical Review Letters* **1976,** 36, (22), 1335.

(55) CRC-Handbook, Handbook of chemistry and physics. In 77th ed.; Lide, D. R., 'Ed.'^'Eds.' CRC Press: Boca Raton, Florida, 1996-1997; 'Vol.' p^pp **12**.

(56) Burroughs, P.; Hamnett, A.; Orchard, A. F.; Thornton, G., Satellite Structure in the X-Ray Photoelectron Spectra of some Binary and Mixide Oxides of Lanthanum and Cerium. *Journal of the Chemical Society-Dalton Transactions* **1976,** 17, 1686.

(57) Wagner, C. D.; Riggs, W. M.; Davis, L. E.; Moulder, J. F.; Muilenbedrg, G. E., *Handbook of X-Ray Photoelectron Spectroscopy*. ed.; Perkin-Elmer Corporation: Minnesota, 1978.

(58) Carley, A. F.; Chalker, P. R.; Riviere, J. C.; Roberts, M. W., The Identification and Characterization of Mixed Oxidation-States at Oxidized Titanium Surfaces by Analysis of X-Ray Photoelectron-Spectra. *Journal of the Chemical Society-Faraday Transactions I* **1987,** 83, 351.

(59) Mayer, J. T.; Diebold, U.; Madey, T. E.; Garfunkel, E., Titanium and Reduced Titania Overlayers on Titanium Dioxide(110). *Journal of Electron Spectroscopy and Related Phenomena* **1995,** 73, (1), 1.

(60) Leung, C. M.; Weinert, M.; Allen, P. B.; Wentzcovitch, R. M., First-principles study of titanium oxides. *Physical Review B* **1996,** 54, (11), 7857.

(61) Mullins, D. R.; Overbury, S. H.; Huntley, D. R., Electron spectroscopy of single crystal and polycrystalline cerium oxide surfaces. *Surface Science* **1998,** 409, (2), 307.

(62) Mullins, D. R.; Radulovic, P. V.; Overbury, S. H., Ordered cerium oxide thin films grown on Ru(0001) and Ni(111). *Surface Science* **1999,** 429, (1-3), 186.

(63) Henderson, M. A.; Perkins, C. L.; Engelhard, M. H.; Thevuthasan, S.; Peden, C. H. F., Redox properties of water on the oxidized and reduced surfaces of CeO_2 (111). *Surface Science* **2003,** 526, (1-2), 1.

(64) Yao, H. C.; Yao, Y. F. Y., Ceria in automotive exhaust catalysts I.Oxygen storage. *Journal of Catalysis* **1984,** 86, 254.

(65) Tsyganenko, A. A.; Pozdnyakov, D. V.; Filimonov, V. N., Infrared Study of Surface Species Arising from Ammonia Adsorption on Oxide Surfaces. *Journal of Molecular Structure* **1975,** 29, (2), 299.

(66) Gates, B. C.; Topsoe, H., Reactivities in deep catalytic hydrodesulfurization: Challenges, opportunities, and the importance of 4-methyldibenzothiophene and 4,6-dimethyldibenzothiophene. *Polyhedron* **1997,** 16, (18), 3213.

(67) Topsoe, H.; Clausen, B. S.; Massoth, F. E., *Hydrotreating Catalysis*. ed.; Springer-Verlag: Berlin, 1996.

(68) Tsyganenko, A. A.; Can, F.; Mauge, F., IR study of the adsorption and isotopic scrambling of thiophene on CaO. *Journal of physical Chemistry B* **2003,** 107, 8578.

(69) Quigley, W. W. C.; Yamamoto, H. D.; Aegerter, P. A.; Simpson, G. J.; Bussell, M. E., Infrared spectroscopy and temperature-programmed desorption study of adsorbed thiophene on gamma-Al_2O_3. *Langmuir* **1996,** 12, (6), 1500.

(70) Jirsak, T.; Dvorak, J.; Rodriguez, J. A., Chemistry of thiophene on ZnO, S/ZnO, and Cs/ZnO surfaces: Effects of cesium on desulfurization processes. *Journal of Physical Chemistry B* **1999,** 103, (26), 5550.

(71) Liu, G.; Rodriguez, J. A.; Hrbek, J.; Long, B. T.; Chen, D. A., Interaction of thiophene with stoichiometric and reduced rutile TiO_2(110) surfaces: role of Ti^{3+} sites in desulfurization activity. *Journal of Molecular Catalysis a-Chemical* **2003,** 202, (1-2), 215.

(72) Hedhili, M. N.; Yakshinskiy, B. V.; Schlereth, T. W.; Gouder, T.; Madey, T. E., The interactions of thiophene with polycrystalline UO_2. *Surface Science* **2005,** 574, (1), 17.

(73) Tarbuck, T. L.; McCrea, K. R.; Logan, J. W.; Heiser, J. L.; Bussell, M. E., Identification of the adsorption mode of thiophene on sulfided Mo catalysts. *Journal of Physical Chemistry B* **1998,** 102, (40), 7845.

(74) Mills, P.; Phillips, D. C.; Woodruff, B. P.; Main, R.; Bussell, M. E., Investigation of the adsorption and reactions of thiophene on sulfided Cu, Mo, and Rh catalysts. *Journal of Physical Chemistry B* **2000,** 104, (14), 3237.

(75) Wu, W. C.; Wu, Z. L.; Feng, Z. C.; Ying, P. L.; Li, C., Adsorption and reaction of thiophene and H_2S on Mo_2C/Al_2O_3 catalyst studied by in situ FT-IR spectroscopy. *Physical Chemistry Chemical Physics* **2004,** 6, (24), 5596.

(76) Wu, Z. L.; Li, C.; Wei, Z. B.; Ying, P. L.; Xin, Q., FT-IR spectroscopic studies of thiophene adsorption and reactions on Mo_2N/gamma-Al_2O_3 catalysts. *Journal of Physical Chemistry B* **2002,** 106, (5), 979.

(77) Nicholson, D. E., Identification of Adsorbed Species by Intrared Spectrometry. *Analytical Chemistry* **1962,** 34, (3), 370.

(78) Ratnasam.P; Fripiat, J. J., Surface Chemistry of Sulphides .1. Infra-red Study of Molybdenum and Germanium Sulphides and of Their Reaction with H_2, H_2O, Thiophene and Ethanethiol. *Transactions of the Faraday Society* **1970,** 66, (575), 2897.

(79) Mills, P.; Korlann, S.; Bussell, M. E.; Reynolds, M. A.; Ovchinnikov, M. V.; Angelici, R. J.; Stinner, C.; Weber, T.; Prins, R., Vibrational study of organometallic

complexes with thiophene ligands: Models for adsorbed thiophene on hydrodesulfurization catalysts. *Journal of Physical Chemistry A* **2001,** 105, (18), 4418.

(80) Sengupta, S. K.; Ahn, H.; Whitten, J. E., Adsorption of thiophene on Al(111) and deposition of aluminum on condensed thiophene. *Surface Science* **2002,** 520, (3), 207.

(81) Whitten, J. E., Adsorption of thiophene and pyridine on W(110). *Surface Science* **2003,** 546, (2-3), 107.

(82) St Clair, T. P.; Oyama, S. T.; Cox, D. F., Adsorption and reaction of thiophene on alpha-Mo_2C(0001). *Surface Science* **2002,** 511, (1-3), 294.

(83) Huntley, D. R.; Mullins, D. R.; Wingeier, M. P., Desulfurization of thiophenic compounds by Ni(111): Adsorption and reactions of thiophene, 3-methylthiophene, and 2,5-dimethylthiophene. *Journal of Physical Chemistry* **1996,** 100, (50), 19620.

(84) Schoofs, G. R.; Preston, R. E.; Benziger, J. B., Adsorption and Desulfurization of Thiophene on Nickel(111). *Langmuir* **1985,** 1, (3), 313.

(85) Kobayashi, M.; Flytzani-Stephanopoulos, M., Reduction and sulfidation kinetics of cerium oxide and Cu-modified cerium oxide. *Industrial & Engineering Chemistry Research* **2002,** 41, (13), 3115.

(86) Watanabe, S.; Ma, X.; Song, C., Characterization of Structural and Surface Properties of $Ti_XCe_{1-X}O_2$ Mixed Oxides by XRD, XPS, TPR and TPD. **in submission**.

(87) Smirnov, M. Y.; Kalinkin, A. V.; Pashis, A. V.; Sorokin, A. M.; Noskov, A. S.; Bukhtiyarov, V. I.; Kharas, K. C.; Rodkin, M. A., Comparative XPS study of Al_2O_3 and CeO_2 sulfation in reactions with SO_2, SO_2+O_2, SO_2+H_2O, and SO_2+O_2+H_2O. *Kinetics and Catalysis* **2003,** 44, (4), 575.

(88) Smirnov, M. Y.; Kalinkin, A. V.; Pashis, A. V.; Sorokin, A. M.; Noskov, A. S.; Kharas, K. C.; Bukhtiyarov, V. I., Interaction of Al_2O_3 and CeO_2 surfaces with SO_2 and SO_2+O_2 studied by X-ray photoelectron spectroscopy. *Journal of Physical Chemistry B* **2005,** 109, (23), 11712.

(89) Ferrizz, R. M.; Gorte, R. J.; Vohs, J. M., TPD and XPS investigation of the interaction of SO_2 with model ceria catalysts. *Catalysis Letters* **2002,** 82, (1-2), 123.

(90) Smith, K. E.; Mackay, J. L.; Henrich, V. E., Interaction of SO_2 with Nearly Perfect and Defect TiO_2(110) Surfaces. *Physical Review B* **1987,** 35, (11), 5822.

(91) Sayago, D. I.; Serrano, P.; Bohme, O.; Goldoni, A.; Paolucci, G.; Roman, E.; Martin-Gago, J. A., Adsorption and desorption of SO_2 on the TiO_2(110)-(1X1) surface: A photoemission study. *Physical Review B* **2001,** 6420, (20).

(92) Sayago, D. I.; Serrano, P.; Bohme, O.; Goldoni, A.; Paolucci, G.; Roman, E.; Martin-Gago, J. A., A photoemission study of the SO_2 adsorption on TiO_2 (110) surfaces. *Surface Science* **2001,** 482, 9.

(93) Raza, H.; Harte, S. P.; Muryn, C. A.; Wincott, P. L.; Thornton, G.; Casanova, R.; Rodriguez, A., NEXAFS studies of the reaction of SO_2 with TiO_2(100)-(1x1) and -(1x3). *Surface Science* **1996,** 366, (3), 519.

(94) Liu, G.; Rodriguez, J. A.; Chang, Z.; Hrbek, J.; Gonzalez, L., Adsorption of methanethiol on stoichiometric and defective TiO_2(110) surfaces: A combined experimental and theoretical study. *Journal of Physical Chemistry B* **2002,** 106, (38), 9883.

(95) Watanabe, S.; Ma, X.; Song, C., **in submission**.

(96) Bozon-Verduraz, F.; Bensalem, A., IR Studies of Cerium Dioxide : Influence of Impurities and Defects. *Journal of the Chemical Society-Faraday Transactions* **1994,** 90, (4), 653.

(97) Li, C.; Domen, K.; Maruya, K.; Onishi, T., Dioxygen Adsorption on Well-Outgassed and Partially Reduced Cerium Oxide Studied by FT-IR. *Journal of the American Chemical Society* **1989,** 111, (20), 7683.

(98) Li, C.; Domen, K.; Maruya, K.; Onishi, T., IR Spectra of Dioxygen Species Formed on CeO_2 at Room-Temperature. *Journal of the Chemical Society-Chemical Communications* **1988**, (23), 1541.

(99) Li, C.; Domen, K.; Maruya, K.; Onishi, T., Oxygen-Exchange Reactions over Cerium Oxide - an FT-IR Study. *Journal of Catalysis* **1990,** 123, (2), 436.

(100) Che, M.; Tench, A. J., Characterization and Reactivity of Molecular Oxygen Species on Oxide Surfaces. *Advances in Catalysis* **1983,** 32, 1.

(101) Bielanski, A.; Haber, J., *Oxygen in Catalysis*. ed.; Marcel Dekker, Inc.: New York, 1991.

(102) Rico, M.; Orza, J. M.; Morcillo, J., Fundamental vibrations of thiophene and its deuterated derivatives. *Spectrochimica Acta* **1965,** 21, 689.

(103) El-Azhary, A. A.; Hilal, R. H., Vibrational analysis of the spectra of furan and thiophene. *Spectrochimica Acta Part a-Molecular and Biomolecular Spectroscopy* **1997,** 53, (9), 1365.

(104) Nakamoto, K., *Infrared and Raman Spectra of Inorganic and Coordination Compounds Part B: Applications in Coordination, Organometallic, and Bioinorganic Chemistry*. Fifth ed.; John Wiley & Sons, Inc.: New York, 1997.

(105) Saur, O.; Bensitel, M.; Saad, A. B. M.; Lavalley, J. C.; Tripp, C. P.; Morrow, B. A., The Structure and Stability of Sulfated Alumina and Titania. *Journal of Catalysis* **1986,** 99, (1), 104.

(106) Waqif, M.; Saur, O.; Lavalley, J. C.; Perathoner, S.; Centi, G., Nature and Mechanism of Formation of Sulfate Species on Copper Alumina Sorbent Catalysts for SO_2 Removal. *Journal of Physical Chemistry* **1991,** 95, (10), 4051.

(107) Bensitel, M.; Saur, O.; Lavalley, J. C.; Morrow, B. A., An Infrared Study of Sulfated Zirconia. *Materials Chemistry and Physics* **1988,** 19, (1-2), 147.

(108) Luo, T.; Vohs, J. M.; Gorte, R. J., An examination of sulfur poisoning on Pd/ceria catalysts. *Journal of Catalysis* **2002,** 210, (2), 397.

(109) Tanaka, K. I., Intermediate of Oxygen-Exchange Reaction over Illuminated Titanium-Dioxide. *Journal of Physical Chemistry* **1974,** 78, (5), 555.

(110) Sato, S.; Kadowaki, T.; Yamaguti, K., Photocatalytic Oxygen Isotopic Exchange between Oxygen Molecule and the Lattice Oxygen of TiO_2 Prepared from Titanium Hydroxide. *Journal of Physical Chemistry* **1984,** 88, (14), 2930.

(111) Yu, J. C.; Lin, J.; Lo, D.; Lam, S. K., Influence of thermal treatment on the adsorption of oxygen and photocatalytic activity of TiO_2. *Langmuir* **2000,** 16, (18), 7304.

(112) Takami, A.; Harada, K.; Tsushio, Y., Behavior of oxygen of cerium composite oxides on catalytic combustion of carbon particulate. *Journal of the Japan Petroleum Institute* **2007,** 50, (2), 102.

(113) Sanjines, R.; Tang, H.; Berger, H.; Gozzo, F.; Margaritondo, G.; Levy, F., Electronic-Structure of Anatase TiO_2 Oxide. *Journal of Applied Physics* **1994,** 75, (6), 2945.

(114) Descorme, C.; Madier, Y.; Duprez, D., Infrared study of oxygen adsorption and activation on cerium-zirconium mixed oxides. *Journal of Catalysis* **2000,** 196, (1), 167.

(115) Suda, Y., Interaction of Benzene, Cyclohexene, and Cyclohexane with the Surface of Titanium-Dioxide (Rutile). *Langmuir* **1988,** 4, (1), 147.

(116) Corma, A.; Garcia, H., Lewis Acids as Catalysts in Oxidation Reactions: Form Homogeneous to Heterogeneous Systems. *Chemical Reviews* **2002,** 102, 3837.

(117) Brown, K. N.; Espenson, J. H., Stepwise oxidation of thiophene and its derivatives by hydrogen peroxide catalyzed by methyltrioxorhenium(VII). *Inorganic Chemistry* **1996,** 35, (25), 7211.

(118) Attar, A.; Corcoran, W. H., Desulfurization of Organic Sulfur-Compounds by Selective Oxidation .1. Regenerable and Nonregenerable Oxygen Carriers. *Industrial & Engineering Chemistry Product Research and Development* **1978,** 17, (2), 102.

(119) Pouzet, P.; Erdelmeier, I.; Ginderow, D.; Mornon, J. P.; Dansette, P.; Mansuy, D., Thiophene S-Oxides - Convenient Preparation, First Complete Structural Characterization and Unexpected Dimerization of One of Them, 2,5-Diphenylthiophene-1-Oxide. *Journal of the Chemical Society-Chemical Communications* **1995**, (4), 473.

(120) Heldt, W. Z., Coupling of Aromatic Rings .I. Pyrolysis of Aryl Sulfides and Aryl Sulfones to Substituted Biphenyls. *Journal of Organic Chemistry* **1965,** 30, (11), 3897.

(121) Pitchen, P.; Dunach, E.; Deshmukh, M. N.; Kagan, H. B., An Efficient Asymmetric Oxidation of Sulfides to Sulfoxides. *Journal of the American Chemical Society* **1984,** 106, (26), 8188.

(122) McGregor, S. D.; Lemal, D. M., Fragmentations . Thermal 5 to 4+1 Reaction. *Journal of the American Chemical Society* **1966,** 88, (12), 2858.

(123) Chou, T. S.; Chang, S. Y., A Convenient Method for the Extrusion of Sulfur-Dioxide from 2,2,5,5-Tetrasubstituted 3-Sulfolenes. *Journal of the Chemical Society-Perkin Transactions 1* **1992**, (12), 1459.

(124) Mock, W. L., Stereochemical Consequences of Orbital Symmetry Control in Reversible Combining of Sulfur-Dioxide with Conjugated Systems (Sulfolene Reactions). *Journal of the American Chemical Society* **1975,** 97, (13), 3666.

(125) LaCount, R. B.; Friedman, S., Oxidation of Dibenzothiophene and Reaction of Dibenzothiophene 5,5-Dioxide with Aqueous Alkali. *Journal of Organic Chemistry* **1977,** 42, (16), 2751.

(126) Shiraishi, Y.; Tachibana, K.; Hirai, T.; Komasawa, I., Photochemical production of biphenyls from oxidized sulfur compounds obtained by oxidative desulfurization of light oils. *Energy & Fuels* **2003,** 17, (1), 95.

(127) Jenks, W. S.; Taylor, L. M.; Guo, Y. S.; Wan, Z. H., Photochemistry of Dibenzothiophene-S,S-Dioxide - Reactions of a Highly Constrained Biradical. *Tetrahedron Letters* **1994,** 35, (39), 7155.

(128) Watanabe, S.; Sun, F.; Ma, X.; Song, C., Mechanistic Insights into the Adsorption of Thiophene on $Ti_{0.9}Ce_{0.1}O_2$ Mixed Oxide by XPS, in-situ IR and TPD. **in submission**.

(129) Laachir, A.; Perrichon, V.; Badri, A.; Lamotte, J.; Catherine, E.; Lavalley, J. C.; Elfallah, J.; Hilaire, L.; Lenormand, F.; Quemere, E.; Sauvion, G. N.; Touret, O., Reduction of Ceo2 by Hydrogen - Magnetic-Susceptibility and Fourier-Transform Infrared, Ultraviolet and X-Ray Photoelectron-Spectroscopy Measurements. *Journal of the Chemical Society-Faraday Transactions* **1991,** 87, (10), 1601.

(130) Sing, K. S. W.; Everett, D. H.; Haul, R. A. W.; Moscou, L.; Pierotti, R. A.; Rouquerol, J.; Siemieniewska, T., Reporting Physisorption Data for Gas Solid Systems with Special Reference to the Determination of Surface-Area and Porosity (Recommendations 1984). *Pure and Applied Chemistry* **1985,** 57, (4), 603.

(131) Kim, J. H.; Ma, X. L.; Zhou, A. N.; Song, C. S., Ultra-deep desulfurization and denitrogenation of diesel fuel by selective adsorption over three different adsorbents: A study on adsorptive selectivity and mechanism. *Catalysis Today* **2006,** 111, (1-2), 74.

(132) Gray, J. H.; Handwerk, G. E., Petroleum Refining. In 4 ed.; 'Ed.'^'Eds.' Marcel Dekker: 2001; 'Vol.' p^pp 16.

(133) Ma, X. L.; Zhou, A. N.; Song, C. S., A novel method for oxidative desulfurization of liquid hydrocarbon fuels based on catalytic oxidation using molecular oxygen coupled with selective adsorption. *Catalysis Today* **2007,** 123, (1-4), 276.

(134) Turk, B. S.; Gupta, R. P., RTI's trend process for deepdesulfurization of naphtha. *Prepr. Pap. - Am. Chem. Soc., Div. Fuel Chem.* **2001,** 46, 392.

(135) Rehms, D. L., Laboratory evaluation of promoted alumina adsorbent for fuel desulfurization. *Prepr. Pap. - Am. Chem. Soc., Div. Fuel Chem.* **2002,** 47, (2), 454

(136) Angelici, R. J., Structural Aspects of Thiophene Coordination in Transition-Metal Complexes. *Coordination Chemistry Reviews* **1990,** 105, 61.

(137) Angelici, R. J., Thiophenes in organotransition metal chemistry: Patterns of reactivity. *Organometallics* **2001,** 20, (7), 1259.

(138) Harris, S., Bonding and Reactivity in Transition-Metal Complexes Containing Thiophenic Ligands. *Organometallics* **1994,** 13, (7), 2628.

(139) Kundakovic, L.; Flytzani-Stephanopoulos, M., Reduction characteristics of copper oxide in cerium and zirconium oxide systems. *Applied Catalysis a-General* **1998,** 171, (1), 13.

(140) Ma, X. L.; Velu, S.; Kim, J. H.; Song, C. S., Deep desulfurization of gasoline by selective adsorption over solid adsorbents and impact of analytical methods on ppm-level sulfur quantification for fuel cell applications. *Applied Catalysis B-Environmental* **2005,** 56, (1-2), 137.

(141) Kung, H. H., Desirable Catalyst Properties in Selective Oxidation Reactions. *Industrial & Engineering Chemistry Product Research and Development* **1986,** 25, (2), 171.

(142) King, D. L.; Faz, C.; Flynn, T., Desulfurization of gasoline feedstocks for application in fuel reforming. *Society of automotive engineers papaer 2000-01-0002* **2000**, 1.

(143) Weitkamp, J.; Schwark, M.; Ernst, S., Removal of Thiophene Impurities from Benzene by Selective Adsorption in Zeolite Zsm-5. *Journal of the Chemical Society-Chemical Communications* **1991**, (16), 1133.

(144) Iwamoto, M.; Yoda, Y.; Yamazoe, N.; Seiyama, T., Study of Metal-Oxide Catalysts by Temperature Programmed Desorption .4. Oxygen-Adsorption on Various Metal-Oxides. *Journal of Physical Chemistry* **1978,** 82, (24), 2564.

(145) Garcia, C. L.; Lercher, J. A., Adsorption and Surface-Reactions of Thiophene on ZSM-5 Zeolites. *Journal of Physical Chemistry* **1992,** 96, (6), 2669.

(146) Smith, A. L., *Applied Infrared Spectroscopy*. ed.; John Wiley & Sons: 1979.

(147) Kataoka, S.; Lee, E.; Tejedor-Tejedor, M. I.; Anderson, M. A., Photocatalytic degradation of hydrogen sulfide and in situ FT-IR analysis of reaction products on surface of TiO2. *Applied Catalysis B-Environmental* **2005,** 61, (1-2), 159.

(148) Waqif, M.; Pieplu, A.; Saur, O.; Lavalley, J. C.; Blanchard, G., Use of CeO_2-Al_2O_3 as a SO_2 sorbent. *Solid State Ionics* **1997,** 95, (1-2), 163.

(149) Rodriguez, J. A.; Jirsak, T.; Perez, M.; Chaturvedi, S.; Kuhn, M.; Gonzalez, L.; Maiti, A., Studies on the behavior of mixed-metal oxides and desulfurization: Reaction of H_2S and SO_2 with Cr_2O_3(0001), MgO(100), and $Cr_XMg_{1-X}O$(100). *Journal of the American Chemical Society* **2000,** 122, (49), 12362.

(150) Davydov, A. A., *Molecular spectroscopy of oxide catalyst surfaces*. ed.; Jon Wiley & Sons Inc.: 2003.

(151) Rodriguez, J. A.; Jirsak, T.; Freitag, A.; Hanson, J. C.; Larese, J. Z.; Chaturvedi, S., Interaction of SO2 with CeO2 and Cu/CeO2 catalysts: photoemission, XANES and TPD studies. *Catalysis Letters* **1999,** 62, (2-4), 113.

(152) Arata, K.; Matsuhashi, H.; Hino, M.; Nakamura, H., Synthesis of solid superacids and their activities for reactions of alkanes. *Catalysis Today* **2003,** 81, (1), 17.

Appendix E

Adsorptive Desulfurization of Various Fuels over Several Metal Oxides

E-1 Experimental

The adsorbents were prepared using cerium ammonium nitrates and titanium oxysulfate sulfuric acid hydrate (Aldrich Chem. Co.) by urea gelation/co-precipitation method. Precipitation was employed at 90~95 ^{o}C for 8 hours. Precipitants were dried 110^{o}C over night, and calcined at 450^{o}C for 6 hrs in air employing a temperature ramp of 2^{o}C/min.

A continuous flow fixed-bed apparatus was used in adsorbent evaluation. The stainless steel reactor tubes are 15 cm in length and have an internal diameter of 4.6 mm. It was housed in an oven capable of heating to 400 ^{o}C. An HPLC pump (Alltech Series 426) was used to measure and pump the liquid feedstock into the reactor. The feed was sent into the reactor from bottom to top by liquid hourly space velocity (LHSV) 1.2 h^{-1}. Temperature in the oven was monitored and maintained using four K-type Omega thermocouples. The powder adsorbents were packed in columns, and the columns were placed in a multi-channel convection oven for the adsorption experiments. The effluent from the adsorbent bed was collected, and analyzed using Antek 9000S total sulfur analyzer.

Mass balance of sulfur was determined by Leco SC-144DR under O_2 flow at 850 ^{o}C. After adsorptive desulfurization of JP-5 using $Ti_{0.9}Ce_{0.1}O_2$, the spent adsorbent was

dried in the stainless steel column under N_2 flow at 70 ^oC for overnight. The dried spent and fresh samples were determined their sulfur content.

E-1-1 Sulfur removal of low sulfur gasoline containing methanol over various metal oxides

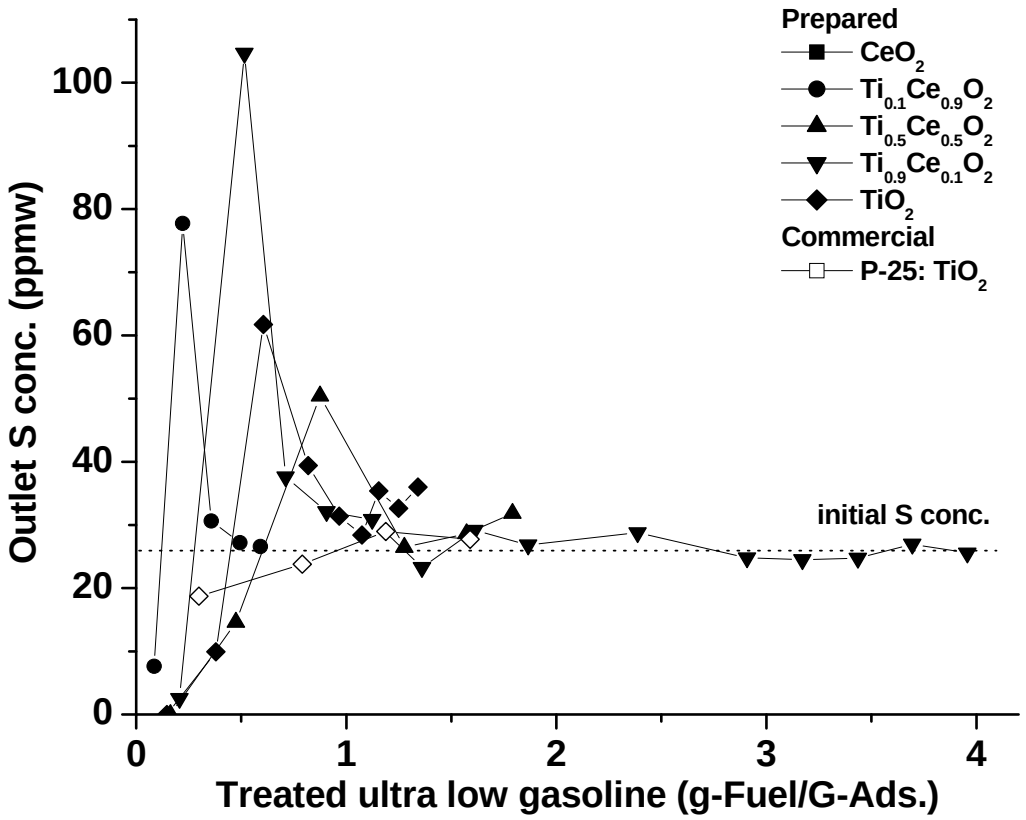

Figure **E-1**: Breakthrough curves of ADS of gasoline (26 ppmw-S) containing methanol over various metal oxide adsorbents: LHSV: 1.2 h-1, operation temperature: room temperature. Pretreatment at 300 ^oC under air flow.

E-1-2 Sulfur removal of JP-8 over the various metal oxides

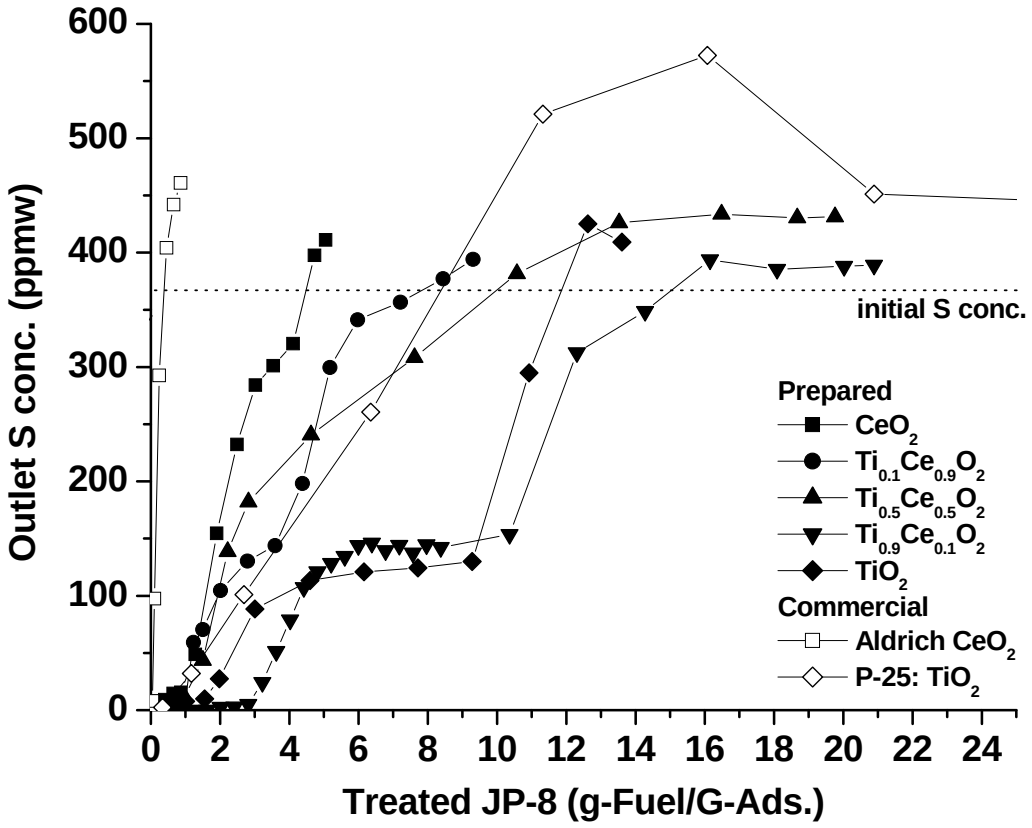

Figure **E-2**: Breakthrough curves of ADS of JP-8 (365 ppmw-S) over various metal oxide adsorbents: operation temperature: LHSV: 1.2 h^{-1}, room temperature. Pretreatment at 300 ^{o}C under air flow.

E-1-3 Sulfur removal of ultra low sulfur diesel over the various metal oxides

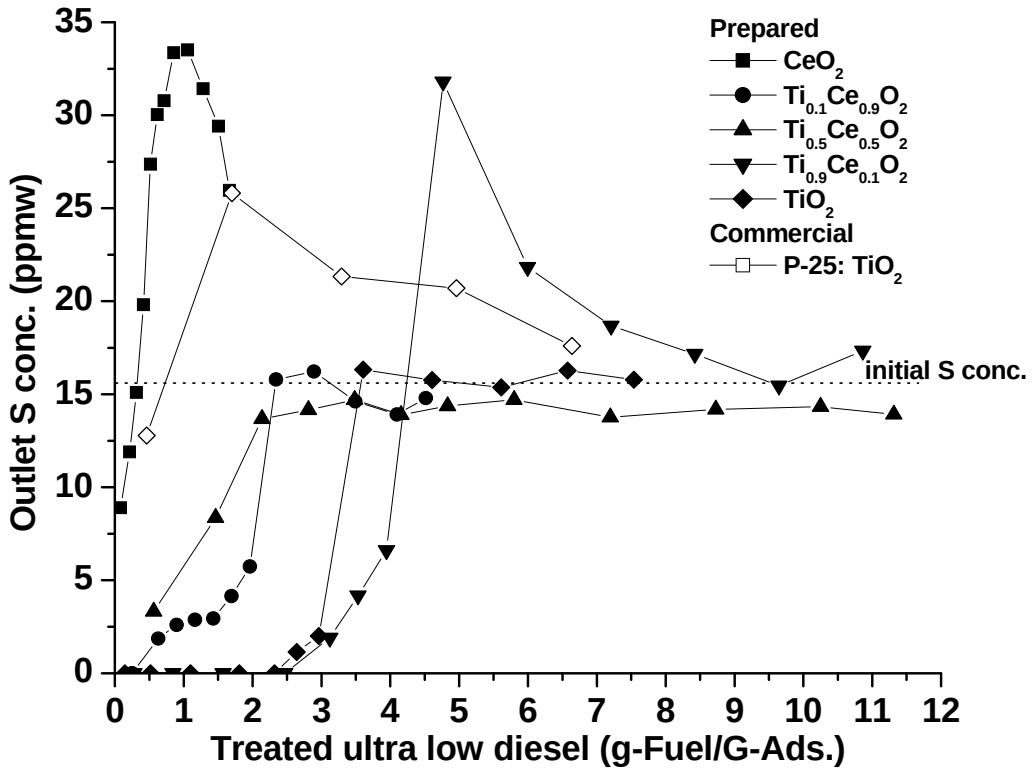

Figure **E-3**: Breakthrough curves of ADS of ultra low diesel (16 ppmw-S) over various metal oxide adsorbents: LHSV: 1.2 h^{-1}, operation temperature: room temperature. Pretreatment at 300 ^{o}C under air flow.

E-1-4 Sulfur removing performance of $Ti_{0.9}Ce_{0.1}O_2$ for the different fuels

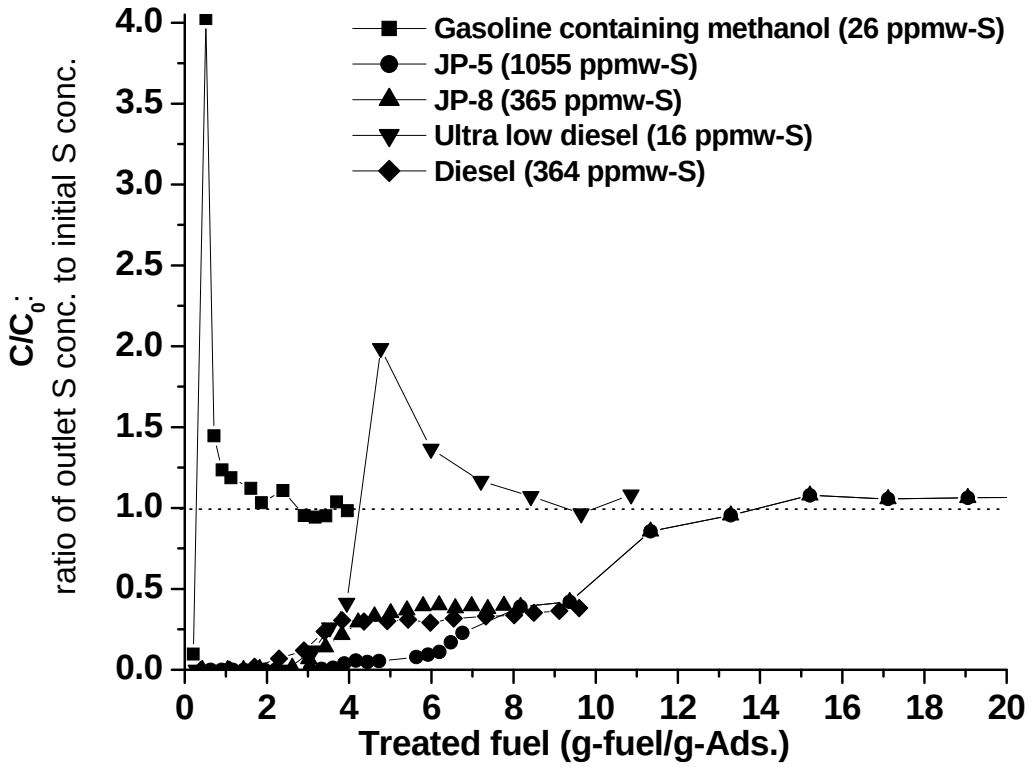

Figure **E-4**: Breakthrough curves of ADS for various fuels over $Ti_{0.9}Ce_{0.1}O_2$: operation temperature: room temperature. Pretreatment at 300 ^{o}C under air flow.

E-2 Sulfur Balance in ADS of JP-8 using $Ti_{0.9}Ce_{0.1}O_2$

Table **E-1**: Sulfur Balance in ADS of JP-8

	S wt. %
Before ADS of JP-8	0.72
After ADS of JP-8	0.93
Result by Leco	0.21
S removal Capacity (saturation)	0.28

* analyzed by Leco SC-144DR under O_2 flow at 850 ^oC

Appendix F

Additional Characterization

XPS spectra of two different $Ti_{0.9}Ce_{0.1}O_2$ samples

Two $Ti_{0.9}Ce_{0.1}O_2$ samples were prepared by urea precipitation at the different time.

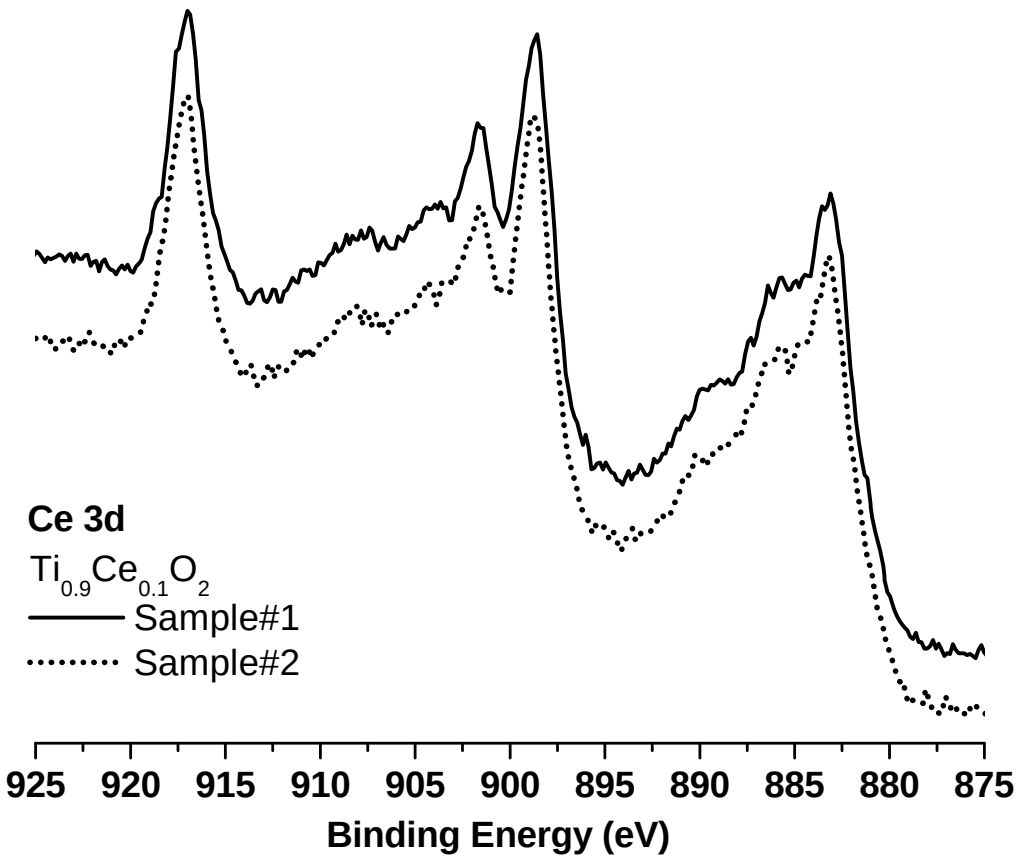

Figure **F-1**: XPS Ce 3d spectra of two $Ti_{0.9}Ce_{0.1}O_2$ samples prepared different time

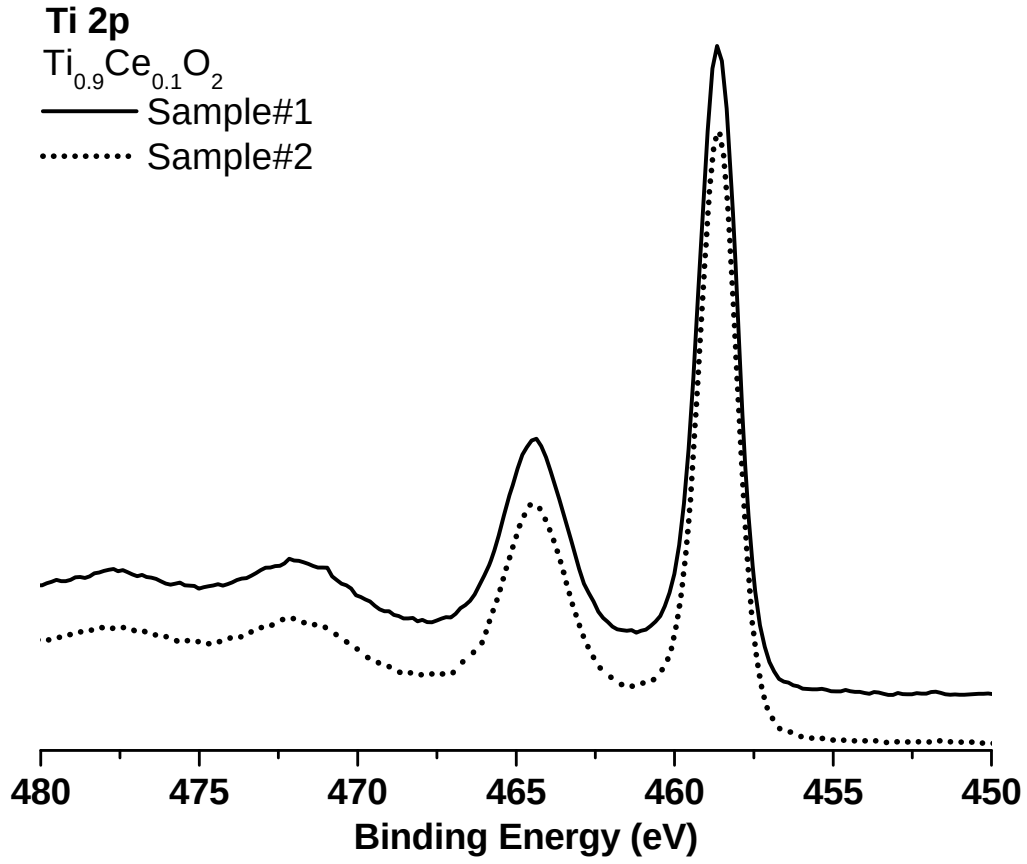

Figure **F-2**: XPS Ti 2p spectra of two $Ti_{0.9}Ce_{0.1}O_2$ samples prepared different time

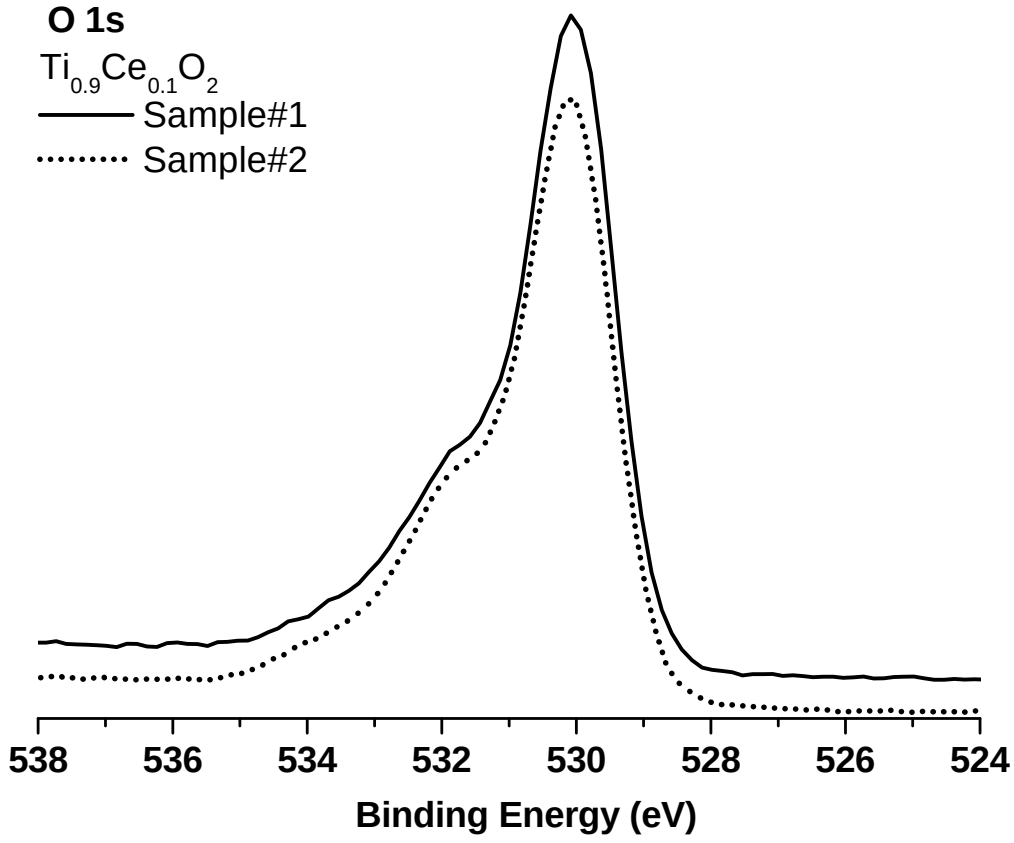

Figure **F-3**: XPS O 1s spectra of two $Ti_{0.9}Ce_{0.1}O_2$ samples prepared different time

VITA

Shingo Watanabe

Shingo Watanabe was born on August 29th, 1977 in Noshiro, Akita, Japan, to the loving parents Eiichi and Yoko Watanabe. He grew up in a small city, Noshiro, until graduated from Noshiro high school. After high school, he attended Akita University where he majored in Applied Chemistry and Material Science. In the senior year, he started a research on intercalation compounds in a ceramics lab under the Dr. Zenbe-e Nakagawa. At the same time, he could have an opportunity to go to St. Cloud State University as an exchange student. He studied Organometallic Chemistry and Inorganic Chemistry along with Spanish and Announcing. After coming back to Akita University, he had another opportunity to know Dr. John Armor who introduced Dr. Chunshan Song. Thanks to Dr. Song's exceptional guidance, he obtained his doctoral degree in Energy and Geo-Environmental Engineering in the fall of 2007. This research has been filed to the patent application in fall of 2007.